ERK1 AND ERK2 IN HEMATOPOIESIS, MAST CELL FUNCTION, AND THE MANAGEMENT OF NF1-ASSOCIATED LEUKEMIA AND TUMORS

Karl W. Staser

Submitted to the faculty of the University Graduate School
in partial fulfillment of the requirements
for the degree
Doctor of Philosophy
in the Department of Biochemistry and Molecular Biology,
Indiana University

March, 2012

Accepted by the Faculty of Indiana University, in partial

fulfillment of the requirements for the degree of Doctor of Philosophy.

_____

D. Wade Clapp, M.D., Chair

_____

Maureen A. Harrington, Ph.D.

Doctoral Committee

_____

Mark G. Goebl, Ph.D.

_____

Feng Chun Yang, M.D., Ph.D.

July 7, 2011

ACKNOWLEDGEMENTS

I thank my committee members for immeasurable insight, support, criticisms, and benedictions, which have critically shaped the direction and discoveries of my graduate research. I also am grateful for the faculty and staff of the Department of Biochemistry, whose intellectual and financial support facilitated this project while providing the fundamental didactic and inductive tutelage that guides meaningful inquiry. Likewise, I thank the students of the Department of Biochemistry who, through the peculiarities and profundities of weekly seminar, have expanded the globe of my scientific exploration.

I thank every single member of the Clapp and Yang laboratories, including several graduate students and technicians who have continued on elsewhere. Of note, I would like to acknowledge Su-Jung Park, who has challenged and tutored me, both technically and intellectually. Her mentorship invaluably underpins this thesis, and I happily anticipate consulting her particular and profound expertise throughout my career.

I am especially grateful for Dr. Wade Clapp's guidance and friendship. Without Wade's encouragement, this thesis would be absent from the scientific repertoire. He ardently promoted and ultimately fulfilled my nascent desire to develop my career goals toward those of a physician-scientist. Thus, from the depths of a previous obscurity my enduring aim of lifelong scientific discovery and service has emerged, and I treasure Wade as a mentor and friend.

ABSTRACT

Karl W. Staser

ERK1 AND ERK2 IN HEMATOPOIESIS, MAST CELL FUNCTION, AND THE MANAGEMENT OF NF1-ASSOCIATED DISEASE

Neurofibromatosis type 1 is a genetic disease that results from either heritable or spontaneous autosomal dominant mutations in the NF1 gene, which encodes a protein serving, at least in part, to accelerate the intrinsic hydrolysis of active Ras-GTP to inactive Ras-GDP. A second-hit *NF1* mutation precedes predominant NF1 neoplasms, including juvenile myelomoncytic leukemia (JMML) and plexiform neurofibroma formation, potentially fatal conditions with no medical therapy. While *NF1* loss of heterozygosity (LOH) in myeloid progenitor cells sufficiently engenders leukemogenesis, plexiform neurofibroma formation depends on LOH in Schwann cells and *Nf1* heterozygosity in the hematopoietic system. Specifically, recruited $Nf1^{+/-}$ mast cells accelerate tumorigenesis through secreted cytokines and growth factors. $Nf1^{+/-}$ mast cells depend upon deregulated signaling in c-kit pathways, a receptor system conserved in hematopoietic stem cells (HSCs). Accordingly, $Nf1^{-/-}$ myeloid progenitor cells, which can induce a JMML-like disease in mice, also demonstrate deregulated c-kit receptor signaling. C-kit-activated $Nf1^{+/-}$ mast cells and $Nf1^{-/-}$ myeloid progenitors both show increased latency and potency of active Erk1 and Erk2, the principal cytosolic-to-nuclear effectors of canonical Ras-Raf-Mek signaling.

Thus, Erk represents a potential regulator of leukemogenesis and tumor-associated inflammation. However, single and combined Erk1 and Erk2 roles in HSC function, myelopoiesis, and mature mast cell physiology remain unknown, and recent hematopoietic studies relying on chemical Mek-Erk inhibitors have produced conflicting results. Here, we show that hematopoietic stability, myelopoiesis, and mast cell generation require Erk1 or Erk2, but individual isoforms are largely dispensable. Principally, *Erk*-disrupted hematopoietic stem cells incorporate BrdU but are incapable of dividing, a novel and cell type-specific Erk function. Similarly, mast cell proliferation requires Erk but cytokine production proceeds through other pathways, elucidating molecule-specific functions within the c-kit cascade. Based on these findings, we have reduced tumor mast cell infiltration by treating genetically-engineered tumor model mice with PD0325901, a preclinical Mek-Erk inhibitor. Moreover, we have devised a quadruple transgenic HSC transplantation model to examine dual Erk disruption in the context of Nf1 nullizygosity, testing whether diseased hematopoiesis requires Erk. These insights illuminate cell-specific Erk functions in normal and Nf1-deficient hematopoiesis, informing the feasibility of targeting Mek-Erk in NF1-associated disease.

D. Wade Clapp, M.D., Chair

TABLE OF CONTENTS

ABBREVIATIONS

7-AAD:	7-Aminoactinomycin D.
APC:	Allophycocyanin.
BCA:	Bicinchoninic acid.
BSA:	Bovine serum albumin.
DAPI:	4',6-diamidino-2-phenylindole.
DMEM:	Dulbecco's Modified Eagle Medium.
EPO:	Erythropoietin.
ERK:	Extracellular regulated kinase.
FBS:	Fetal bovine serum.
FITC:	Fluorescein isothiocyanate.
Flt3L:	Flt (Fms-like receptor tyrosine kinase 3) ligand.
G-CSF:	Granulocyte-colony stimulating factor.
GM-CSF:	Granulocyte-macrophage-colony stimulating factor.
GAP:	GTPase activating protein.
GDP:	Guanosine diphosphate.
GMP:	Granulocyte-macrophage progenitor.
GTP:	Guanosine triphosphate.
HPPC:	High proliferation potential cell.
HSC:	Hematopoietic stem cell.
Hst:	Hoechst.
IL-3:	Interleukin-3.
IL-6:	Interleukin-6.
IL-13:	Interleukin-13.
IL-17:	Interleukin-17.
IMDM:	Iscove's Modified Dulbecco's Medium.
I.P.:	Intraperitoneal.
I.V.:	Intravenous (tail vein).
LPPC:	Low proliferation potential cell.
MAPK:	Mitogen activated protein kinase.
M-CSF:	Macrophage-colony stimulating factor.
MCP-1:	Monocyte chemotactic protein 1.
MEP:	Megakaryocyte-erythroid progenitor.
MIP-1a:	Macrophage inflammatory protein 1 alpha.
MIP-1b:	Macrophage inflammatory protein 1 beta.
MP:	Myeloid progenitor.
MPP:	Multipotent progenitor.
MTT:	3-(4,5-dimethylthiazol-2-yl)-2,5-diphenyltetrazolium bromide.
NaN_3:	Sodium azide.
NF1:	Neurofibromatosis type 1.
NGF:	Nerve growth factor.
PBS:	Phosphate buffered saline.
PDGF:	Platelet-derived growth factor.
PE:	Phycoerythrin.

PEI:	Polyethyleneimines.
PerCP:	Peridinin chlorophyll protein.
PI:	Propidium iodide.
PI-3K:	Phosphatidylinositol 3-kinases.
PY:	Pyronin Y.
PVDF:	Polyvinylidene fluoride.
RANKL:	Receptor activator of nuclear factor kappa-B ligand.
RAS:	Rat Sarcoma protein.
SCF:	Stem cell factor.
SLAM:	Signaling lymphocytic activation molecule.
SDS-PAGE:	Sodium dodecyl sulfate polyacrylamide gel electrophoresis.
TNF-α:	Tumor necrosis factor alpha.
VEGF:	Vascular endothelial growth factor.
WT:	Wild-type.

INTRODUCTION

Neurofibromatosis type 1 (NF1, von Recklinghausen's disease) is a genetic disorder caused by autosomal dominant mutations in the *NF1* gene, which encodes Neurofibromin, a protein that accelerates the hydrolysis of Ras from its GTP- to GDP-bound conformation. The disease afflicts approximately 1 in 3500 persons worldwide in a pandemic fashion, and it is the most common genetic disorder with a predisposition to cancer (1). NF1 manifests with both non-tumorigenic and tumorigenic maladies, including learning disabilities, skeletal dysplasia, non-healing fractures (pseudarthrosis), myeloid leukemia (JMML), and tumors such as optic glioma and the namesake neurofibroma. The disease's hallmark signs include hyper-pigmented areas of the skin (café au lait macules) and hamartomas on the iris (Lisch nodules), which serve as important diagnostic criteria and may be observed in infancy or childhood of afflicted individuals (2, 3). Because prominent NF1 symptoms arise from neural crest-derived tissue (e.g. glia, Schwann cells, melanocytes), some reports have characterized NF1 as a disorder of the neural crest. However, NF1 pathologies arise in organs derived from all embryonic germ layers, and we should consider NF1 not only a tumor predisposition syndrome but also a systemic developmental disorder (4).

NF1-like cutaneous tumor syndromes appeared in the literature during the 18th century (5-7), and in the 1880s Friedrich von Recklinghausen published seminal observations detailing cutaneous tumors comprised of both neuronal and fibroblastic tissue, deeming the tumors neurofibromen (8). NF1's pathognomonic neurofibromas are slowly progressing, heterogeneous solid tumors comprised of

Schwann cells, fibroblasts, vascular cells, and infiltrating hematopoietic cells, predominantly degranulating mast cells (9-14). Cutaneous and subcutaneous neurofibromas derive from small peripheral nerve branches during adolescence or adulthood and are found in nearly all individuals with NF1 (15). By comparison, plexiform neurofibromas afflict half or fewer individuals with NF1 and develop from cranial and large-peripheral nerve sheaths, possibly initiating during gestation or early infancy from abnormally differentiated nonmyelinating Schwann cells or their less-differentiated precursors (16, 17).

Plexiform neurofibromas are typically a lifelong source of disfigurement, disability, and mortality. In many cases, plexiform neurofibromas compress cranial nerves and/or peripheral nerve roots at the vertebral column and create an array of morbidity, including paresthesia, paralysis, drooling, sleeplessness, respiratory and gastrointestinal distress, blindness, and loss of bowel and bladder control (18, 19). A plexiform neurofibroma also has the potential to transform into a malignant peripheral nerve sheath tumor (MPNST), a highly morbid, metastatic cancer afflicting up to 10% of NF1 patients in their lifetime (20, 21).

Plexiform neurofibroma treatment consists primarily of symptom management and/or surgical resection. In many cases, the tumor's close involvement with vital nerve tissue, vasculature, or other viscera complicates surgery (18, 19, 22). Currently, the tumors have no medical therapy or cure, although several molecularly-targeted compounds are in preclinical or clinical testing (23-27). Problematically, nerve sheaths and heavily collagenized areas

may resist drug bioavailability, complicating direct pharmacological inhibition of the tumorous mass. Therefore, therapeutic strategies targeting components of the tumor microenvironment, including vascular cells and infiltrating mast cells, may prove viable alternatives (28).

Mast Cells, Tumors, and the NF1 Hematopoietic System

Mast cells are granular hematopoietic cells that arise from myeloid progenitor cells prior to granulocyte/monocyte lineage commitment (29). Mast cell precursors migrate from the bone marrow into the vasculature and enter dermal tissue where they mature into immune effector cells. Mast cells fight pathogens, protect against venoms and toxins, and may perform other immunomodulatory functions, both pro- and anti-inflammatory (30-33). While mast cells are predominantly known as the mediators of allergy and allergic asthma via IgE/FcεR pathways, they additionally depend on stem cell factor (SCF) signaling at the c-kit receptor tyrosine kinase for their generation and, in some contexts, pathophysiological activation (34-37). Indeed, mice naturally mutated at the c-kit receptor tyrosine kinase (*W*, or “white spotting locus” mutants, which reduces c-kit kinase activity >85%) exhibit profoundly reduced numbers of tissue-resident mast cells (35). Some *W* mice have anemia and deficient hematopoiesis, as the hematopoietic stem cell (HSC) also depends upon SCF/c-kit signaling.

The pro-inflammatory activities of recruited mast cells and other immune effector cells have been shown to sustain tumor microenvironments in various disease models (reviewed in (38-40)). In this inflammatory microenvironment

hypothesis, tumorigenic cells recruit and co-opt the functions of non-tumorigenic hematopoietic cells via unchecked mitogenic and chemotactic signals. These recruited cells, in turn, coordinate vascular in-growth, collagen deposition, and the pathological inflammation promoting extracellular matrix remodeling, tumor expansion, invasion, and metastasis. Specifically, mast cells can synthesize and secrete matrix metalloproteinases (MMPs), various cytokines (e.g. IL-6 and TNF-α), and multiple mitogens (e.g. NGF, VEGF, and PDGF) (32, 33) with putative roles in tumor initiation, maintenance, and growth.

Mast cells have been associated with NF1 since 1911, when H. Greggio first noted *les cellules granuleuses* in neurofibroma tissue (14). Decades later, several investigators confirmed their presence using traditional histology and electron microscopy (9-13). By the 1980s, mast cells were widely-recognized inflammatory effectors and hallmark histological features (albeit of unknown significance) of the neurofibroma. Vincent Riccardi first hypothesized that mast cells may critically contribute to neurofibroma formation, proposing that mast cell degranulation explained his clinical observations of coincident pruritus and cutaneous neurofibroma formation (41). Indeed, a small human study with a mast cell granule stabilizer (ketotifen) reduced pruritus and/or slowed neurofibroma growth (42), but a subsequent multiphase trial confirmed only anti-pruritic and analgesic effects, not neurofibroma reduction (43). These inquiries provided important evidence of aberrant mast cell degranulatory activity in neurofibroma tissue yet suggested that local inhibition of degranulation alone does not change overall disease course. As discussed in this review, recent biochemical,

transplantation, and pharmacological studies have implicated a preponderant role for SCF-mediated mast cell gain-in-functions in orchestrating the neurofibroma microenvironment. This SCF-mediated coordination of mast cell inflammation and tumor growth may inform a novel approach to NF1 therapeutics.

Intriguingly, the mast cell shares functional and phenotypic similarities with hematopoietic stem and progenitor cells, potentially informing mechanisms of the coincident occurrence of JMML in NF1 patients. This myelomonocytic neoplasia, which has no therapy or cure and is uniformly fatal, results from loss of *NF1* heterozygosity in hematopoietic stem and progenitor cells, which become hypersensitive to multiple cytokines, including GM-CSF and SCF (44, 45). Like mast cells, all hematopoietic stem and progenitor cells express the c-kit receptor tyrosine kinase and utilize SCF signaling for their proliferation, differentiation, and survival (46). Thus, we can consider the NF1 hematopoietic system to be one of myeloid dysfunction at the level of hematopoietic stem and progenitor cells, including mast cell precursor cells (Figure 1).

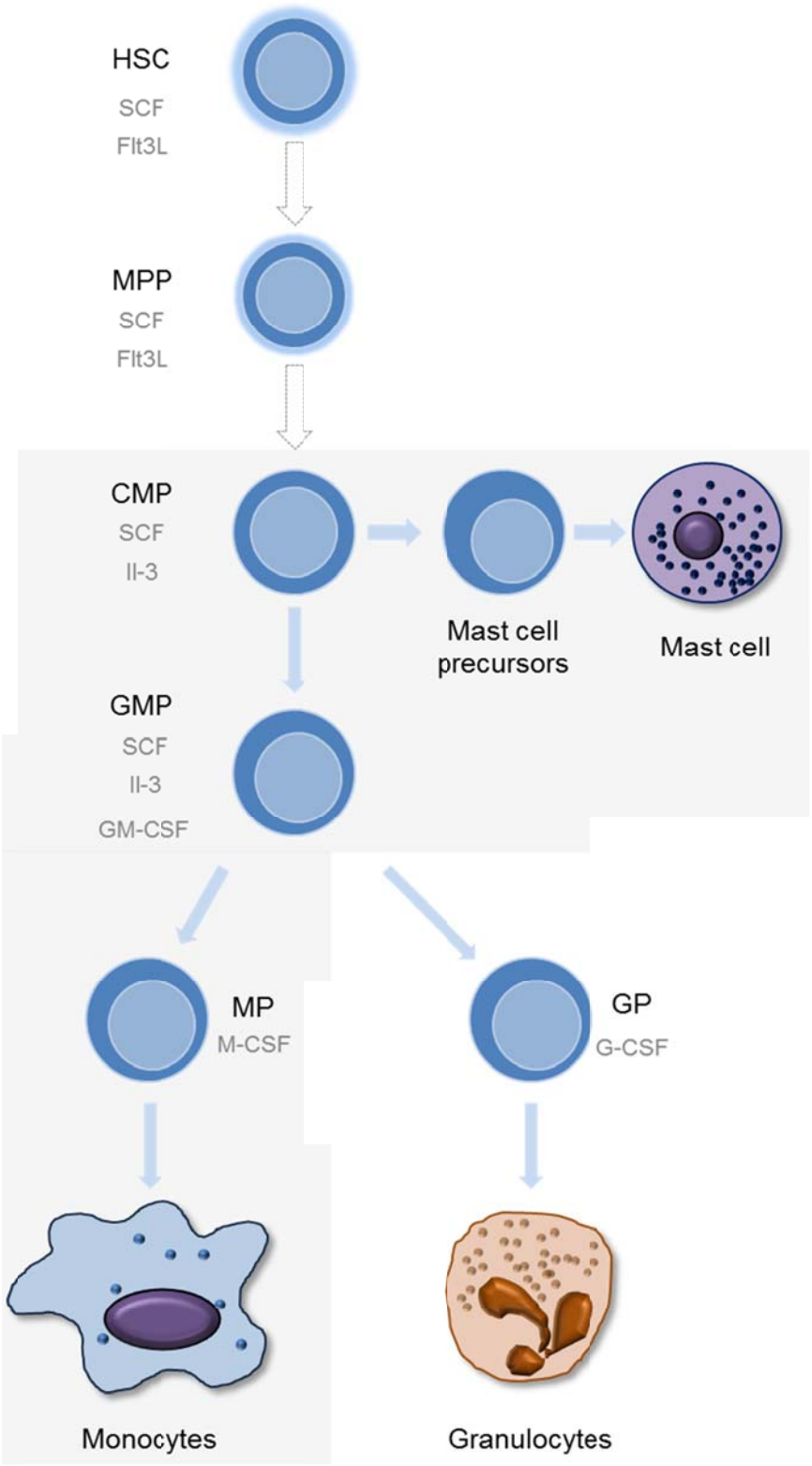
HSC
SCF
Flt3L
MPP
SCF
Flt3L
CMP
SCF
Il-3
Mast cell precursors
Mast cell
GMP
SCF
Il-3
GM-CSF
MP
M-CSF
GP
G-CSF
Monocytes
Granulocytes

Figure 1

Figure 1: Myeloid hierarchy with an emphasis on cells known to be dependent on Neurofibromin signaling. The hematopoietic stem cell (HSC) gives rise to multipotent progenitors (MPP), which can differentiate to the common myeloid progenitor (CMP) or the common lymphoid progenitor (not shown). The CMP gives rise to granulocyte-macrophage progenitors (GMP), mast cell precursors, and erythroid lineages (not shown). The GMP, in turn, gives rise to the granulocyte progenitor (GP) and the macrophage/monocyte progenitor (MP), which can differentiate into multiple cell types, including macrophages, osteoclasts, and dendritic cells. The shaded box indicates lineages known to be hyper-responsive to the indicated cytokines, subsequent to mono- or biallelic inactivation of *Nf1/NF1*. SCF: stem cell factor, Flt3L: Flt3 (fms-like receptor tyrosine kinase 3) ligand, Il-3: interleukin-3, GM-CSF: granulocyte-macrophage colony stimulating factor, M-CSF: macrophage colony stimulating factor, G-CSF: granulocyte colony stimulating factor.

NF1 Genetics

A century after von Recklinghausen's seminal case reports, genetic linkage studies in NF1-afflicted families identified the pericentromeric region of chromosome 17 as the genomic region harboring the gene responsible for the disease (47, 48). Further studies in patients with translocations of chromosome 17 (49-52) facilitated the identification and full-length sequencing of the *NF1* gene (53), which spans 350 kilobases of human chromosome 17 (17q11.2) and encodes 59 exons producing a 2818 amino acid protein (49, 54-56). Of note, human Neurofibromin and its mouse homolog share 98% identity at the protein level (57).

Approximately half of *NF1* mutations in humans arise spontaneously (58), with the majority of mutations leading to premature truncation of the protein neurofibromin (59, 60). When *NF1* mutations occur post-meiotically, individuals may exhibit segmental NF1 with manifestations confined regionally or to a subset of normally affected cell types (e.g. only pigmentation defects) (61). Different *NF1* frameshift and point mutations do not necessarily correlate with phenotypic severity, although some studies have shown that microdeletions encompassing the entire *NF1* locus (which account for less than 10% of mutations) associate with earlier onset and more profound disease manifestations (62, 63). Phenotypic variation tends to be high even within families, and pedigree analyses indicate that while *NF1* mutations are fully penetrant, variation in genes independent of the *NF1* locus critically modulates time-to-onset and course of the disease (64, 65). Parallel to the human data, different *Nf1*-mutant mouse strains exhibit both

varied expression levels of neurofibromin and variable susceptibility to different NF1-like disease manifestations (66). Overall, with the exception of the documented severity associated with *NF1* locus-encompassing microdeletions and a uniquely mild phenotype associated with a 3-base pair deletion in exon 17 (67), particular genetic mutations or genomic variations which may correlate to specific disease outcomes are largely unknown.

NF1 encodes neurofibromin, a protein which functions, at least in part, as a $p21^{ras}$ (Ras) guanosine tri-phosphatase (GTP) activating protein (GAP) (68-72). Neurofibromin and other Ras-GAPs logarithmically accelerate the intrinsic hydrolysis of Ras-GTP to its inactive guanosine di-phosphate- (GDP)-bound conformation (73). In response to multiple mitogenic stimuli, active Ras-GTP orchestrates diverse protein signaling networks, including mitogen activated protein kinase- (MAPK)- and Akt-directed pathways (74-78). Hence, by accelerating the conversion of Ras-GTP to Ras-GDP, neurofibromin negatively regulates Ras-dependent signaling cascades and, generally, serves to downregulate mitogenic events across diverse protein networks. In cases of NF1 heterozygosity or nullizygosity, as observed in somatic cells and in tumor cells of individuals with NF1, respectively, downstream Ras-mediated phosphorylation and transcriptional events can increase in duration and total output. This global upregulation of Ras-dependent activity in *NF1/Nf1*-disrupted tissue typically leads to cellular gain-in-functions, including enhanced proliferation, migration, and survival in multiple cell types (reviewed in (79-83). Of note, the specific Ras effectors potentiated by loss of *NF1* may vary by cell and receptor type, and

biochemical consequences in one cell-receptor system may or may not be observed in another.

Nf1 Gene Dosage

Although *NF1* is classified as a classical Knudson tumor suppressor gene, multiple studies have shown that *NF1* heterozygosity critically modulates cell fate and function by altering Ras-dependent biochemical pathways in distinct cell types (reviewed in (82)). Moreover, physiological Ras activity regulates embryogenesis, early development, and normal tissue maintenance. Therefore, neurofibromin may be viewed not only as a tumor suppressor but also as a regulator of histiogenesis, cellular maintenance, and repair (4). Accordingly, NF1 is a disorder of both tumor predisposition and of developmental dysplasia.

While somatic cells in an individual with NF1 are heterozygous for *NF1*, loss of heterozygosity (LOH) in different cell types typically precedes hallmark hyperplastic, dysplastic, and neoplastic disease manifestations. LOH has been shown in human tissue samples and confirmed in NF1 mouse models of certain NF1 pathologies via multiple molecular techniques, coinciding with *NF1*'s designation as a classical tumor suppressor gene. As examples, LOH in Schwann cells or their precursors permits neurofibroma formation (17, 84-86) and LOH in myeloid progenitor cells induces myelomonocytic leukemia (44).

Individuals with NF1 also have an increased prevalence of multiple generalized manifestations which do not appear to require cell-specific biallelic inactivation of *NF1*, including skeletal and mesenchymal dysplasia (e.g. short stature, osteoporosis, and soft tissue malformation), disorders of neurocognitive

development (e.g. retardation, spatial/visual coordination, and autism), and vascular pathologies (e.g. fistulae, infarcts, and aneurysms). Hence, *NF1* heterozygosity alone alters Ras-dependent pathways to a degree sufficient for the pathological alteration of normal developmental and homeostatic processes in multiple organ systems.

Indeed, *Nf1* haploinsufficient mast cells and fibroblasts, major constituents of the heterogeneous plexiform neurofibroma, demonstrate multiple gain-in-function phenotypes that include enhanced proliferation, survival, migration, and cytokine production in response to specific stimuli (87, 88). These data parallel findings in *Nf1* haploinsufficient microglia (89), which critically modulate the inflammatory microenvironment of NF1-associated optic glioma (90-92).

In some mouse models of plexiform neurofibroma and optic glioma formation, tumorigenesis requires *Nf1* haploinsufficiency in non-tumorigenic cells. Specifically, hematopoietic stem cell transplantation studies in the $Nf1^{flox/flox}$*; Krox20°Cre* and $Nf1^{flox/flox}$*; P0aCre* models (which experience biallelic *Nf1* inactivation in a subset of Schwann cell/Schwann cell precursors) have shown that neurofibroma genesis requires *Nf1* haploinsufficiency and c-kit-mediated signaling in the hematopoietic compartment (24). In these experiments, $Nf1^{flox/flox}$*; Krox20°Cre* mice required $Nf1^{+/-}$ hematopoietic stem cell transplants to engender tumorigenesis, while WT hematopoietic stem cell transplants protected against tumorigenesis in $Nf1^{flox/-}$*;Krox20°Cre* mice. These data, combined with cell culture studies of $Nf1^{+/-}$ mast cells, roundly implicate the *Nf1* haploinsufficient hematopoietic compartment (and, specifically, deregulated myeloid and mast

cells), as a principal pathologic component of the plexiform neurofibroma microenvironment.

By comparison, clonal outgrowth in NF1-associated JMML depends on *Nf1/NF1* LOH in hematopoietic stem and progenitor cells (c-kit^{+} cells) with no requirement for an *Nf1*$^{+/-}$ cellular background. As evidence, transplantation of *Nf1*$^{-/-}$ hematopoietic stem cells into WT mice engenders a myeloproliferative disorder (MPD) recapitulating human JMML (44, 45, 93). However, in human cases of NF1-associated JMML, we expect all surrounding somatic cells in the individual to be essentially *NF1*$^{+/-}$. Of note, no report has directly investigated possible contributions of an *Nf1*$^{+/-}$ stroma to the time-to-onset, progression, and severity of NF1-associated MPD.

Mek-Erk Signaling in Mast Cells

SCF regulates mast cell and hematopoietic progenitor cell cytopoiesis, proliferation, survival, and cytokine synthesis, and *Nf1* deficiency can potentiate these functions. In fact, the study of SCF-stimulated *Nf1*$^{+/-}$ mast cells provided foundational evidence that haploinsufficiency of a “tumor suppressor” could modulate multi-lineage cell fate and function in tissue culture and in vivo (87). This study additionally demonstrated that *Nf1* haploinsufficiency increases the latency and potency of GTP-bound Ras in SCF-stimulated cells. Subsequent studies have detailed the biochemical mechanisms modulating SCF-mediated gain-in-functions, showing alterations arising from deregulated signaling events in multiple Ras-dependent networks. In response to ligand binding at diverse cell surface receptors, Ras activates to its GTP-bound state and promotes

phosphorylation in downstream protein networks, including those orchestrated by MAPKs and phosphoinositide-3-kinase (PI-3K) (75-78). Neurofibromin, which contains a highly-conserved GAP-related domain (GRD) with homology to the yeast gene products IRA1 and IRA2, logarithmically accelerates the intrinsic hydrolysis of active GTP-bound Ras to its GDP-bound state (50, 55, 68, 71, 79, 94). Generally, loss-of-function mutations in genes encoding Ras-GAPs promote cell growth, proliferation, migration, and survival (40). In myeloid progenitor cells, microglia, and mast cells, loss of one or both alleles of *Nf1* leads to increased duration of Ras-GTP activity and phosphorylation of specific effectors within Raf-Mek-Erk, PI-3K-Rac-Pak-P38, and PI-3K-Akt cascades (44, 45, 87, 92, 95-100).

Cell culture and in vivo studies of genetically-disrupted mast cells indicate that the Raf-Mek-Erk pathway may primarily modulate SCF-mediated proliferation and protein synthesis while the PI-3K-Rac2-Pak-p38 pathway controls F-actin dynamics and cellular motility (97, 98, 100-103). Biochemical investigations have additionally shown that the PI-3K-dependent pathway reinforces the classical Raf-Mek-Erk cascade through the activity of the p21 activated kinases (Paks) (98, 102). In this schema, PI-3K-activated Rac2 induces Pak1 to phosphorylate Mek at serine 298 as well as Raf1 at serine 338, potentiating Raf1's phosphorylation of Mek at serine 217/222. These activities potentiate phosphorylation of the extracellular regulated kinases, Erk1 and Erk2. Erk1 and Erk2 phosphorylate cytoplasmic targets (e.g. $p90^{rsk}$), translocate to the nucleus, and activate multiple mitogenic transcription factors (e.g. c-Fos, Elk1, C/EBP).

However, direct genetic studies of Mek-Erk signaling in the SCF-stimulated mast cell are lacking. All prior investigations have relied on chemical inhibitors of Mek (e.g. PD98059), which are known to have non-selective inhibitions and cellular toxicities. Moreover, Erk1 and Erk2's specific modulation of the mast cell cycle, as well as Erk-dependent transcriptional events, including the production of inflammatory cytokines, are not documented. Finally, it is unknown whether Erk1 and Erk2 have isoform specific roles in the modulation of SCF-mediated mast cell function (Figure 2).

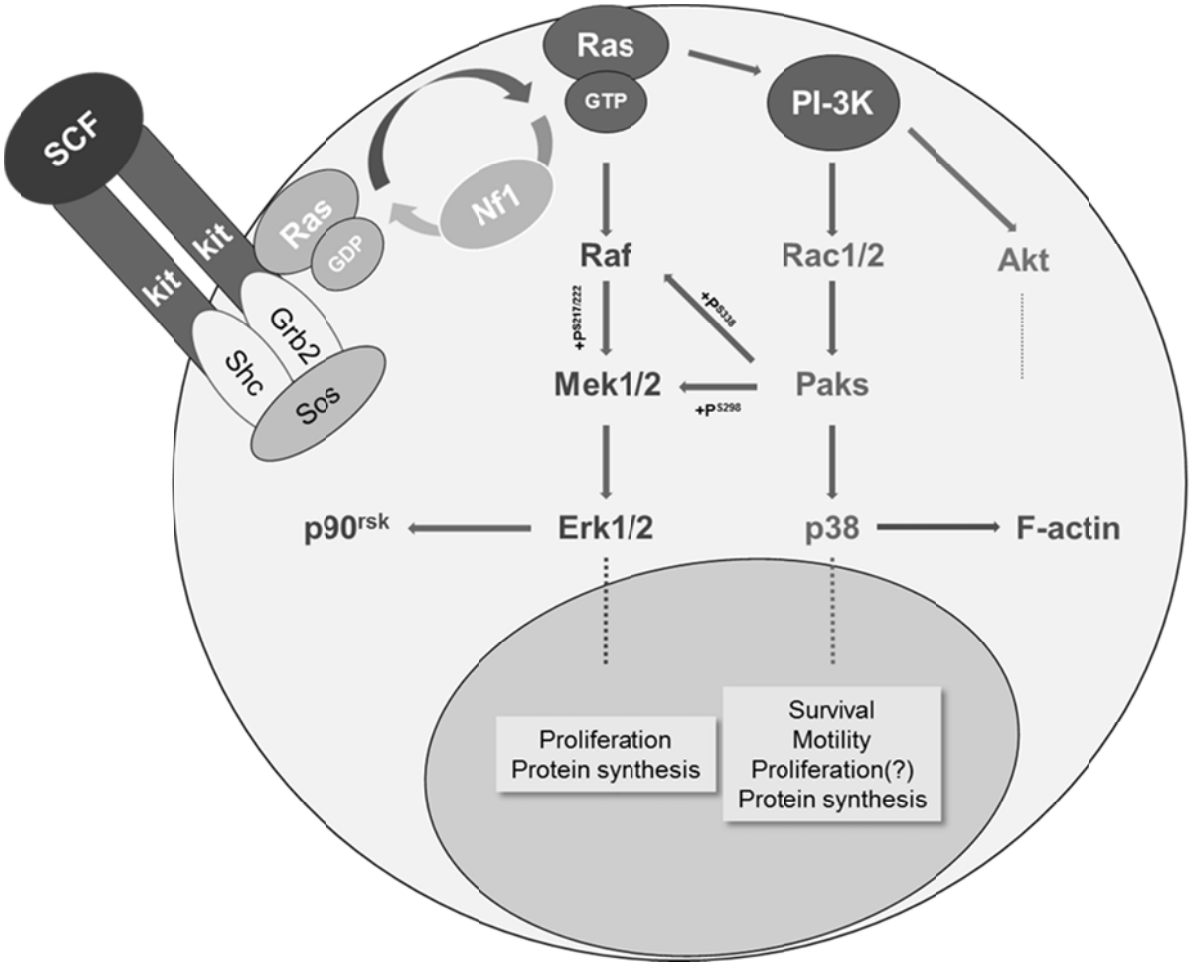
SCF
kit
kit
Ras
GDP
Nf1
Ras
GTP
PI-3K
Raf
Rac1/2
Akt
+PS217/222
+PS338
Grb2
Shc
Sos
Mek1/2
+PS298
Paks
p90rsk
Erk1/2
p38
F-actin
Proliferation
Protein synthesis
Survival
Motility
Proliferation(?)
Protein synthesis

Figure 2

Figure 2: Hyperactive SCF:c-kit pathways in the *Nf1*$^{+/-}$ mast cell. Kit-ligand (SCF) binding at the c-kit receptor tyrosine kinase induces receptor dimerization, activates Ras to its GTP-bound conformation, and induces Ras-Raf-Mek-Erk and PI-3K-Rac-Pak-p38 signaling pathways. While Mek-Erk signals may principally mediate mast cell proliferation, PI-3K activation mediates survival, motility and, through its Pak-dependent crosstalk with Raf-Mek, proliferation. Neurofibromin accelerates the intrinsic hydrolysis of Ras-GTP to inactive Ras-GDP and serves, at least in part, to negatively regulate Mek-Erk- and PI-3K-directed pathways. Although SCF-c-kit interactions initiate other molecular events, this schematic highlights only those thus far shown to be hyperactive in the *Nf1*$^{+/-}$ mast cell. Dashed lines indicate multiple downstream effectors not fully detailed.

Mek-Erk Signaling in Hematopoietic Stem and Progenitor Cells

Like the SCF-stimulated *Nf1*$^{+/-}$ mast cell, *Nf1*$^{-/-}$ myeloid progenitor cells (c-kit^{+}) stimulated with various combinations of SCF, IL-3, and GM-CSF show increased potency and latency of phospho-Erk1/2. This finding corresponds to increased proliferation, colony formation, and the ability of these cells to initiate a JMML-like disease in mice (44, 45). These three cytokines are critical to the proliferation and differentiation of hematopoietic stem cells (HSCs), multipotent progenitor (MPPs), and myeloid progenitors (MPs), and they induce the phosphorylation of Erk1 and Erk2 in both normal and *Nf1*-deficient signaling contexts.

However, genetic hematopoietic studies of single and dual *Erk1* and *Erk2* disruption have focused on only T and B lymphocytes (104, 105). Of note, myelopoietic studies relying on Mek-Erk chemical inhibitors in tissue culture have produced seemingly contradictory results (106-108). In the single previous assessment of dual Erk1/2 disruption in hematopoietic stem cells (Mx1Cre^{+}Erk1$^{-/-}$ Erk2$^{flox/flox}$), Yasuda et al reported defects in pre-B cell expansion (105). They did not examine myelopoiesis, long-term hematopoiesis, or HSC proliferation. Moreover, recent hematopoietic studies using Mek-Erk chemical inhibitors in tissue culture have reached conflicting conclusions (reviewed in (109)), suggesting contrasting effects of chemical Mek-Erk inhibition on monocyte, granulocyte, and myeloid progenitor differentiation (106-108, 110). These studies reinforce the notion that data derived from chemical inhibitors in tissue culture may not accurately represent in vivo physiology. Therefore, genetic in vivo data

are needed to elucidate Erk1 and Erk2's importance (or dispensability) in HSC proliferation, myelopoiesis, and mature effector cell (e.g. mast cell) function.

Global Observations on the Functions of Erk1 and Erk2

Globally, Erk1 and Erk2, 44 and 42 kDa proline-directed protein kinases which share about 83% homology at the amino acid level, appear to ramify critical signals across diverse cell types and ligand-receptor systems (111). Indeed, many tissue culture-based studies have broadly implicated Erk1 and Erk2 kinase activity in the control of cell differentiation, proliferation, survival, motility, and protein synthesis. Generally, ligand binding at cell surface receptors induces Mek1/2 to phosphorylate Erk1 and Erk2, which phosphorylate a number of cytoplasmic targets before translocating to the nucleus to phosphorylate mitogenic transcription factors. Of note, the Raf-Mek-Erk cascade is increasingly being targeted in preclinical and clinical trials of novel, small molecule anti-cancer drugs (112), and the recently developed Mek-Erk inhibitor PD0325901 demonstrates high selectivity, potency (IC_{50} at nanomolar to sub-nanomolar concentrations), and low toxicity (113). Thus, the clinical application of Mek-Erk inhibition in disease management verges on the immediate horizon.

Of concern, though, many of the mechanistic and functional conclusions regarding Erk1 and Erk2 derive either from the use of older generation Mek inhibitors (e.g. PD98059, U0126) or from dominant-negative overexpression in cell lines. While these multitudinous studies have vastly delineated Erk1 and Erk2's importance in various cell functions, amalgamations of these cell culture

studies have created potentially erroneous cell-type specific conclusions for Erk1 and Erk2 roles in vivo.

For example, many cell culture studies have shown that Erk1 and Erk2 kinase activity, via transcription factors such as c-Fos and c-Jun, regulates the G1/S transition, leading to a broad conclusion that Erk1 and Erk2 globally control DNA synthesis (i.e. “the master regulator of G1/S”) but not later cell cycle progression (114). However, a recent genetic in vivo study found that even though Erk1/2 regulates G1/S in fibroblasts, the kinases appear to specifically influence G2/M in keratinocytes (115), indicating lineage-specificity of Erk’s proliferative control. Of note, many tissue culture-based studies of Mek-Erk function have relied on NIH 3T3 or mouse embryonic fibroblasts, both of which have a fibroblastic origin. Intriguingly, lineage-specific study in primary embryonic stem cells found that Erk1/2 activity controls cellular differentiation but not proliferation (116), and, using these insights, investigators are applying PD0325901 to embryonic and induced pluripotent stem cells to encourage their self-renewal ex vivo (117-119). Taken together, these findings raise the possibility that Erk1/2 activity is dispensable for DNA synthesis and/or proliferation in certain cell types (including hematopoietic stem cells, progenitor cells, and mast cells) while highlighting the importance of genetic in vivo studies restricted to specific cell lineages. Cell-specific insights hold a practical relevance, as demonstrated by embryonic stem cell research, where delineation of Erk function has endowed an unexpected usefulness for chemical Mek-Erk inhibition.

The generation of an *Erk1* knockout mouse (*Erk1*$^{-/-}$) (120) and, more recently, an *Erk2* conditional knockout mouse (*Erk2*$^{flox/flox}$) (121, 122) have permitted delineation of singular and combined functions of Erk1 and Erk2. Interestingly, isoform specific roles have emerged in some cell types but not others (123). *Erk1* disruption enhances striatal-dependent learning (124), susceptibility to cocaine addiction (125), hepatocyte survival (126) but not proliferation (127), and the proliferative capacity of fibroblasts (128) while suppressing adipogenesis (129). In the hematopoietic system, *Erk1* disruption alters thymocyte differentiation (120), favors Th1 cell polarization (130), and increases splenic erythropoiesis (131). In some studies, *Erk1* disruption potentiates Mek-Erk2 signaling, suggesting a mechanism for unexpected gain-in-functions (124, 125, 128). However, genetic studies in fibroblasts have shown both isoforms to positively contribute to proliferation, in a gene dose-dependent and isoform-independent manner (132, 133). Enhanced proliferation in some *Erk1*-disrupted cells, then, may result solely from Erk2 over-compensation (i.e. not from intrinsic negative-regulator properties).

Accordingly, *Erk2* disruption principally suppresses cell function, including embryonic lethality at E11.5 due to failed placental vascularization (121). In hepatocytes, *Erk2* disruption reduces proliferative capacity (127), an observation reproduced in vitro and in vivo with normal and transformed fibroblasts (128). Similarly, *Erk2* excision in neurons reduces cognitive function (122), including impaired long-term memory (134). In humans, *ERK2* mutations correlate with cognitive deficits, developmental delays, microcephaly, and cardiac outflow tract

abnormalities, all of which are symptoms of DiGeorge syndrome, a chromosome microdeletion disease which can affect *ERK2*'s locus on chromosome 22 (135, 136). Based on current publications, then, Erk2 may be viewed as the preponderant operator among the two kinases. However, this supposition needs genetic validation in specific cell lineages, and several in vivo studies have found no detectable phenotypic consequence of singular *Erk1* or *Erk2* disruption.

Notwithstanding, the potential for isoform-specific roles for Erk1 and Erk2 in specific cell lineages holds a particular medical relevance. A recent crystal structure of human ERK1 revealed substantial differences in D-motif and backside binding sites, as compared to ERK2, indicating the feasibility of selective ERK1 or ERK2 inhibitory agents (137). Given the suspected critical contribution of combined ERK1/2 signaling to multiple cell types, singular ERK1 or ERK2 inhibition may engender highly-selective targeting of aberrant biological activity in diseased cells while avoiding systemic toxicities.

Indeed, in the few organ systems thus far examined, dual *Erk1/2* disruption leads to profound diminution of cell function, including critical regulation of endothelial cell proliferation and migration (138), luteinizing hormone-induced female fertility from the normal maintenance of granulosa cells (139), radial gliomagenesis and cortical lamination (140), and osteoblast differentiation (141). With the exception of the neuronal studies, the authors observed mild, if any, effects of singular *Erk* disruption.

Given these previous studies, Erk1 and Erk2 may differentially, reciprocally, or inconsequentially influence normal and diseased hematopoiesis

and SCF-mediated mast cell function. Finally, given plethoric studies of Erk1/2 signaling suggesting broad and diverse roles for the molecules, the putative consequences of *Erk* disruption in hematopoietic cells may hinge on altered proliferation, differentiation, survival, and/or protein synthesis.

THESIS OVERVIEW

NF1 deficiency induces increased latency and potency of Erk1 and Erk2 phosphorylation in SCF-stimulated mast and myeloid progenitor cells. *NF1* deficiency and hyper-phosphorylated effectors in c-kit-regulated pathways correlate with abnormally increased proliferation, survival, and protein synthesis. Accordingly, Erk1 and/or Erk2 could be feasible targets for the medical management of plexiform neurofibromas and NF1-associated JMML, especially given the recent development of the pharmacological grade Mek-Erk inhibitor PD0325901. However, foundational genetic studies regarding Erk1 and Erk2's singular and/or combined functions in hematopoietic stem cell and mast cell function are lacking. Here, we use genetic approaches to disrupt *Erk1*, *Erk2*, and *Erk1/2* in hematopoietic stem cells, assessing the functional consequences on myelopoiesis and global hematopoiesis. We then assess the consequence of *Erk1*, *Erk2*, and *Erk1/2* disruption in SCF-stimulated mast cells in tissue culture while examining the efficacy of systemic PD0325901 administration in treating mast cell invasion and plexiform neurofibroma maintenance in a mouse tumor model. We additionally describe an ongoing, long-term experiment to test genetic *Erk1/2* disruption in the context of Nf1-dependent leukemia.

MATERIALS AND METHODS

Mice, Genotyping, and *Mx1Cre* Induction

Previously described *Erk1*$^{-/-}$ (120) and *Erk2*$^{flox//flox}$ (104) mice were bred with *Mx1Cre* transgenic mice and each other. Genotyping was performed as described previously (104, 120, 142). Cre expression was induced in age/sex-matched cohorts by seven intraperitoneal injections of poly I poly C (polyIC, Sigma) dissolved in sterile PBS, using a 27-gauge 0.5" inch needle inserted into the left peritoneal cavity just above the inguinal ligament. To minimize toxicity at initial doses, we used a graded dosing scheme, starting at 15 μg/g body weight and ending at 25 μg/g on the seventh dose. Mice were weighed periodically throughout the dosing regimen, and the average dose throughout amounted to ~20-22 μg/g body weight. Transplanted mice received 6 doses of polyIC, graded between 10 and 20 μg/g body weight (average dose, ~15-17.5 μg/g body weight).

PolyIC is a synthetic dsRNA which induces cells to produce and release IFN-β, driving transcription via JAK-STAT signals at the *Mx1* gene promoter and thus inducing Cre expression in *Mx1Cre* transgenic mice. Previous studies have demonstrated that *Mx1Cre* potently expresses in hematopoietic stem and progenitor cells subsequent to polyIC administration (143, 144). All mice in an experiment received identical doses of polyIC throughout, based on body weight, regardless of genotype. Mice were maintained at Indiana University School of Medicine according to the Institutional Animal Care and Use Committee and Institutional Review Board guidelines.

Marrow Isolation

After Cre induction, femoral, tibial, and/or iliac bone marrow was flushed in Iscove's Modified Dulbecco's Media (IMDM, Gibco/Invitrogen), supplemented with 0.5-1.0% bovine serum albumin (BSA, Sigma) or 2% fetal bovine serum (FBS, Hyclone, ThermoScientific) using a 23-gauge 1.5" inch needle. In quantitative studies, all femurs received the same number of flushes with the same quantity of media. Low density mononuclear cells were isolated by density gradient (Histopaque, Sigma), as described (45). Briefly, harvested cells were carefully layered onto an equivalent volume of Histopaque and centrifuged for 20 minutes at 2000 rpm on a gh-3.8 rotor (Beckman Coulter). Cells were washed in IMDM or other media, as appropriate, before beginning enumeration, colony assays, or flow cytometry-based experiments. Enumeration was performed by hemcytometer and trypan blue exclusion, with three replicates counted and averaged per biologically-independent sample.

Colony Assays

Methylcellulose-based colony forming unit assays and LPPC-HPPC assays were performed as described (45, 145). For LPPC-HPPC, 25,000 low-density mononuclear cells were mixed in 0.33% agar and placed on solidified 1% agar containing 20% FBS, 100 ng/mL SCF, 10 ng/mL GM-CSF, 5 ng/mL IL-3, 10 ng/mL M-CSF, 10 ng/mL G-CSF (Peprotech), and 4U/mL EPO (Amgen). Colony plates were then placed at low oxygen (5%) and 5% CO_2/37°C. Colonies were enumerated by inverted light microscope after one week (LPPC) and two weeks

(HPPC), with HPPCs described as a densely-cored colony covering at least three-quarters of a 2 mm^2 area on a 35 mm^2 Nunclon gridded plate (Thermo Scientific).

For the methylcellulose-based protocol, 25,000 low density mononuclear cells were mixed in 1 mL 1% methylcellulose (Stem Cell Technologies) enriched with 30% FBS, 10^{-4} M β-Mercaptoethanol, and the cytokines/concentrations as listed above (LPPC-HPPC), or as listed for individual experiments, and then plated in duplicate or triplicate on 35 mm^2 Nunclon gridded plate using a16-gauge 1.5" inch needle. After one week growth in room oxygen and 5% CO_2/37°C, colonies were enumerated by inverted light microscope, with a colony defined as an aggregation of at least 50 bone marrow cells originating from a central point.

Single Cell Colony Assays

For single-cell colony assays, freshly-isolated low-density marrow cells were stained with fluorophore-conjugated antibodies to HSC-defining cell surface proteins (see below) and sorted by FACS (FACSAria, BD) into a 96-well flat bottom plate containing 100 µL of 1% methylcellulose enriched with 30% FBS, 100 ng/mL SCF, 10 ng/mL IL-3, 10 ng/mL Flt3-ligand, and 4 U/mL EPO and allowed to grow for seven to ten days in 5% CO_2/37°C. After enumeration of large colonies (>50 cells), each well was then fixed in 4% PFA, washed twice with PBS, and resuspended in 4',6-diamidino-2-phenylindole (DAPI, Invitrogen) containing PBS, allowing efficient visualization of low cell numbers. The ability of the FACSAria to accurately perform single-cell plating is regularly evaluated by

members of the Indiana University School of Medicine Flow Cytometry Core by spotting individual events on glass slides.

Bone Marrow Histology

For histological analyses, we placed the right femur of age/sex-matched mice in a phosphate-buffered 10% formalin solution immediately after killing and fixed for up to two weeks. Femurs were then decalcified in Ethylenediaminetetraacetic acid (EDTA), embedded in paraffin, and cut into 8 μm sections by our in-laboratory histology core. Tissue sections were mounted onto glass slides and stained with H&E or Masson's tri-chrome using standard histological techniques.

Hematopoietic Stem Cell Transplantation

For competitive transplantation assays, bone marrow cells were first isolated, as described above, from CD45.2^{+} *Erk* mutant and CD45.1^{+} WT BoyJ mice, which were obtained from the Indiana University School of Medicine In Vivo Therapeutics Core. Viable bone marrow cells were counted by hemcytometer with Trypan blue exclusion and standardized by concentration in PBS. *Erk* mutant and WT cells were then mixed, at ratios indicated in individual experiments, and injected with a 27 gauge 0.5" needle into the lateral tail vein of lethally-irradiated (1100 cGy, split dose, cesium isotope source) CD45.1/2^{+} WT mice, which were obtained from the Indiana University School of Medicine In Vivo Therapeutics Core. In all experiments, each mouse received 2x10^{6} total low density bone marrow cells suspended in 200 μL PBS. Mice were housed in a

pathogen-minimized room. Mice were considered long-term reconstituted four months post-transplantation.

Peripheral Blood Isolation

At the indicated times after transplantation and before/after polyIC injection, 50-100 µL of blood was extracted from the lateral tail vein of transplant recipients via a superficial excision, perpendicular to the vein, created by a disposable feather scalpel. Blood was collected in a microcapillary tube (Kimble Kimax), transferred to an EDTA coated tube (BD Biosciences), mixed well to avoid clotting, and transferred to a 5 mL flow cytometry tube (BD Biosciences) containing 2 mL of RBC lysis buffer (Qiagen). Whole blood was incubated in this lysis buffer for 10 to 15 minutes at room temperature then washed twice with PBS. After washing, cells were resuspended in 100 µL of 3% FBS/0.09% NaN_3 in PBS ("flow buffer") and kept on ice for further treatment prior to analysis by flow cytometry.

Secondary Transplantation

Erk mutant and CD45.1$^+$ WT BoyJ marrow cells were mixed at a 19:1 ratio and injected I.V. into lethally-irradiated (1100 cGy, split dose) CD45.1/2$^+$ WT mice (total of $2x10^6$ bone marrow cells in 200 µL PBS), as described in the "Hematopoietic Stem Cell Transplantation" section. After four months, primary transplant recipients were injected with a six-dose regimen of polyIC, allowed one month recovery, then one mice from each cohort killed to extract bone marrow for analysis and secondary transplantation. Secondary transplantation

was performed in a non-competitive fashion by injection of $2.0x10^6$ bone marrow cells suspended in 200 µL PBS into lethally-irradiated (1100 cGy, split dose) CD45.1/2$^+$ WT recipients. Secondary transplant recipients were housed in the same pathogen-minimized room as the primary recipients. Peripheral blood was isolated and analyzed as described above.

Flow Cytometry

Acquisition: For both isolated peripheral white blood cells and bone marrow cells, cells were incubated at 4°C for 30 to 60 minutes with saturating concentrations of anti-mouse antibodies in flow buffer supplemented with 0.25 µg Anti-mouse CD16/CD32 ("Fc Block"). Data were acquired on a BD FACSCalibur or a BD LSR II 407 flow cytometer outfitted with red (633 nm, 2 detectors), blue (488 nm, 5 detectors), and violet lasers (407 nm, 2 detectors) using FACSDiva software (BD). For most experiments, single color compensation controls were obtained using 1-to-2 drops of polystyrene microbeads (BD Biosciences) treated with each experimental fluorophore-conjugated antibody and suspended in 400 µL PBS.

Analysis: Compensation matrices were calculated using a defined algorithm in FlowJo 7.6.3 software (TreeStar), with the single-color data acquired from fluorophore-conjugated antibody-stained polystyrene microbeads. Compensation parameters were then applied to all samples. Initial gates were set using characteristic forward and side scatter parameters. Further gating was typically determined using fluorescence minus-one controls. Gates were set on a single sample in a blinded fashion and then automatically applied to all samples.

Quantitative data were assembled by batch export of gated values. Statistical analyses were performed as described below.

Flow Cytometry Antibodies

All flow cytometry fluorophore-conjugated antibodies were from BD Biosciences, unless otherwise noted. For mature hematopoietic lineage analysis, we used the following panel of antibodies: anti-CD45.1-APC, anti-CD45.2-PerCP-Cy5.5, anti-CD3e-FITC, anti-B220-HorizonV500, anti-CD8-PacificBlue, anti-CD4-APC eFluor 780 (eBiosciences), anti-11b/Mac1-PE, anti-Ly6G/Gr1-PE-Cy7 with or without biotinylated anti-Ter119 and streptavidin-conjugated PE-Texas Red (Molecular Probes, Invitrogen). For progenitor cell analysis, we used the following panel: FITC-conjugated anti-lineage markers (CD4, CD4, CD8, B220, Mac1, Gr1, Ter119), anti-CD16/32-PE, anti-CD34-PacificBlue, anti-Sca1-APC-Cy7, and anti-c-Kit-PerCP-Cy5.5. For HSC analysis, we used the following panel: anti-lineage-FITC, as above, anti-CD48-FITC (eBiosciences), anti-CD41-FITC (eBiosciences), anti-CD150-APC (eBiosciences), anti-Sca1-APC-Cy7, and anti-c-Kit-PerCP-Cy5.5. For single-cell sorting of HSCs in colony assays, we used the same, but without anti-c-Kit-PerCP-Cy5.5 to prevent possible interference at the c-kit receptor tyrosine kinase during subsequent stimulation with SCF. In BrdU/PI experiments, we substituted anti-Sca1-PE-Cy7 and anti-c-Kit-APC-Cy7 antibodies to reduce detector spillover from the PI dye. In Hoechst/Pyronin Y experiments, we used anti-lineage-FITC, as above, anti-CD48-FITC (eBiosciences), anti-CD41-FITC (eBiosciences), anti-CD150-APC (eBiosciences), and anti-Sca1-APC-Cy7.

BrdU HSC Analysis

For bromodeoxyuridine (BrdU) incorporation experiments, mice were injected I.P. using a 27-gauge 0.5” needle for four days with 2 mg of bromodeoxyuridine (Sigma) dissolved at 10 mg/mL in PBS, starting two days after the last dose of polyIC. The day after the last dose, mice were killed and bone marrow cells isolated as described above. Extracted marrow cells were then stained with cell surface protein antibodies directed against HSC cell surface markers and subsequently fixed and permeabilized according to the manufacturer’s protocol (BrdU Flow Kit, BD Biosciences). Briefly, cells were washed with flow buffer, permeabilized by incubation with 100 µL of BD Cytofix/Cytoperm for 15 minutes at room temperature, washed in 1 mL BD Wash Buffer (which contains the permeabilizing reagent saponin), re-fixed in 100 µL BD Cytofix/Cytoperm Plus (or either substituted with 10% DMSO/Cytofix/Cytoperm or freezing at -80°C in 90% FBS/10% DMSO, according to BD’s alternate protocol) for 10 minutes on ice, washed in 1 mL BD Wash Buffer, and re-fixed in Cytofix/Cytoperm for 5 minutes at room temperature. After further washing in 1 mL BD wash buffer, cells were incubated with 30 µg DNAse for one hour at 37°C to expose BrdU binding sites, washed in 1 mL BD Wash Buffer, stained with saturating concentration of anti-BrdU-PacificBlue, and resuspended with 0.125 µg PI in 100 µL flow buffer. Cells were then analyzed by flow cytometry on an LSR II flow cytometer, as described in the section entitled Flow Cytometry.

PY/Hst HSC Analysis

For Pyronin Y(PY)/Hoechst (Hst) experiments, marrow cells were incubated for 30 minutes at 37°C in 1 mL per 10^6 cells of 3.33 μM Hoechst 33342 (Invitrogen) in a solution of 10% FBS/20 mM HEPES/0.1% dextrose/PBS. Without washing, 10 μL of concentrated PY (Sigma) was added (final = 1 μg/mL PY) and the cells incubated for 30 minutes at 37°C, followed by washing and HSC antibody incubation, as above. Cells were continuously stored on ice and immediately processed by flow cytometry.

Marrow Enrichment

In some experiments, including BrdU and PY/Hst-based experiments, low-density bone marrow cells were first enriched by lineage depletion or by c-kit selection using the MACS Lineage Depletion or C-kit Isolation kits (Miltenyi Biotec), according to the manufacturer's protocol. Briefly, bone marrow cells were incubated with biotinylated lineage antibody cocktail or anti-c-kit antibody-conjugated beads in MACS buffer (PBS with 0.5% BSA and EDTA). For lineage depletion, cells were then incubated with streptavidin-conjugated magnetic beads, passed through an LS magnetic column (Miltenyi), and the flow-through collected as lineage depleted cells. For c-kit enrichment, antibody-treated bone marrow cells were passed through an MS magnetic column (Miltenyi), the flow-through discarded, and the adherent cells (i.e. c-kit$^+$) washed from the column and collected. Cells were then washed in PBS or flow buffer for further experiments.

Pcl7CREeGFP Generation

The pcl7eGFP lentiviral construct was a kind gift of Helmut Hannenberg at the Indiana University School of Medicine. This construct contains an *eGFP* cassette and a multiple cloning site (MCS) downstream of the spleen focus-forming virus (SFFV) promoter, which potently drives transcription in eukaryotic cells. The *eGFP* cassette was swapped with a *CREeGFP* fusion construct (Addgene), inserted between the MCS and the BsrgI site at the C-terminus of *eGFP*, using standard molecular cloning techniques.

Virus Generation

To generate virus, NIH 293T cells at 95% confluence on 10 cm dishes were transfected with 5 µg each of pcl7CREeGFP or pcl7eGFP, gag-pol expressing plasmid, and foamyviral envelope plasmid (pCOPE01) in 6 mL Dulbecoo's Modified Eagle Media (DMEM, Gibco/Invitrogen) containing 10% FBS and 0.0075 mg/mL polyethyleneimine (PEI, Sigma). After overnight transfection at 37°C, transfection media was aspirated and replaced with 6 mL fresh DMEM containing 10% FBS, 50 U/mL penicillin, 50 µg/mL streptomycin-streptomycin, 2 mM L-Glutamine, and 10% FBS. After 24 hours, all supernatants were collected, like cultures pooled (to 30 mL maximum), filtered through a 0.22 µm polyethersulfone (PES) membrane Stericup unit (Millipore), and centrifuged at 25-30,000x g at 4°C for 2 hours in a polycarbonate Oak Ridge centrifuge tube (Nalgene). Supernatant was decanted, bleached, and disposed in biohazardous waste, and the viral pellet resuspended in 1 mL IMDM containing 20% FBS.

Virus was stored in aliquots at -80°C and all thawed sample was either immediately used or appropriately discarded. Viral titer (infectious particles per mL) was determined by percent GFP-positivity of serially transduced HT1080 cells, plated at 100,000 per well of a six well plate in 1 mL DMEM/10% FBS. The serial dilution started at 10^{-3} dilution from stock and ended with 10^{-8} dilution. The following equation was used for titer computation:

$$Titer\left(infectious\frac{particles}{mL}\right) = \frac{GFP\ cells\ \% * 100{,}000\ total\ cells}{1\ mL\ media * 10^{-x}\ dilution\ factor}$$

Viral Transduction

A similar protocol was used for the transduction of both low density mononuclear cells and of mature mast cells. Briefly, each well of a six-well plate was coated overnight at 4°C or for four hours at room temperature with 40 µg recombinant fibronectin (Retronectin, Takara) in 1 mL PBS. This fibronectin/PBS solution was aspirated and replaced with 50-100 infectious particles per target cell (mononuclear or mast cell) diluted in a 1 mL solution of IMDM containing 20% FBS, 50 U/mL penicillin, 50 µg/mL streptomycin-streptomycin, 2 mM L-Glutamine supplemented with either 100 ng/mL SCF, 10 ng/mL IL-6, and 10 ng/mL IL-3 (mononuclear cell transduction protocol) or only 10 ng/mL IL-3 (mast cell transduction protocol). After one hour virus/fibronectin incubation at 37°C, 1-2 million target cells were added in a 50 µL volume of the aforementioned transduction media to each 1 mL solution containing well. After 16 to 24 hours of

incubation at 37°C, the cells were harvested, washed in IMDM, and resuspended in appropriate culture media or immediately used for experiments.

Mast Cell Culture

To generate mast cells in tissue culture, non-adherent low-density bone marrow cells (isolated as described above) were passaged twice weekly for 4-6 weeks in mast cell media ("MCM": IMDM containing 10% FBS, 50 U/mL penicillin, 50 µg/mL streptomycin-streptomycin, and 2 mM L-Glutamine supplemented with 7.5 ng/mL interleukin-3 (IL-3, Peprotech)), as described previously (87, 146). Mast cells were identified by characteristic morphology on Giemsa/toluidine blue staining and via flow cytometry with fluorescently conjugated primary antibodies directed against FcεR and c-kit, as described previously (98). After four weeks of culture in IL-3, mast cell purity ($Fc\varepsilon R^{+}$c-kit^{+}) approached 95% of the culture population. Actual culture homogeneity is shown in the results section.

Inhibitors

The Mek-Erk inhibitor PD0325901 was purchased from Cayman Chemicals, dissolved at 10 mM in DMSO, stored in 10 µL aliquots at -20°C, and diluted fresh in cell culture media for each experiment to a concentrated solution of 100 µM (~1000x). Final concentrations are indicated in specific experiments and range from 10 to 800 nM. Final DMSO concentration in PD0325901-based experiments was < 0.008%, and equivalent DMSO concentrations were applied to non-treated samples. Samples were pre-incubated with inhibitor or DMSO only

for about one hour at 37°C prior to stimulation. SB203580 (p38 inhibitor), SP600125 (JNK inhibitor), rapamycin (mTOR inhibitor), FH535 (β-catenin inhibitor) and LY-294002 (PI-3K inhibitor) were all purchased from Sigma, dissolved to a 1000x stock solution in DMSO, and used at indicated concentrations.

Mast Cell Proliferation Assays

Hemcytometer-based: Four- to six-week old mast cells were deprived of IL-3 and FBS for 16 to 20 hours ("overnight") and then resuspended in RPMI or IMDM with 10% FBS, 50 U/mL penicillin, 50 µg/mL streptomycin-streptomycin, and 2 mM L-Glutamine. Cells were standardized to a concentration of 2 to $4x10^5$ cells per mL and then 1 mL placed into each well of a 24-well plate. Cells were stimulated with recombinant murine SCF, at the concentrations indicated in individual experiments. For each condition, duplicate or triplicate wells were assayed. After 72 hours at 37°C, viable mast cells were counted by hemcytometer with trypan blue exclusion using an inverted light microscope. The single value for each individual sample was considered the mean of the replicates. The standard error of the mean was computed from multiple means of biologically-independent samples.

MTT-based: 3-(4,5-dimethylthiazol-2-yl)-2,5-diphenyltetrazolium bromide-(MTT)-based assay of mast cell proliferation/cellularity was performed according to the manufacturer's protocol (Roche). As above, mast cells were deprived of growth factors overnight and then resuspended in RPMI or IMDM with 10% FBS, 50 U/mL penicillin, 50 µg/mL streptomycin-streptomycin, and 2 mM L-Glutamine.

A total of 32,500 cells were plated per well of a 96-well plate in 100 µL final volume (final concentration was $3.25x10^5$ cell per mL). Cells were stimulated with recombinant murine SCF, at concentrations ranging from 10 to 100 ng/mL. For each condition, quadruplicate or sextuplet wells were assayed. At 24, 48, and 72 hours following SCF stimulation at 37°C, MTT reagent (Roche, 10 µL) was added to each well and the cells incubated for four hours at 37°C. Next, solubilization buffer (Roche, 100 µL) was added and the cells incubated overnight at 37°C. Absorbance was read by spectrophotometer at 550 nm wavelength (Molecular Devices). Wells containing media only were used as reference/blank, which was averaged and subtracted from all sample values prior to analysis. Data were acquired with SoftMax Pro software (Molecular Devices). The mean value of all replicates for a sample was considered the single value for an individual sample. Using these single values for biologically-independent samples, the standard error of the mean was computed.

3H-Thymidine-based: Mast cells were deprived of growth factors overnight and then resuspended in IMDM with 50 U/mL penicillin, 50 µg/mL streptomycin-streptomycin, and 2 mM L-Glutamine. A total of 50,000 cells were plated per well of a 96-well plate in 100 µL final volume (final concentration was $5.0x10^5$ cell per mL). Between four and six replicates of each condition were typically assayed. Cells were pre-treated one hour with the indicated concentrations of PD0325901 or vehicle alone and subsequently stimulated with 10% FBS and 80 ng/mL SCF supplemented with 1 µCi ^{3}H-thymidine. In some experiments, 1 µCi ^{3}H-thymidine was added 16 hours after SCF/FBS stimulation. For experiments with multiple

time points, identical plates were established for each condition, and plates were placed at -20°C to stop proliferation at the indicated time point. After the conclusion of the experiment, all plates were thawed and assayed at the same time. Measurement of ^{3}H-thymidine incorporation was performed with a Beckman-Coulter scintillation counter. Given high inter-well variability secondary to imprecision in the high-throughput scintillation counter, the highest and lowest values among replicates were eliminated, in an unbiased manner, and the remaining values used to compute a mean value. In all cases, standard errors of the mean are presented only if multiple mean values from biologically-independent samples were obtained.

Mast Cell Cycle Analysis

Four- to six-week old mast cells were deprived of IL-3 and FBS overnight and then resuspended in IMDM with 0.5%-1.0% BSA, 50 U/mL penicillin, 50 µg/mL streptomycin-streptomycin, and 2 mM L-Glutamine. Cells were standardized to a concentration of $2.25x10^{6}$ cells per mL and then 4 mL placed in 15 mL conical Falcon tubes. Some samples were pre-incubated with 100 nM PD0325901. Cells were then stimulated with 80 ng/mL recombinant murine SCF and 10% FBS, aliquoted to 1.6 mL Eppendorf tubes, allowed to grow for 24 hours at 5% CO_2/37°C, then pulsed with 10 µM BrdU for 2 hours. After BrdU pulse, cells were washed with PBS to remove the unincorporated BrdU. Some cultures were then re-treated with 100 nM PD0325901. Cells were then stopped by addition of 100 µL BD Cytofix/Cytoperm solution at three, six, and twelve hours following the BrdU pulse. Cells were washed in 1 mL flow buffer and stored at -

80°C in 300 µL 90% FBS/10% DMSO. After thawing, the BD BrdU Flow protocol was followed, starting with the five minute re-fixation in 100 µL BD Cytofix/Cytoperm, as described above. In this experiment APC-conjugated BrdU antibody (instead of PacificBlue-conjugated) was used to detect BrdU incorporation, and 20 µL 7-AAD solution was used to detect nuclear content. Samples were analyzed with a FACSCalibur flow cytometer equipped with blue and red lasers.

Mast Cell Survival Assay

Four- to six-week old mast cells were deprived of IL-3 and FBS overnight and then resuspended in RPMI or IMDM with 0.5%-1.0% BSA, 50 U/mL penicillin, 50 µg/mL streptomycin-streptomycin, and 2 mM L-Glutamine. Cells were standardized to a concentration of $2x10^5$ cells per mL and then 1 mL placed into each well of a 24-well plate. Cells were stimulated with recombinant murine SCF (without FBS), at the concentrations indicated in individual experiments. For each condition, duplicate or triplicate wells were assayed. After 72 hours at 37°C, viable mast cells were counted by hemcytometer on light microscopy, with trypan blue exclusion. The single value for each individual sample was considered the mean of the replicates. The standard error of the mean was computed from multiple means of biologically-independent samples.

Deconvolution Microscopy

Four- to six-week old mast cells were deprived of IL-3 and FBS overnight. In some experiments, mast cells were deprived of only IL-3 overnight (i.e.

cytokine-deprived). The cells were then resuspended in RPMI or IMDM with 0.5%-1.0% BSA or with 10% FBS, as indicated, 50 U/mL penicillin, 50 µg/mL streptomycin-streptomycin, and 2 mM L-Glutamine. Cells were standardized to a concentration of $2.5x10^6$ cells per mL, pre-incubated with PD0325901, where indicated, and stimulated with 80 ng/mL recombinant murine SCF and/or with 10% FBS at 5% CO_2/37°C. Cells were aliquoted to 1.6 mL Eppendorf tubes and the stimulated terminated by addition of 4% paraformaldehyde for 15 minutes at room temperature. After, fixation, cells were resuspended in 1 mL PBS. Approximately 200,000 cells were then loaded in PBS onto a cytospin funnel mounted to a glass slide and spun for 10 minutes at 800 g. Following cytospin, fixed cells were extracted by washing in 0.3% Triton-X, blocked in 5% FBS, incubated with primary antibody in 0.1% BSA/PBS overnight at 4°C, washed three times in PBS, and subsequently incubated for one hour at room temperature with fluorophore-conjugated anti-mouse or anti-rabbit antibodies (Molecular Probes, Invitrogen). After washing, one drop of a DAPI mounting solution (Molecular Probes, Invitrogen) was applied and a cover slip sealed over the samples using lacquer. Data were acquired on a DeltaVision deconvolving microscopy system (Applied Precision) and analyzed with ImageJ. Typical controls included cells incubated with secondary (fluorophore-conjugated) antibody but not primary antibody.

Cytokine Array

To screen for cytokines potently induced to secretion by SCF-stimulation, we performed a qualitative assessment using an immunoblot-based array

(Mouse Cytokine Array Panel A, R&D Systems). Six-week old mast cells were deprived of IL-3 and FBS overnight and then resuspended in RPMI with 0.5% BSA, 50 U/mL penicillin, 50 µg/mL streptomycin-streptomycin, and 2 mM L-Glutamine. Cells were standardized to a concentration of $2.5x10^6$ cells per mL and then 2 mL per condition placed in 15 mL Falcon tubes. Cells were then stimulated with 50 ng/mL SCF for six hours at 5% CO_2/37°C, and centrifuged. The supernatant was then harvested and stored at -20°C. After thawing, the cytokine array experiment was performed on the mast cell supernatants according to the manufacturer's protocol. Briefly, array membranes, which are pre-coated with antibodies to 40 known mouse cytokines and growth factor, were blocked in 2 mL Array Buffer 6, washed, and then incubated with 1.5 mL mast cell supernatant treated with Array Buffer 4, Array Buffer 5, and 15 µL Detection Antibody Cocktail. After overnight incubation at 4°C with gentle rocking, membranes were washed and then incubated with streptavidin-conjugated horseradish peroxidase (streptavidin-HRP). Following washes, conjugated enzyme was detected by enhanced chemiluminescence (ECL, Amersham, GE Healthcare). Signal density was measured using NIH free software (ImageJ). Background intensity was averaged and subtracted from all sample values. Supernatants from non-stimulated mast cells served as control.

Multiplex Assay

Five-week old mast cells were deprived of IL-3 and FBS overnight and then resuspended in IMDM with 1.0% BSA, 50 U/mL penicillin, 50 µg/mL streptomycin-streptomycin, and 2 mM L-Glutamine. Cells were standardized to a

concentration of $2.5x10^6$ cells per mL and then 200 µL placed into each well of a 96-well round bottom plate. Cells were pre-incubated with inhibitors, as indicated, and then stimulated with recombinant murine SCF, at the concentrations indicated. After 6 hours at 37°C, the 96-well plate was centrifuged for 10 minutes at 800g, and the supernatant carefully transferred to a new 96-well plate and stored at -80°C. Cytokines and growth factors were assayed with multiplex simultaneous quantification of ten fluorescent antibody capture beads directed against M-CSF, TNF-α, MCP-1, MIP-1α, MIP-1β, G-CSF, GM-CSF, IL-10, IL-13, IL-6. These cytokines were selected based on preliminary screening experiments using the cytokine array detection kit (see above).The multiplex assay was performed according to the manufacturer's protocol (Millipore Milliplex). Briefly, 25 µL of mast cell supernatant was incubated with analyte antibody capture beads, washed three times with provided buffer, incubated with secondary antibody containing streptavidin-PE, washed three times, suspended in 100 µL sheath fluid (i.e. saline), and analyzed on a Luminex 200 cytometer with StarStation software (Luminex). Standard curves were computed using a cubic spline fit, according to the manufacturer's instruction.

Western Blotting

Sample isolation: Four- to six-week old mast cells were deprived of IL-3 and FBS overnight. In some experiments, mast cells were deprived of only IL-3 overnight (i.e. cytokine-deprived). The cells were then resuspended in RPMI or IMDM with 0.5%-1.0% BSA or with 10% FBS, as indicated, 50 U/mL penicillin, 50 µg/mL streptomycin-streptomycin, and 2 mM L-Glutamine. Cells were

standardized to a concentration of $2.5x10^6$ cells per mL and pre-incubated, as indicated, with PD0325901 or with vehicle alone. Each sample was stimulated with the indicated concentration of SCF and then one to 1.5 mL of cells aliquoted to individual 1.6 mL Eppendorf tubes for each time point following stimulation. At the indicated time point, tubes were placed on ice and immediately centrifuged for 3 minutes at 1200g at 4°C. After carefully aspirating the supernatant, SDS-PAGE buffer containing β-mercaptoethanol was added at a final concentration of 1 µL buffer per 5,000-20,000 cells, depending on the experiment. Cells in SDS-PAGE were then sonicated and clarified by centrifugation. In some experiments, protein lysis buffer (ProteoJet, Fermentas, ThermoFisher) supplemented with Complete Mini Protease Inhibitor Cocktail (Roche), sodium fluoride, and sodium orthovananate was used instead of SDS-PAGE buffer for initial isolation, followed by clarification of supernatant, quantification of protein by the bicinchoninic acid method (BCA, Thermo Scientific), standardization, and suspension in SDS-PAGE buffer. After sample standardization, equivalent quantities were loaded into a 4-12% Bis-Tris gel (Invitrogen) and electrophoresed. Electrophoresed samples were transferred to PVDF membrane for immunoblotting.

Immunoblotting protocol: PVDF membranes were blocked for more than 24 hours in 5% non-fat milk/0.01% NaN_3/PBS. Samples were then incubated with antibodies in 5% non-fat milk in PBS overnight with gentle rocking. Following three to six washes in 0.1% Tween-20/PBS, membranes were incubated for one hour with mouse or rabbit anti-Fc antibody conjugated to streptavidin (GE Healthcare) diluted 1:5000 in 0.5-2% non-fat milk in PBS. Following three to six

more washes, HRP enzyme was detected with ECL or SuperSignal West Dura chemiluminescent kit (ThermoScientific), according to the manufacturers' protocols. Signal density was measured using NIH free software (ImageJ).

Quantification of Mast Cells In Vivo

Following previously described protocols (98, 147), WT BoyJ mice which had been reconstituted with WT, *E1-KO*, and *E2-KO* hematopoietic stem cells for approximately one year were given an infusion of SCF or vehicle (PBS) via micro-osmotic pumps (Alzet). Pumps were placed subcutaneously at the mid-flank. The micro-osmotic pumps released SCF or vehicle at a rate of 0.5 µL an hour over the course of seven days. After killing the mice, approximately one to two cm sections of skin were excised, fixed in phosphate buffered 10% formalin, embedded in paraffin, and section at 10 micron. Sections were then stained with toluidine blue to identify mast cells. Cells were quantified by counting 2-mm^2 sections.

PD0325901 Treatment of Plexiform Neurofibroma Model

The *Nf1*$^{flox/-}$; *PeriostinCre*$^{+}$ tumor model was used to assess in vivo efficacy of PD0325901 treatment in modulating the hematopoietic inflammation associated with plexiform neurofibroma development. Five tumor model mice with PET-CT-verified plexiform neurofibromas were fed with drug by oral gavage every day for six weeks. The dose was 12.5 mg/kg PD0325901 in a solution of 0.5% methylcellulose/0.2% Tween-80 in water at a concentration of 12.5 mg/mL. A typical dose comprised 200 µL of solution. After the six-week treatment, all

mice were killed and assessed by histology of the dorsal root ganglia, as described previously (24).

Statistics

All statistical analyses were performed with GraphPad Prism 5.0. One- or two-way ANOVA was performed, as appropriate, with Bonferroni post-hoc corrections. For two variable comparisons, unpaired two-tailed student's t tests were used. All tests, number of biologically-independent replicates, and significance levels are found within the figure legends.

RESULTS

Erk and Hematopoiesis

To test the consequence of *Erk* disruption in hematopoietic stem and progenitor cells, we employed two primary methods. First, we performed functional and descriptive studies of the bone marrow cells harvested from mice disrupted for *Erk1*, *Erk2*, and *Erk1/2*. Second, we transplanted *Erk* mutant hematopoietic stem cells in a competitive fashion into lethally-irradiated WT host mice, waited for complete hematopoietic reconstitution, induced Cre expression, and performed long-term hematopoietic studies in vivo.

Inducible deletion of *Erk1*/2 in the bone marrow.

We intercrossed *Erk1* knockout mice with conditional knockout ("floxed") *Erk2* mice (104), generating $Erk1^{-/-}Erk2^{flox/flox}$ animals. We bred these $Erk1^{-/-}Erk2^{flox/flox}$ mice with mice bearing the *Mx1Cre* transgene, an inducible construct expressing in all marrow cells, including but not limited to hematopoietic stem and progenitor cells (Figure 3a) (143, 144, 148). We analyzed four genotypes: $Erk2^{flox/flox}$ (WT), $Erk1^{-/-}Erk2^{flox/flox}$ *(E1-KO),* $Erk2^{flox/flox}Mx1Cre^{+}$ *(E2-KO),* and $Erk1^{-/-}Erk2^{flox/flox}Mx1Cre^{+}$ *(DKO)* (Figure 3a-b). After moderate polyIC dosing, *E2-KO* mice had efficient *Erk2* deletion, but putative *DKO* mice required extended doses (20-25 μg/g body weight, seven doses) to achieve low/undetectable Erk2 levels (Figure 3c). Moreover, *DKO* primary mutants succumbed to various complications during or within six weeks of Cre induction, suggesting a critical requirement for one Erk isoform in hematopoietic and/or non-hematopoietic tissues. Particularly, we found that $Mx1Cre^{+}$ potently drives $Erk2^{flox/flox}$ excision in

hepatic tissue, precluding our ability to eliminate the possibility that liver toxicity induced lethality in non-transplanted animals.

Of note, we administered the same weight-based polyIC regimen to all mice, regardless of genotype, throughout the following studies. We also performed experiments at varying times after the last dose of polyIC, although typically within one to five days after, as indicated in individual experiments. The imminent death and hematopoietic gene excision instability of the *DKO* animals prevented us from waiting longer. To circumvent these complications, we performed our paramount hematopoietic studies in long-term transplanted animals, as discussed later.

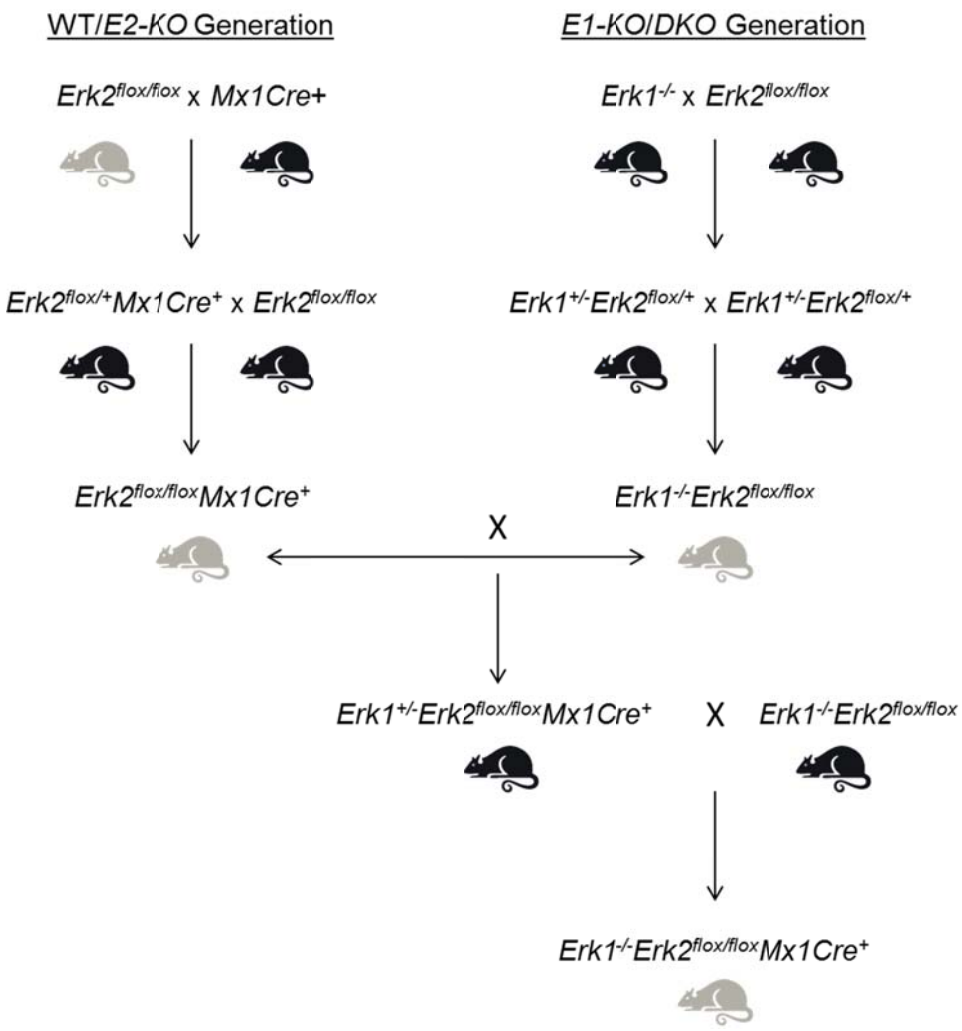
WT/E2-KO Generation
E1-KO/DKO Generation
Erk2flox/flox x Mx1Cre+
Erk1-/- x Erk2flox/flox
Erk2flox/+Mx1Cre+ x Erk2flox/flox
Erk1+/-Erk2flox/+ x Erk1+/-Erk2flox/+
Erk2flox/floxMx1Cre+
Erk1-/-Erk2flox/flox
X
Erk1+/-Erk2flox/floxMx1Cre+
X
Erk1-/-Erk2flox/flox
Erk1-/-Erk2flox/floxMx1Cre+

Figure 3a

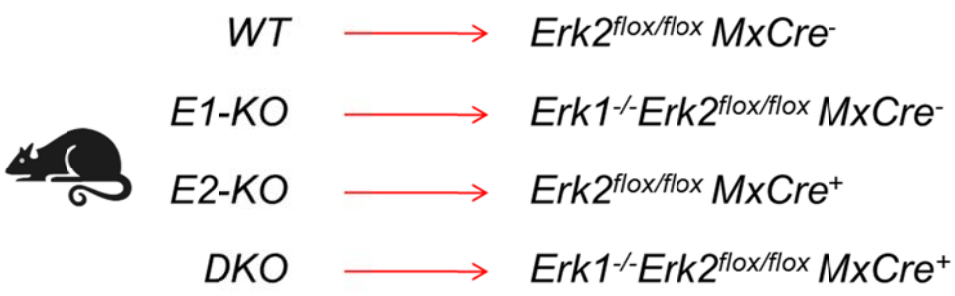
WT
Erk2flox/flox MxCre-
E1-KO
Erk1-/-Erk2flox/flox MxCre-
E2-KO
Erk2flox/flox MxCre+
DKO
Erk1-/-Erk2flox/flox MxCre+

Figure 3b

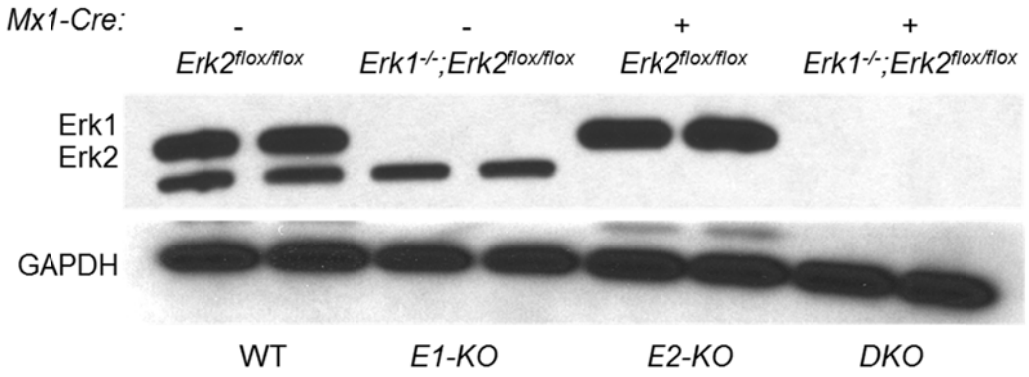
Mx1-Cre:
-
-
+
+
Erk2flox/flox
Erk1-/-;Erk2flox/flox
Erk2flox/flox
Erk1-/-;Erk2flox/flox
Erk1
Erk2
GAPDH
WT
E1-KO
E2-KO
DKO

Figure 3c

Figure 3: Model system and successful *Erk* deletion in the bone marrow. *Erk1*$^{-/-}$ mice, *Erk2*$^{flox/flox}$ mice, and *Mx1Cre*$^{+}$ mice were intercrossed according to the indicated schema (a). Essential breeding (i.e. experimental) genotypes are indicated in gray. After creation of the desired *Erk* mutant and *Mx1Cre*$^{+}$ mice, purebred mice were interbred with their *Mx1Cre*$^{-}$ littermates to generate *Cre*$^{+}$ and *Cre*$^{-}$ littermates for all experiments. *Flox*: flanking loxp sites. For ease, WT, *E1-KO*, *E2-KO*, and *DKO* are the nomenclature used throughout, indicative of the shown genotypes (b). The extended polyIC regimen (20-25 µg/g body weight, 7 doses, every other day) led to undetectable Erk2 in *Mx1Cre*$^{+}$, as detected by anti-Erk1/2 antibody immunoblot of whole bone marrow cells (c).

Loss of myeloid cellularity and granulocytes in *DKO* bone marrow.

Given previous findings from lymphocyte-focused studies of *Erk1/2* disruption in the hematopoietic system (including excision driven by *Mx1Cre* (105)), we did not anticipate a gross myeloid phenotype. However, we found a two to two-and-a-half fold reduction in total marrow cellularity (Figure 4), which corresponded to striking histological changes, including diminished white blood cellularity, vacant marrow spaces, and distended sinuses (Figure 5a). By flow cytometry, we found a prominent reduction in the frequency of the characteristic myeloid $FSC^{hi}SSC^{hi}$ population (Figure 5a, bottom row). Intriguingly, we observed none of these deficiencies in single *KO* animals.

Quantitative analyses of these flow cytometry data revealed diminished myeloid cells as a frequency and as a total quantity of bone marrow cells (Figure 5b). Moreover, while the characteristic lymphocyte $FSC^{low}SSC^{low}$ population was increased as a frequency, adjustment for total cellularity revealed no change overall (Figure 5b, bottom graph). Thus, in these short-term experiments, the redistribution from the characteristic myeloid scatter to lymphoid scatter principally resulted from a loss in total myeloid cells and not from a change in the putative lymphoid population.

To further examine marrow composition, we employed eleven-parameter flow cytometry capable of simultaneously assaying the expression of the major cell surface proteins marking hematopoietic lineage commitment. These markers included Gr1 (granulocytes), Mac1 (monocytes), B220 (B cells), CD3 (T cells), CD4, CD8, and Ter119 (erythroid cells). Accurate identification of mature myeloid

lineages requires initial gating on the non-lymphocyte population, as activated lymphocytes can express some myeloid markers. Accordingly, cells were first gated on $CD3^-$ and $B220^-$ using unbiased histogram analyses based on fluorescence-minus-one controls. In doing so, we found prominent reductions in the frequency and absolute number of strictly-defined mixed marrow granulocytes ($CD3^-B220^-Gr1^+Mac1^+$), as shown qualitatively (Figure 6a) and quantitatively, both as a frequency and as adjusted for the reduced overall cellularity (Figure 6b), recapitulating and extending the initial findings from the abnormal redistribution in forward and side scatters.

To detect a possible unexplained induction of lymphocyte marker expression on myeloid cells in the *DKO* samples, we also examined the absolute frequency of $Gr1^+$ and/or $Mac1^+$ expressing cells (without $CD3^-B220^-$ gating). As above, the frequency of absolute $Gr1^+$ or $Mac1^+$ cells were reduced (Figure 7a, top panel). Moreover, although the frequency of cells expressing lymphocyte markers was increased in *DKO* samples (Figure 7a, bottom panel; Figure 7b, top graph), the total number of $B220^+$ and $CD3^+CD4^+$ cells were diminished while the total number of $CD3^+CD8^+$ cells remained unchanged (Figure 7b, bottom graph).

In the short-term, dual *Erk1/2* disruption in the bone marrow dramatically diminishes total cellularity, which principally results from reduced granulocyte numbers. Moreover, short-term *Erk1/2* disruption moderately reduces B lymphocyte and $CD4^+$ T lymphocyte cellularity. By contrast, single isoform disruption produces no distinct phenotype from WT samples.

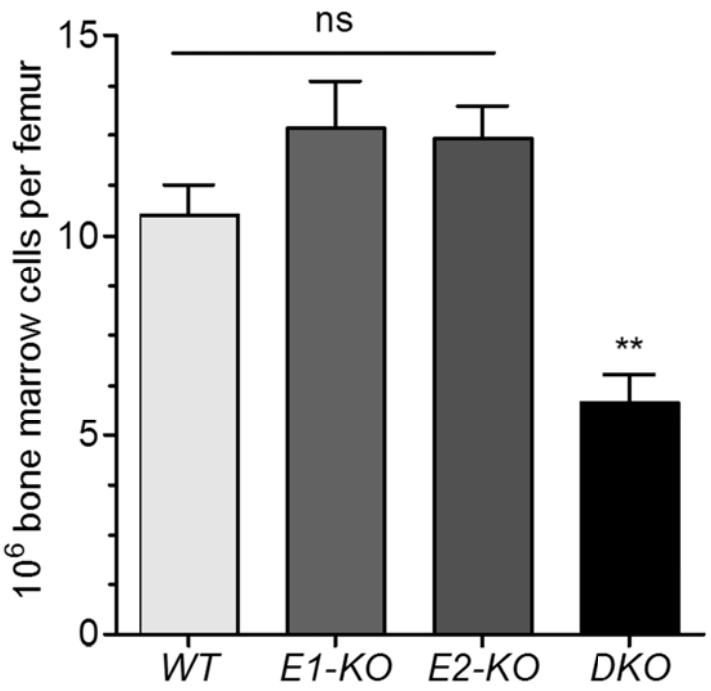

Figure 4

Figure 4: Reduced overall cellularity of *DKO* bone marrow. DKO samples show a 2 to 2.5-fold reduction in total low density bone marrow cellularity, as quantified per femur. E1-KO and E2-KO bone marrow samples show no difference from WT (n = 3-7, **p<0.01 vs. all groups, 1-way ANOVA with Bonferroni correction). Error bars represent the standard error of the mean. These data are representative of at least five separate experiments with multiple biologically independent replicates per experiment.

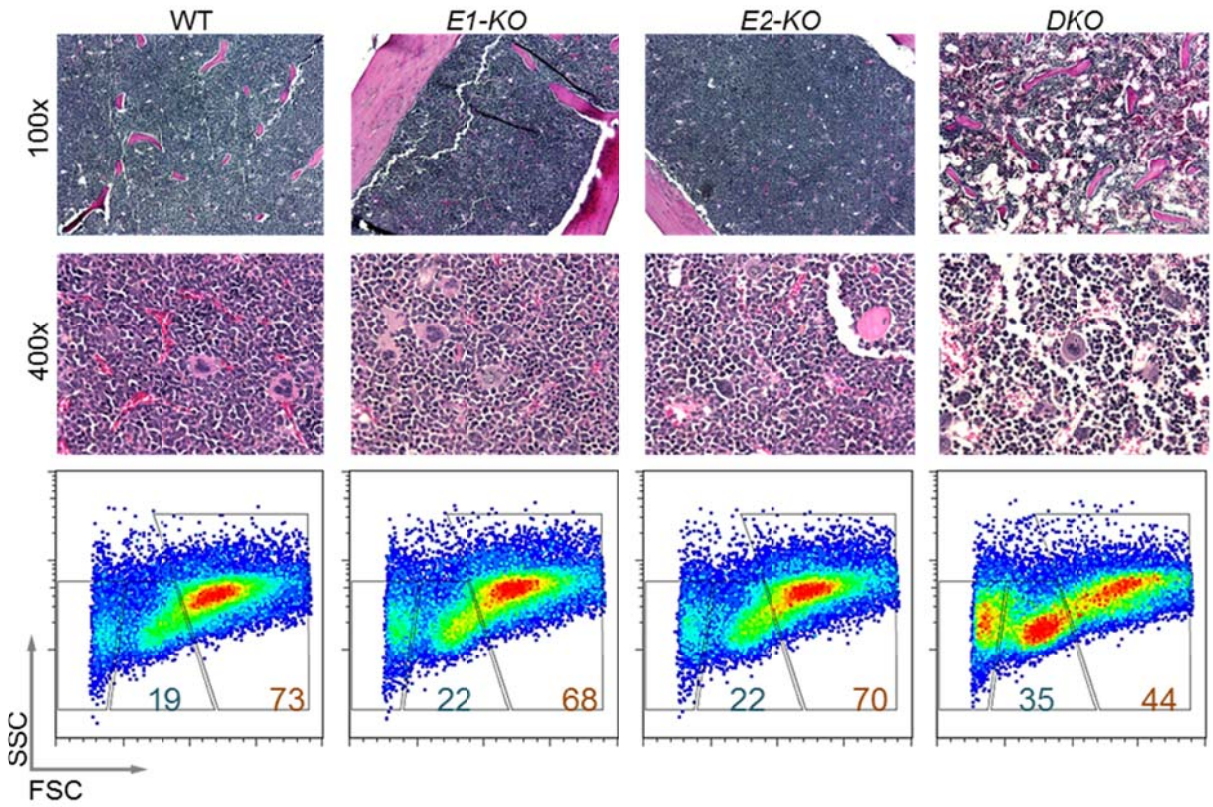

Figure 5a

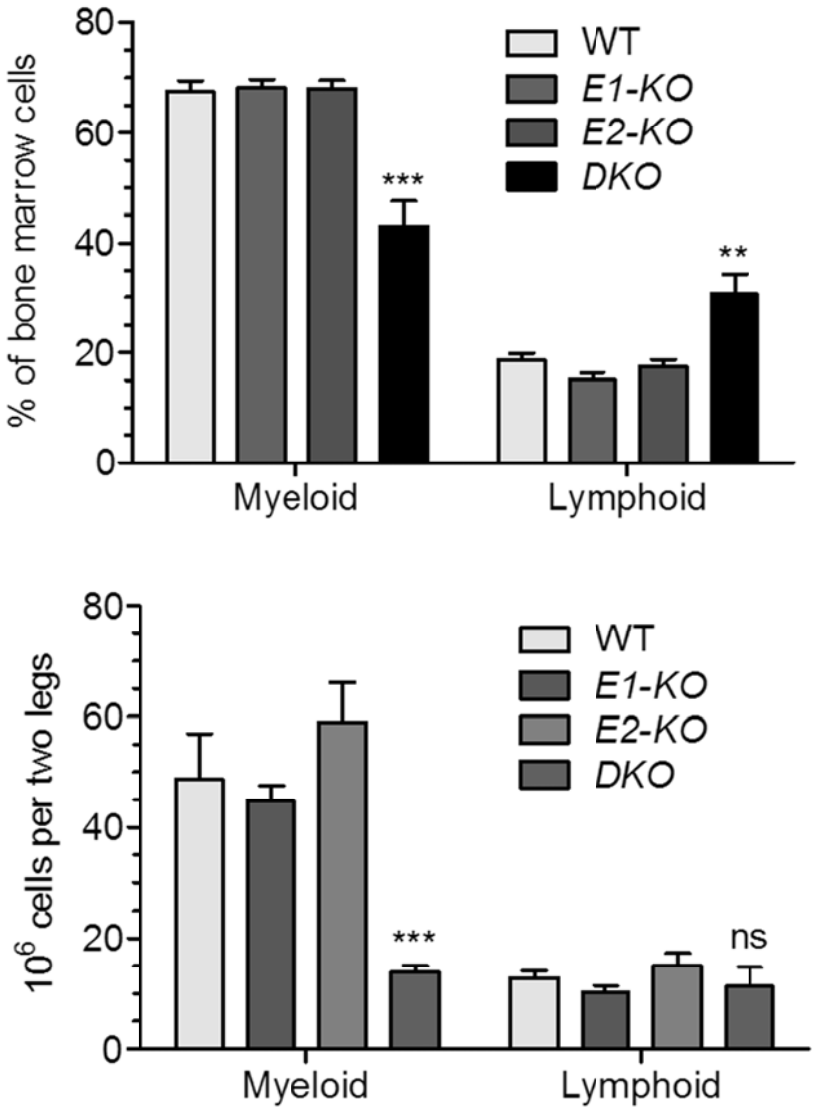
% of bone marrow cells
80
60
40
20
0
WT
E1-KO
E2-KO
DKO
***
**
Myeloid
Lymphoid
10^6 cells per two legs
80
60
40
20
0
WT
E1-KO
E2-KO
DKO
***
ns
Myeloid
Lymphoid

Figure 5b

Figure 5: Histological and flow cytometric analyses show loss of *DKO* bone marrow myeloid cellularity. The reduction in total *DKO* bone marrow cellularity corresponds to vacant marrow spaces and distended sinuses, as shown at 100x and 400x by H&E stain of 8 μM femoral sections on light microscopy (a, top two rows). By flow cytometric analyses, the *DKO* samples show a prominent shift in frequency from the characteristic myeloid $FSC^{hi}SSC^{hi}$ population to a lymphoid $FSC^{low}SSC^{low}$ population (a, bottom row). These data are quantified as a frequency and by total number of cells in the two graphs, revealing a preferential reduction in the absolute number of the characteristic myeloid population (b) (n=3-7, **p<0.01, ***p<0.001, DKO vs. all, 2-way ANOVA with Bonferroni correction). Error bars represent the standard error of the mean. These data are representative of several experiments, each with multiple biologically-independent replicates per experiment.

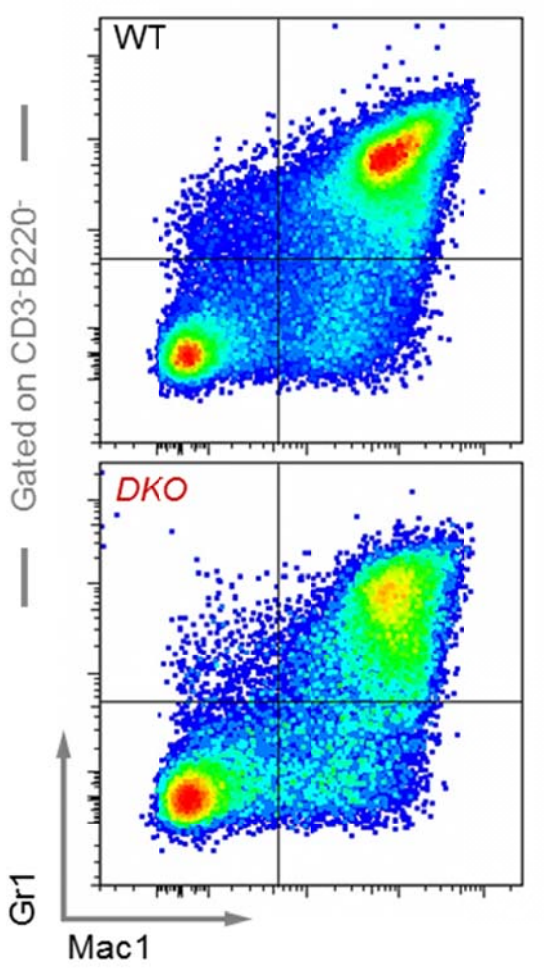

Figure 6a

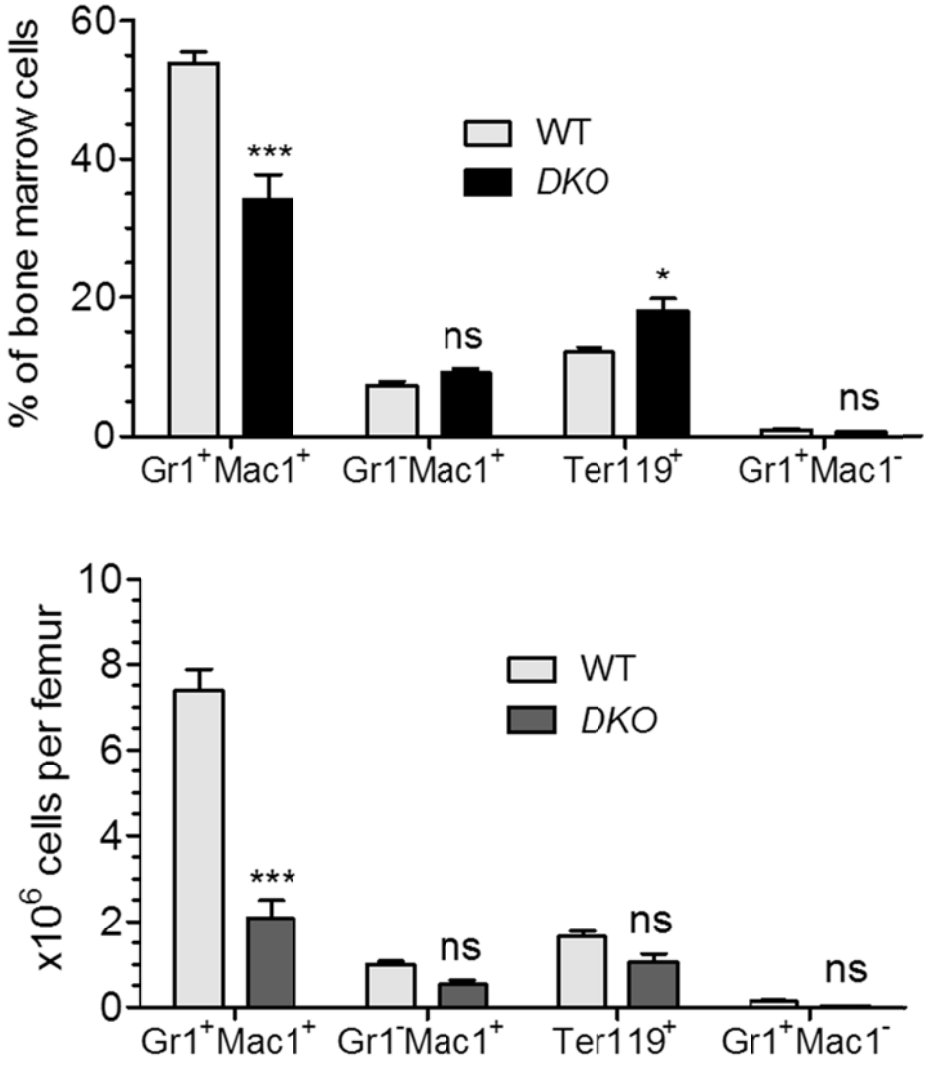
% of bone marrow cells
60
40
20
0
WT
DKO
***
ns
*
ns
Gr1+Mac1+
Gr1-Mac1+
Ter119+
Gr1+Mac1-
x10^6 cells per femur
10
8
6
4
2
0
WT
DKO
***
ns
ns
ns
Gr1+Mac1+
Gr1-Mac1+
Ter119+
Gr1+Mac1-

Figure 6b

Figure 6: Reduction in the frequency and absolute number of *DKO* marrow granulocytes. Bone marrow cells were incubated with saturating concentrations of nine distinct fluorophore-conjugated antibodies directed against cell surface markers of mature hematopoietic lineages. Granulocytes were defined as the $CD3^{-}B220^{-}Gr1^{+}Mac1^{+}$ population, representing mixed marrow mature and immediate precursor granular cells. *DKO* samples showed preferential reduction in this population, as demonstrated by representative flow cytometry (a, gated on $CD3^{-}B220^{-}$) and as quantified by frequency (b, top) and total cellularity (b, bottom, all gated on $CD3^{-}B220^{-}$; for both graphs, n=7, *p<0.05, ***p<0.001, 2-way ANOVA with Bonferroni correction). Error bars represent the standard error of the mean.

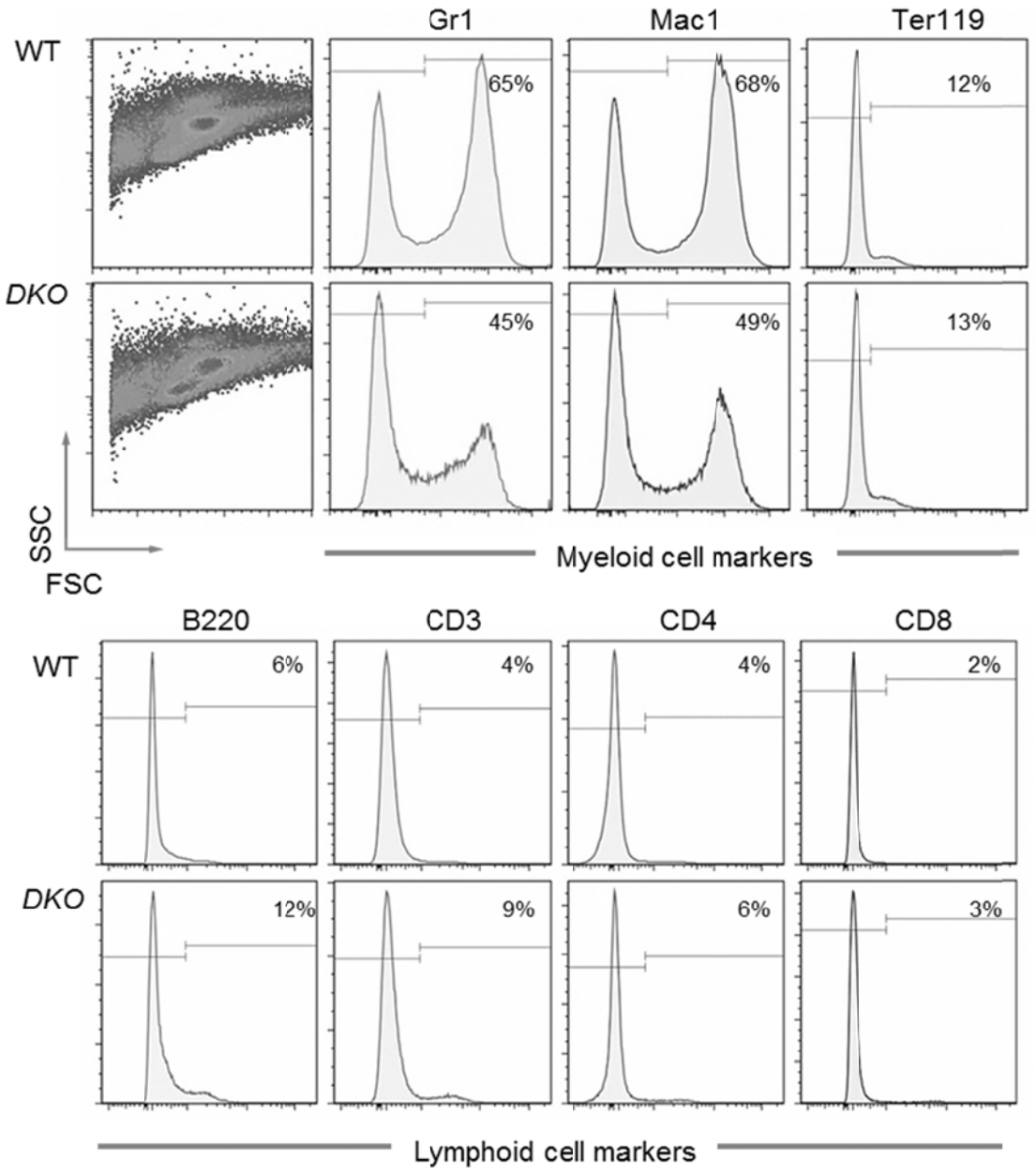
Gr1
Mac1
Ter119
WT
65%
68%
12%
DKO
45%
49%
13%
SSC
FSC
Myeloid cell markers
B220
CD3
CD4
CD8
WT
6%
4%
4%
2%
DKO
12%
9%
6%
3%
Lymphoid cell markers

Figure 7a

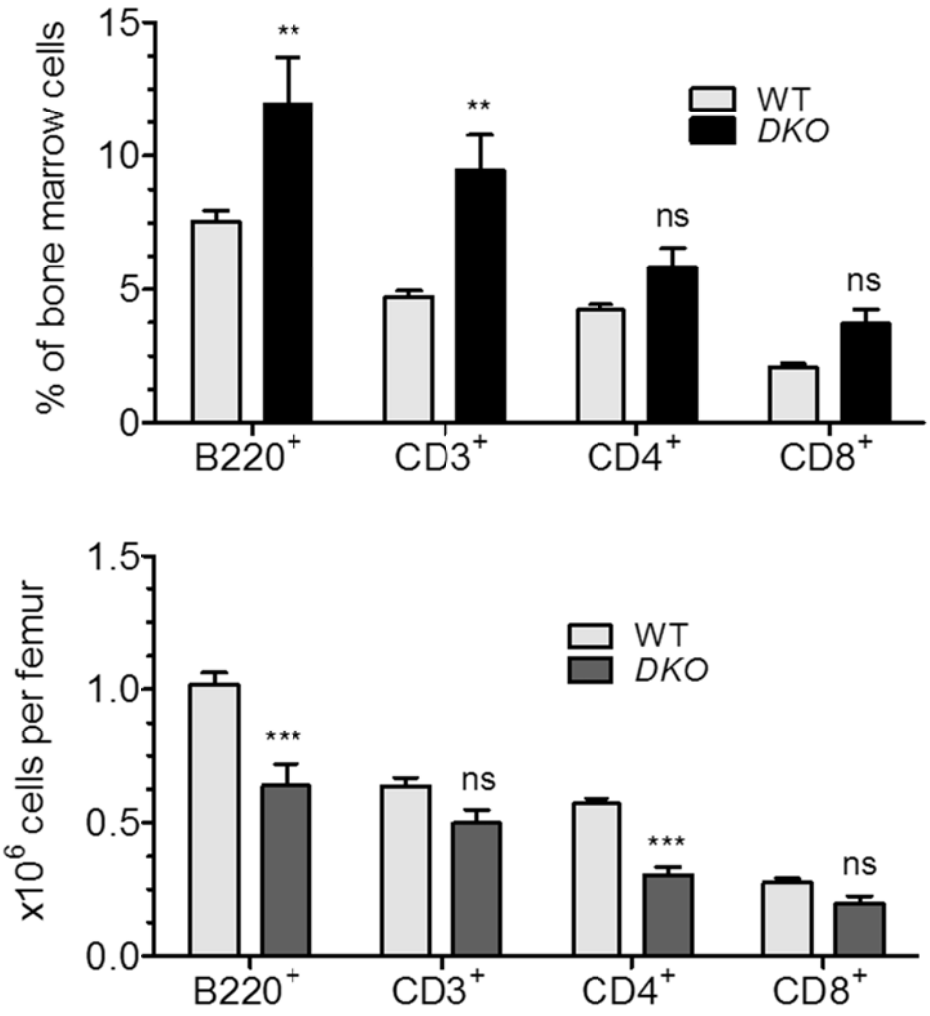
% of bone marrow cells
15
10
5
0
**
**
ns
ns
WT
DKO
B220+
CD3+
CD4+
CD8+
x10^6 cells per femur
1.5
1.0
0.5
0.0
***
ns
***
ns
WT
DKO
B220+
CD3+
CD4+
CD8+

Figure 7b

Figure 7: Absolute reduction in *DKO* myeloid markers and in total lymphoid cellularity. Ungated flow cytometric analyses of individual myeloid markers shows reduced frequency of total *DKO* $Gr1^+$ and $Mac1^+$ marrow cells with no difference in the frequency of $Ter119^+$ cells (a) (representative of n=7). While *DKO* marrow shows increased frequency of cells positive for lymphocyte markers (B220, CD3, CD4, CD8), quantification reveals that total lymphoid cell number is still depressed in *DKO* marrow (b) (n=7, **p<0.01, ***p<0.001, 2-way ANOVA with Bonferroni correction). Error bars represent the standard error of the mean.

Loss of myeloid colony formation in *DKO* bone marrow.

To test if this observed loss of myeloid cellularity arises in myeloid precursors (versus apoptosis or other deficiency in mature monocytes and granulocytes), we performed colony assays on enriched methylcellulose with saturating concentrations of SCF, EPO, IL-3, GM-CSF, M-CSF, and G-CSF. This combination of cytokines induces clonal proliferation and differentiation of progenitors along the entire myelopoietic hierarchy, from the hematopoietic stem cell to late-stage monocytic and granulocytic precursors (see Figure 1).

Through these assays, we found that mixed *DKO* precursors produced few, if any, colonies, with no differences detected among *E1-KO, E2-KO,* and WT specimens (Figure 8). Intriguingly, protein analysis of the few *DKO* colonies revealed an outgrowth of Erk2-expressing progenitors (i.e. *E1-KO* cells), indicating that only those cells escaping Cre-mediated recombination (and, thus, disruption of *Erk2*) can produce colonies. As expected, adjustment of these data for loss of femoral bone marrow cellularity further accentuates the diminution in *DKO* colony production while revealing no difference in single *KO* samples (data not shown). We performed additional colony assays using single and varied combinations of cytokines (e.g. IL-3 alone, IL-3 in combination with SCF, as discussed later), largely recapitulating the results from the mixed myeloid colony assay

To further assess the hematopoietic capacity of *DKO* bone marrow, we performed low and high proliferative potential cell colony forming unit assays (LPPC-CFU and HPPC-CFU). While using similar combinations of myelopoietic

cytokines, these experiments rely on different experimental conditions (e.g. agar-based media, longer growth term, lower oxygen tension) to encourage the clonal outgrowth of hematopoietic stem and multipotent progenitor cells. By definition, these colonies have a large, dense core and can be replated to grow more colonies, thus demonstrating high clonal proliferative potential. In practice, this assay approximates the more primitive hematopoietic potential of an admixed population of bone marrow cells. As part of the assay, colonies resembling mixed myeloid colonies can be observed after one week of growth (LPPC colonies). In these experiments, we found no quantitative differences among WT, *E1-KO*, and *E2-KO* bone marrow cells in their capacity to produce colonies (Figure 9). However, as above, *DKO* bone marrow cells produced few, if any, colonies.

Although we did not detect differences among the *E1-KO*, *E2-KO*, and WT bone marrow cells in our initial analyses, we caution against generalizing that individual Erk isoforms are dispensable for the generation of all myeloid lineages. It should be noted that the aforementioned experiments assess gross myeloid phenotypes using high doses of multiple myeloid- and early progenitor cell-acting cytokines. Indeed, in lineage-specific analyses not depicted here, lower concentrations and combinations of particular myelopoietic cytokines produce intriguing, isoform-dependent results, especially when considering functional aspects of particular lineages. For example, we have found that *E1-KO* bone marrow cells demonstrate a diminished capacity to produce osteoclast colonies in M-CSF/RANKL supplemented methylcellulose, while *E2-KO* bone marrow cells demonstrate no deficiency as compared to WT cells. While these data are

not shown here, they are currently submitted for publication as part of a manuscript. Thus, in the currently discussed hematopoietic investigation, we are assessing only gross hematopoietic and myeloid phenotypes, principally concerning WT versus *DKO* cells. We reiterate, with caution, that specific hematopoietic cell types may depend on variable doses of Erk1 and/or Erk2 for their generation and function, and that subtler functional assays may be required to detect these phenotypes.

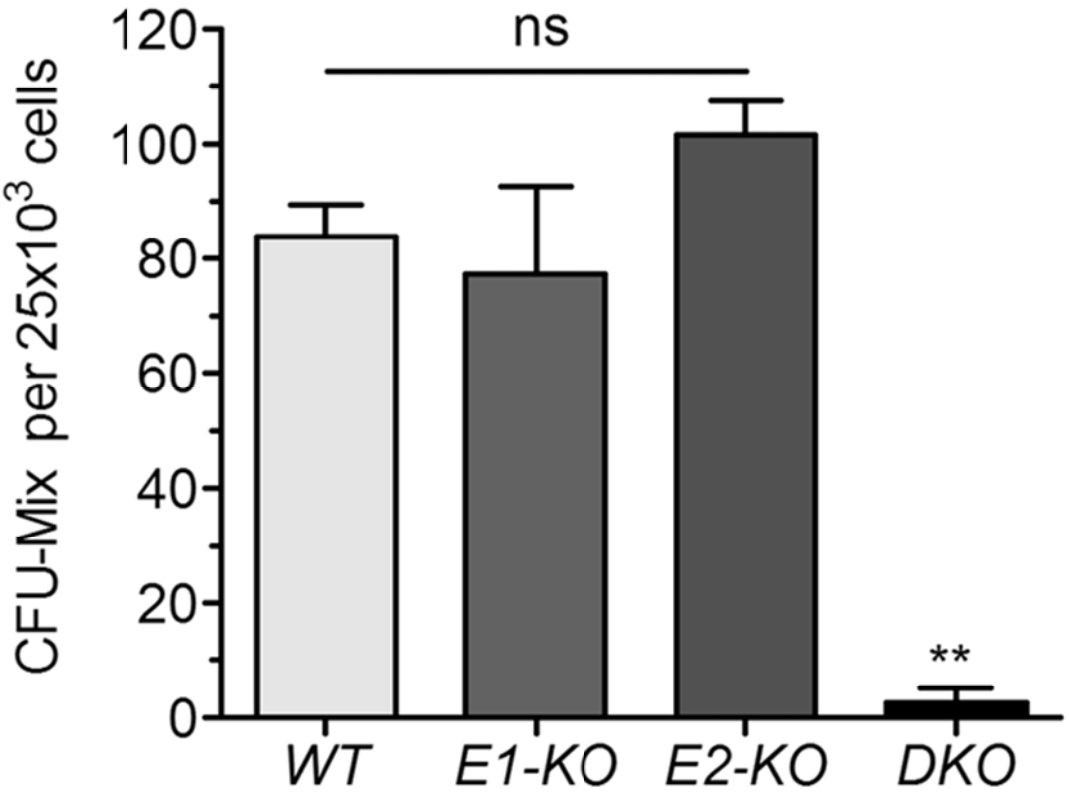
ns
120
100
80
60
40
20
0
CFU-Mix per 25x10^3 cells
**
WT
E1-KO
E2-KO
DKO

Figure 8

Figure 8: Myeloid colony formation requires one isoform of Erk. While WT, *E1-KO*, and *E2-KO* bone marrow cells produced similar numbers of colonies, *DKO* cells formed few mixed myeloid colonies in methylcellulose supplemented with SCF, IL-3, EPO, GM-CSF, G-CSF, and M-CSF (n=3-4, **p<0.01 vs. all, 1-way ANOVA with Bonferroni correction). Error bars represent the standard error of the mean. These results are representative of at least three experiments performed on separate occasions, each with multiple biologically-independent replicates. Each biologically independent sample was plated in triplicate, and the mean number of colonies formed per plate was considered the value for the sample.

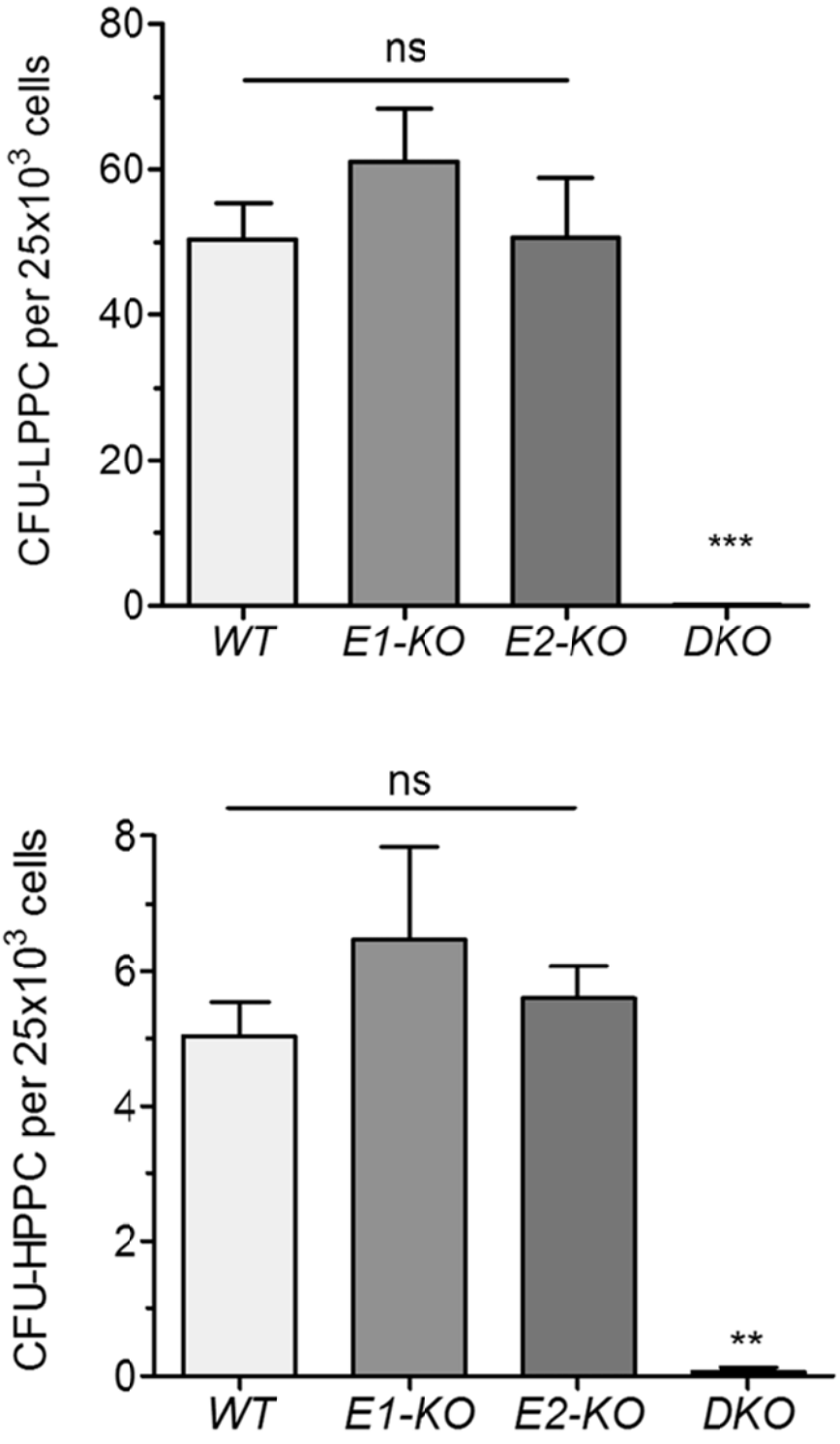
CFU-LPPC per 25x10^3 cells
80
60
40
20
0
ns
***
WT
E1-KO
E2-KO
DKO
CFU-HPPC per 25x10^3 cells
8
6
4
2
0
ns
**
WT
E1-KO
E2-KO
DKO

Figure 9

Figure 9: Hematopoietic stem and multipotent progenitor cell colony formation requires one isoform of Erk. As with the assays on methylcellulose, *DKO* bone marrow cells produced few colonies in LPPC and HPPC assays, experiments which encourage the clonal outgrowth of multipotent progenitor cells. No difference was detected among WT, *E1-KO*, and *E2-KO* bone marrow cells in their capacity to form LPPC/HPPC colonies. Cytokines included SCF, IL-3, EPO, GM-CSF, M-CSF, and G-CSF (n=5-6, **p<0.01 vs. all, 1-way ANOVA with Bonferroni correction). Error bars represent the standard error of the mean. Each biologically-independent sample was plated in triplicate, and the mean number of colonies formed per plate was considered the value for the sample.

Stable chimerism requires one isoform of Erk.

We next performed competitive HSC transplantation experiments to test HSC-autonomous, long-term *Erk* deletion in vivo. Competitive transplantation experiments rely on congenic antigens to distinguish hematopoietic source in transplant recipient mice. In these experiments, we employed mice with congenic CD45, which is a cell surface protein tyrosine phosphatase expressed on all leukocytes (CD45 was originally termed the “leukocyte common antigen). The *Erk* mutants are bred on a C57BL/6 background, which contains two alleles of the CD45.2 variant on all leukocytes. Using flow cytometry, the CD45.2 cell surface marker can easily be distinguished from the CD45.1 variant, which expresses on all leukocytes from WT B6.SJL-PtrcaPep3b/BoyJ (BoyJ) mice. Moreover, the first generation progeny of mice with CD45.2-expressing cells bred with mice with CD45.1-expressing cells (C57 x BoyJ) produce mice containing leukocytes with one allele each of CD45.1 and CD45.2, thus creating “double-positive” CD45.1/2 leukocytes. By flow cytometry, these F1-derived CD45.1/2^{+} cells are also easily distinguished from CD45.1- or CD45.2-expressing cells.

We transplanted CD45.2^{+} *Erk* mutant bone marrow cells mixed with WT BoyJ cells into lethally-irradiated “F1” CD45.1/2^{+} hosts and allowed four months for complete hematopoietic stem cell reconstitution of the recipients (Figure 10). This experiment produced chimeric mice with three sources of hematopoiesis: CD45.2^{+} *Erk* mutant hematopoietic stem cells, CD45.1^{+} WT BoyJ hematopoietic stem cells, and residual (~5-10%) CD45.1/2^{+} WT hematopoietic stem cells. After an assessment of chimerism at the four month time point, we injected all

transplant recipients with six doses, every other day, of polyIC, thus inducing Cre-mediated allele excision in *Mx1Cre*$^{+}$ hematopoietic stem cell recipients. We then drew blood from the tail vein of live animals to progressively track overall peripheral blood chimerism (CD45.1^{+} versus CD45.2^{+} versus CD45.1/2^{+}) as well as the production of mature marrow effector cells by chimeric source.

This experimental design confers multiple advantages. First, based on the lethality of Cre induction in primary *Mx1Cre*$^{+}$*Erk1*$^{-/-}$*Erk2*$^{flox/flox}$ and the failure of *DKO* bone marrow precursor cells to form colonies in tissue culture, we hypothesized that dual *Erk* disruption profoundly abrogates homeostasis in hematopoietic and non-hematopoietic lineages. Competitive transplantation into WT F1 hosts not only isolates the phenotype to hematopoietic stem cells and their progeny, but it also provides a supportive (and easily distinguishable) CD45.1^{+} WT hematopoietic system. Thus, we were able to track mutant- and WT-derived long-term hematopoiesis in vivo. Moreover, we have both external and internal WT controls (i.e. WT BoyJ vs. *Erk2*$^{flox/flox}$ cohort as well as the WT BoyJ component in both cohorts).

Four months post-transplantation, we detected no difference between the *Erk1*$^{+/+}$*Erk2*^{floxflox} and *Erk1*$^{-/-}$*Erk2*$^{flox/flox}$*Mx1Cre*$^{+}$ (essentially *E1-KO*) hematopoietic stem cell recipients (Figure 11). However, one month after Cre induction, *DKO* CD45.2^{+} blood cell chimerism fell to approximately half pre-induction levels. By six months, CD45.2^{+} peripheral blood chimerism in the *DKO* cohort dropped more than seven-fold, with no change detected in the control group.

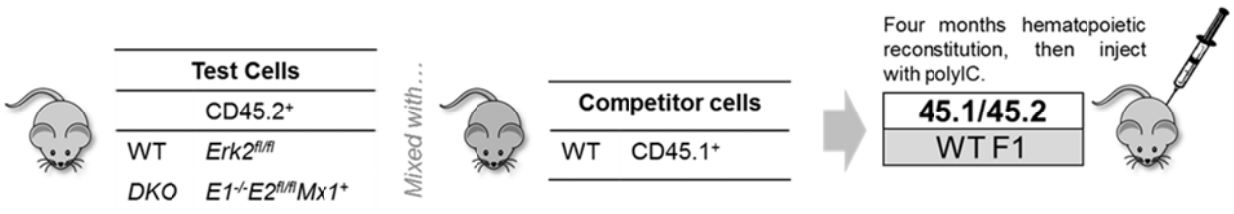
Test Cells
CD45.2+
WT
Erk2fl/fl
DKO
E1-/-E2fl/flMx1+
Mixed with…
Competitor cells
WT
CD45.1+
Four months hematopoietic reconstitution, then inject with polyIC.
45.1/45.2
WT F1

Figure 10

Figure 10: General transplant schema. Lethally-irradiated CD45.1/2^{+} mice were transplanted with mixed CD45.2^{+} (*Erk* mutant) and CD45.1^{+} marrows cells (BoyJ WT). After four months of hematopoietic stem cell reconstitution (to achieve stable chimerism), mice were injected with six doses, every other day, of polyIC to induce Cre-mediated allele excision in *Mx1Cre*$^{+}$ mice. Chimerism and lineage commitment were tracked by flow cytometry of peripheral blood extracted from the tail vein. Various ratios of test to competitor cells were used, as indicated in individual experiments.

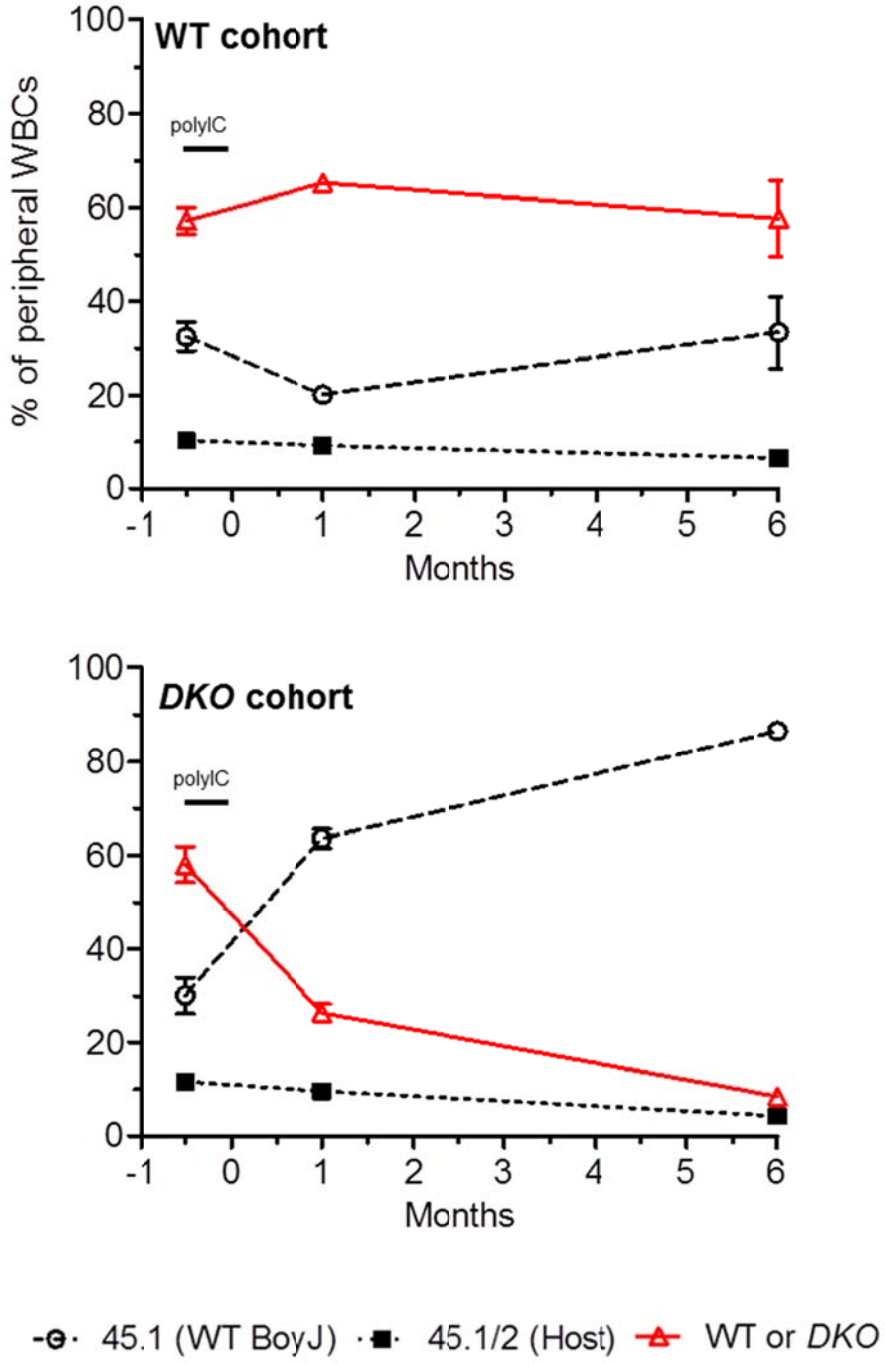
WT cohort
polyIC
% of peripheral WBCs
100
80
60
40
20
0
-1
0
1
2
3
4
5
6
Months
DKO cohort
polyIC
45.1 (WT BoyJ)
45.1/2 (Host)
WT or DKO

Figure 11

Figure 11: Stable hematopoiesis requires Erk. In this experiment, we mixed *Erk* mutant and WT BoyJ bone marrow cells at a 1:1 ratio and transplanted them into lethally-irradiated F1 mice. Four months post-transplant (-0.5 month time point), we detected no difference between the CD45.2^{+} peripheral blood chimerism of the *Erk2*$^{flox/flox}$ and *Mx1Cre*$^{+}$*Erk1*$^{-/-}$*Erk2*$^{flox/flox}$ (i.e. essentially *E1-KO*) cohorts. However, after Cre induction, the WT CD45.2^{+} recipients demonstrated stable chimerism (top) while the *DKO* recipients demonstrated rapid and progressive loss of CD45.2^{+} chimerism (bottom) (n=5 recipients in WT cohort and n=10 in *DKO* cohort. WT vs. *DKO* -0.5 month 45.2^{+}chimerism was not significant by student's t-test or 2-way ANOVA with Bonferroni correction, ***p<0.001 at one and six months, 2-way ANOVA with Bonferroni correction). Error bars represent the standard error of the mean.

We performed additional transplant experiments to further assess the hematopoietic potential of single and dually-disrupted *Erk* mutants. First, we transplanted WT BoyJ mice with *E1-KO* or *E2-KO* marrow, finding that these hematopoietic stem cells successfully engrafted and reconstituted major bone marrow lineages. Approximately six months post-transplant, we extracted 100 μL of peripheral blood from the tail vein of five mice in each cohort. We lysed the red blood cells, added lysis buffer, and standardized protein content using the BCA method protein assay. We then electrophoresed equivalent quantities of these samples, transferred the samples to a PVDF membrane, and probed with anti-Erk1/2 antibody. We detected no Erk1 protein or Erk2 protein in the *E1-KO* and *E2-KO* hematopoietic stem cell recipients, respectively (Figure 12). These data indicate that the loss of a single Erk isoform does not preclude long-term stable hematopoietic reconstitution or peripheral blood production. However, we did detect quantitative differences in lineage commitment between WT, *E1-KO,* and *E2-KO* stem cell recipients, as discussed in detail below.

To further confirm the loss-of-chimerism results in *DKO* HSC recipients, we competitively transplanted mice with *Mx1Cre*$^{+}$*Erk2*$^{fl/fl}$ and WT BoyJ hematopoietic stem cells admixed at a 1:1 ratio into lethally-irradiated F1 mice. This experiment controls for possible loss of chimerism observed in *DKO* cells due to Cre expression (and not due specifically to the disruption of the *Erk2* isoform). Although no previous report has found the *Mx1Cre* construct to disrupt hematopoietic stem cell stability, we aimed to confirm this in the context of *Erk* disruption. Again, we allowed four months of hematopoietic reconstitution before

inducing Cre expression with polyIC. As hypothesized, we detected no loss in chimerism in the *E2-KO* recipients, tracked up to seven months after polyIC injection (Figure 13).

We next transplanted 19 *Erk* mutant cells per 1 BoyJ bone marrow cell into primary and secondary F1 hosts. This experiment tests the hypothesis that a higher "dose" of *DKO* mutant cells could protect against the loss-of-chimerism phenotype. However, after four months of hematopoietic reconstitution and one month following Cre-induction, we found a 14-fold expansion of CD45.1$^+$ WT competitor cells in the peripheral blood of CD45.2$^+$ *DKO* recipients (Figure 14). Because the long-term persistence of lymphocytes can inflate the peripheral blood chimerism relative to the bone marrow chimerism, we also killed one mouse from each transplant cohort to assess marrow-based chimerism. Astonishingly, we found a 35-fold expansion in CD45.1$^+$ WT bone marrow chimerism (from 2% stable peripheral blood chimerism to 76% bone marrow chimerism) in just one month following Cre-induction. Thus, a higher dose of *DKO* HSCs does not protect against the loss-of-chimerism phenotype.

We then transplanted bone marrow cells from these two mice into new cohorts of lethally-irradiated F1 recipients, essentially testing the ability of *DKO* HSCs to engraft and self-renew. Two months following this secondary transplantation, peripheral blood CD45.2$^+$ chimerism had fallen to 8% and, after six months, to 6% (Figure 15). Thus, *DKO* CD45.2 chimerism fell over fifteen-fold from the initial 94% CD45.2$^+$ chimerism in the primary transplant recipients. In sum, these experiments demonstrate that dual *Erk* disruption results in hematopoietic stem

cell instability and failure to self-renew in a cell dose-independent and marrow-autonomous manner.

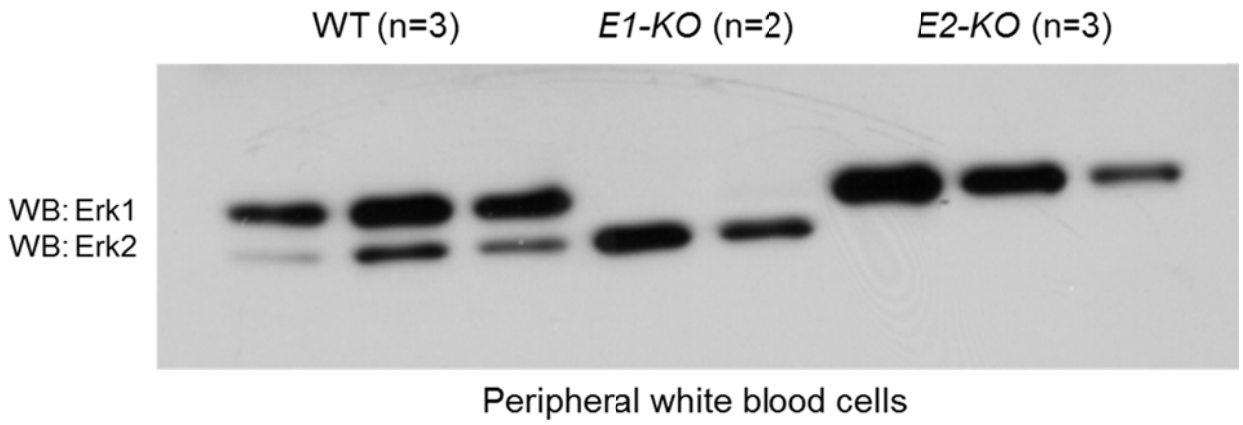
WT (n=3)
E1-KO (n=2)
E2-KO (n=3)
WB: Erk1
WB: Erk2
Peripheral white blood cells

Figure 12

Figure 12: Single *Erk1-KO or Erk2-KO* in HSCs is stable in long-term hematopoietic reconstitution. Cohorts of 9-13 BoyJ WT mice were transplanted with WT (*Erk2*$^{flox/flox}$), *E1-KO*, or *E2-KO* hematopoietic stem cells. After more than six months after transplantation, peripheral blood was extracted from the tail vein, purified in RBC lysis solution, protein extracted, and the protein quantity standardized by BCA protein assay. Equivalent quantities were electrophoresed on SDS-PAGE gel, transferred to a PVDF membrane, and probed for Erk1 and Erk2 protein with Anti-Erk1/2 antibody. Shown are representative immunoblots from a total of five mice assayed in each cohort.

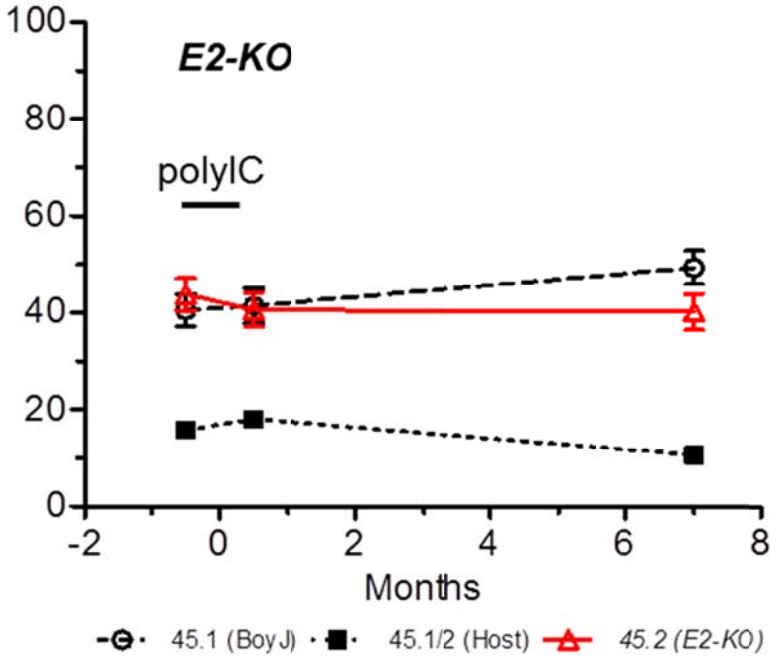
E2-KO
polyIC
100
80
60
40
20
0
-2
0
2
4
6
8
Months
45.1 (BoyJ)
45.1/2 (Host)
45.2 (E2-KO)

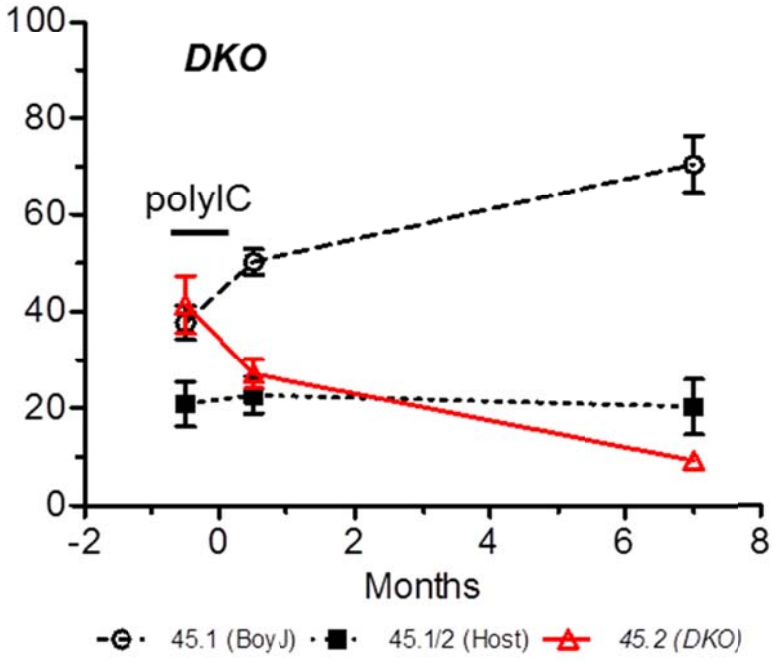
DKO
polyIC
100
80
60
40
20
0
-2
0
2
4
6
8
Months
45.1 (BoyJ)
45.1/2 (Host)
45.2 (DKO)

Figure 13

Figure 13: *Mx1Cre* expression and loss of *Erk2* do not affect HSC stability. Cohorts of WT F1 mice were competitively transplanted with BoyJ and *Erk* mutant marrow (*Mx1Cre*$^{+}$*Erk2*$^{flox/flox}$ and *Mx1Cre*$^{+}$*Erk1*$^{-/-}$*Erk2*$^{flox/flox}$). Cre-expression and *Erk2* allele excision was induced by polyIC injection after four months of hematopoietic reconstitution. Chimeric analyses shows no change in chimerism among *E2-KO* CD45.2+ peripheral white blood cells, as compared to the CD45.1+ fraction and to the *DKO* CD45.2+ white blood cells (n=10, both groups, $p>0.05$ for *E2-KO* %CD45.1^{+} cells versus %CD45.2^{+} cells, all time points; $p<0.01$ and $p<0.001$ for *DKO* %CD45.1^{+} cells versus %CD45.2^{+} cells, 0.5 months and seven months, respectively, two-way ANOVA with Bonferroni correction). Error bars represent the standard error of the mean.

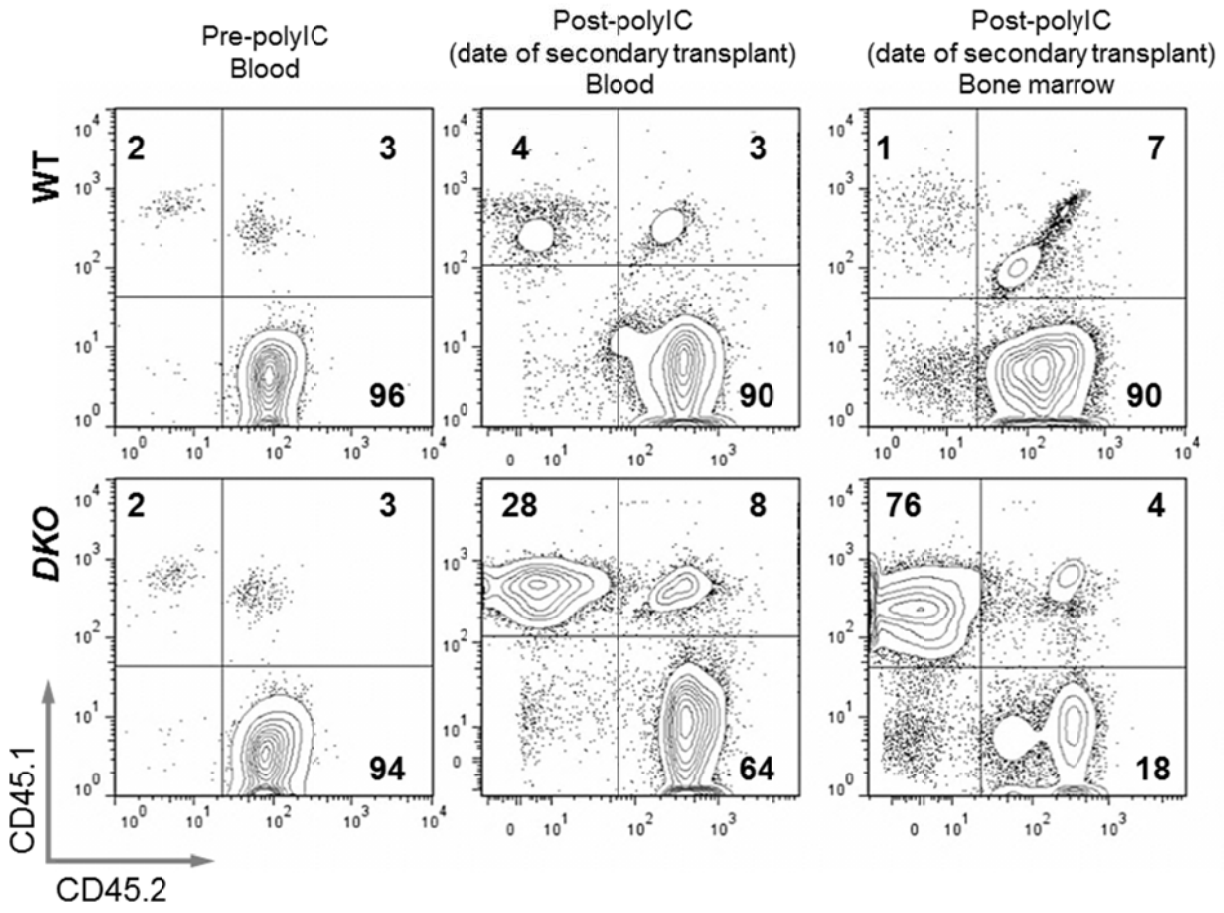
Pre-polyIC
Blood
Post-polyIC
(date of secondary transplant)
Blood
Post-polyIC
(date of secondary transplant)
Bone marrow
WT
DKO
2
3
96
4
3
90
1
7
90
2
3
94
28
8
64
76
4
18
CD45.1
CD45.2

Figure 14

Figure 14: A high-dose of *DKO* HSCs does not protect against the loss-of-chimerism phenotype. Nineteen *Erk* mutant bone marrow cells were transplanted per one WT BoyJ cell, in a total quantity of $2x10^6$ cells per recipient. After four months of hematopoietic reconstitution, peripheral blood chimerism largely reflected this 19-to-1 ratio (i.e. ~95% $CD45.2^+$). Two weeks after initiation of Cre expression, *DKO* $CD45.2^+$ peripheral blood chimerism fell to 64%while the WT $CD45.1^+$ fraction expanded fourteen-fold (second column). In the bone marrow, *DKO* $CD45.2^+$ chimerism fell to 18% two weeks after initiation of Cre expression (third column). First two columns are representative of n=5 in WT group and n=10 in *DKO* group. Third column is from one mouse killed in each cohort (the same mice whose blood chimerism is shown in the second column).

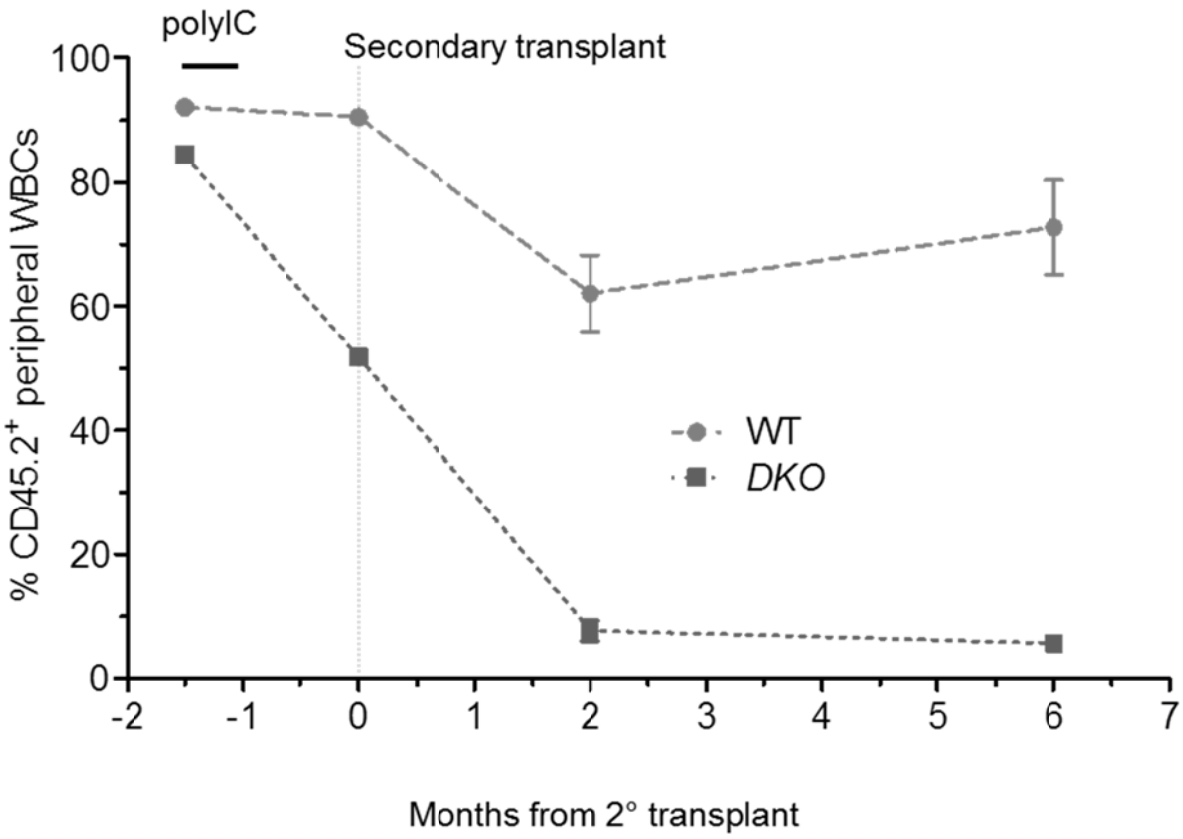
polyIC
Secondary transplant
100
80
60
40
20
0
% CD45.2+ peripheral WBCs
-2
-1
0
1
2
3
4
5
6
7
WT
DKO
Months from 2° transplant

Figure 15

Figure 15: Secondary transplantation of high-dose HSC transplant reveals rapid loss-of-chimerism and failure of *DKO* HSCs to self-renew. Bone marrow cells extracted from the mouse killed in each cohort from the 19-to-1 *Erk*-to-WT transplant experiment were transplanted (in a non-competitive fashion) into new lethally-irradiated F1 recipients. *DKO* recipients showed a profound loss of $CD45.2^+$ chimerism while WT recipients showed only minor losses, a variation typical of secondary transplantation experiments ($n=7\text{-}9$, $p<0.001$, $\%CD45.2^+$, WT versus *DKO* at 2 months and 6 months, 2-way ANOVA with Bonferroni correction).

Erk1/2 disruption rapidly and permanently abolishes myelopoiesis.

Based on our initial findings from primary mutant mice and our long-term transplantation studies, we hypothesized that the rapid loss-of-chimerism in *DKO* transplant recipients resulted from defective myelopoiesis. However, given previous findings of defective lymphopoiesis in dually-disrupted *Erk1/2* mutants (104, 105), the loss-of-chimerism phenomenon could potentially hinge on deficient lymphopoiesis. Indeed, mature lymphocytes ($CD3^+$ and $B220^+$) typically constitute two-thirds or more of the total peripheral blood cellularity of C57/BL6 mice (but less than one-third of the bone marrow cellularity). To assay Erk-dependent lymphopoiesis and myelopoiesis, in a marrow-autonomous manner, we examined tail vein blood of transplanted mice using ten-parameter flow cytometry. This protocol permitted simultaneous and comprehensive assessment of all major mature white blood cell surface markers as well as of the CD45.1 and CD45.2 congenic markers.

By just two weeks following the polyIC regimen, we found few non-lymphocytic ($CD3^-B220^-$) cells in the $CD45.2^+$ fraction of *DKO* HSC recipients (Figure 16a, second column). Within these few non-lymphocytic cells, we further found frequency redistribution away from the expectedly preponderant $CD3^-B220^-Gr1^+Mac1^+$ population, which represents circulating neutrophils (Figure 16a, third column). Although monocyte ($CD3^-B220^-Gr1^-Mac1^+$) frequency distribution in the non-lymphoid *DKO* $CD45.2^+$ fraction approximated the frequency in the non-lymphoid WT $CD45.2^+$ fraction, the absolute frequency of *DKO* monocytes was severely diminished, given the overall reduction in both

DKO chimerism and total non-lymphoid cells. As expected from the loss in non-lymphoid cellularity, we found a reciprocal increase in the frequency distribution of $B220^+$ cells (B cells) and $CD3^+$ cells (T cells), as a percentage of the *DKO* $CD45.2^+$ fraction. By contrast, we found no skewing in the frequency distribution of $CD3^+CD4^+CD8^-$ (CD4 T cells) or $CD3^+CD4^-CD8^+$ (CD8 T cells), as a percentage of the parental $CD3^+$ population (Figure 16a, fourth column).

We employed two strategies to quantify these results. First, we assessed the total lymphopoietic and myelopoietic capacities of $CD45.1^+$ (WT BoyJ) and $CD45.2^+$ (WT or *DKO*) marrow systems. To do so, we computed the overall percentage of each hematopoietic subpopulation (T cells, B cells, neutrophils, and monocytes) in the peripheral blood, separated by chimeric source (Figure 16b). These analyses reveal a near-complete absence of *DKO* $CD45.2^+$-derived circulating monocytes and neutrophils, while additionally demonstrating a compensatory production of myeloid cells from WT BoyJ $CD45.1^+$ marrow. Moreover, these analyses revealed an absolute reduction in circulating *DKO* $CD45.2^+$ B cells, with no change (at this time point) in circulating *DKO* $CD45.2^+$ T cells (Figure 16c).

Secondly, we analyzed potential skewing in lineage commitment, independent of the loss-of-chimerism phenotype. To accomplish this, we computed the ratio of the observed percentage of $CD45.2^+$ cells within each subpopulation to the expected, or overall, percentage of $CD45.2^+$ cells. For example, if overall $CD45.2^+$ chimerism of a mouse is 20%, then we would expect approximately 20% of all circulating neutrophils to be $CD45.2^+$, thus giving a 1.0

ratio for the observed-to-expected ratio. As predicted, WT myeloid populations all had an observed-to-expected $CD45.2^+$ ratio close to 1.0, while *DKO* overall myeloid, monocyte, and neutrophil populations were between ten and twenty-fold lower than the expected 1.0 ratio (Figure 17a). Intriguingly, *DKO* marrow skewed toward circulating $CD3^-B220^-Gr1^+Mac1^-$ cells, an undefined population of unknown significance. However, it should be noted that a prior publication argued that $Mac1^+$ cell maturation may hinge on Mek-Erk signaling (108), suggesting that dual *Erk* disruption inhibits terminal differentiation toward $Mac1^+Gr1^+$ cells. Given the loss of myeloid cells, the lymphoid ratio skewed above 1.0, representing an abnormal persistence of *DKO* lymphoid cells (Figure 17b).

In sum, these data show an absolute loss in the ability of *DKO* HSCs to produce mature monocytes and neutrophils. This myeloid deficiency is independent of the overall loss-in-chimerism phenotype. Finally, lymphocytes appeared to be less rapidly effected by *Erk* disruption than myelocytes, probably correlating with their long lifespans in the periphery.

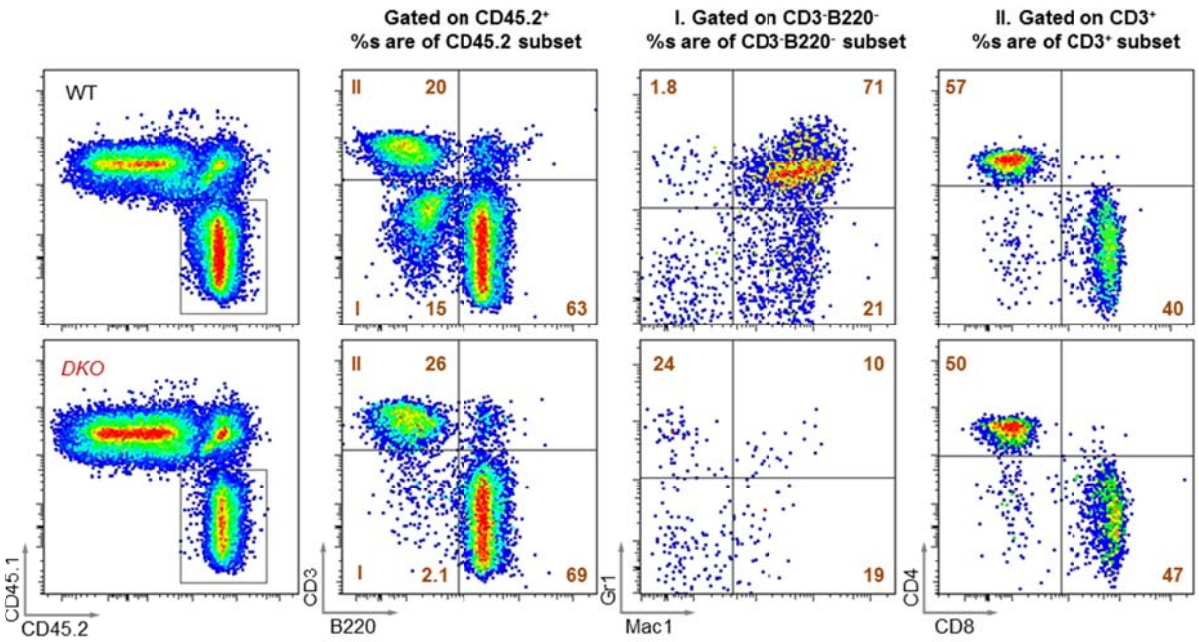
Gated on CD45.2+
%s are of CD45.2 subset
I. Gated on CD3-B220-
%s are of CD3-B220- subset
II. Gated on CD3+
%s are of CD3+ subset
WT
DKO
II
20
I
15
63
II
26
I
2.1
69
1.8
71
21
24
10
19
57
40
50
47
CD45.1
CD45.2
CD3
B220
Gr1
Mac1
CD4
CD8

Figure 16a

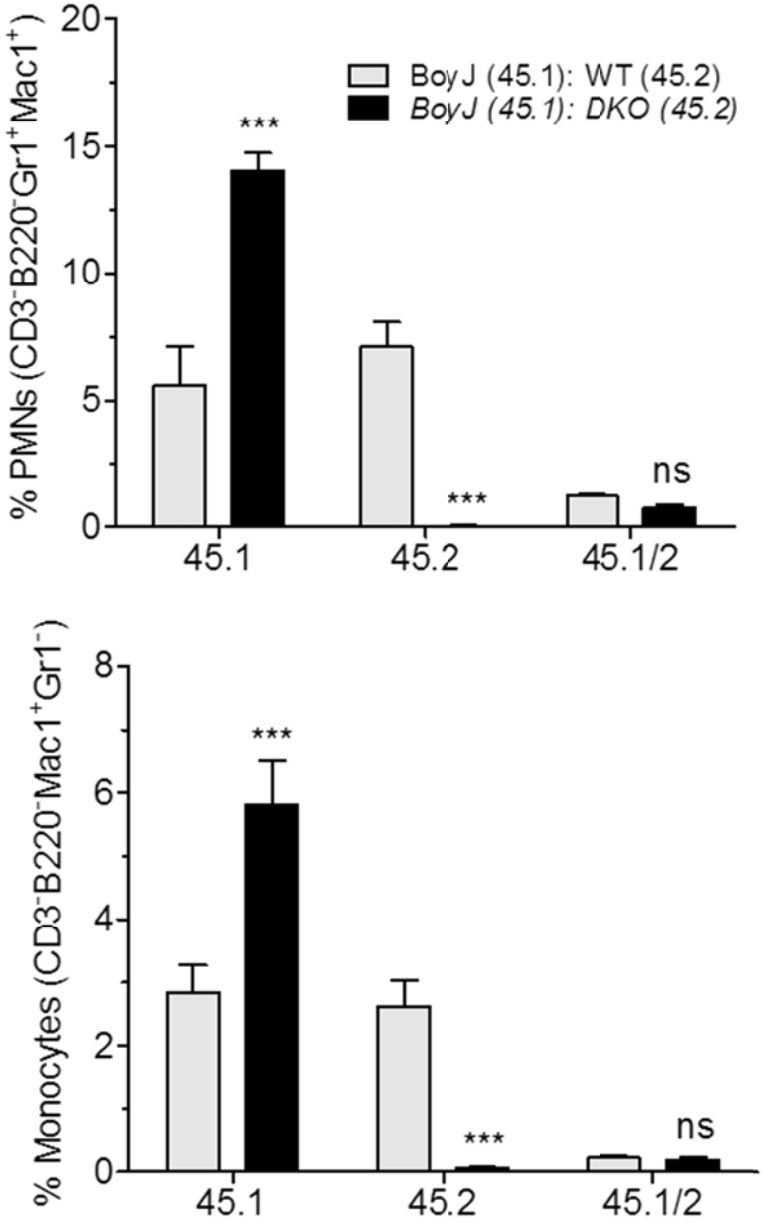
BoyJ (45.1): WT (45.2)
BoyJ (45.1): DKO (45.2)
% PMNs (CD3-B220-Gr1+Mac1+)
20
15
10
5
0
***
***
ns
45.1
45.2
45.1/2
% Monocytes (CD3-B220-Mac1+Gr1-)
8
6
4
2
0
***
***
ns
45.1
45.2
45.1/2

Figure 16b

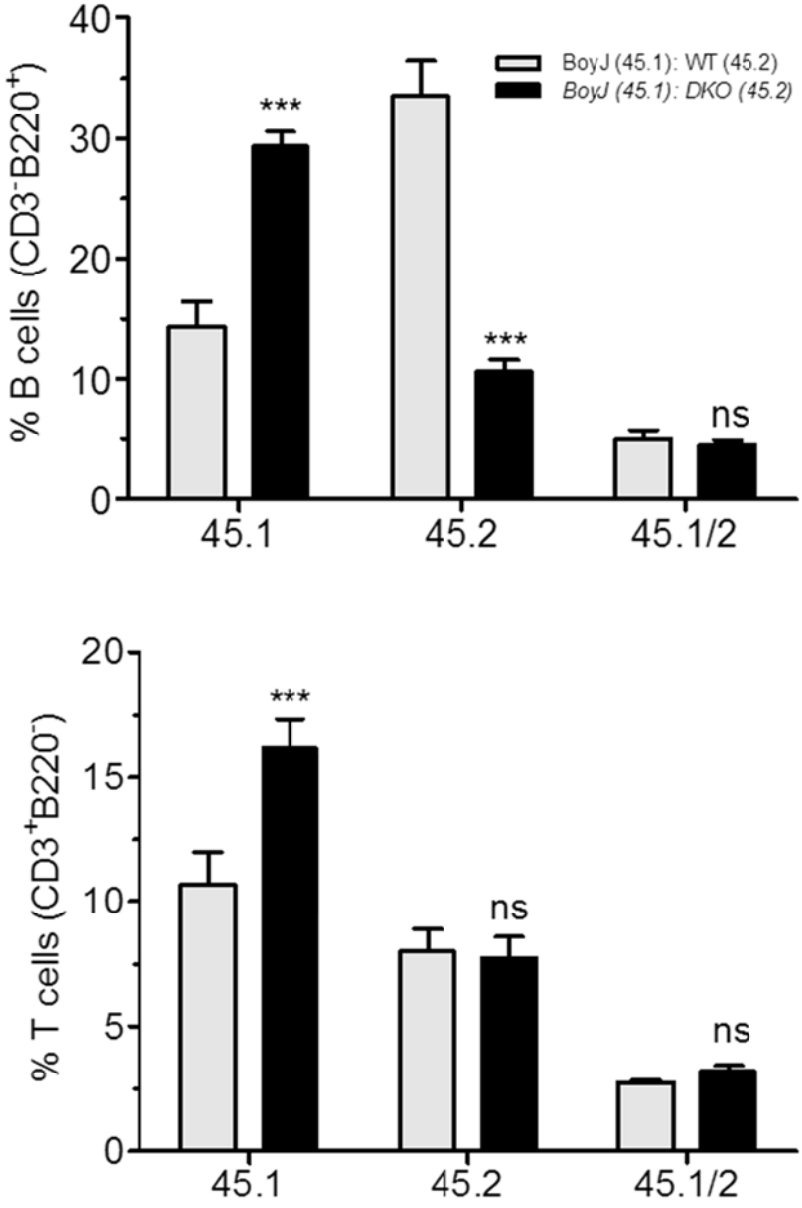
40
30
20
10
0
% B cells (CD3-B220+)
BoyJ (45.1): WT (45.2)
BoyJ (45.1): DKO (45.2)
***
***
ns
45.1
45.2
45.1/2
20
15
10
5
0
% T cells (CD3+B220-)
***
ns
ns
45.1
45.2
45.1/2

Figure 16c

Figure 16: Erk disruption ablates absolute myelopoiesis in a marrow-autonomous manner. Ten-parameter flow cytometric analyses of peripheral blood two months after Cre induction demonstrates ablated *DKO*-derived $CD45.2^+$ circulating granulocytes ($CD3^-B220^-Gr1^+Mac1^+$) and monocytes ($CD3^-B220^-Gr1^-Mac1^+$) (third column) with no distribution change in $CD3^+CD4^+$ or $CD3^+CD8^+$ lymphocytes (second and fourth columns) (percentages are of total $CD45.2^+$ fraction) (a). Quantification of these data, by chimeric source, shows severe reduction in circulating *DKO* $CD45.2^+$ granulocytes, monocytes, and B-cells, with reciprocal compensation from the $CD45.1^+$ WT BoyJ chimeric fraction. In the WT cohort, the granulocyte/monocyte production from $CD45.1^+$ and $CD45.2^+$ HSCs are equivalent (b-c) (n=4 and n=9, WT and *DKO* cohorts, respectively, ***$p<0.001$, 2-way ANOVA with Bonferroni correction). Error bars represent the standard error of the mean.

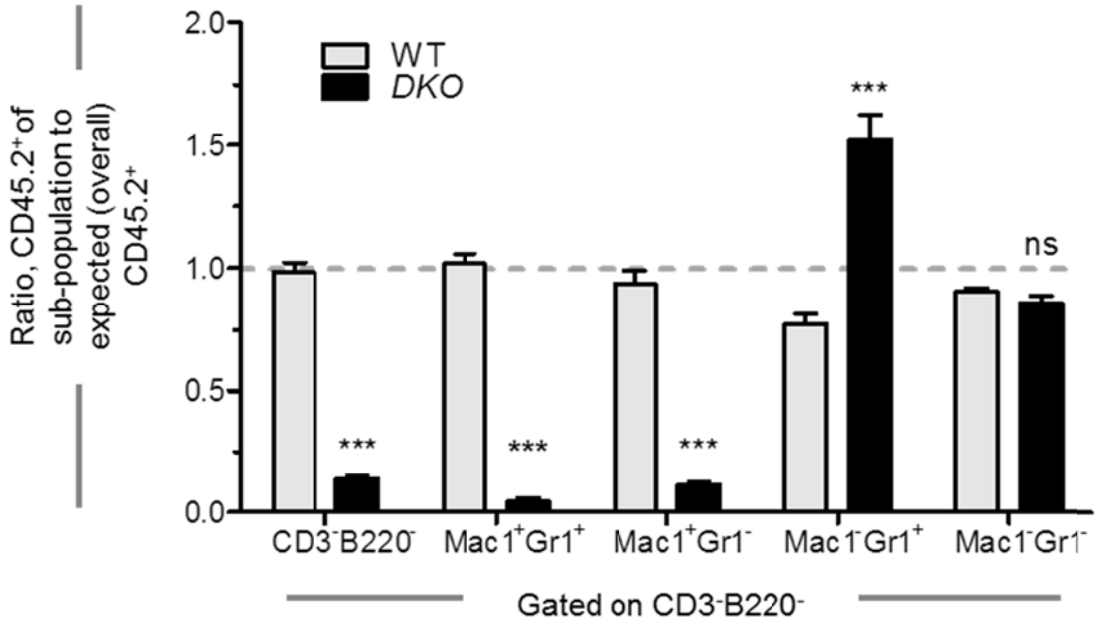
Ratio, CD45.2+ of sub-population to expected (overall) CD45.2+
2.0
1.5
1.0
0.5
0.0
WT
DKO
***
***
***
***
ns
CD3-B220-
Mac1+Gr1+
Mac1+Gr1-
Mac1-Gr1+
Mac1-Gr1-
Gated on CD3-B220-

Figure 17a

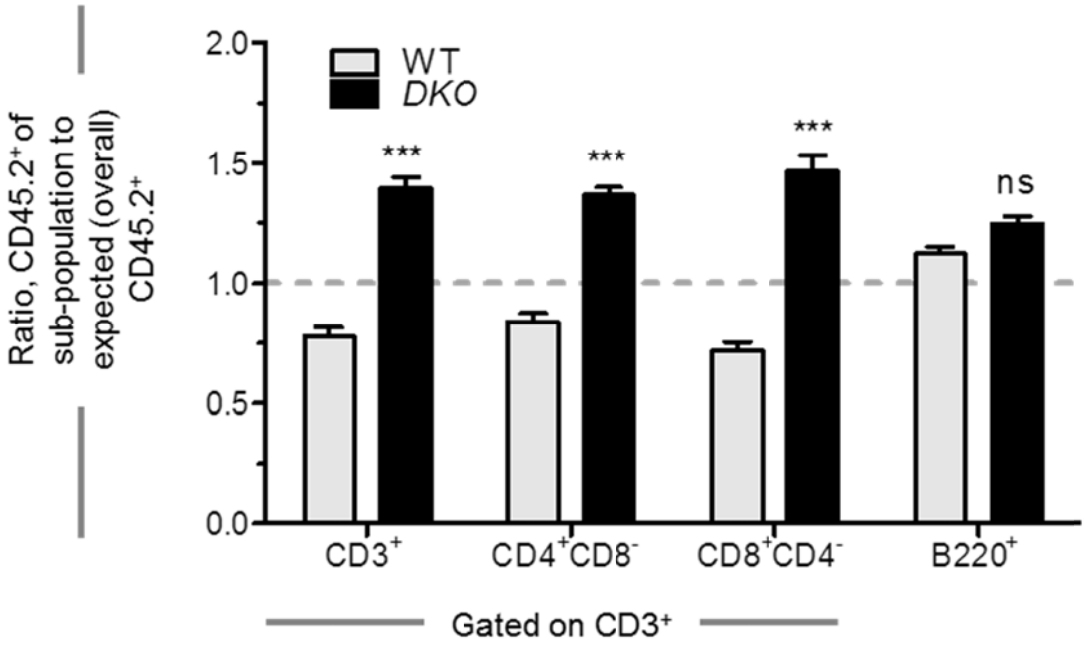
Ratio, CD45.2+ of sub-population to expected (overall) CD45.2+
2.0
1.5
1.0
0.5
0.0
WT
DKO
***
***
***
ns
CD3+
CD4+CD8-
CD8+CD4-
B220+
Gated on CD3+

Figure 17b

Figure 17: *Erk* disruption ablates absolute myelopoiesis in a chimerism-independent manner. Standardizing $CD45.2^+$ % of each lineage to the expected (overall) $CD45.2^+$ % corrects for loss-of-chimerism and reveals potential lineage skewing. The dashed lines indicate the expected 1.0 ratio, whereby a chimerism of x% would be expected to contribute x% of the particular cell population. *DKO* $CD45.2^+$ cells produced far fewer myeloid cells than expected, even when corrected for the loss-of-chimerism in these analyses. Moreover, *DKO* $CD45.2^+$ cells abnormally skewed to undefined $CD3^-B220^-Mac1^-Gr1^+$ cells as well as increased skewing toward lymphocytes (a-b) (n=9 for WT and n=19 for *DKO*, ***p<0.001, 2-way ANOVA with Bonferroni correction). Error bars represent the standard error of the mean.

Erk1/2 disruption abrogates the exponential expansion of hematopoietic progenitor cells.

Based on the striking in vivo myelopoietic consequence of *Erk1/2* disruption, we assessed progenitor cell frequency and quantity in *DKO* bone marrow. Previous studies have demonstrated that hematopoietic stem and progenitor cells undergo an exponential expansion (149). As progenitor cells become more differentiated, their proliferative rate increases, peaking at the level of the common myeloid progenitor (CMP) and granulocyte-macrophage progenitor (GMP). By contrast, the near-terminally differentiated direct granulocytic precursors (e.g. $CD3^-B220^-Gr1^+Mac1^+$ cells) have a much lower proliferative rate, relying on the exponential expansion of precursors – the CMP and GMP – to replenish the rapid egress and turnover of this cell population (150). Table 1 shows the abbreviations, phenotypic definition, and relative proliferative rate of these different populations.

In our analyses of hematopoietic stem and progenitor cell frequency and number, we incubated mononuclear cells with a cocktail of fluorophore-conjugated antibodies directed against cell surface proteins marking mature lineage commitment (lin: CD3, CD4, CD8, B220, Gr1, Mac1, Ter119) as well as distinct fluorophore-conjugated antibodies directed against c-kit, Sca1, CD34, and FcγRII/III. The flow cytometry-based gating strategy for analyzing these progenitor populations, as well as representative data from WT and *DKO* samples, are shown in Figure 18a.

We found striking reductions in the frequency of multipotent progenitors (MPP: $Lin^-Sca1^+c\text{-}Kit^+$), myeloid progenitors (MP: $Lin^-Sca1^-c\text{-}Kit^+$), common myeloid progenitors (CMP: $Lin^-Sca1^-c\text{-}Kit^+CD34^+FcγRII/III^{-/low}$), granulocyte-monocyte progenitors (GMP: $Lin^-Sca1^-c\text{-}Kit^+CD34^+FcγRII/III^+$), and megakaryocyte-erythroid progenitors (MEP: $Lin^-Sca1^-c\text{-}Kit^+CD34^-FcγRII/III^-$) (Figure 18b-c, left/top). Adjusting for the diminished *DKO* cellularity per femur exaggerated these differences (Figure 18b-c, right/bottom), revealing a profound diminution of total myeloid progenitor numbers in *DKO* bone marrow. Dual *Erk* disruption most dramatically impacted the CMP population, which showed a near 20-fold reduction in total number. The total GMP population was the second most affected, showing a six-to-seven-fold reduction compared to WT. Of note, these populations are the direct precursors to granulocytes and monocytes, and they demonstrate the highest proliferative rates among all known hematopoietic populations in the bone marrow. Overall, the total pool of MPs (including MEPs) was reduced approximately six-fold in *DKO* bone marrow.

We next quantified the SLAM-LSK population ($CD150^+Lin^-CD48^-CD41^-Sca1^+c\text{-}Kit$), which represents long-term multi-lineage repopulating HSCs and constitutes about 0.007% of bone marrow cells (151). Intriguingly, in these analyses, we found no difference in HSC frequency between WT and *DKO* bone marrow (Figure 19a-b). These data suggest a linear relationship between HSC loss and overall bone marrow cellularity. Combined with the data of exponential loss in total myeloid progenitor number, these data implicate a proliferative defect at the level of the HSC.

Population		Phenotype definition	Phenotype abbreviation	Proliferative rate
Hematopoietic stem cell	**HSC**	$CD150^{+}Lin^{-}CD48^{-}CD41^{-}Sca1^{+}c\text{-}Kit^{+}$	SLAM-LSK	↑
Multipotent progenitor	**MPP**	$Lin^{-}Sca1^{+}c\text{-}kit^{+}$	LSK	↑↑
Myeloid progenitors	**MP**	$Lin^{-}Sca1^{-}c\text{-}kit^{+}$	LK	↑↑↑
Common myeloid progenitor	**CMP**	$Lin^{-}Sca1^{-}c\text{-}kit^{+}CD34^{+}FcγRII/III^{-/low}$	---	↑↑↑↑
Granulocyte-macrophage progenitor	**GMP**	$Lin^{-}Sca1^{-}c\text{-}kit^{+}CD34^{+}FcγRII/III^{+}$	---	↑↑↑↑
Megakaryocyte-erythroid progenitor	**MEP**	$Lin^{-}Sca1^{-}c\text{-}kit^{+}CD34^{-}FcγRII/III^{-}$	---	↑↑↑
Granulocytes	**G**	$CD3^{-}B220^{-}Gr1^{+}Mac1^{+}$	---	↑
Lineage negative	**Lin^{-}**	$CD3^{-}$, $CD4^{-}$, $CD8^{-}$, B220, $Gr1^{-}$, $Mac1^{-}$, $Ter119^{-}$	Lin^{-}	

Table 1. Phenotypic definitions and relative proliferative rate of hematopoietic stem and progenitor cells.

Table 1. Phenotypic definitions and relative proliferative rate of hematopoietic stem and progenitor cells.

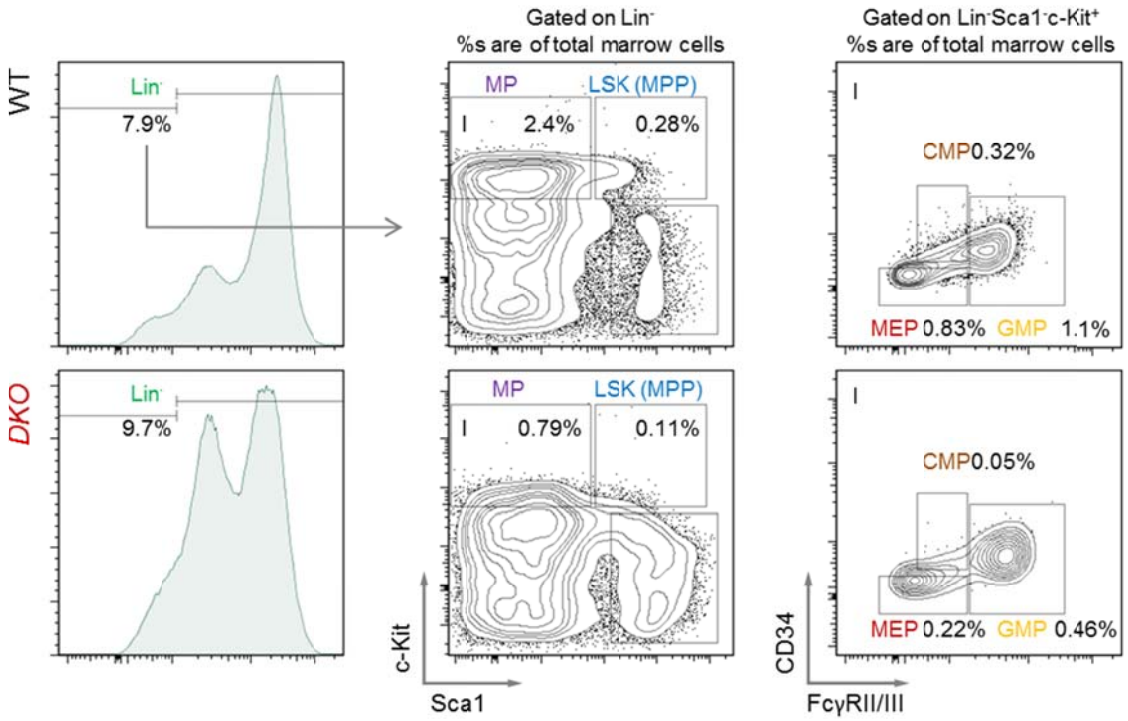
WT
DKO
Lin-
7.9%
Lin-
9.7%
Gated on Lin-
%s are of total marrow cells
MP
LSK (MPP)
2.4%
0.28%
0.79%
0.11%
c-Kit
Sca1
Gated on Lin-Sca1-c-Kit+
%s are of total marrow cells
CMP0.32%
MEP 0.83% GMP 1.1%
CMP0.05%
MEP 0.22% GMP 0.46%
CD34
FcγRII/III

Figure 18a

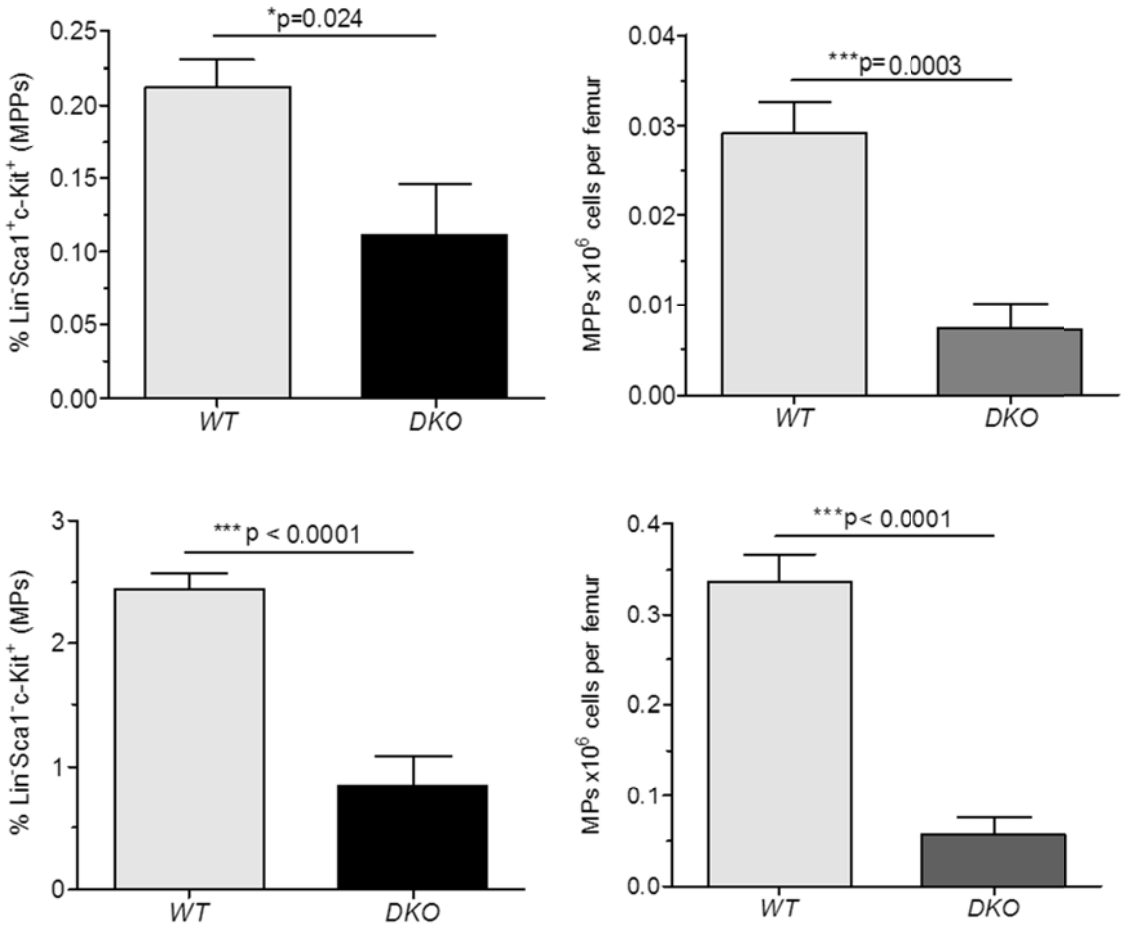
*p=0.024
% Lin-Sca1+c-Kit+ (MPPs)
0.25
0.20
0.15
0.10
0.05
0.00
WT
DKO
***p= 0.0003
MPPs x10^6 cells per femur
0.04
0.03
0.02
0.01
0.00
WT
DKO
*** p < 0.0001
% Lin-Sca1-c-Kit+ (MPs)
3
2
1
0
WT
DKO
***p< 0.0001
MPs x10^6 cells per femur
0.4
0.3
0.2
0.1
0.0
WT
DKO

Figure 18b

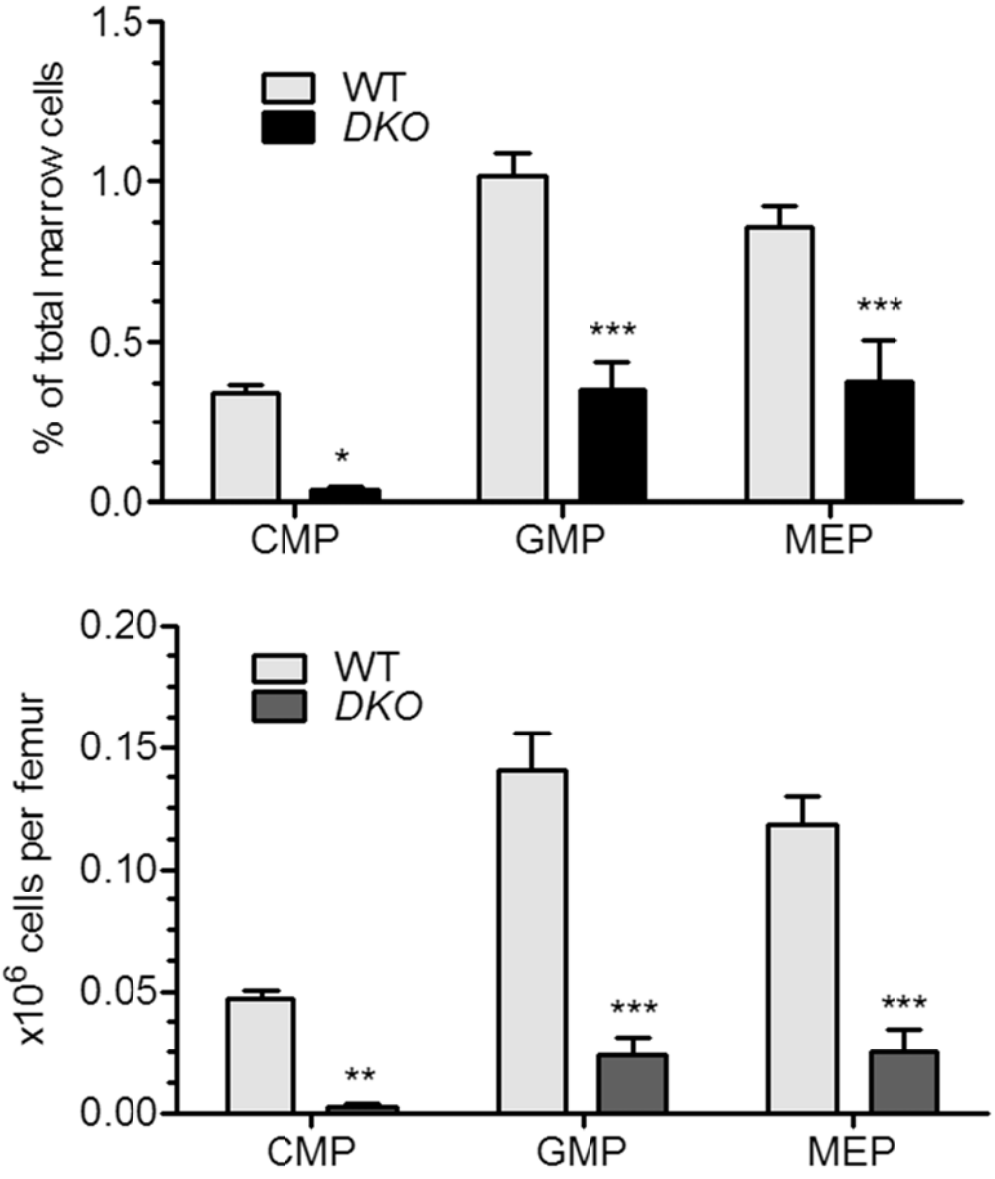
1.5
1.0
0.5
0.0
% of total marrow cells
WT
DKO
*
***
***
CMP
GMP
MEP
0.20
0.15
0.10
0.05
0.00
x10^6 cells per femur
WT
DKO
**
***
***
CMP
GMP
MEP

Figure 18c

Figure 18: *DKO* bone marrow has exponential reduction in myeloid progenitor number. Representative flow pictographs show progressive loss in the frequency of *DKO* multipotent progenitors (MPP, $Lin^{-}Sca1^{+}c\text{-}Kit^{+}$), myeloid progenitors (MP, $Lin^{-}Sca1^{-}c\text{-}kit^{+}$), and common myeloid progenitors (CMP, $Lin^{-}Sca1^{-}c\text{-}Kit^{+}CD34^{+}FcγRII/III^{low}$), as well as deficiencies in the more committed megakaryocyte-erythrocyte progenitors (MEP, $Lin^{-}Sca1^{-}c\text{-}Kit^{+}CD34^{-}FcγRII/III^{-}$) and granulocyte-macrophage progenitors (GMP, $Lin^{-}Sca1^{-}c\text{-}Kit^{+}FcγRII/III^{+}$) (a) Quantitative analyses show diminished frequency in MPPs, MPs, CMPs, MEPs, and GMPs (b-c, left column and top graph), with a profound diminution in the total number of MPs, CMPs, and GMPs (b-c, right column and bottom graph), the bone marrow populations that are the direct precursors of monocytes and granulocytes and that have the highest proliferative rate (n=7, p values derived from unpaired student's t-tests; in the CMP/GMP/MEP graphs, *$p<0.05$, **$p<0.01$, ***$p<0.001$, 2-way ANOVA with Bonferroni correction). Error bars represent the standard error of the mean. Progenitor analyses were performed on two separate occasions, each with multiple biologically-independent samples.

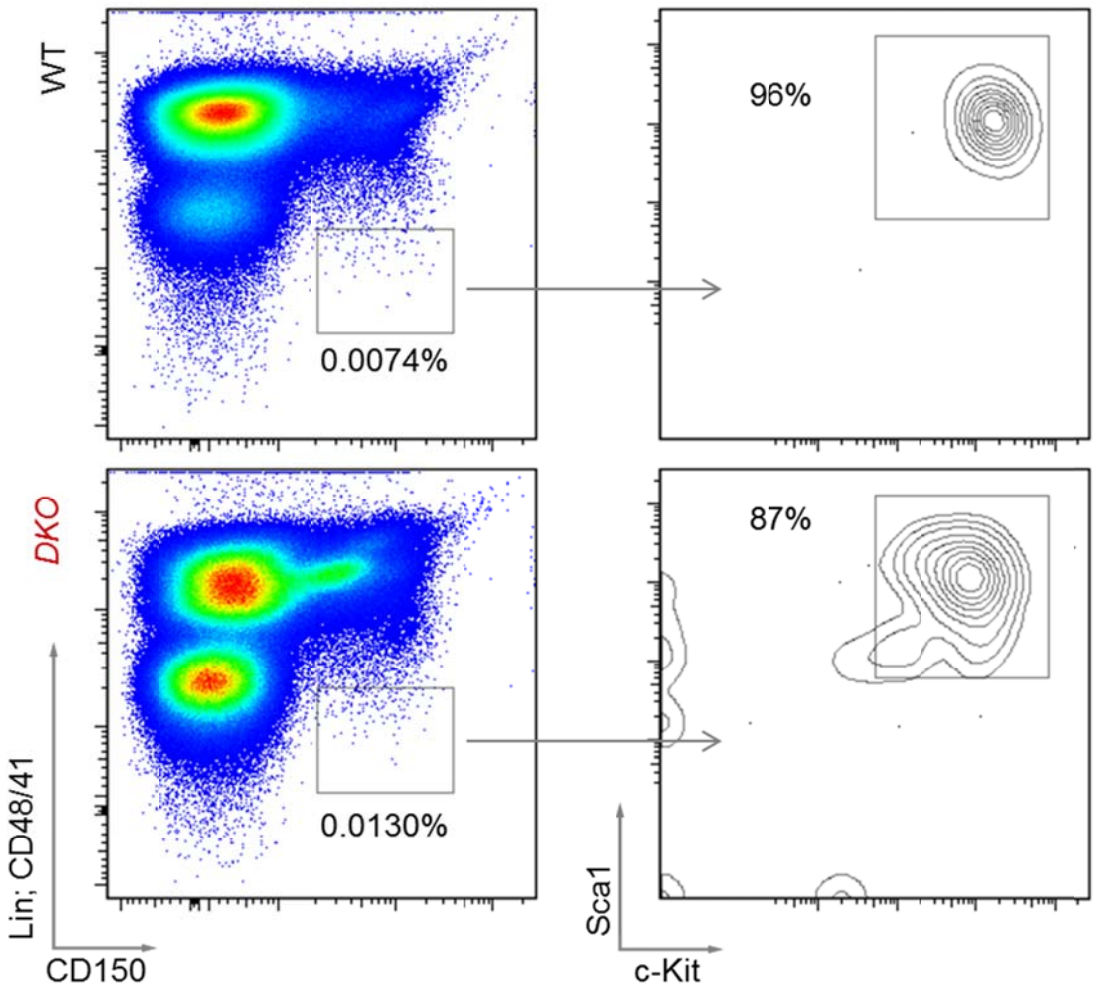

Figure 19a

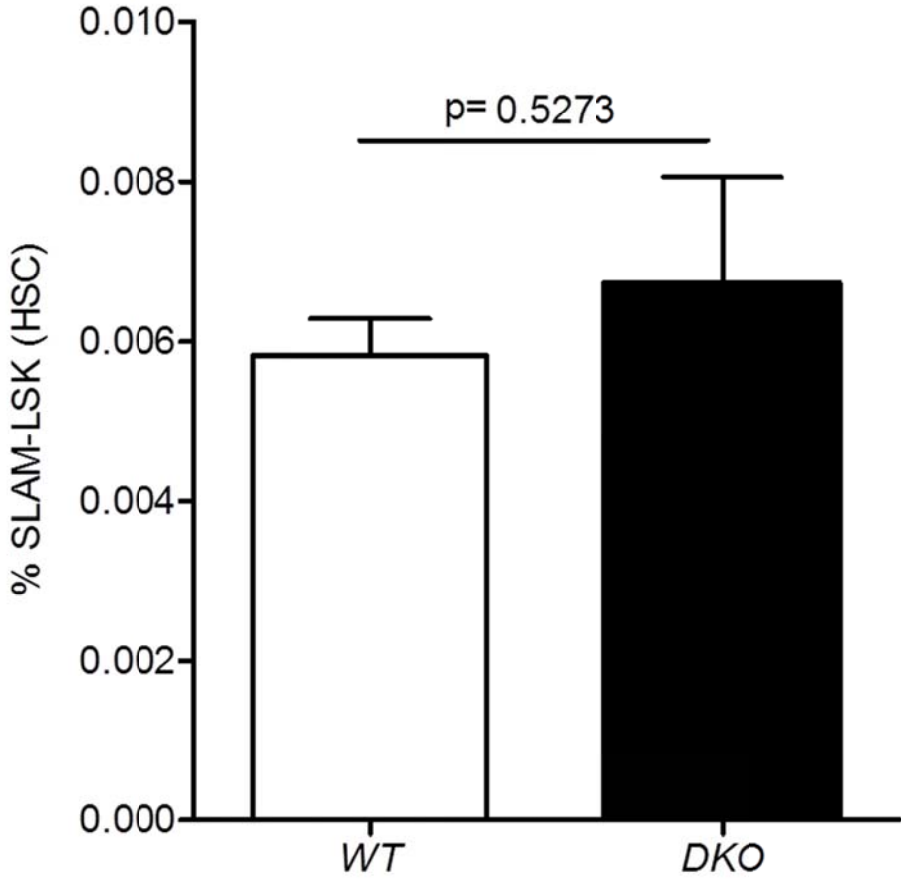

Figure 19b

Figure 19: *DKO* HSCs decline linearly with loss of *DKO* bone marrow cellularity. *DKO* bone marrow showed no difference in the frequency of SLAM-LSK cells ($Lin^-CD48^-CD41^-CD150^+Sca1^+c\text{-}kit^+$), which represents the most phenotypically precise known definition of the long-term, multi-lineage repopulating hematopoietic stem cell (n=7, p value derived from an unpaired student's t-test). Error bars represent the standard error of the mean. Statistical data are derived from one experiment with multiple biologically-independent replicates. HSC analyses were performed on at least three separate occasions with multiple biologically-independent replicates.

Erk1/2 disruption prevents stem cell colony formation but not BrdU incorporation.

To further assess the consequence of *Erk* disruption on HSC proliferation, we performed multiple experiments analyzing HSC proliferative status. First, we injected mice with four sequential doses (2 mg/dose) of BrdU, starting two days after completion of the polyIC regimen (Figure 20a). We then harvested bone marrow, stained with cell surface markers for the HSC population, fluorophore-conjugated anti-BrdU antibody, and propidium iodide (PI). Surprisingly, *DKO* HSCs demonstrated no difference (and, potentially, increases) in BrdU uptake (Figure 20b-c), implying that *DKO* stem cells readily synthesize DNA.

To further assess this finding, we performed an alternative experiment using Hoechst (Hst) and Pyronin Y (PY) dyes. These are well-characterized dyes of total DNA and RNA content, respectively, and they are frequently used to assess the cell cycle status of hematopoietic stem and progenitor cells (152-154). In these experiments, we found increased DNA and RNA content in *DKO* HSCs with no difference in the size and granularity of the HSC population (Figure 21a-b). The size and granularity analysis ensures that the increase in Hst and PY does not correlate only to abnormal morphology secondary to *Erk* disruption. The relative increases in RNA and DNA (Hst^+ and PY^+) hypothetically represents an active cell cycle status (i.e. compartmentalization to G1, S, G2, or M).

These data could indicate at least two scenarios: first, that *DKO* HSCs are somehow hyper-proliferating and, second, that *DKO* HSCs enter the cell cycle but do not complete mitosis. To test the counterintuitive possibility that these *DKO* HSCs were hyper-proliferating, we sorted single HSCs into methylcellulose

enriched with SCF, Flt3-ligand, and IL-3 (all of which stimulate HSC proliferation), finding no colony formation or evidence of progeny after seven to ten days in culture (Figure 21c). Thus, we concluded that HSC proliferation but not BrdU incorporation (and, thus, perhaps not G1/S entry), requires at least one Erk isoform.

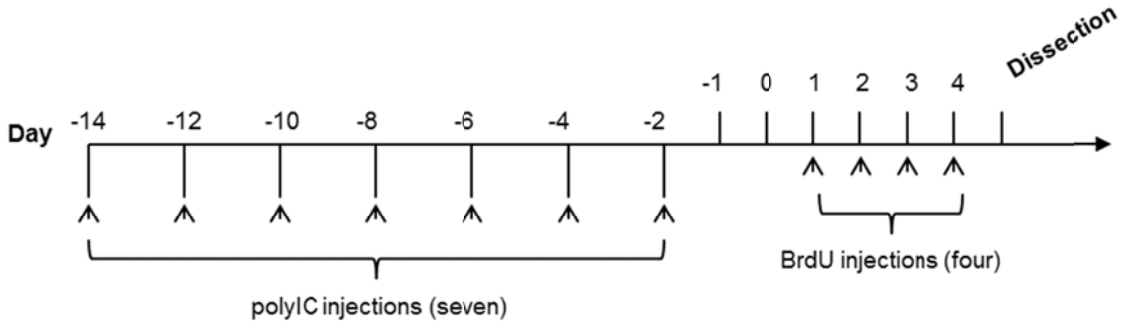
Day
-14
-12
-10
-8
-6
-4
-2
-1
0
1
2
3
4
Dissection
BrdU injections (four)
polyIC injections (seven)

Figure 20a

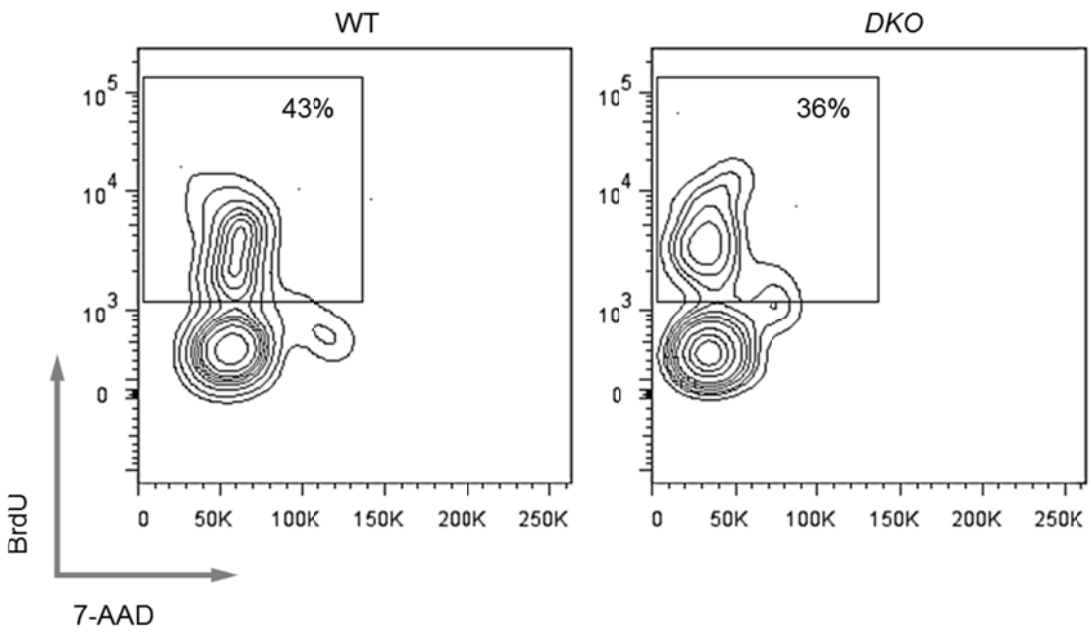

Figure 20b

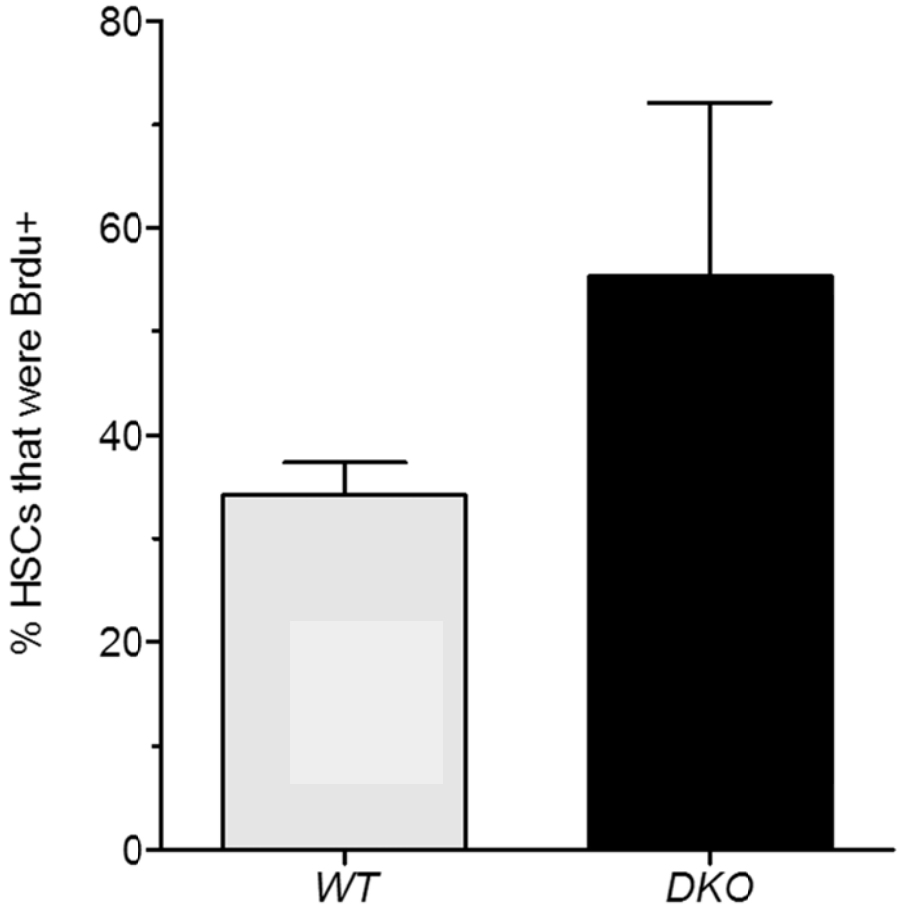

Figure 20c

Figure 20: *DKO* HSCs incorporate BrdU. Mice were given four doses of BrdU (2 mg/mouse) over four days following the polyIC regimen (a). After killing, bone marrow cells were stained for HSC markers and BrdU and analyzed by flow cytometry, revealing that both WT and *DKO* HSCs incorporate BrdU (b). Quantification revealed no difference between $BrdU^+$ *DKO* and WT HSCs (c) (n=3-7, $p>0.05$, student's unpaired t-test). Error bars represent the standard error of the mean.

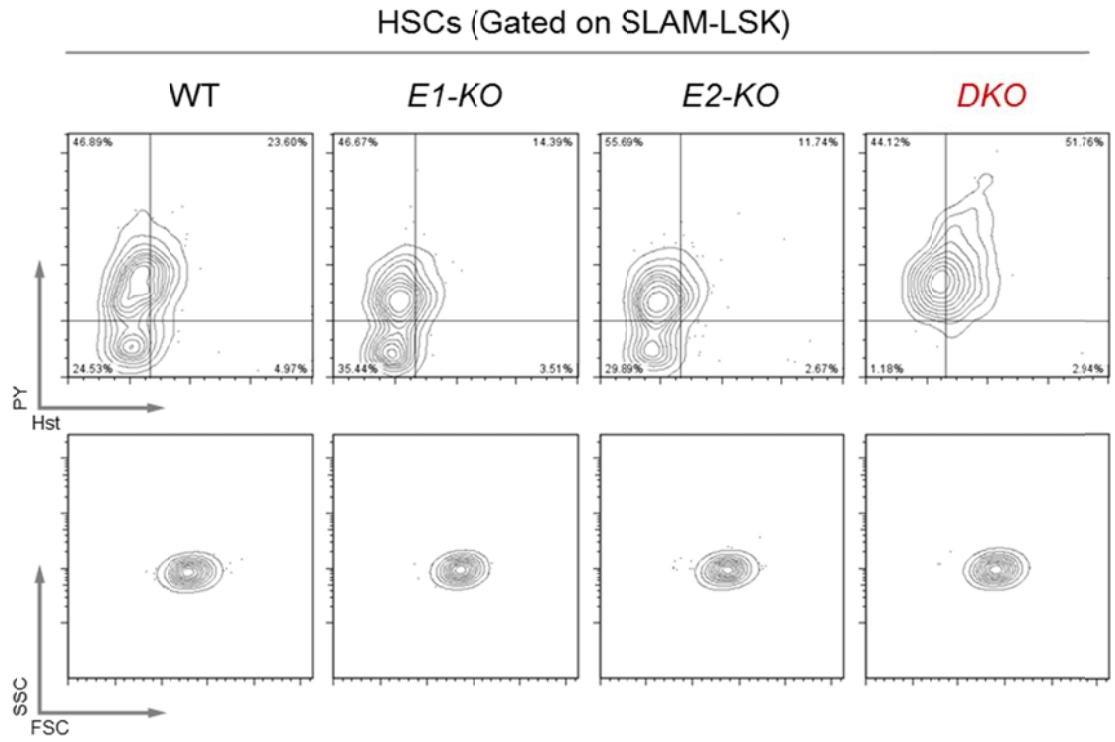
HSCs (Gated on SLAM-LSK)
WT
E1-KO
E2-KO
DKO
46.89%
23.60%
24.53%
4.97%
46.67%
14.39%
35.44%
3.51%
55.69%
11.74%
29.89%
2.67%
44.12%
51.76%
1.18%
2.94%
PY
Hst
SSC
FSC

Figure 21a

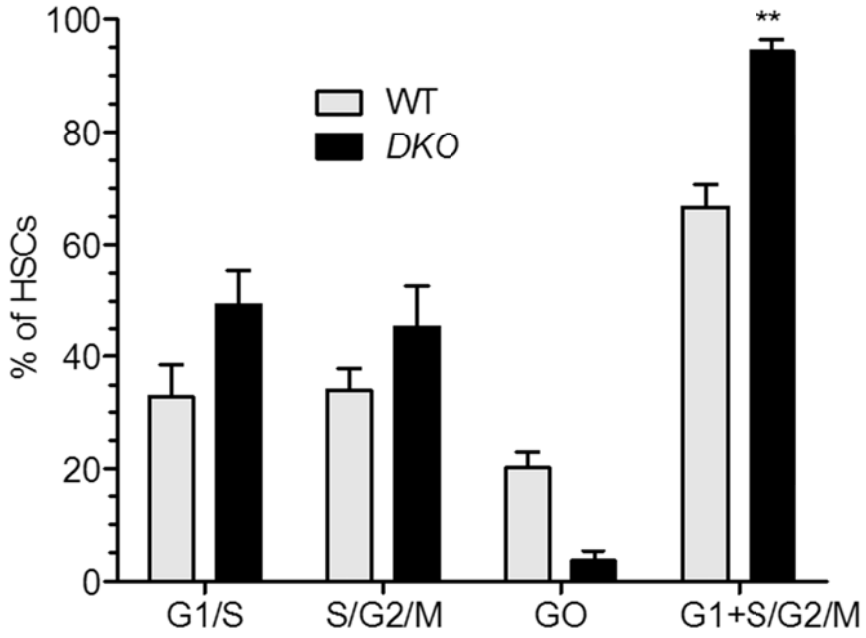

Figure 21b

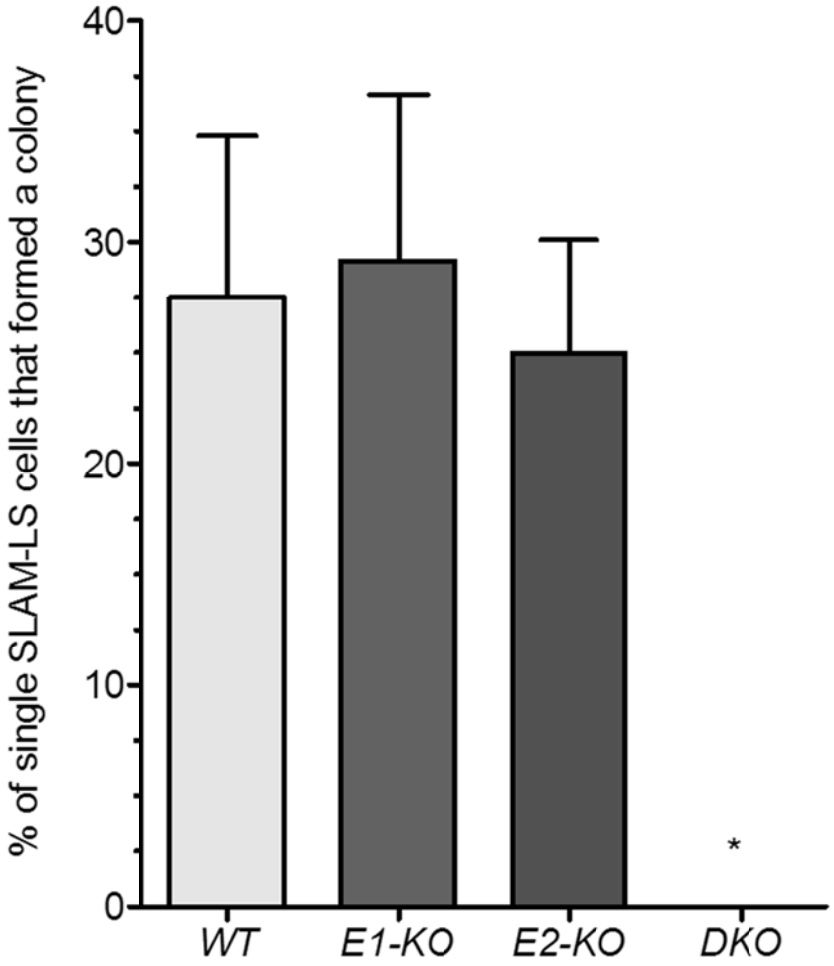
40
30
20
10
0
% of single SLAM-LS cells that formed a colony
*
WT
E1-KO
E2-KO
DKO

Figure 21c

Figure 21 DKO HSCs have increased DNA and RNA content but do not form colonies. Staining for HSC markers and for Pyronin Y and Hoechst one day after polyIC revealed increased DNA and RNA content in *DKO* HSCs, with no apparent change in overall size and granularity (a). Quantification revealed an increase of *DKO* HSCs in the cell cycle (b) (n=4-7, **p<0.01, 2-way ANOVA with Bonferroni correction). Single *DKO* SCs failed to produce any colonies or progeny after being sorted into 96-well plates containing methylcellulose enriched with serum, SCF, Flt3L, and IL-3, while no differences were detected among WT, *E1-KO*, and *E2-KO* HSCs (c) (n = 4-9, *p<0.05, 1-way ANOVA with Bonferroni correction). On all graphs, error bars represent the standard error of the mean.

Erk1/2 control HSC proliferation: additional evidence.

We performed a number of other complementary studies to assess the influence of Erk activity on proliferation and survival. First, we assayed apoptosis using flow cytometric detection of fluorophore-conjugated Annexin V, a phospholipid binding protein with high affinity for exposed phosphatidylserine residues on the inverted membrane leaflets of cells undergoing apoptosis (155). In these assays, we found no consistent difference in *DKO* cells over *E1-KO, E2-KO*, and WT cells, although *DKO* cells tended to show mildly higher levels (Figure 22a). We then probed protein samples extracted from bone marrow and spleen cells to assay the levels of cleaved PARP, a biochemical indicator of activation in pro-apoptotic pathways. In these analyses, we found no differences in cleaved PARP among *E1-KO*, *E2-KO*, and *DKO* samples (Figure 22b).

To assess proliferation and survival ex vivo, we sorted LSK cells (MPPs) from the bone marrow of dozens of WT mice and performed proliferation/survival studies with the Mek-Erk inhibitor PD0325901. We plated equivalent numbers of MPPs into each well of 96-well plates containing serum and SCF. After three days of stimulation, we counted these cells with trypan blue, which darkly stains cells with disrupted membranes (i.e. apoptotic or necrotic). We performed this experiment on three separate occasions, finding that 100 nM of PD0325901 reduced LSK cell proliferation between two and 10-fold (Figure 22c). By contrast, we did not detect consistent changes in the number of trypan blue positive cells per well betweenPD0325901-treated and non-treated samples.

We performed western blot on protein extracted from bone marrow cells to assess the expression level of different cyclins. Cyclin levels fluctuate as cells progress through the cell cycle, and their relative levels indicate the cell cycle status of proliferating cells (156). Generally, cyclin D increases during G1, cyclins E and A increase during late G1 and S-phase, and cyclin B increases during G2/M phases. Our protein analyses revealed severely diminished cyclin D and increased levels of cyclin B in *DKO* bone marrow cells (Figure 22d), indicating an abnormal compartmentalization toward later stages of the cell cycle. These data correlate with our findings from the BrdU- and PY/Hst-based experiments, albeit in the whole marrow compartment. Interestingly, *E1-KO* and *E2-KO* samples both demonstrated mildly diminished levels of cyclin D, although this did not correlate with any immediately observable phenotype.

We also assessed cell cycle status of only the myeloid $FSC^{hi}SSC^{hi}$ myeloid subset using Pyronin Y and Hoechst dyes. This experiment yielded similar results as our HSC cell cycle analysis, whereby the *DKO* samples demonstrated increased DNA and RNA content, indicating abnormal compartmentalization to S/G2/M (Figure 22e). Thus, the precise mechanism of abnormal proliferation in *Erk*-disrupted myeloid cells may be similar to Erk-disrupted HSCs.

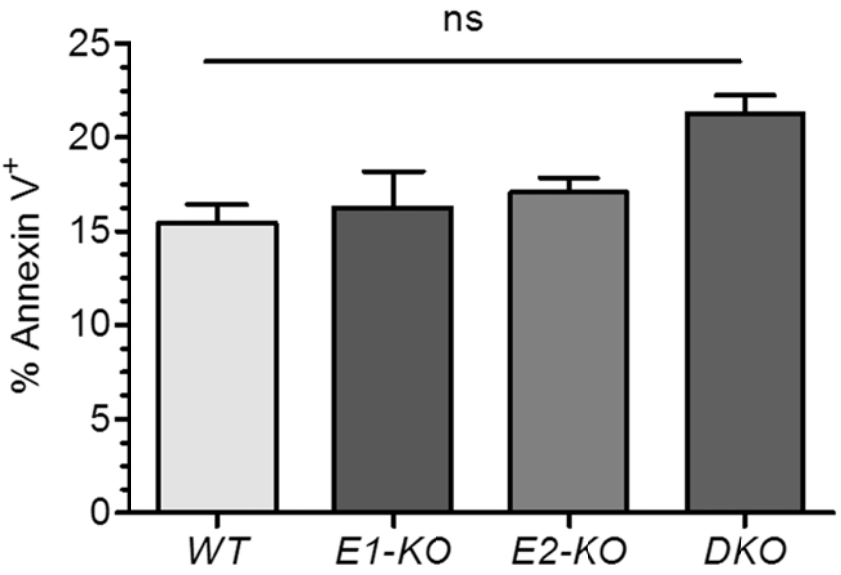

Figure 22a

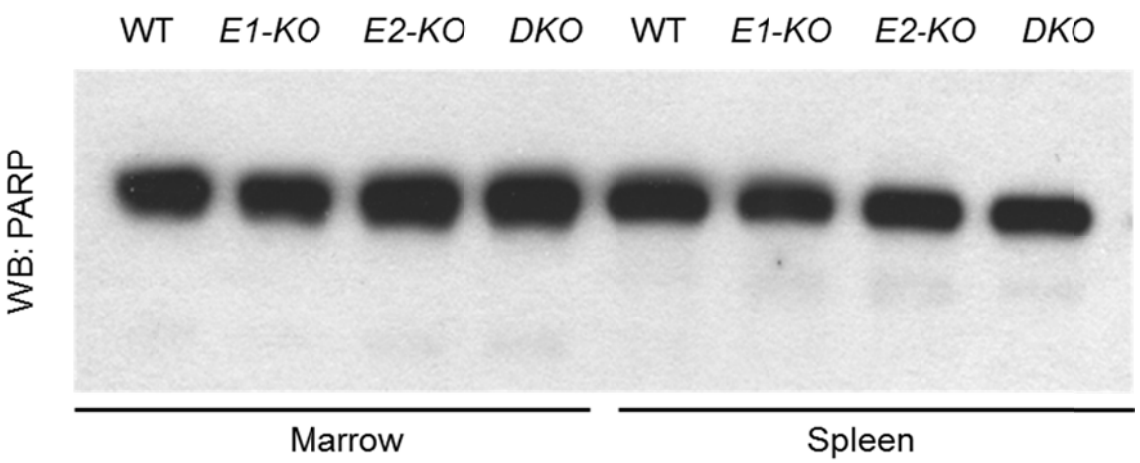

Figure 22b

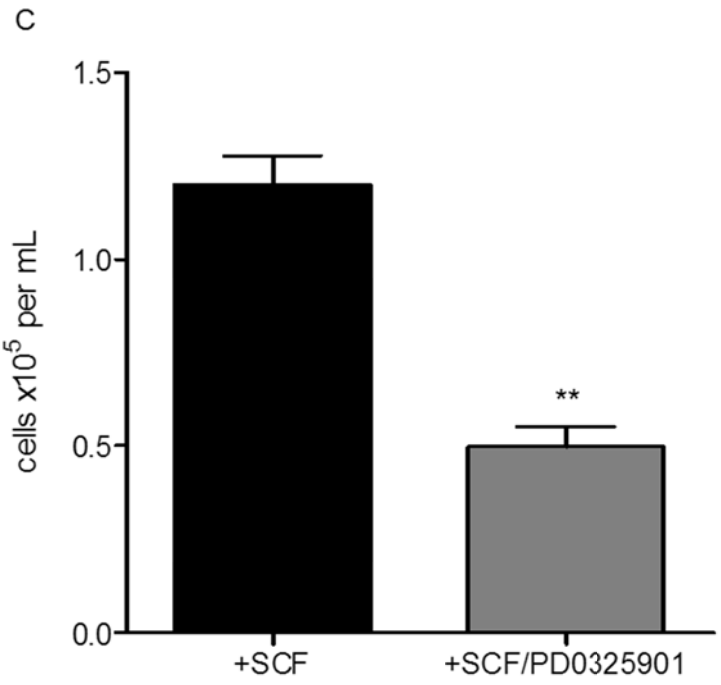

Figure 22c

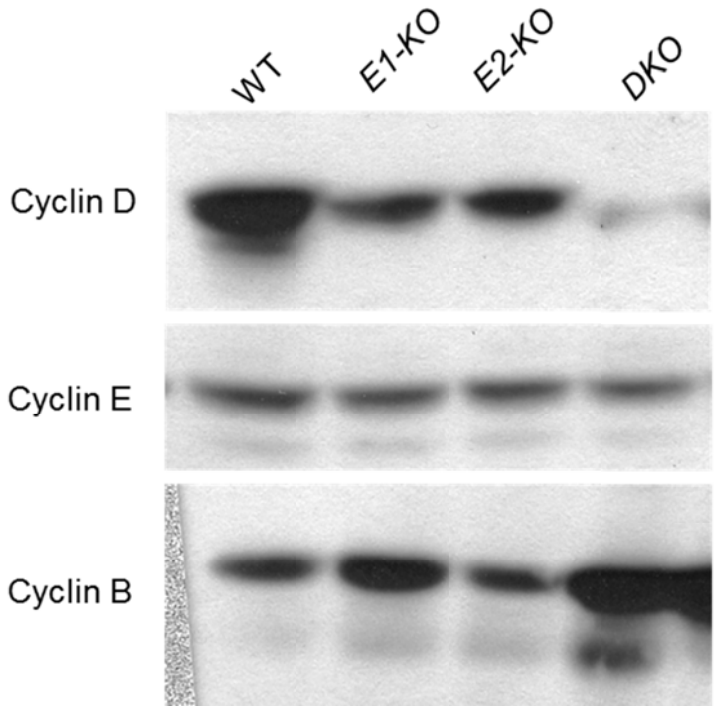

Figure 22d

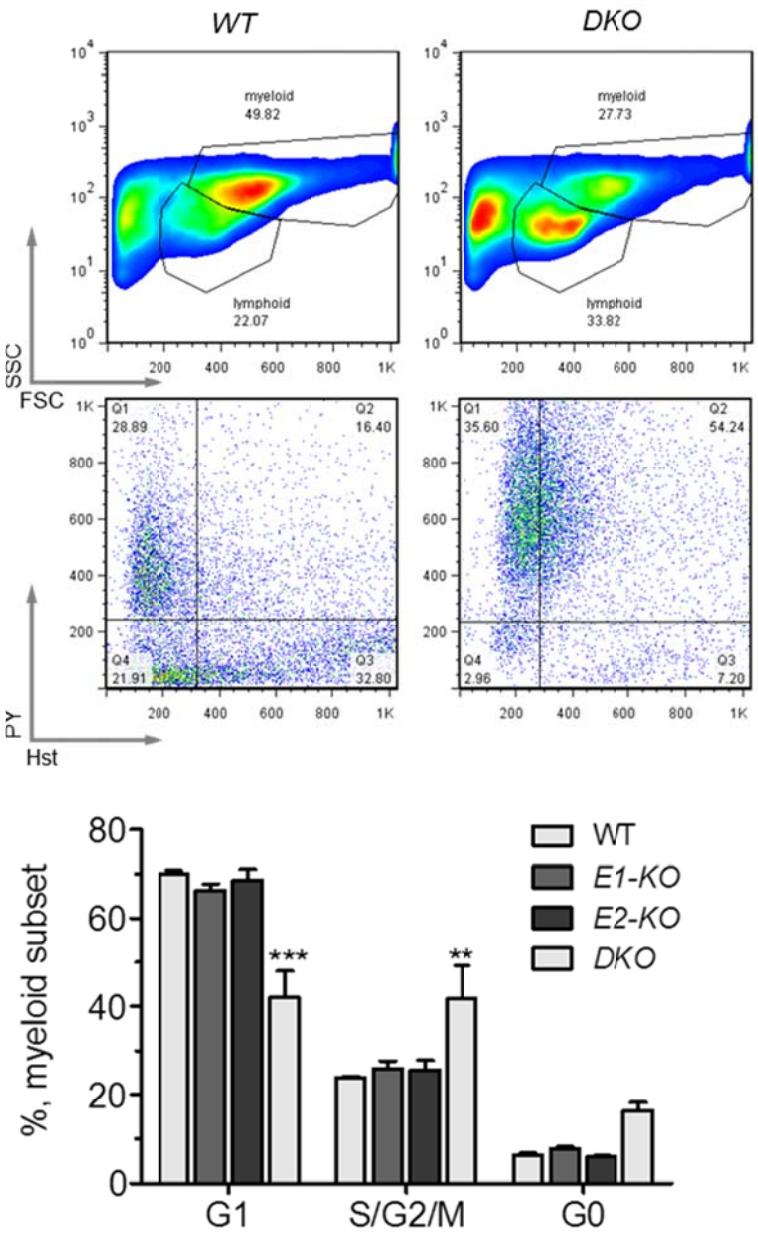
WT
DKO
myeloid
49.82
lymphoid
22.07
myeloid
27.73
lymphoid
33.82
SSC
FSC
Q1
28.89
Q2
16.40
Q4
21.91
Q3
32.80
Q1
35.60
Q2
54.24
Q4
2.96
Q3
7.20
PY
Hst
%, myeloid subset
WT
E1-KO
E2-KO
DKO
***
**
G1
S/G2/M
G0

Figure 22e

Figure 22: Additional genetic evidence that Erk's preponderant role in the hematopoietic system is in the control of proliferation. Flow cytometric Annexin V-based detection of apoptosis in bone marrow cells revealed no difference between WT, *E1-KO*, *E2-KO*, and *DKO* samples (a) (n=3, $p>0.05$ for all comparison, one-way ANOVA with Bonferroni correction). Western blot of protein extracted from bone marrow cells and from the spleen showed no difference in cleaved PARP levels between WT, *E1-KO*, *E2-KO*, and *DKO* samples (b). $Lin^{-}Sca1^{+}c\text{-}kit^{+}$ MPPs were FACS-sorted using admixed bone marrow of multiple (10-20 per experiment) wild-type mice, separated into triplicate wells per condition containing 10,000 cells each, pre-inhibited (one hour) with either 100 nM PD0325901 or vehicle only, then stimulated with 80 ng/mL SCF and FBS for three days. PD0325901-inhibited cells showed consistent reductions in total proliferative output (c) (n=3 replicates, $^{**}p=0.0017$, student's t test). Data are representative of one experiment performed on three separate occasions. Cyclin level analysis was performed by western blot of equivalent quantities of bone marrow cells lysed in SDS-PAGE buffer, revealing profound diminution of cyclin D levels in *DKO* cells with a reciprocal increase in cyclin B levels (d). *E1-KO* and *E2-KO* cells also showed a moderate depression in cyclin D levels. Gating on the characteristic $FSC^{hi}SSC^{hi}$ myeloid population revealed an increased frequency of $PY^{+}Hst^{+}$ (i.e. S/G2/M) cells (e) (n=3, $^{**}p<0.01$, $^{***}p<0.001$, 2-way ANOVA with Bonferroni correction). In all graphs, error bars represent the standard error of the mean.

Single *Erk1* or *Erk2* disruption have specific long-term consequences.

As indicated in the prior experiments, we detected few readily observable phenotypes in *E1-KO* and *E2-KO* bone marrow samples. We additionally performed experiments with bone marrow samples harboring only one allele of *Erk*: *Mx1Cre*$^{+}$*Erk1*$^{+/-}$*Erk2*$^{flox/flox}$ mice injected with polyIC (or, *E1*$^{+/-}$*E2-KO*). These experiments tested the hypothesis that *Erk1* and *Erk2* operate in a gene dosage dependent manner and that by further reducing the total Erk1/2 level, a readily observable phenotype may emerge. However, we found no phenotype comparable to the *DKO* phenotype in the *E1*$^{+/-}$*E2-KO* bone marrow cells, as indicated by bone marrow cellularity and colony formation (Figure 23a). Thus, the observed *DKO* phenotype – at least in terms of colony formation in tissue culture and maintenance of myeloid cellularity – appears to require binary and complete ablation of *Erk*1/2, without an obvious gene dose dependency. We did not test *E1*$^{-/-}$*E2*$^{+/-}$ samples, although we would expect similar results.

Intriguingly, though, we found a prominent loss of circulating lymphoid cells in BoyJ WT mice transplanted long-term with *E2-KO* hematopoietic stem cells (Figure 23b). Using our ten-parameter flow cytometric analyses of peripheral blood chimerism and lineage commitment, we found a three-fold reduction in the percentage of CD3^{+}CD4^{+} and CD3^{+}CD8^{+} T cells in *E2-KO* HSC recipients (Figure23b, top graph). The percentage of circulating CD3^{-}B220^{-} Gr1^{+}Mac1^{+} PMNs and CD3^{-}B220^{-}Gr1^{-}Mac1^{+} monocytes showed a reciprocal increase as a frequency of peripheral blood cells (Figure 23b, bottom graph), while B220^{+} B cells showed no change as a percentage of peripheral blood cells.

Thus, the increase in peripheral myeloid cell frequency in *E2-KO* HSC recipients inversely correlates to the decrease in peripheral T cell frequency.

Based on this intriguing observation, we next examined if *E2-KO* hematopoietic stem and progenitor cells possess an intrinsic ability to overproduce myeloid cells. While we had not detected a difference in our previous experiments, here we employed lower concentrations of single cytokines to test possible subtle consequences of *Erk2* ablation. We additionally performed these experiments on bone marrow cells extracted from the long-term HSC transplant recipients, thus isolating putative phenotypes to a marrow-autonomous etiology. However, we found no difference between WT and *E2-KO* transplanted marrow cells in their ability to form colonies on methylcellulose, at all tested concentrations of IL-3 and GM-CSF (Figure 23c). Of note, we also found no difference in total bone marrow cellularity between WT and *E2-KO* transplant recipients (data not shown). Accordingly, we concluded that the increased frequency of circulating myeloid cells probably results directly from the diminished frequency of T cells and not from an intrinsic capacity of *E2-KO* progenitor cells to overproduce myeloid cells.

Finally, we note a mild depression in circulating myeloid cell frequency in the *E1-KO* HSC recipients, which can be appreciated in Figure 23b. In another set of experiments not discussed in detail here, we have found that the bone marrow of *E1-KO* mice contains reduced numbers of osteoclast-specific monocyte progenitors and that *E1-KO* cultured osteoclasts demonstrate impairment in multiple functional assays. These observations correspond with

increased bone mineral density in primary *E1-KO* mice and in WT mice transplanted with *E1-KO* HSCs, indicating a marrow-autonomous consequence of *Erk1* disruption on bone physiology. Interestingly, *E1-KO* osteoclasts show diminished $p90^{rsk}$ phosphorylation in response to M-CSF stimulation while *E2-KO* osteoclasts have no change in their $p90^{rsk}$ phosphorylation levels, as compared to WT mice. As evidenced, myeloid/monocyte-derived osteoclasts appear to preponderantly depend upon Erk1 activity over Erk2 activity for functional and biochemical aspects. Thus, while we generally argue for Erk1 and Erk2's singular dispensability in global hematopoietic stem and progenitor cell maintenance, we again caution against generalizing these observations toward specific effector cell number and function.

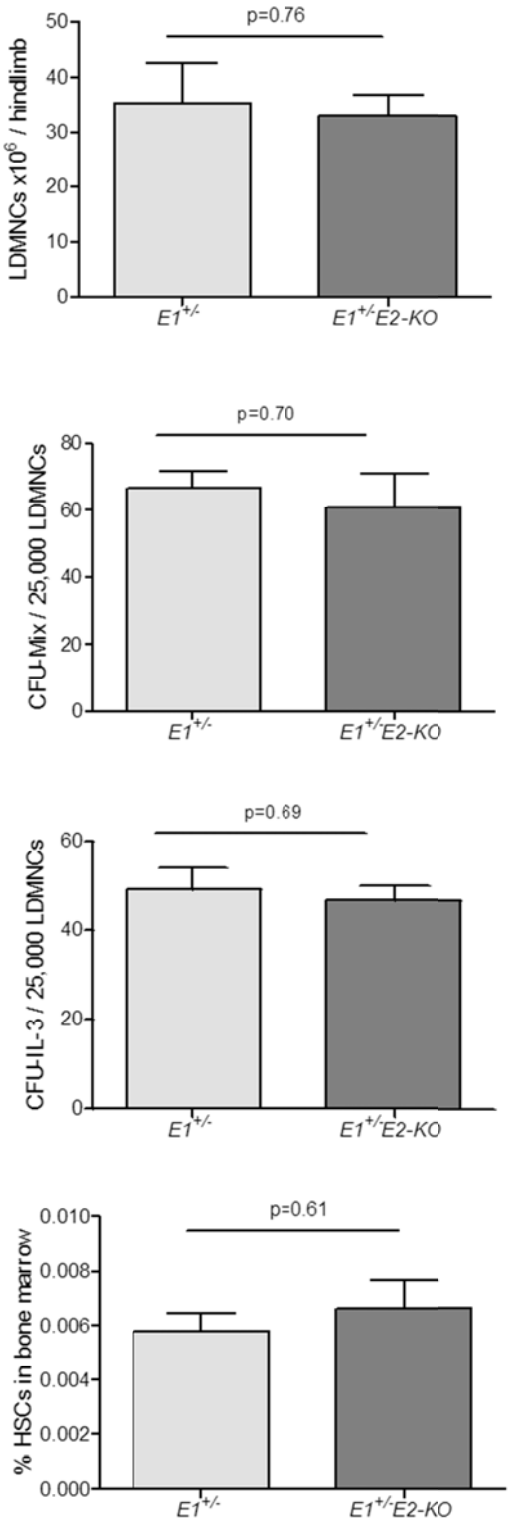
p=0.76
LDMNCs x10^6 / hindlimb
50
40
30
20
10
0
E1+/-
E1+/-E2-KO
p=0.70
CFU-Mix / 25,000 LDMNCs
80
60
40
20
0
E1+/-
E1+/-E2-KO
p=0.69
CFU-IL-3 / 25,000 LDMNCs
60
40
20
0
E1+/-
E1+/-E2-KO
p=0.61
% HSCs in bone marrow
0.010
0.008
0.006
0.004
0.002
0.000
E1+/-
E1+/-E2-KO

Figure 23a

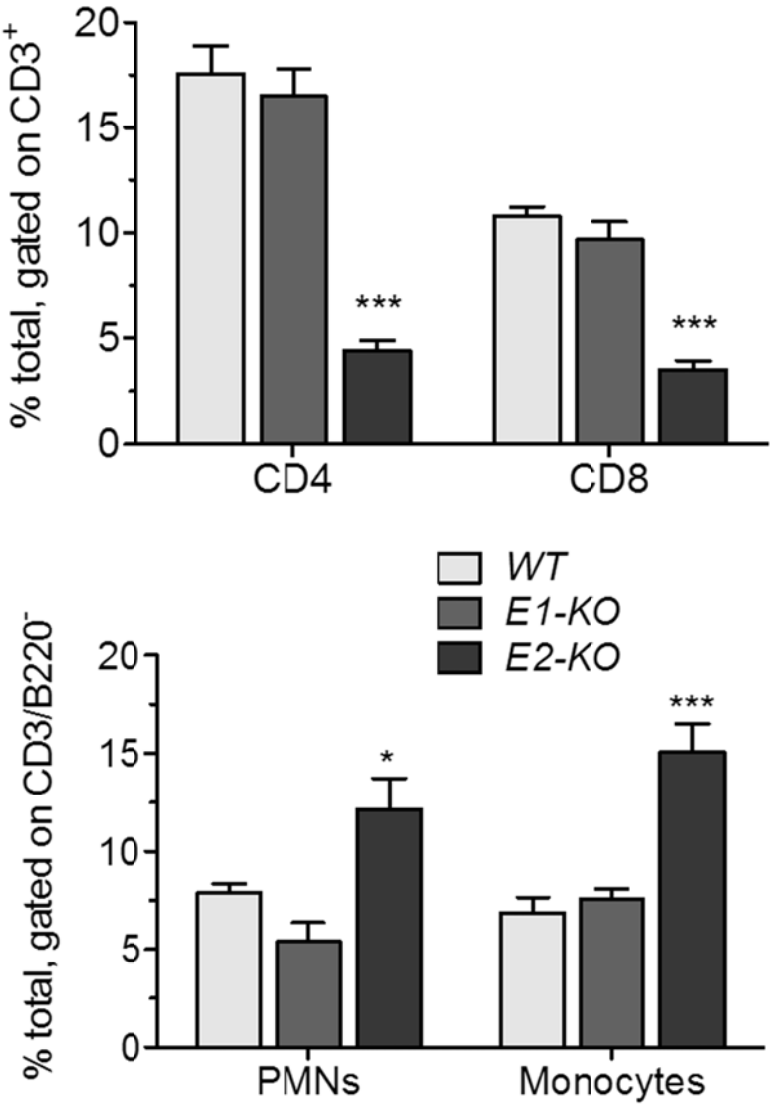
% total, gated on CD3+
20
15
10
5
0
***
***
CD4
CD8
WT
E1-KO
E2-KO
% total, gated on CD3/B220-
20
15
10
5
0
*
***
PMNs
Monocytes

Figure 23b

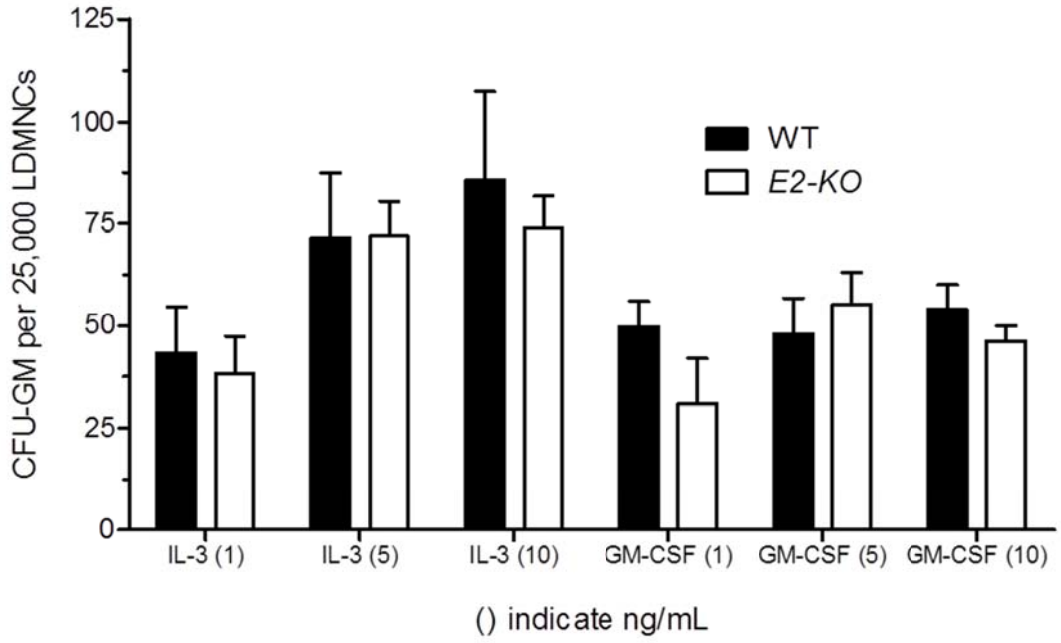
125
100
75
50
25
0
CFU-GM per 25,000 LDMNCs
WT
E2-KO
IL-3 (1)
IL-3 (5)
IL-3 (10)
GM-CSF (1)
GM-CSF (5)
GM-CSF (10)
() indicate ng/mL

Figure 23c

Figure 23. Additional assessment of the hematopoietic consequence of single *Erk* isoform disruption. Loss of three *Erk* alleles produced no immediately discernible phenotype in experiments assaying cellularity, colony formation, and HSC frequency (a) (n=3-5, p values derived from student's t-test). Mice transplanted more than four months with *E2-KO* hematopoietic stem cells had reduced frequency of circulating $CD4^+$ and $CD8^+$ T cells (b, top graph) but increased frequency of circulating $CD3^-B220^-$ PMNs and monocytes (b, bottom graph), with little difference peripheral blood lineage commitment between WT and *E1-KO* HSC recipients (n=5, *p<0.05, ***p<0.001, 2-way ANOVA with Bonferroni correction). Bone marrow cells from WT and *E2-KO* HSC transplanted mice were extracted and assayed for myeloid colony formation using varying concentrations of IL-3 and GM-CSF, as indicated, but no differences were found (c) (n=3-4, in all comparisons p>0.05, by student's two-tailed unpaired t-test or by two-way ANOVA with Bonferroni correction). In all graphs, error bars represent the standard error of the mean.

Erk disruption and *Nf1*-deficient hematopoiesis.

Based on our findings here, Erk appears critical for the long-term maintenance of the hematopoietic system. Specifically, the rapid generation of myeloid cells in vivo requires at least one isoform of Erk. These data seem particularly relevant in light of the increased levels of phosphorylated Erk1 and Erk2 observed in the bone marrow cells of patients with NF1-associated juvenile myelomonocytic leukemia and in the cells of mice with a JMML-like myeloproliferative disease.

A recent pharmacological study found that Mek-Erk chemical inhibitors (e.g. CI-1040 and PD0325901) tripled survival in mice transplanted with $Nf1^{-/-}$ progenitor cells additionally transformed with a Moloney-4070A LTR virus (MOL4070LTR), a hybrid virus shown to preferentially induce myeloid neoplasms (157). In this study, $Nf1^{-/-}$ progenitor cells infected with MOL4070LTR produced an acute myelogenous leukemia (AML) hypersensitive to pharmacological Mek-Erk inhibition. Despite the overall improvement in survival, Mek-Erk-independent genetic events enabled fatal leukemic progression. However, given the pharmacological approach, low levels of Erk phosphorylation contributing to AML progression could not be ruled out. Moreover, viral transformation of $Nf1^{-/-}$ progenitor cells may not accurately exemplify Mek-Erk signaling in NF1-associated MPD. Interestingly, in another recent study, the same research group demonstrated that PD0325901 can virtually abrogate MPD caused by oncogenic Ras expression in the hematopoietic system (158) . As yet, though, the specific

requirement for Mek-Erk signaling in the context of *Nf1*-deficiency remains unknown.

In an ongoing study, we are assessing the progression of $Nf1^{-/-}$ induced MPD in the context of genetically disrupted *Erk1/2*, testing our hypothesis that the diseased hematopoiesis of NF1-associated MPD requires Erk. Our laboratory and others have previously shown that transplantation of *Nf1* deficient progenitor cells into WT mice is sufficient to induce a myeloproliferative disorder resembling human JMML (44, 45, 93, 159, 160). Accordingly, we have initiated a study to test *Erk* disruption in the context of marrow-autonomous *Nf1*-deficiency and putative MPD genesis. To do so, we have generated $Nf1^{flox/flox}Erk1^{-/-}$ $Erk2^{flox/flox}Mx1Cre^{+}$ mice (*Nf1*$^{-/-}$*; DKO*). We have transplanted mononuclear cells from *Nf1*$^{-/-}$*; DKO* (experimental), $Nf1^{flox/flox}Mx1Cre^{+}$ (*Nf1*$^{-/-}$; positive control), *DKO,* and *E1-KO* (negative controls) mice mixed at a 1:4 ratio with WT BoyJ bone marrow cells into the tail vein of lethally-irradiated (1100 cGy) F1 mice (n=10 recipients per group, 40 total mice) (Figure 24). Two months following transplantation, we will assess initial chimerism and lineage commitment, followed by polyIC injection and tracking, as described above. Currently, we are within the two month reconstitution period.

Initially, we expect ~20% $CD45.2^{+}$ (test) and ~80% $CD45.1^{+}$ (WT BoyJ) chimerism in all recipient groups. In the *Nf1*$^{-/-}$*; DKO* group, we expect one of three outcomes: 1). Elimination of the $CD45.2^{+}$ *Nf1*$^{-/-}$*; DKO* fraction, but perhaps at a slower rate than in *DKO* only; 2). progression to MPD, with stable deletion of

Nf1 and *Erk2,* if diseased hematopoiesis does not require Erk; and 3). progression to MPD, with stable *Nf1* deletion but continued Erk2 expression. Importantly, we will carefully assess *Erk2* and *Nf1* allele recombination efficiency in the CD45.2^{+} fraction via PCR and immunoblot, as above. If we conclude that NF1-associated MPD does not require Erk (in other words, MPD exists in the CD45.2^{+} fraction, *Nf1* is excised, and *Erk2* is excised), we will analyze *Nf1*$^{-/-}$*; DKO*-dependent hematopoiesis in vivo and in tissue culture. To do so, we will assay lineage commitment in the peripheral blood of the CD45.2 *(Nf1*$^{-/-}$*; DKO*) fraction via flow cytometry, and we will use FACS to isolate this fraction for molecular and functional analyses, including peripheral blood colony forming unit assays. We will then kill mice, isolate the CD45.2^{+} fraction, and perform further colony assays, flow cytometric phenotyping, and biochemical experiments, as above and described previously (148). In the scenario that NF1-associated MPD does not require Erk, a revelatory experiment may include next-generation RNA-Seq using the ABI SOLiD 4 platform, comparing mRNA expression in *Nf1*$^{-/-}$*; DKO* myeloid progenitors (e.g. lin^{-}c-kit^{+} cells) to WT, *Nf1*$^{-/-}$, and *DKO* myeloid progenitors.

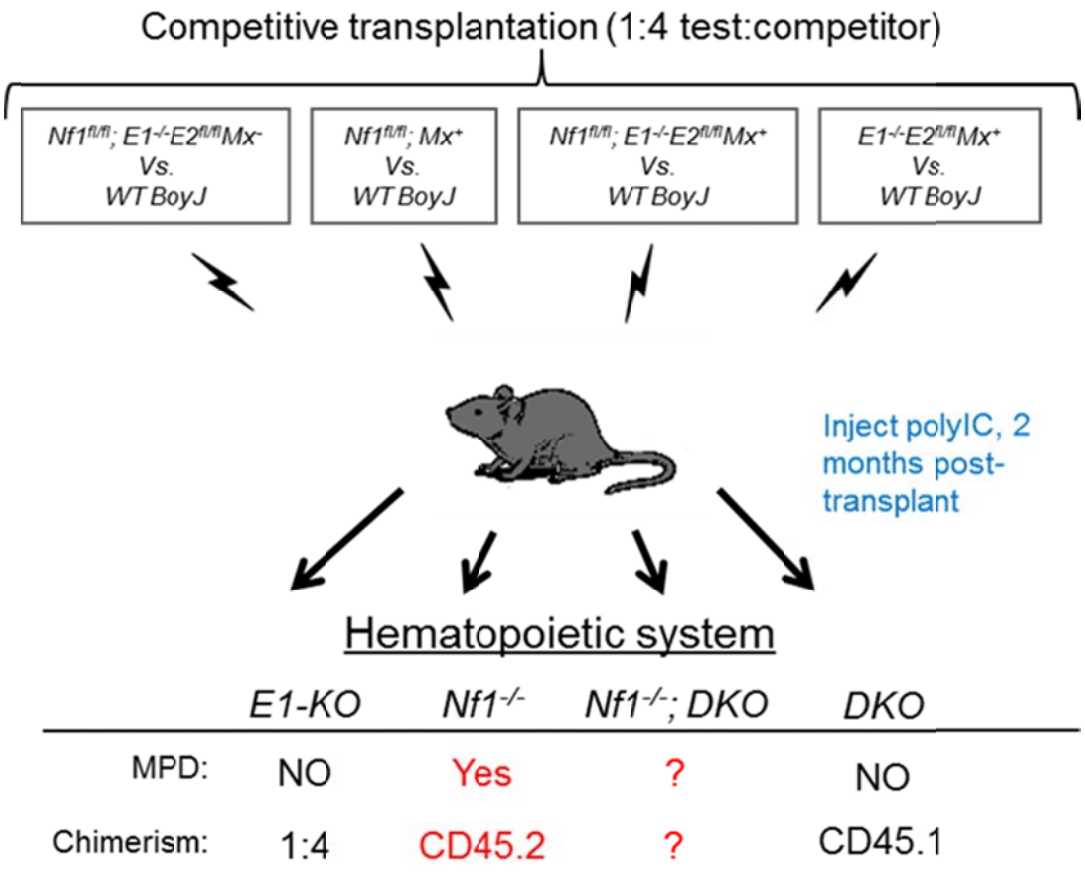
Competitive transplantation (1:4 test:competitor)
Nf1fl/fl; E1-/-E2fl/flMx- Vs. WT BoyJ
Nf1fl/fl; Mx+ Vs. WT BoyJ
Nf1fl/fl; E1-/-E2fl/flMx+ Vs. WT BoyJ
E1-/-E2fl/flMx+ Vs. WT BoyJ
Inject polyIC, 2 months post-transplant
Hematopoietic system
E1-KO
Nf1-/-
Nf1-/-; DKO
DKO
MPD:
NO
Yes
?
NO
Chimerism:
1:4
CD45.2
?
CD45.1

Figure 24

Figure 24: Experimental design to assay hematopoietic *Erk* disruption in the context of *Nf1* deficiency.

Erk and the mast cell

Mast cell cytopoiesis requires Erk.

To generate mast cells in vitro, we extracted bone marrow from the long bones of adult mice killed after the polyIC regimen, as described above. Non-adherent bone marrow cells were passaged twice weekly for four to six weeks in media containing 7.5 ng/mL interleukin-3 ("MCM"), as described previously (87, 146). Homogeneity of cultures were assessed by Giemsa/toluidine blue staining of typical mast cell morphology and by flow cytometric fluorophore-conjugated antibody-based detection of the FcεR and c-kit, cell surface markers of mast cell maturity, as described previously (98).

No differences were observed in the capacity of WT, *E1-KO*, or *E2-KO* bone marrow cells to generate a near-homogenous population of $FcεR^+$ and c-kit^+ cells by 4-6 weeks of MCM culture (Figure 25a), indicating normal mast cell differentiation from single *E1-KO and E2-KO* myeloid progenitor cells. We also tracked the expression of c-kit and $FcεR^+$ for six weeks of multiple cultures, finding no substantial difference in mast cell homogeneity, differentiation, or time-to-maturity among the single *KO* specimens.

By contrast, we found that *DKO* bone marrow cells could not differentiate into mast cells in MCM, confirming a critical reciprocity for Erk1 and Erk2 in mast cell precursor growth and differentiation. We also repeated methylcellulose-based colony assays using combined SCF and IL-3, two cytokines important to mast cell cytopoiesis. mast cell cytopoiesis. Similar to previous assays using mast cell cytopoiesis. Similar to our assays using mixed myeloid cytokines, no

DKO mast cell colonies formed (Figure 25b). We then attempted to grow colonies from bone marrow cells first enriched for c-kit expression using magnet-conjugated anti-c-kit antibody beads, but we were similarly unable to grow colonies from *DKO* c-kit^{+} cells (data not shown).

We found gross failure of *DKO* bone marrow cells to proliferate and adhere in liquid media (Figure 25c). In addition to MCM, we attempted to grow *DKO* bone marrow cells in liquid culture supplemented with M-CSF and RANKL, but these conditions yielded no proliferative or adhesive capacity. By contrast, we detected no differences in proliferation or adhesion among WT, *E1-KO*, and *E2-KO* samples.

During MCM-based culture of bone marrow cells, we tracked membrane leaflet inversion by flow cytometric detection of phosphatidylserine residues using APC-conjugated Annexin V. Generally, this loss of membrane integrity indicates an apoptotic cell. In these assays, we found little difference in the frequency of apoptotic cells between WT, *E1-KO*, *E2-KO*, and *DKO* bone marrow cells on the first day of culture. However, further culture of *DKO* bone marrow cells revealed a rapid induction of apoptosis and, by four weeks, only scant and apoptotic or necrotic (Annexin V and propidium iodide double positive) cells remained (Figure 25d).

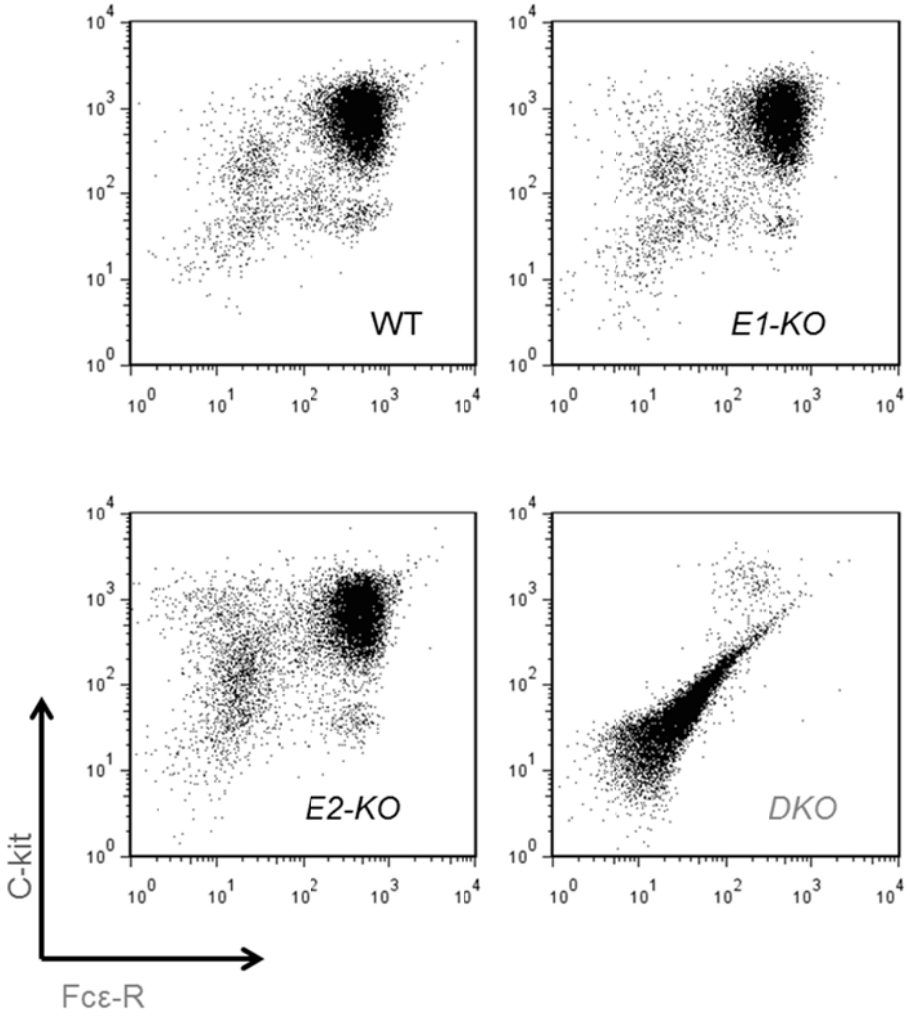

Figure 25a

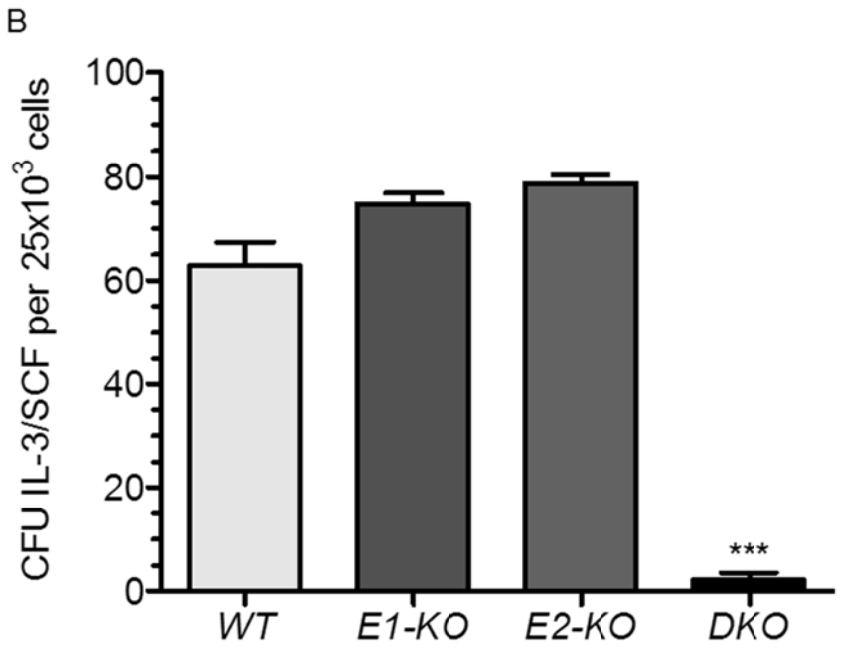

Figure 25b

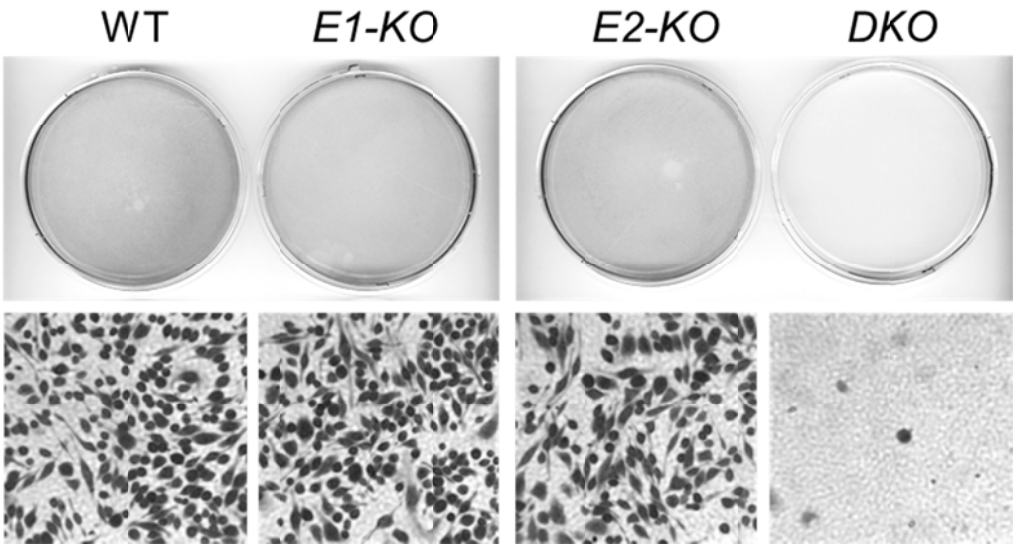

Figure 25°C

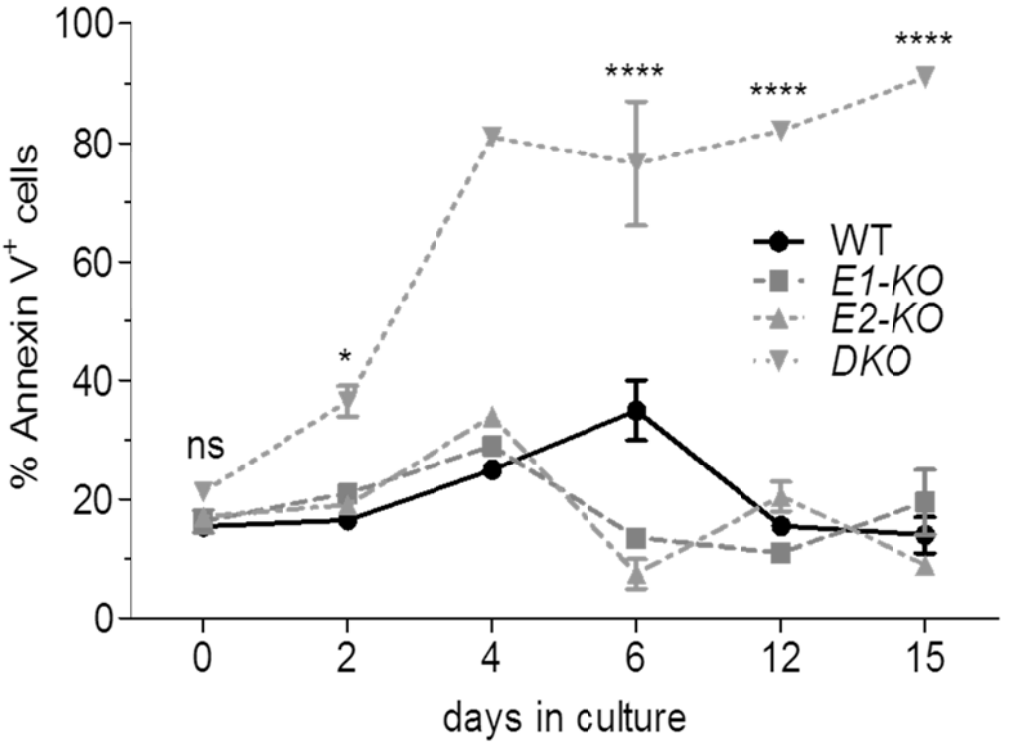
100
80
60
40
20
0
% Annexin V+ cells
ns
*
****
****
****
WT
E1-KO
E2-KO
DKO
0
2
4
6
12
15
days in culture

Figure 25d

Figure 25: Mast cell cytopoiesis, colony formation, and bone marrow cell growth require Erk. Non-adherent bone marrow cells were passaged twice weekly for four weeks in IMDM containing 10% FBS and 7.5 ng/mL IL-3 (MCM), revealing a critical requirement for either Erk1 or Erk2 in mast cell cytopoiesis, as assessed by flow cytometric detection of c-kit and FcεRI, cell surface markers of mast cell maturity (a). No differences were detected in mast cell cytopoiesis at four weeks between *E1-KO, E2-KO,* and WT cultures. Data are representative of at least six independent cultures for each genotype. *DKO* bone marrow cells produced few colonies in methylcellulose media supplemented with IL-3 and M-CSF (n=3-4, ***p<0.001, *DKO* vs. all, one-way ANOVA with Bonferroni correction). Crystal violet staining demonstrates that *DKO* bone marrow cells have a dramatically diminished capacity to adhere and proliferate in liquid culture, with no differences detected among *E1-KO, E2-KO,* and WT cultures (c). In these photographs, adherent cells were principally (although not exclusively) monocyte/macrophages. Data are representative of at least six independent cultures for each genotype. Apoptosis was assessed by flow cytometric detection of phosphatidylserine by APC-conjugated Annexin V, revealing a rapid and persistent induction of cell death in *DKO* bone marrow cells grown in liquid culture (n=2-3 at time points with statistical analyses, ****p<0.0001, *DKO* vs. all, two-way ANOVA with Bonferroni correction).

Chemical Mek-Erk inhibition in mast cells.

As our data indicate that mast cell cytopoiesis requires one isoform of Erk, we have devised alternative chemical and genetic approaches to study dual Erk inhibition in mature mast cells. First, we have treated cultured mast cells with PD0325901, a small molecule inhibitor of Mek1/2 that prevents the phosphorylation and activation of Erk1/2. Compared to previous generation Mek-Erk inhibitors (e.g. PD98059, U0126, CI-1040), PD0325901 exhibits greater selectivity, potency, and oral bioavailability, thus making the molecule a more suitable research tool and a potentially effective pharmacological agent (Figure 26) (113, 161, 162). Several investigations have found that PD0325901 can inhibit cancer cell growth at nanomolar to sub-nanomolar concentrations in vitro (163-167). Based on these findings, investigators have used PD0325901 to attenuate the progression and severity of certain murine-modeled cancers, including glioma, hepatocellular carcinoma, thyroid cancer, prostate cancer, a virally-induced acute myelogenous leukemia, and an oncogenic Ras-dependent leukemia (158, 163, 166-168). Moreover, two phase II clinical trials have assessed PD0325901 efficacy in the treatment of metastatic, chemotherapy refractory cancers (169, 170), although few clinical studies have examined PD0325901's efficacy in less-progressed neoplasia. Likewise, few studies have examined PD0325901 in the context of primary, non-transformed cultured cells.

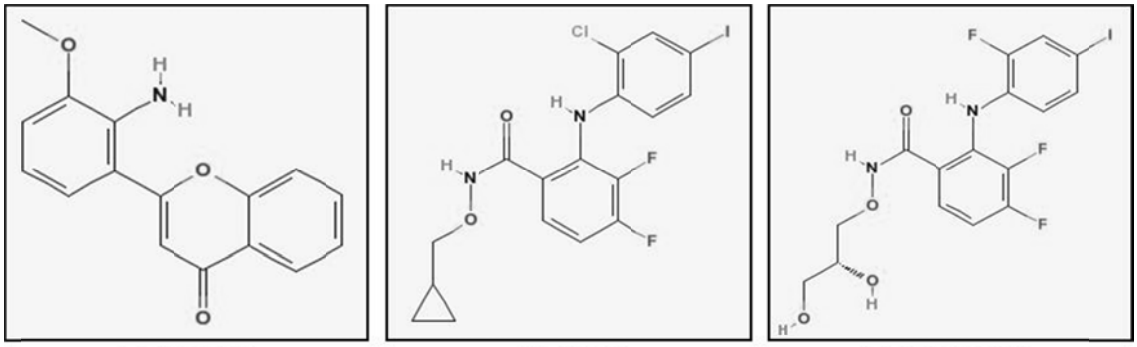
PD98059
IC50: 10 to 100 μM
CI-1040
IC50: 1 to 10 μM
PD0325901
IC50: 0.1 to 10 nM
Structures are from PubMed Compound

Figure 26

Figure 26: PD0325901 is a new generation, pharmacological grade Mek-Erk inhibitor. PD98059 (left) is the best-characterized and most widely-used inhibitor of Mek phosphorylative activity on Erk1/2. However, PD98059 has poor solubility, a non-pharmacological IC_{50} (10-100 μM in most cell types), a tendency to crystalize, and multiple off-target effects. Structural modifications in the PD98059 led to the development of CI-1040, the first Mek-Erk inhibitor to be used in clinical trials (middle). Further modification of CI-1040 led to the development of PD0325901 (*N*-((*R*)-2,3-dihydroxy-propoxy)-3,4-diXuoro-2-(2-Xuoro-4-iodo-phenylamino)-benzamide), which demonstrates the greatest potency and metabolic stability of the small molecule Mek-Erk inhibitors (right).

PD0325901 inhibits SCF-mediated Erk1/2 phosphorylation.

Because PD0325901 is a relatively new Mek-Erk inhibitor found in far fewer published studies than its predecessors (e.g. PD98059, U0126), we first aimed to establish its potency, efficacy, and selectivity in inhibiting Erk1/2 phosphorylation in SCF-stimulated primary mast cells. To do so, we pre-incubated growth factor deprived mast cells with varying concentrations of PD0325901, stimulated the cells for five minutes with SCF, extracted protein, and subsequently performed western blots to assess the phosphorylation level of Erk1/2 and other kinases. We chose five minutes as the endpoint because our prior experiments have shown that phospho-Erk1/2 levels peak between two and five minutes following SCF stimulation. In other experiments discussed below, we assessed other time points following SCF-stimulation.

We found that 25 nM of PD0325901 reduced the phosphorylation level of Erk1/2 in SCF-stimulated mast cells by nearly one-half the phosphorylation level of mast cells pre-treated with vehicle only (Figure 27a). At over 200 nM PD0325901, Erk1/2 phosphorylation could barely be detected. Moreover, the phosphorylation level of $p90^{rsk}$, which is a putatively specific measure of Erk kinase activity, directly correlated with the phosphorylation level of Erk1/2 was effectively inhibited by PD0325901 in the SCF-stimulated mast cell.

At this five minute time point, we detected a high degree of variability in the level of phospho-Akt^{S473}. As we have noted in other experiments, Akt phosphorylation secondary to SCF-stimulation does not demonstrate strictly predictable time-dependency that SCF-mediated Erk1/2 phosphorylation does.

Most importantly, though, the variable level of phospho-Akt did not correlate with increasing concentrations of PD0325901. Because phospho-Akt is a sensitive measure of PI-3K activation, we concluded that up to 400 nM PD0325901 does not inhibit PI-3K, at least in a dose-dependent manner (Further time points and affects are discussed later). We also found that up to 400 nM PD0325901 does not inhibit phosphorylation of GSK3β^{S9} at five minutes, a direct target of activated Akt. However, as discussed later, PD0325901 appears to modulate the phosphorylation status of Akt andGSK3β at later time points through potentially discrete mechanisms.

The IC_{50} for PD0325901's inhibition of Erk1/2 phosphorylation in SCF-stimulated mast cells was 37 nM (Figure 27b). The compound's maximal inhibition of Erk1/2 phosphorylation occurred at 200 to 400 nM. The phosphorylation level of p90^{rsk} directly correlated with Erk1/2 phosphorylation, while Akt^{S473} phosphorylation did not correlate with PD0325901 concentration. These parameters largely reflect findings of high selectivity, high potency, and sub-micromolar efficacy in prior publications concerning the use of PD0325901 in various transformed and non-transformed cell types (113, 163-165, 171-175).

We have concluded that PD0325901 exhibits potency and selectivity for Mek-Erk inhibition, preliminarily serving as a valuable tool for the study of Erk-dependent, SCF-mediated mast cell function. Accordingly, throughout the following experiments, we studied the role of Erk1 and Erk2 in SCF-mediated mast cell physiology and biochemistry using WT, *E1-KO, E2-KO*, and PD0325901-treated WT primary mast cells.

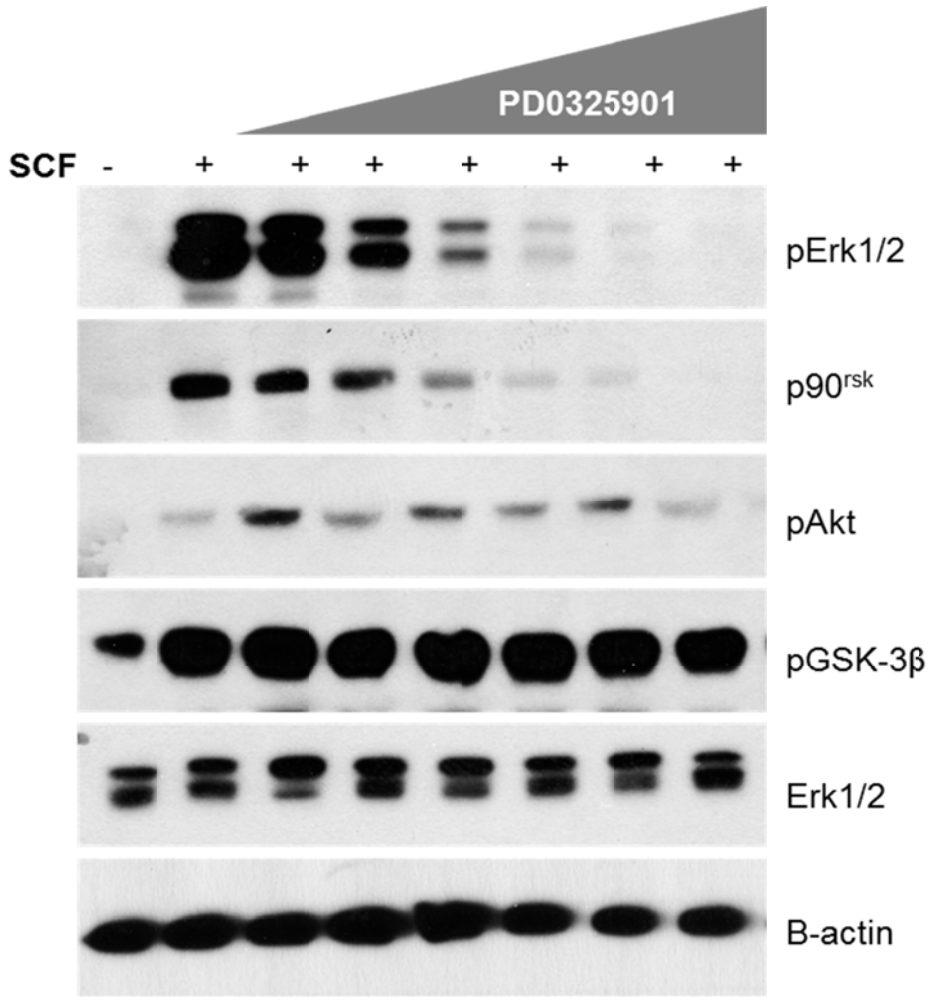

Figure 27a

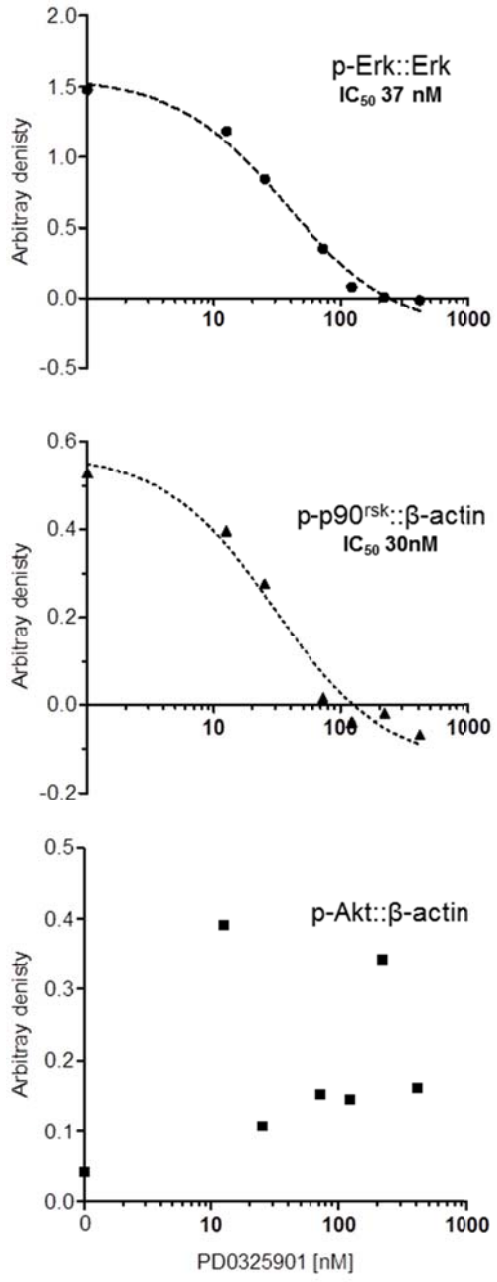
p-Erk::Erk
IC50 37 nM
Arbitray denisty
2.0
1.5
1.0
0.5
0.0
-0.5
10
100
1000
p-p90rsk::β-actin
IC50 30nM
Arbitray denisty
0.6
0.4
0.2
0.0
-0.2
10
100
1000
p-Akt::β-actin
Arbitray denisty
0.5
0.4
0.3
0.2
0.1
0.0
0
10
100
1000
PD0325901 [nM]

Figure 27b

Figure 27: PD0325901 inhibits Erk1/2 phosphorylation. Mast cells were deprived of growth factors overnight, resuspended to a standard concentration, pre-incubated with the indicated concentrations of PD0325901, and stimulated with SCF. After five minutes, cell aliquots were briefly centrifuged at 4°C and resuspended in SDS-PAGE buffer. After electrophoresis and transfer to PVDF membrane, samples were probed with the indicated antibodies. PD0325901 efficiently inhibited Erk1/2 phosphorylation and p90rsk phosphorylation (a putatively specific indicator of Erk kinase activity) (a). PD0325901 did not appear to modulate levels of phospho-AktS473 or phospho-GSK3βS9 in a dose-dependent manner at this time point. The three parameter logarithmic regressions demonstrate a biochemical IC50 of 30-35 nM as well as no relationship between PD0325901 concentration and Akt phosphorylation status (b). To build the dose-inhibition curve, the ratio of phosphorylated to total at the non-stimulated time point was subtracted from all points. (e.g.“0.0” represents density values from protein samples extracted from non-stimulated cells).

Single Erk isoforms are dispensable for SCF-mediated mast cell proliferation.

We performed multiple experiments using different techniques to assess the consequence of *Erk1* disruption, *Erk2* disruption, and PD0325901-treatment on SCF-mediated mast cell proliferation. These methods included total proliferative output (fold change in culture size, starting from a defined cell number), radioactive thymidine incorporation, and MTT-based assessment of metabolic activity, which can serve as a high-throughput surrogate for hemcytometer-based assays of total proliferative output.

First, we assessed whether single *Erk* disruption altered mast cell proliferation. Mast cells were deprived of growth factors overnight, plated in one mL IMDM at 250,000 cells per well in duplicate in a 24-well plate, and stimulated with 10% FBS and 25 ng/mL SCF. After 72 hours at 37°C, cells were stained with trypan blue (a negative marker for cell viability) and enumerated using an inverted light microscope.

In this experiment, we found no difference in the fold change of cell number between WT, *E1-KO*, and *E2-KO* samples, all of which approximately doubled in number during the course of the experiment (Figure 28). We repeated these experiments multiple times as well as by using MTT-based assays (data not shown), again finding no difference in the total proliferative capacity of SCF-stimulated WT, *E1-KO*, and *E2-KO* mast cells. Of note, we trialed various time points (24 to 96 hours) and concentrations of SCF (10 to 100 ng/mL), attempting to uncover dose- or time-dependency of putative consequences of single *Erk* isoform disruption. Throughout these experiments, though, we were unable to

identify any difference between SCF-mediated proliferation in WT, *E1-KO*, and *E2-KO* mast cells. As with HSC stability, single Erk isoforms appear dispensable for the total proliferative output of SCF-stimulated primary cultured murine mast cells.

Based on the biochemical studies of PD0325901 described above, we next examined SCF-mediated mast cell proliferation using increasing concentrations of PD0325901. This hemcytometer-based experiment was performed in a similar manner to the proliferation experiment described above, except that cells were incubated with 100 nM PD0325901 or vehicle alone for approximately one hour prior to stimulation with FBS/SCF.

In this experiment, we found a clear dose-response between PD0325901 inhibition and reduction in SCF-mediated mast cell proliferation, similar to our biochemical experiments assaying Erk1/2 phosphorylation. Intriguingly, 100 nM of drug abrogated proliferation in these cells (Figure 29). Due to the closeness in PD0325901 dosage required to inhibit SCF-mediated Mek-Erk phosphorylation and to abrogate SCF-mediated proliferation, our initial data suggest that SCF-mediated mast cell proliferation largely requires Erk kinase activity.

Of note, we did not observe substantially increased trypan blue uptake in cells treated with 12.5 to 100 nM of PD0325901, indicating that these cells were not undergoing apoptosis. These observations indicate that 100 nM PD0325901 principally halts proliferation but does not induce cytotoxicity or apoptosis.

To further explore the mechanics of Erk-dependent SCF-mediated mast cell proliferation, we performed ^{3}H-thymidine incorporation assays. These

experiments quantitate DNA synthesis by detection of newly-incorporated, radioactively-labeled thymidine bases. As a note of distinction, these assays measure S-phase entry from G0 or G1, not total proliferative output.

In our initial experiments assaying thymidine incorporation after SCF-stimulation, we aimed to characterize the kinetics of the initiation of DNA synthesis in mast cells deprived of growth factors overnight. We standardized cell concentrations and plated 50,000 per well in a 96-well plate, incubated the cells with 100 nM PD0325901, and subsequently stimulated them with 10% FBS and 80 ng/mL SCF supplemented with 1 μCi ^{3}H-thymidine. Starting at two hours after stimulation and at multiple time points following, we froze identically established 96-well plates at -20°C until the conclusion of the experiment, at which time we assayed thymidine incorporation with a scintillation counter.

We found that FBS/SCF-stimulated mast cells incorporated almost no ^{3}H-thymidine in the first ten hours following stimulation (Figure 29b, top graph). This G1 lag phase was followed by a slow but detectable rise in thymidine incorporation between 12 and 16 hours. Thymidine incorporation then rapidly accelerated between 20 and 28 hours following stimulation.

Intriguingly, 100 nM PD0325901 appeared to not affect the quantity of thymidine incorporation during this early induction phase. Of note, in these initial experiments we assayed only pooled samples in replicate (thus precluding our ability to perform biologically-independent statistical analysis).

Based on these preliminary findings, we performed a similar experiment under different timing conditions. Here, we stimulated growth factor-deprived

mast cells with FBS/SCF for sixteen hours and subsequently added ^{3}H-thymidine, thus reducing unnecessary exposure to radiation, which could possibly modulate normal cellular proliferation (176). In this experiment, we again found little thymidine incorporation two and four hours following its addition (representing hours 18 and 20 of total FBS/FBS stimulation) (Figure 29b, bottom graph). However, FBS/SCF-stimulated mast cells incorporated the largest quantity of thymidine between approximately 28 and 36 hours. This increased rate then plateaued by 48 hours. Moreover, 100 nM PD0325901 dramatically reduced the large increase in thymidine incorporation observed between 28 and 36 hours in FBS/SCF stimulated WT, *E1-KO*, and *E2-KO* mast cells.

Overall, these experiments indicated that the transition to S-phase after growth factor deprivation requires at least twelve hours of FBS/SCF-stimulation. Additionally, they demonstrated that maximal DNA synthesis occurs between 28 and 36 hours.

Using these observations, we assessed the dependency of SCF-mediated mast cell thymidine incorporation on increasing doses of PD0325901. We performed these experiments similar to those described above, adding ^{3}H-thymidine 16 hours after stimulation with 10% FBS and 80 ng/mL SCF. The plates were placed at -80°C at 24 and 48 hours (total) following stimulation. Here, we found no statistical difference in the sensitivity of WT, *E1-KO*, and *E2-KO* to increasing concentrations of PD0325901 (Figure 29c). While the computed IC_{50} values for maximal inhibition of thymidine incorporation for WT, *E1-KO*, and *E2-KO* cells were 31 nM, 19 nM, and 51 nM, respectively, at 24 hours and 65 nM, 25

nM, and 26 nM, respectively, for 48 hours (both with broad 95% confidence intervals), 400 nM of PD0325901 failed to inhibit thymidine incorporation to less than 20% of the untreated value in both WT and *E2-KO* cells. Intriguingly, 400 nM of PD0325901 diminished thymidine incorporation in *E1-KO* cells to 5% of their untreated values, and, by using a student's unpaired t-test, these differences between *E1-KO* versus WT and *E2-KO* cells were significant at $p<0.05$. However, they were not significant in the appropriately applied 2-way ANOVA with Bonferroni correction. Whether or not *E1-KO* cells are indeed more sensitive to PD0325901 inhibition requires further examination.

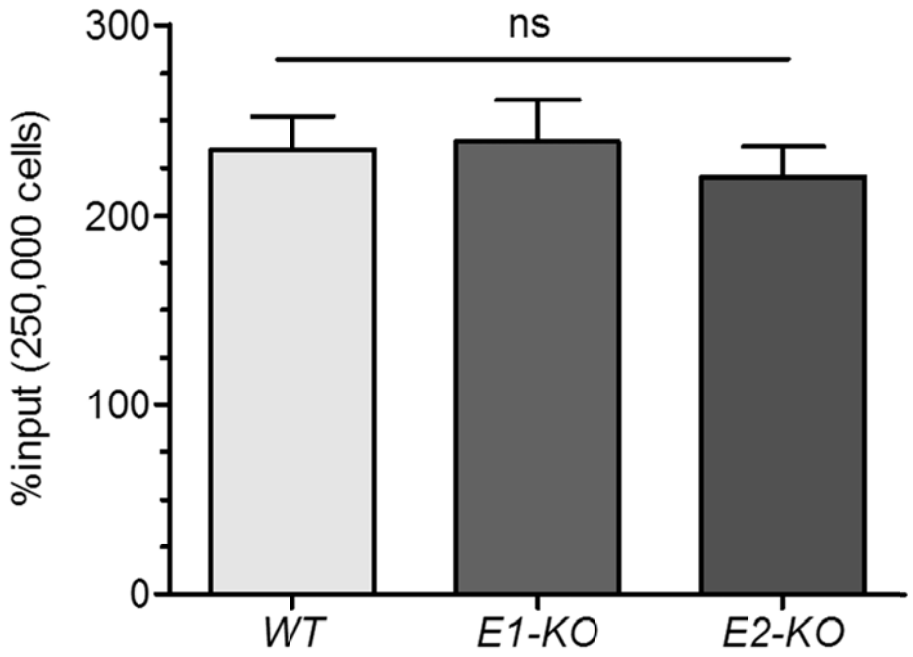

Figure 28

Figure 28. *E1-KO, E2-KO*, and WT mast cells show no difference in SCF-mediated proliferation. Primary cultured mast cells were deprived of IL-3 and FBS overnight and resuspended at 250,000 per mL in IMDM. One mL of cells per condition were plated in duplicate into each well of a 24-well plate. Cells were stimulated with 25 ng/mL SCF and 10% FBS and allowed to grow for 72 hours at 37°C. Cells were then enumerated by hemcytometer using trypan blue exclusion on an inverted light microscope. Cell viability was comparable among all cultures. The mean of duplicate cultures were considered the value for each biologically-independent sample (n=3). P values were not significant by either one-way ANOVA with Bonferroni correction or by student's unpaired t-tests. Error bars represent the standard error of the mean. These data represent at least two experiments performed on separate occasions using multiple biologically-independent samples per experiment.

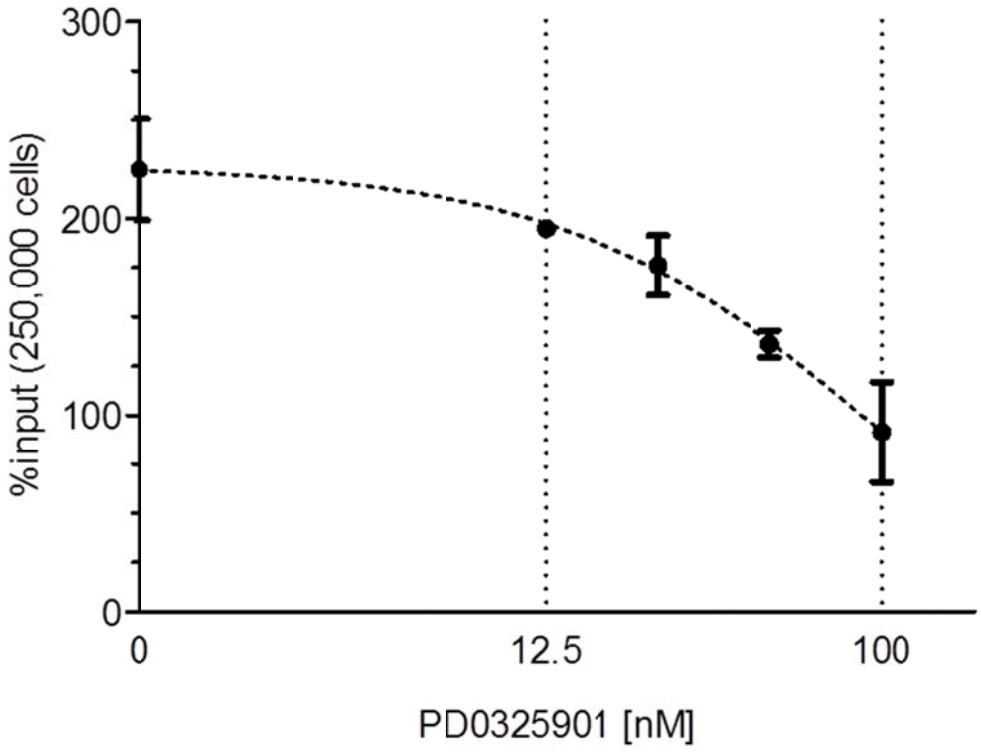

Figure 29a

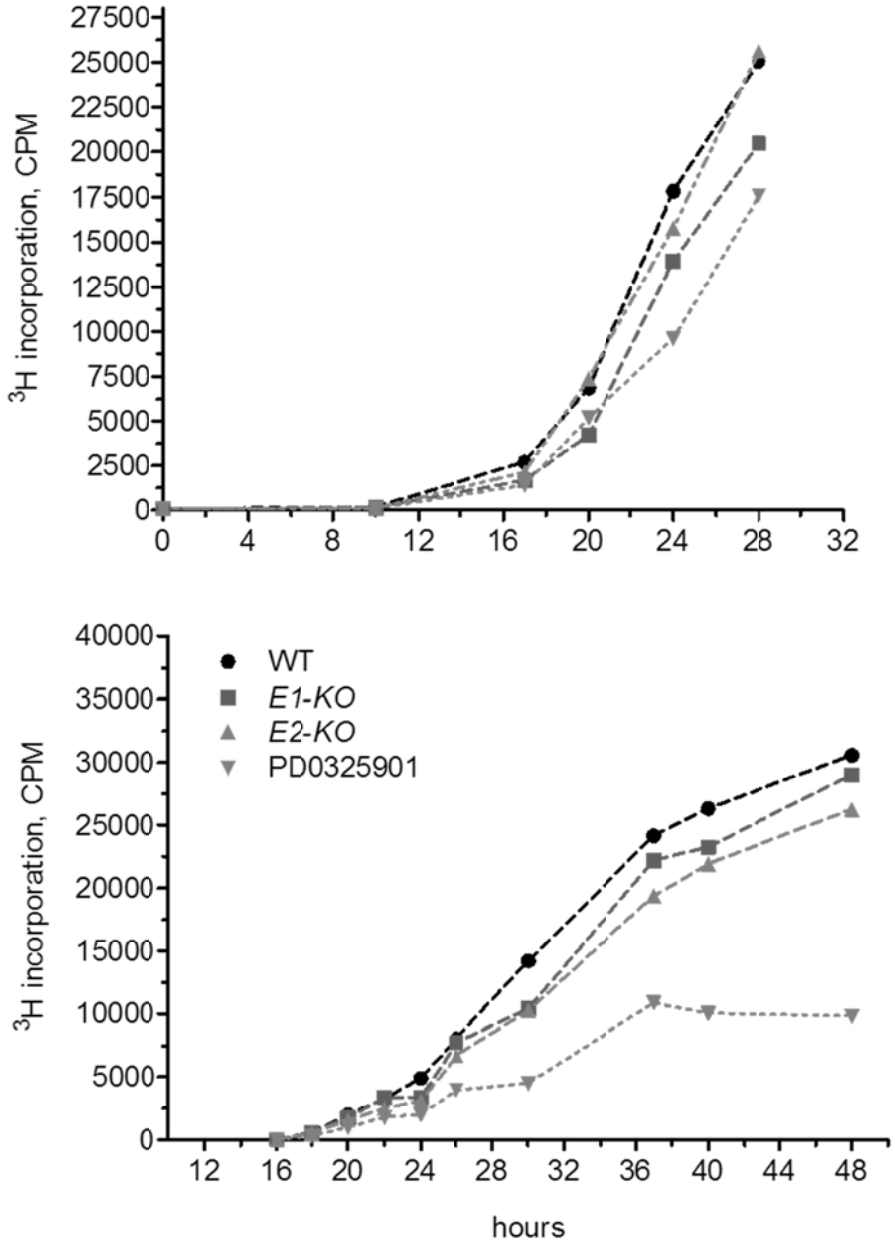
27500
25000
22500
20000
17500
15000
12500
10000
7500
5000
2500
0
^{3}H incorporation, CPM
0
4
8
12
16
20
24
28
32
40000
35000
30000
25000
20000
15000
10000
5000
0
^{3}H incorporation, CPM
WT
E1-KO
E2-KO
PD0325901
12
16
20
24
28
32
36
40
44
48
hours

Figure 29b

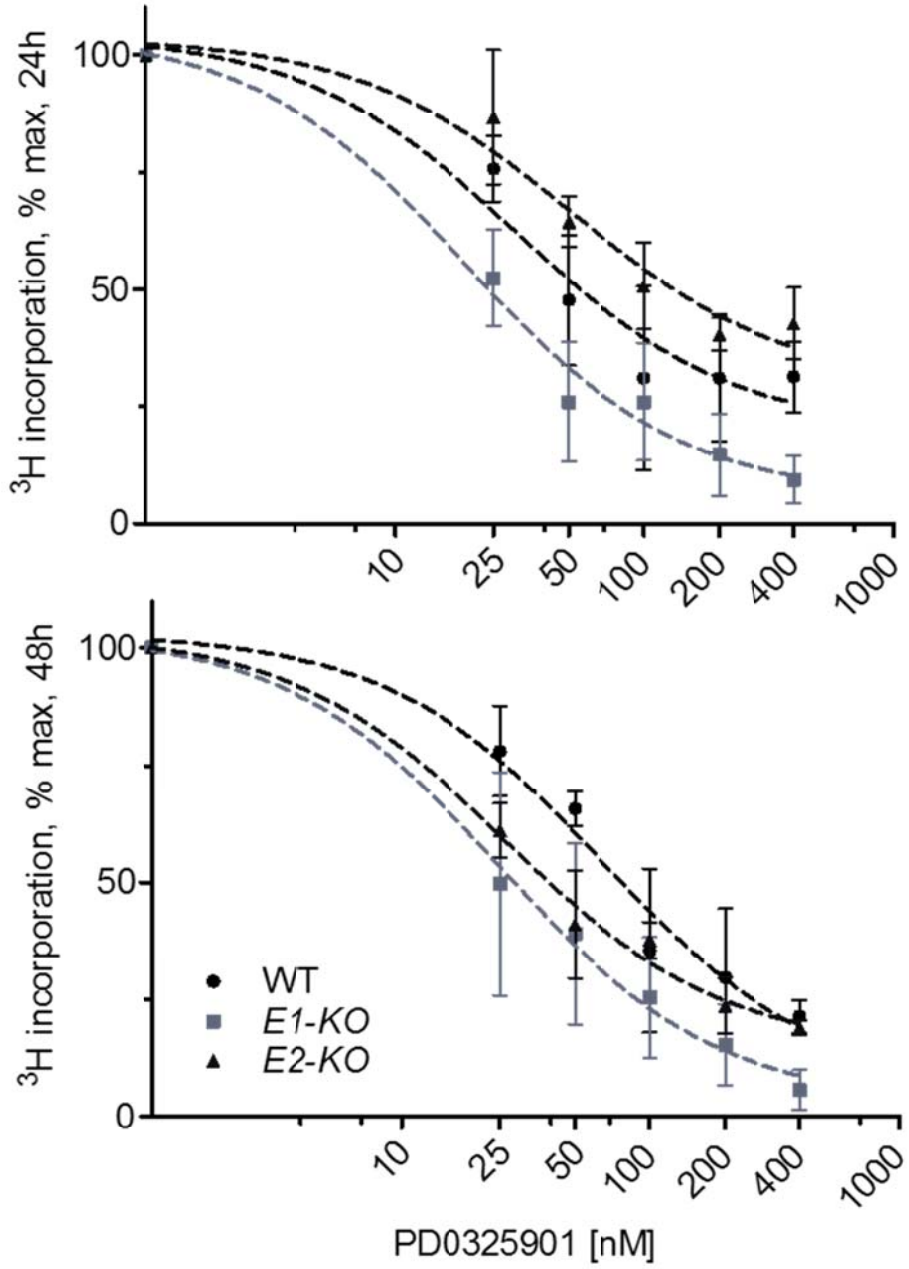
^{3}H incorporation, % max, 24h
100
50
0
10
25
50
100
200
400
1000
^{3}H incorporation, % max, 48h
100
50
0
WT
E1-KO
E2-KO
10
25
50
100
200
400
1000
PD0325901 [nM]

Figure 29c

Figure 29: Quantitative effects of genetic and chemical Mek-Erk inhibition on proliferation and thymidine incorporation. To establish the efficacy of PD0325901 in inhibiting total proliferative output, experiments were performed as described in Figure 28, but mast cells were first incubated for one hour with increasing concentrations of PD0325901 or with vehicle only before SCF/FBS stimulation. 100 nM of PD0325901 completely inhibited total mast cell proliferative output (a) (at 100 nM, mean number was 91% of input, n=3, $p<0.05$ for 100 nM versus 0, 12.5, and 25 nM by student's unpaired t-test). Error bars represent the standard error of the mean. ^{3}H-thymidine incorporation experiments were performed on 50,000 cells per well in 100 µL IMDM in 96-well plates, stimulated with 10% FBS and 80 ng/mL SCF. In initial experiments, we determined that growth factor-deprived mast cells require approximately 16 hours to begin rapidly incorporated of thymidine while finding little evidence of differences between *E1-KO*, *E2-KO*, WT cells (b) (pooled samples performed in replicate; no statistical analyses performed). By titrating PD0325901 dose, we found that IC_{50} values for all three genotypes for inhibiting thymidine incorporation are less than 100 nM, with no significant difference detected between WT, *E1-KO*, and *E2-KO* cells (c) (n=3 for each genotype, all comparisons not significant via 2-way ANOVA with Bonferroni correction). By less rigorous statistical testing, *E1-KO* cells had a significantly increased sensitivity to 400 nM PD0325901 ($p<0.05$ versus WT and *E2-KO*, student's unpaired t-test). Error bars represent the standard error of the mean. In a and c, dotted lines indicate a three-parameter logarithmic non-linear regression.

PD0325901 reduces BrdU incorporation in SCF-stimulated mast cells.

From our experiments above, we concluded that 100 nM PD0325901 can completely inhibit the generation of new mast cell progeny following SCF-stimulation (Figure 29a). However, we still detected thymidine incorporation in SCF-stimulated mast cells up to 400 nM PD0325901, implying that some cells had begun S-phase despite the Mek-Erk inhibition. We considered that similar to our HSC studies, some PD0325901-inhibited mast cells may enter S-phase but ultimately not divide. Alternatively, PD0325901-inhibited mast cells may begin synthesizing DNA but subsequently fail to complete S-phase.

To further explore the cell cycle kinetics of PD0325901-inhibited mast cells, we performed BrdU pulse-chase experiments. Here, mast cells were stimulated with SCF and FBS for 24 hours, pulsed with BrdU for 2 hours, and the BrdU washed out. Some cultures were then re-treated with PD0325901, testing continued Mek-Erk inhibition on cells which had already begun the cell cycle (i.e. those cells detected as $BrdU^+$). We stopped different cultures at three, six, and twelve hours following the BrdU washout, predicting that these would be sufficient times to detect a full cycle of cell division in BrdU-labeled cells.

In our preliminary experiment, we found that 100 nM PD0325901 reduced the frequency of cells incorporating BrdU and, thus, entering S-phase, by approximately half (Figure 30, left column). After washing out the BrdU and reapplying PD0325901, we found no additional reduction in the frequency of cells that completed the cell cycle, as indicated by the shift in 7-AAD staining of total nuclear material (Figure 30, second and third columns). Therefore, once these

SCF-stimulated mast cells incorporated BrdU, 100 nM PD0325901 appeared incapable of preventing completion of mitosis.

These chemical findings contrast our genetic findings in HSCs in vivo, whereby *DKO* HSCs incorporated BrdU and had increased nuclear material but failed to proliferate. Of critical note, though, our mast cell proliferation experiments rely on a single cytokine (SCF) as well as chemical inhibitors in vitro. To further assay this phenomenon, we are now developing more precise methods, including genetic ablation of *Erk1/2* in primary mature mast cells.

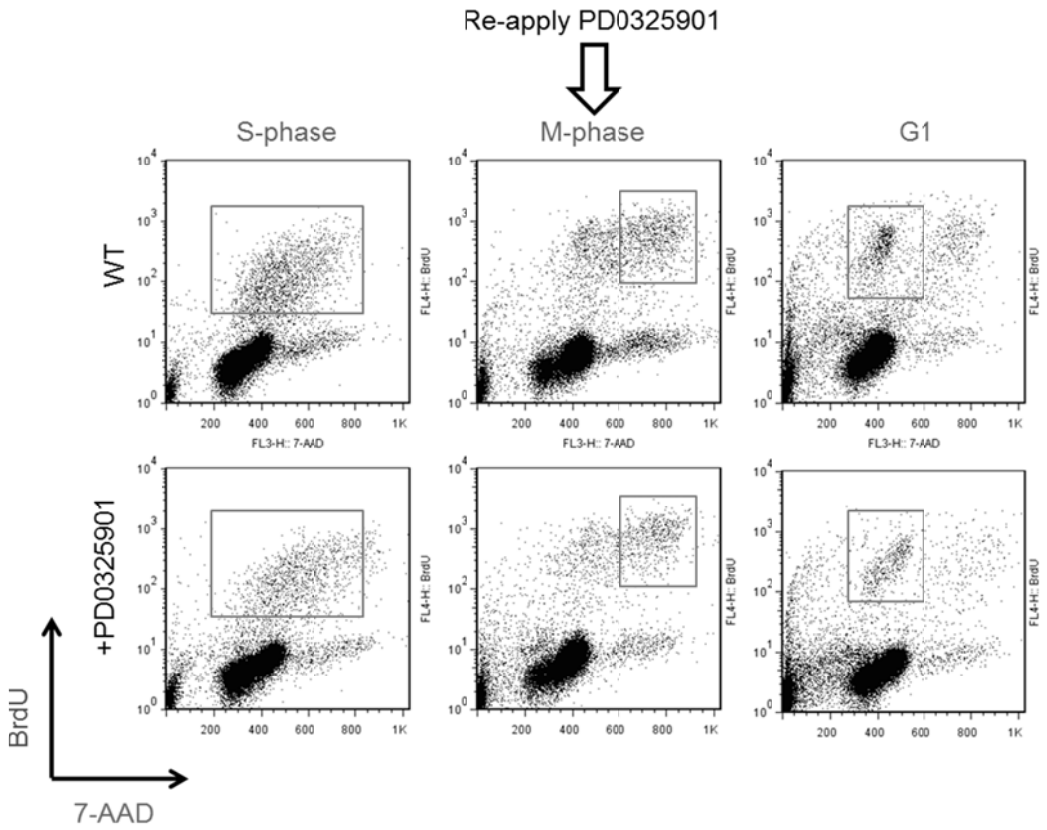
Re-apply PD0325901
S-phase
M-phase
G1
WT
+PD0325901
BrdU
7-AAD
FL3-H:: 7-AAD
FL4-H:: BrdU

Figure 30

Figure 30: PD032901 reduces BrdU incorporation but not mitosis in SCF-stimulated mast cells. Mast cells were deprived of growth factors overnight and stimulated with SCF and FBS. Some cultures were pre-incubated with 100 nM PD0325901. After 24 hours at 37°C, cultures were pulsed with BrdU for two hours and the BrdU subsequently washed out. PD0325901 was then re-introduced to some cultures. While PD0325901 reduced the frequency of cells incorporating BrdU (left column), it did not prevent cells from completing mitosis (middle and right columns). This is non-quantitative and representative of only one experiment.

Erk negatively regulates SCF-mediated mast cell cytokine production.

Mast cells modulate inflammation via the production and secretion of multiple pro- and anti-inflammatory cytokines. To obtain a general assessment of which cytokines SCF-stimulated mast cells elaborate, we first performed a broad-based cytokine array to screen 40 possible candidates. This experiment relies on membranes pre-coated with specific antibodies which are subsequently incubated with supernatant from SCF-stimulated mast cells (i.e. mast cell conditioned media). Mast cells were first deprived of growth factors overnight then stimulated with SCF (only) for six hours. The conditioned media was then harvested for protein assays.

In these experiments, SCF stimulation induced the release of MCP-1 (JE), MIP-1α, IL-6, TNF-α, M-CSF, GM-CSF, and IL-13 (Figure 31). All of these cytokines serve generally inflammatory roles, including the stimulation and recruitment of macrophages, monocytes, and other myeloid cells (e.g. M-CSF, MIP-1α)(177, 178). Interestingly, SCF stimulation reduced the secretion of IL-16, a cytokine which principally modulates T cell function. We found that WT and *Nf1*$^{+/-}$ mast cell secreted a similar panel of cytokines, with the exception that *Nf1*$^{+/-}$ mast cells secreted an increased amount compared to WT mast cells. Of the total 40 proteins tested, only those cytokines with an appreciable change compared to samples from non-stimulated mast cells are shown.

Using the data derived from this qualitative screen, we next performed a quantitative multiplex assay to determine the consequence of single *Erk* genetic inhibition, of PD0325901 treatment, and of increasing SCF concentrations on

cytokine secretion in a quantitative fashion. Conditioned media was prepared similarly to the cytokine array experiment. Following supernatant isolation, samples were processed with a multiplex kit including analytes for M-CSF, TNF-α, MCP-1, MIP-1α, MIP-1β, G-CSF, GM-CSF, IL-10, IL-13, and IL-6.

Largely, we found no difference among *E1-KO*, *E2-KO*, and WT samples in their capacity to generate increasing levels of the six cytokines in response to SCF stimulation (Figure 32a). If anything, single *Erk* disruption tended to increase the quantity of cytokine produced and secreted (although, through this experiment's sample size, the variability of cytokine levels produced from biologically-independent samples was too great to detect any differences). As an intriguing parallel to this possible increase in cytokine production from single *KO* mast cells, pre-incubation with PD0325901 followed by SCF-stimulation potentiated maximal cytokine secretion in a dose-dependent manner. These data are statistically presented for the 100 ng/mL SCF stimulation condition (Figure 32b), revealing that PD0325901 increased the quantity of MCP-1, MIP-1α, MIP-1β, IL-13, andIL-6 in mast cell conditioned media. Only TNF-α secretion did not change with PD0325901 treatment. Potentially, then, Erk negatively regulates the production of multiple cytokines in the SCF-stimulated mast cell. The implications of this, as well as ongoing experiments to further elucidate this observation, are presented in the Discussion.

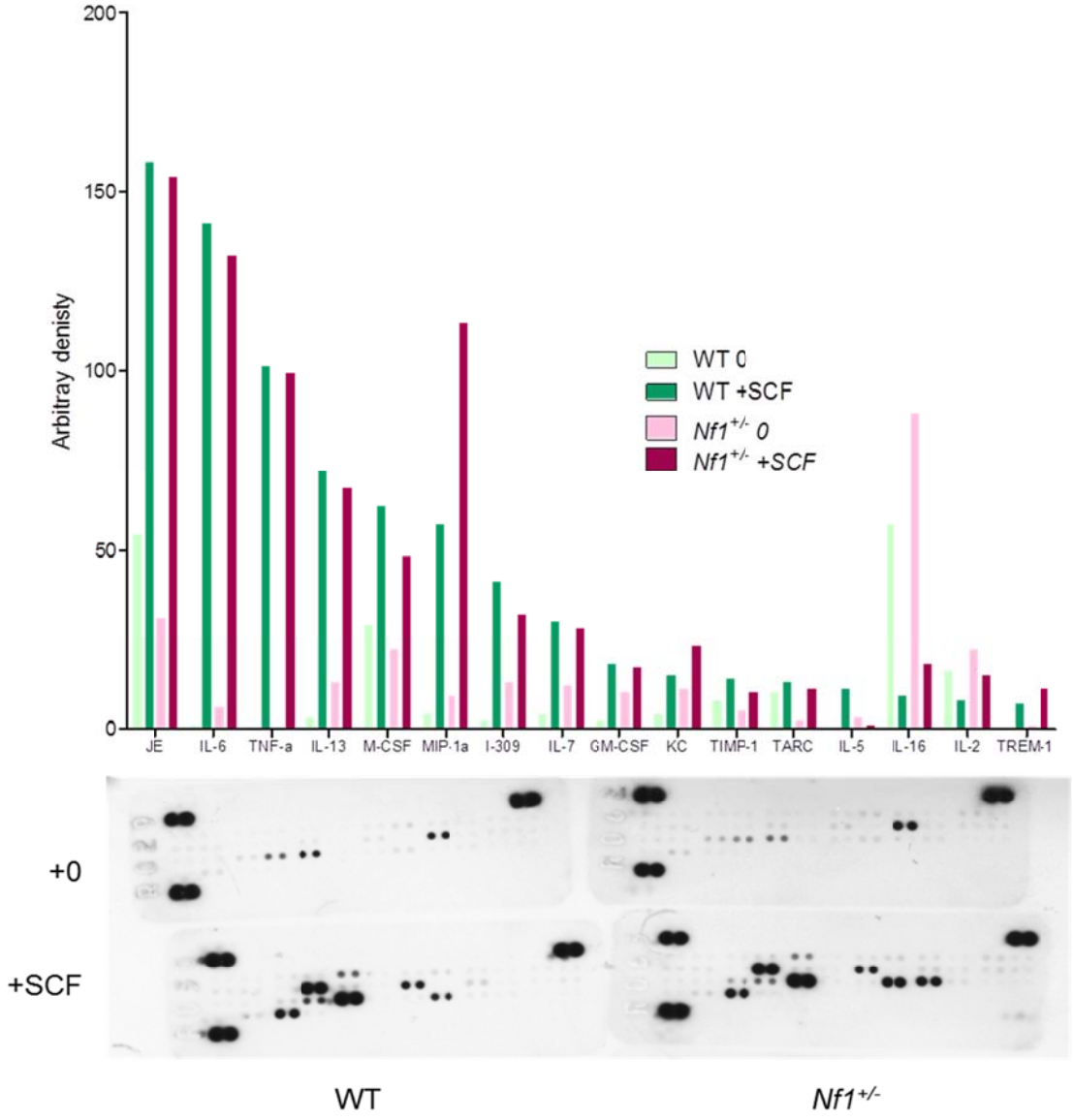
200
150
100
50
0
Arbitray denisty
WT 0
WT +SCF
Nf1+/- 0
Nf1+/- +SCF
JE
IL-6
TNF-a
IL-13
M-CSF
MIP-1a
I-309
IL-7
GM-CSF
KC
TIMP-1
TARC
IL-5
IL-16
IL-2
TREM-1
+0
+SCF
WT
Nf1+/-

Figure 31

Figure 31: Cytokine array delineates multiple cytokines secreted from SCF-stimulated primary mast cells. Mast cells were derived of growth factors overnight and stimulated for six hours with 50 ng/mL SCF at 37°C. The supernatants were harvested and assayed by a mouse-specific cytokine array panel, which detects up to 40 individual proteins using immunological methods. As can be seen on the exposed immunoblot membranes (bottom), each cytokine antibody is spotted in duplicate (the three dense duplicates in the upper left, right and lower left corner are positive controls; lower right is negative control). Using arbitrary density units, all spots were quantified and graphed, revealing several cytokines induced by SCF stimulation. Only those cytokines with an appreciable change between the stimulated and non-stimulated state are shown. Similar experiments were performed on two other occasions.

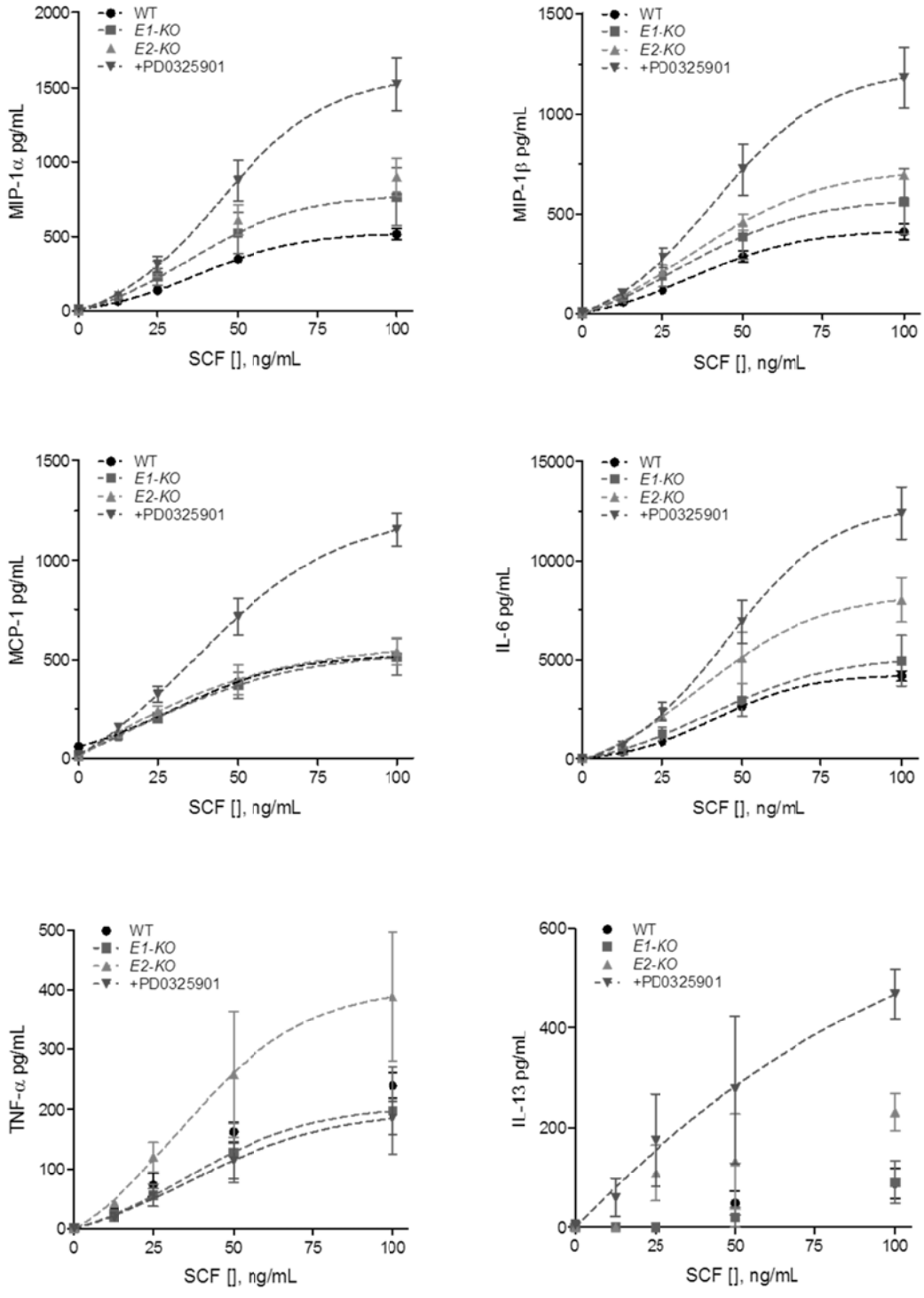
WT
E1-KO
E2-KO
+PD0325901
MIP-1α pg/mL
MIP-1β pg/mL
MCP-1 pg/mL
IL-6 pg/mL
TNF-α pg/mL
IL-13 pg/mL
SCF [], ng/mL

Figure 32a

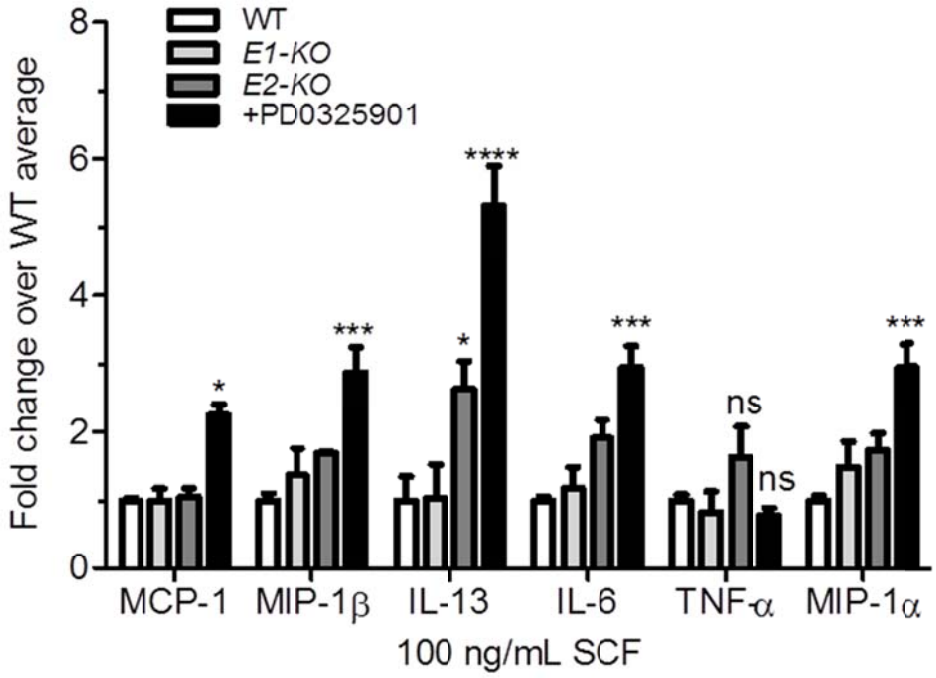
WT
E1-KO
E2-KO
+PD0325901
Fold change over WT average
8
6
4
2
0
*
***
*
****
***
ns
ns
***
MCP-1
MIP-1β
IL-13
IL-6
TNF-α
MIP-1α
100 ng/mL SCF

Figure 32b

Figure 32: Quantitative assessment of *Erk* disruption and PD0325901 treatment on mast cell cytokine production. Mast cell supernatant was produced according to the protocol described for the cytokine array panel, although, in this experiment, cells were pre-treated with 100 nM PD0325901 and stimulated with increasing concentrations of SCF. Few differences were detected between *E1-KO*, *E2-KO*, and WT samples. However, PD0325901 treatment potentiated cytokine production (a) (n=5 for WT, 4 for *E1-KO*, 2 for *E2-KO*, and 3 for PD0325901-treated). Error bars represent the standard error of the mean. The lines indicate a three-parameter logarithmic regression. Detailed analyses comparing the fold change over the mean WT value for each cytokine at 100 ng/mL SCF revealed that all analyzed cytokines except TNF-α were potentiated by PD0325901 treatment (b) (*$p<0.05$, ***$p<0.001$, ****$p<0.0001$, as compared to WT, 2-way ANOVA with Bonferroni correction). *E2-KO* cells also tended to have increased cytokine production, with the value for IL-13 at 100 ng/mL significant at a confidence of $p<0.05$. All other comparisons to WT were not significant. For statistical purposes, each individual WT value was compared to the aggregate WT mean for each cytokine. Error bars represent the standard error of the mean.

Erk-dependent biochemical alterations in the mast cell.

To understand the mechanisms of how single *KO* mast cells functionally compensate for the loss of the complementary Erk isoform, we performed various biochemical experiments on SCF-stimulated mast cells. As foundation, in total bone marrow cells we regularly observed mildly increased Erk1 levels in *E2-KO* cells, as can be seen in Figure 3c and as emphasized in Figure 33a. However, we did not detect a reciprocal increase in Erk2 levels in *E1-KO* cells (in either total bone marrow cells or mature mast cells). These data may indicate a preponderant biochemical importance for Erk2 in marrow and mast cell function, although more precise studies are needed in specific cell lineages.

Intriguingly, and perhaps in complement to the above observations, we found that total Erk2 levels *decreased* in some *E1-KO* mast cells. However, the Erk2 phosphorylation level subsequent to SCF-stimulation approximated WT samples (Figure 33b). Other reports have suggested that loss of Erk1 can lead to hyperphosphorylation of Erk2 and, subsequently, increased biological activity in Erk-mediated functions (124, 128, 179). Hypothetically, then, disruption of *Erk1* increases the availability of Erk2 to phosphorylation by Mek1/2. If true, this observation in cultured mast cells may indicate that the *E1-KO* mast cell down-regulates total Erk2 protein level to prevent abnormal hyperactivation of Erk2. These conjectures are supported by the observation of few, if any, functional differences between SCF-stimulated WT, *E1-KO*, and *E2-KO* mast cells. It should be noted that we observed this down-regulation of Erk2 only under specific conditions (and especially in older culture age mast cells).

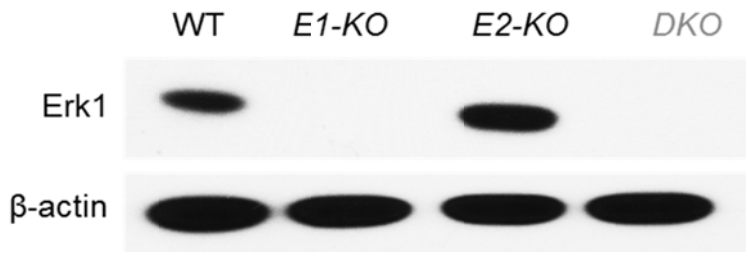

Figure 33a

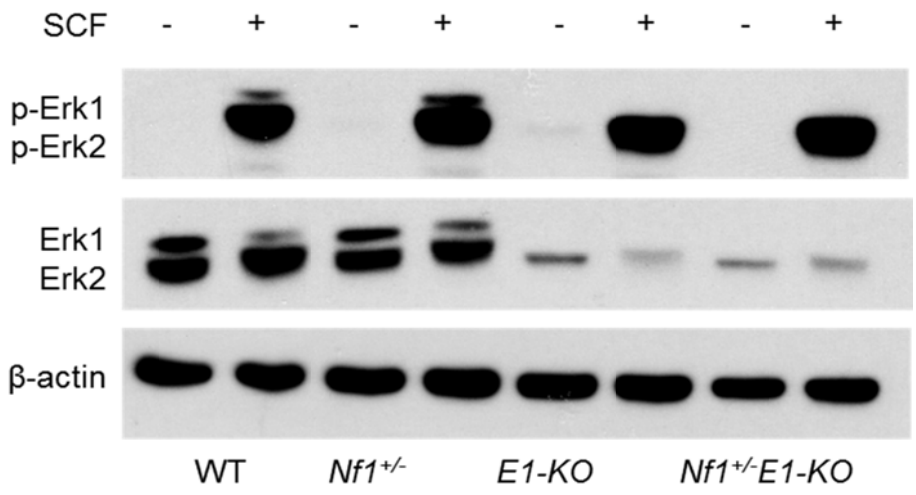

Figure 33b

Figure 33: Biochemical consequence of single *Erk* disruption on the level and phosphorylation status of the complementary isoform. In bone marrow cells, we consistently observed a mild increase in the level of Erk1 protein in *E2-KO* samples (a). We did not detect increased Erk2 levels in protein from *E1-KO* samples. This phenomenon can also be appreciated in Figure 3c. In mature primary mast cells, *E1-KO* cells downregulate Erk2 levels as the cells age (b). However, the total quantity of phosphorylated Erk2 approximates WT levels following SCF-stimulation.

As we considered that *E1-KO* and *E2-KO* mast cells may develop irregularities in PI-3K-directed pathways, we next examined phosphorylation events in the canonical PI-3K pathway. We additionally assayed SCF-mediated regulation of β-catenin, a signaling mechanism as yet not described for primary cultured mast cells. Several reports instigated our interest in β-catenin signaling in the mast cell. These reports demonstrated that PI-3K pathways can influence β-catenin translocation, that Erk1/2 kinase activity can directly influence β-catenin levels through the phosphorylation of GSK3β and $p90^{rsk}$, and that SCF-stimulated mast cell-like leukemia lines demonstrate nuclear β-catenin in vitro (180-182). Based on these publications, we postulated that β-catenin activity may be important to SCF-mediated mast cell function and that Erk may influence this activity.

Indeed, we found that SCF induces the phosphorylation of β-catenin at serine 552 and serine 675 (Figure 34). These findings corresponded with potent phosphorylation of Akt at serine 473 and GSK3β at serine 9, a signaling axis which can modulate β-catenin stability and activity in the context of co-activated receptor tyrosine kinase and Wnt/Frizzled pathways. In this schema, PI-3K activated Akt phosphorylates and inactivates GSK3β, which, along with other events, permits β-catenin to escape sequestration and marking for proteasomal degradation by ubiquitin ligases. Disinhibited β-catenin can then undergo phosphorylation, translocate to the nucleus, and activate mitogenic transcription factors (183).

Intriguingly, PD0325901 inhibited the upregulation of β-catenin in SCF-stimulated primary mast cells (Figure 35a). We typically observed maximal β-catenin levels at thirty minutes to one hour following stimulation with FBS/SCF. At one hour, PD0325901 reduced this level to near non-stimulated levels. To assess the sub-cellular localization of β-catenin, we imaged mast cells via deconvolution microscopy, finding that PD0325901 could inhibit the SCF-stimulated translocation of β-catenin to the nucleus (Figure 35b). While compelling, these findings need further validation and quantification, especially through immunoblot of specific cell fractions under varying conditions (e.g. nucleus, membrane, organelles with/without FBS at various time points).

Of note, we did not detect a change in phospho-Akt levels at thirty minutes, one hour, and three hours following SCF-stimulation and PD0325901-inhibition (Figure 35a). However, phospho-Akt increased substantially at six hours during PD0325901 treatment. While the phosphorylation of GSK3β at serine 9 largely followed the levels of phospho-Akt at thirty minutes and six hours, PD0325901 treatment mildly depressed phospho-GSK3β^{S9} at one and three hours. Interestingly, Hu et al reported that Erk kinase activity directly primes GSK3β for additional phosphorylation at its serine 9 by $p90^{rsk}$ (which is also dependent on Erk activity) (183), leading us to suspect that Mek-Erk directly modulates GSK3β^{S9} phosphorylation and β-catenin levels. Although we have ongoing experiments to assess interactions between Erk, GSK3β, and p90rsk, we have not as yet co-immunoprecipitated these proteins in SCF-stimulated primary mast cells, as Hu et al did in immortalized cell lines (183). In our

alternate strategy, we are using deconvolution microscopy to identify possible co-localizations between the three molecules during SCF/FBS stimulation.

Finally, we have taken a particular interest in the PD0325901-mediated potentiation of phospho-Akt at six hours. As found in the Discussion, we suggest potential mechanisms by which this potentiation of phospho-Akt may explain increased cytokine production in PD0325901-inhibited cells. We also delineate several experiments to further explore these hypotheses.

We next assessed β-catenin levels in *E1-KO* and *E2-KO* mast cells, finding great variability in the basal level of β-catenin in the mutants as compared to WT samples (Figure 35c). In the experiment shown, β-catenin levels in single Erk *KO*s do not follow FBS/SCF-stimulation but rather persist throughout the stimulation period. We have obtained similar results in analyses of *E1-KO* mast cells by confocal microscopy (data not shown), and we are continuing to assess the specifics of this β-catenin deregulation in single *Erk-KO* mast cells. As now, our data suggest that single Erk-KO mast cells compensate biochemically by upregulating β-catenin levels, perhaps through aberrant phosphorylation of Akt^{S473}. However, our data indicate that the short-term induction of β-catenin requires at least some measure of Mek-Erk activity. To address these intricacies, we are examining SCF-stimulated mast cells lacking β-catenin (*Mx1Cre*$^{+}$*Ctnnb1*$^{flox/flox}$) as well as further exploring biochemical alterations in mast cells genetically disrupted for *Erk1/2*, as described below.

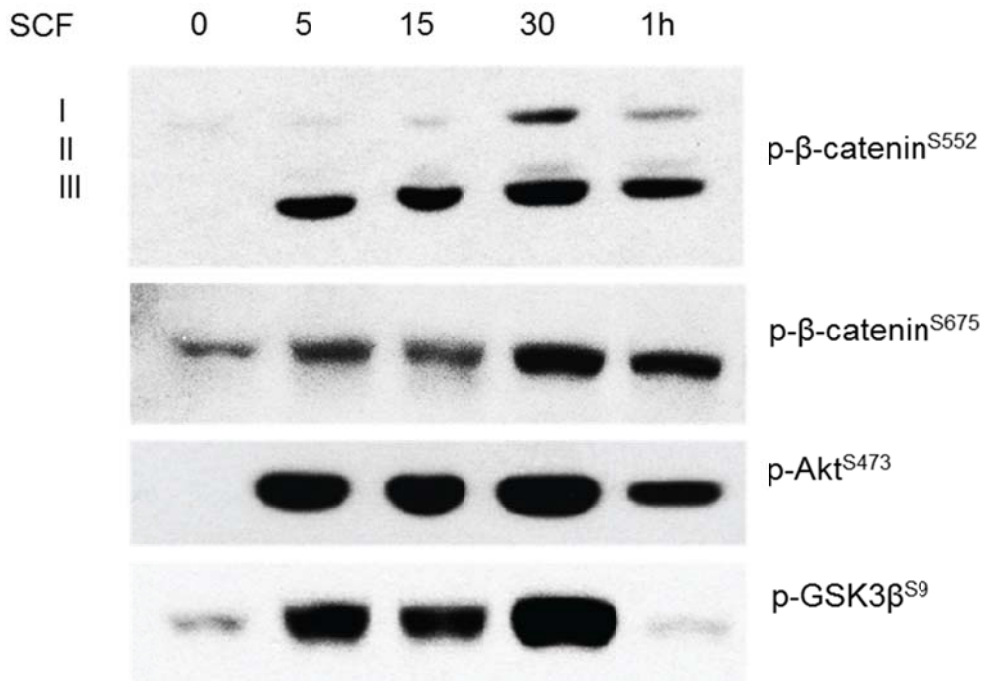
SCF
0
5
15
30
1h
I
II
III
p-β-catenin^{S552}
p-β-catenin^{S675}
p-Akt^{S473}
p-GSK3β^{S9}

Figure 34

Figure 34: SCF induces the phosphorylation of β-catenin. Mast cells were deprived of growth factors overnight, standardized by concentration, and stimulated with recombinant murine SCF. Proteins were extracted in SDS-PAGE buffer, electrophoresed, and transferred to a PVDF membrane for subsequent analysis by immunoblotting. The phosphorylation of β-catenin's serine residue 552 was readily observed after five minutes and peaked at thirty minutes following stimulation. Phosphorylation of serine residue 675 occurred more slowly but also peaked at thirty minutes following stimulation. These phosphorylation events correlated with the activating phosphorylation of Akt^{S473} and the inhibitory phosphorylation of $GSK3\beta^{S9}$ which, in canonical β-catenin signaling, precedes β-catenin activation and nuclear translocation.

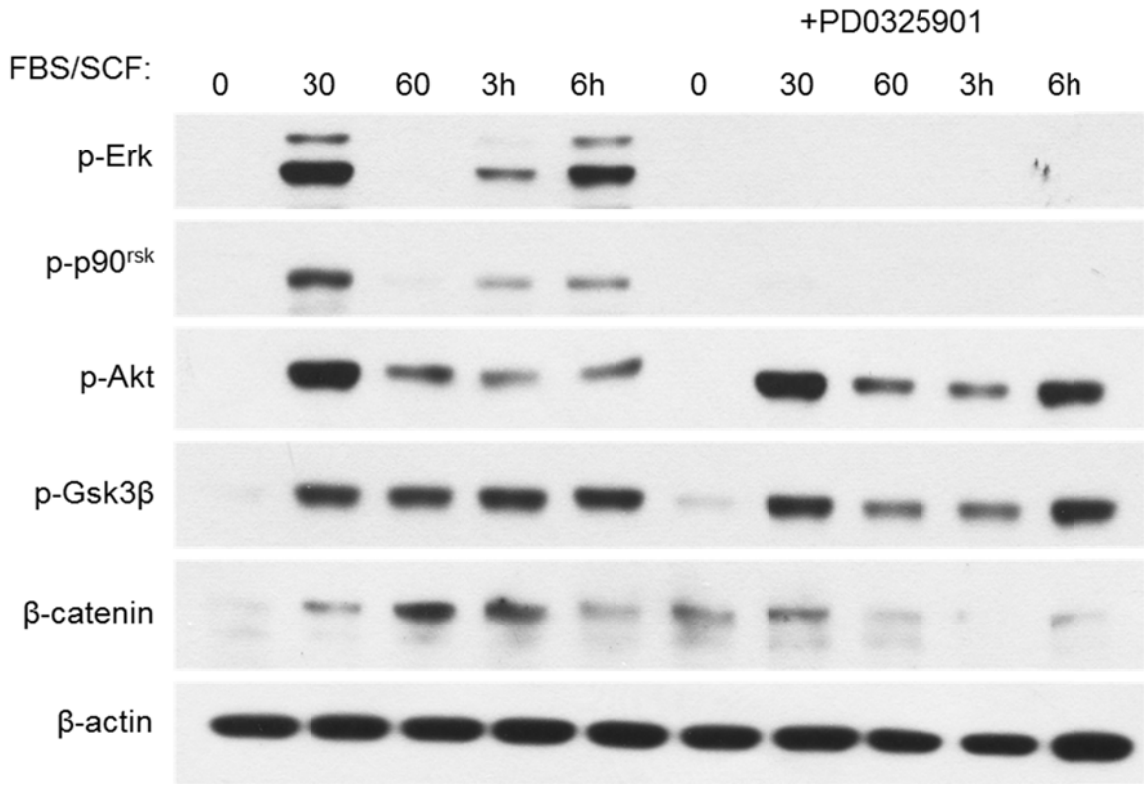
+PD0325901
FBS/SCF:
0
30
60
3h
6h
0
30
60
3h
6h
p-Erk
p-p90rsk
p-Akt
p-Gsk3β
β-catenin
β-actin

Figure 35a

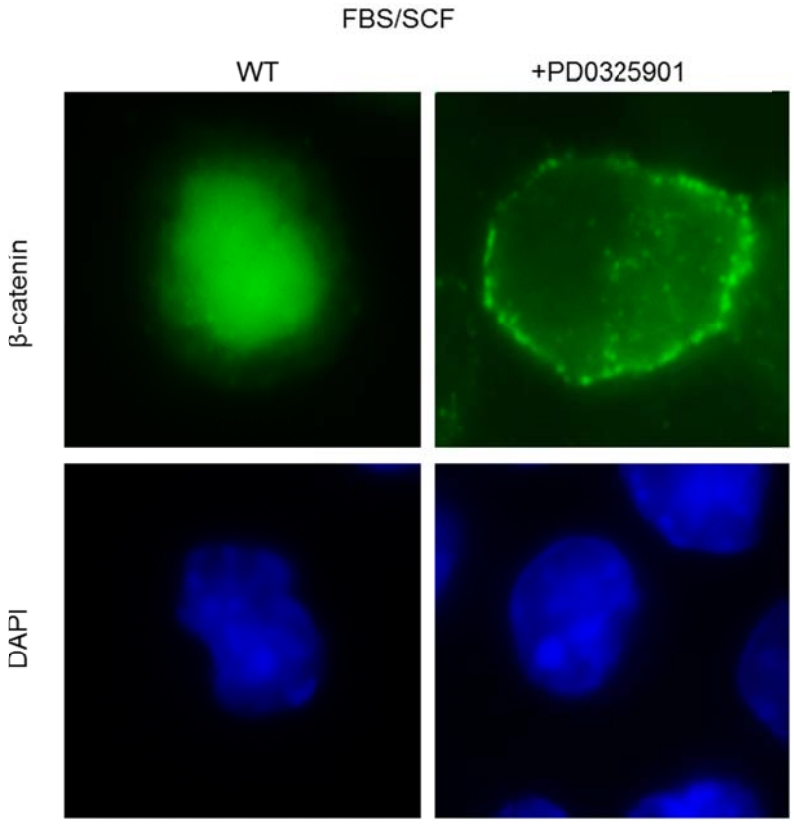

Figure 35b

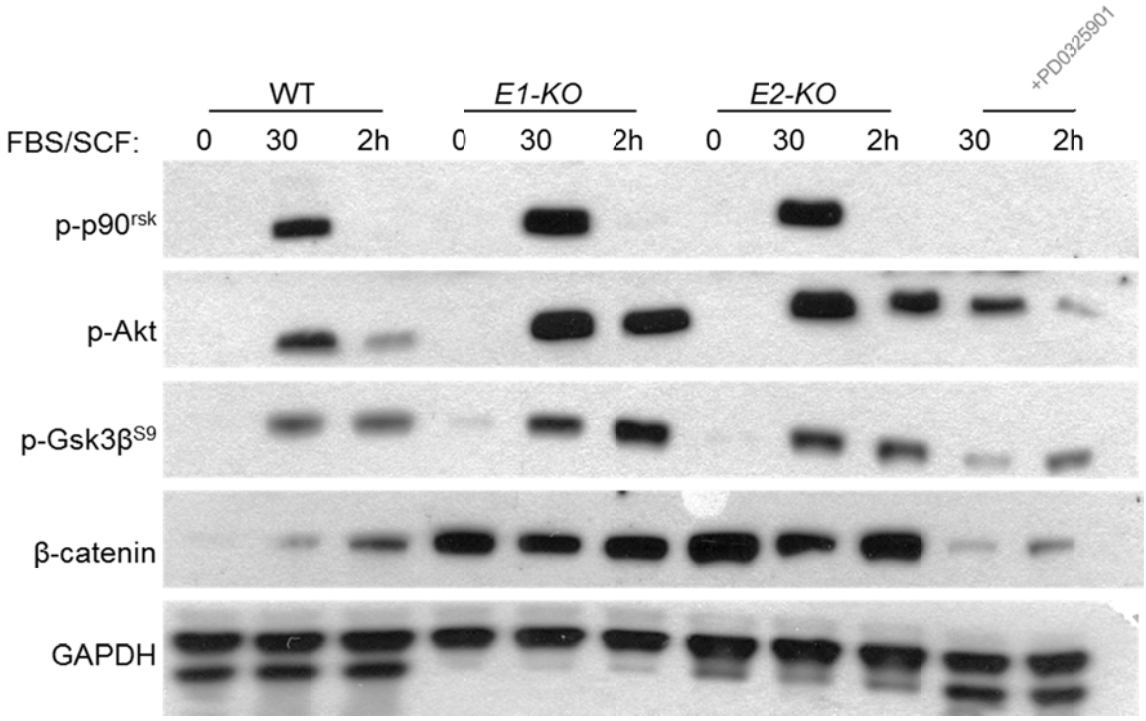
WT
E1-KO
E2-KO
+PD0325901
FBS/SCF:
0
30
2h
0
30
2h
0
30
2h
30
2h
p-p90rsk
p-Akt
p-Gsk3βS9
β-catenin
GAPDH

Figure 35c

Figure 35: β-catenin is upregulated, phosphorylated, and translocates to the nucleus in SCF-stimulated mast cells in a Mek-Erk-dependent manner. Mast cells were deprived of IL-3 overnight, suspended to a standard concentration, and stimulated with FBS/SCF, with or without pre-incubation in100 nM PD0325901. PD0325901 prevented the upregulation of β-catenin, as seen at one hour, three hours, and six hours in non-treated cells (a). PD0325901 also diminished the level of phospho-GSK3β^{S9} while potentiating the level of phospho-Akt^{S473} at six hours following SCF-stimulation. Similar immunoblots were performed on at least three separate occasions. Stimulated mast cells were fixed and processed for deconvolution microscopy, which revealed translocation of β-catenin to the nucleus that could be inhibited by PD0325901 (c) (shown: one hour following SCF/FBS stimulation). *E1-KO* and *E2-KO* mast cells demonstrated deregulated β-catenin levels, even under basal conditions (c). This immunoblot is representative of several different experiments, although the level of β-catenin deregulation varied widely at non-stimulated conditions in *E1-KO* and *E2-KO* mast cells. By contrast, β-catenin levels were consistently negligible in non-stimulated WT cells.

Erk1/2 disruption in primary mature mast cells.

We have developed a foamy/lentiviral gene delivery system to create *DKO* mast cells while bypassing the requirement for Erk in myeloid precursor proliferation and mast cell cytopoiesis. This integrating retrovirus delivers a previously described *Cre:eGFP* fusion construct (184) placed under control of the splenic-focus forming virus promoter (SFFV), which potently drives transcription in eukaryotic cells. We generated this *Cre:eGFP* delivery system in conjunction with our collaborator Helmut Hannenberg, who had previously constructed proprietary elements within the viral, polymerase, and foamyviral envelop plasmids (185, 186)(Figure 36a).

Through this three-plasmid, 293T-based packaging system (modified from protocols described previously (187-189)), we have achieved titers at 10^9 to 10^{10} virions/mL, allowing us to achieve up to 70% transduction efficiency in mast cells, as measured by eGFP-positivity on flow cytometry. Importantly, we did not observe virus-induced toxicity, even at 10^3 virions per mast cell (we have routinely used 25-50 virions/cell). In our initial experiment, we found clear evidence that delivery of *Cre:eGFP* to the genome of primary mature mast cells can successfully excise floxed alleles (Figure 36b). In ongoing experiments, we are using FACS to sort GFP^+ cells prior to analysis, thus ensuring putatively pure populations of *Erk2*-excised mast cells. The immunoblot in 36b shows antibody detection of protein isolated from an unsorted cell population and therefore underrepresents the efficiency of the Cre in excising the *Erk2* allele.

To date, we are unaware of any study demonstrating foamy/lentiviral transduction of primary murine mast cells, although one study achieved lentiviral transduction in human mast cells (190) while another reported adenoviral transduction in rodent mast cells (191). This tool and protocol should prove useful for future studies in primary cultured mast cells. Moreover, our initial data have recapitulated aspects of the PD0325901 data, showing that *Erk1*$^{-/-}$*Erk2*$^{flox/flox}$ cells transduced with *Cre:eGFP* (effectively, *DKO*) diminish to near zero over time (Figure 36c), suggesting a primarily proliferative defect in *DKO* mast cells. We did not observed rapid loss of or increased apoptosis in this population, suggesting that *Erk* disruption does not preclude mast cell survival in tissue culture.

We are currently repeating deconvolution microscopy experiments, the multiplex assays, and our hemcytometer-, thymidine-, and BrdU-based proliferation studies on *Cre:eGFP* transduced mast cells, seeking to refine our PD0325901-based results. Based on our immunoblot data, we hypothesize that although *DKO* mast cells will not proliferate, they may demonstrate enhanced survival secondary to compensatory deregulation in PI-3K-Akt pathways. Potentially, *DKO* cells will demonstrate an ability to enter S-phase or to complete mitosis, providing genetic granularity as to the functions of Erk1/2 in this specific cell and receptor-ligand system.

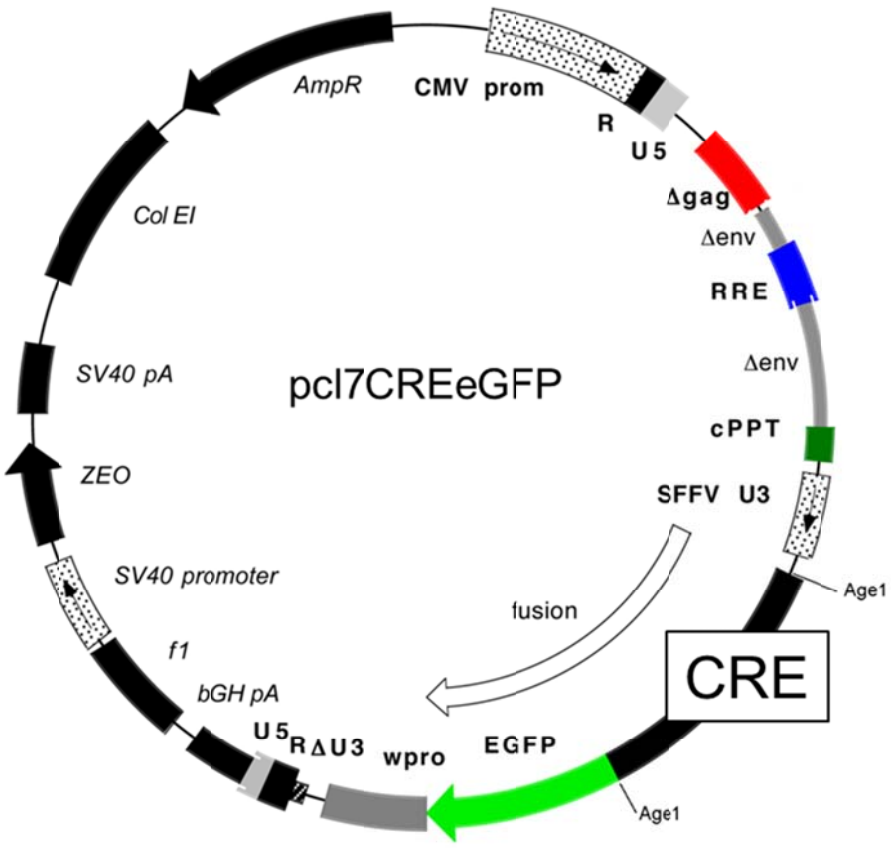
AmpR
CMV prom
R
U5
Δgag
Δenv
RRE
Δenv
cPPT
SFFV U3
Age1
CRE
fusion
EGFP
Age1
wpro
U5
RΔU3
bGH pA
f1
SV40 promoter
ZEO
SV40 pA
Col EI
pcl7CREeGFP

Figure 36a

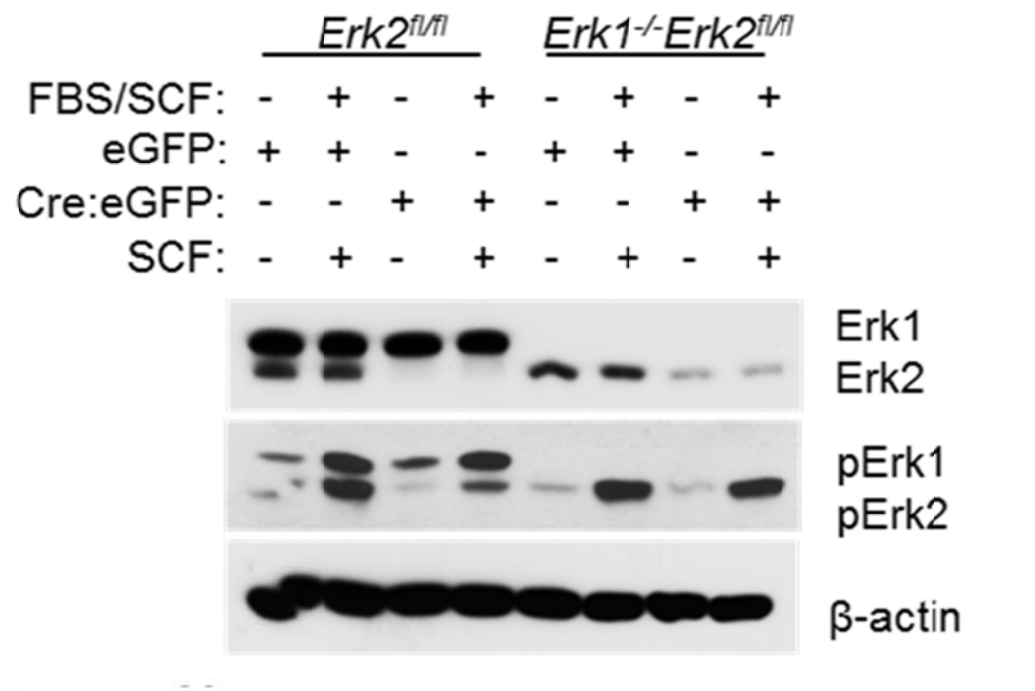
Erk2fl/fl
Erk1-/-Erk2fl/fl
FBS/SCF: - + - + - + - +
eGFP: + + - - + + - -
Cre:eGFP: - - + + - - + +
SCF: - + - + - + - +
Erk1
Erk2
pErk1
pErk2
β-actin

Figure 36b

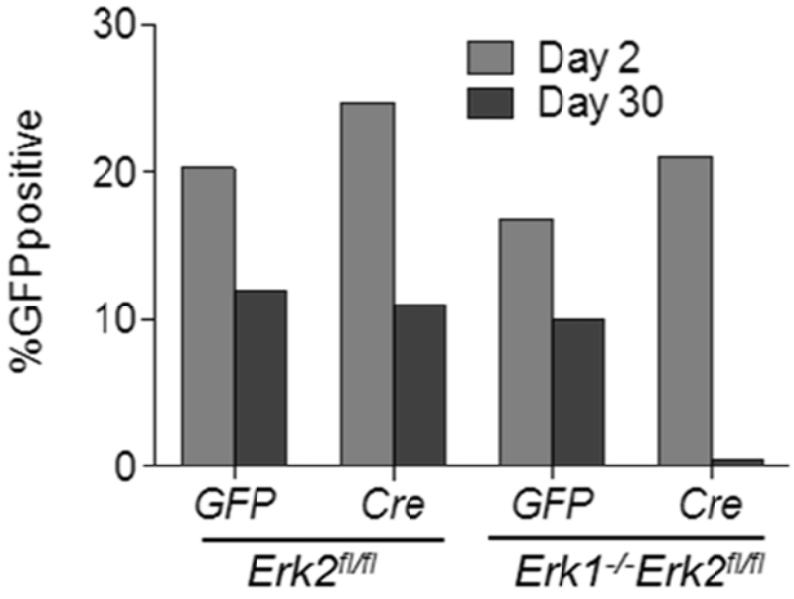
30
20
10
0
%GFPpositive
Day 2
Day 30
GFP
Cre
GFP
Cre
Erk2fl/fl
Erk1-/-Erk2fl/fl

Figure 36c

Figure 36: Efficient transduction of primary mast cells with a *Cre:eGFP* carrying lentivirus. Using standard cloning techniques, we inserted a *Cre:eGFP* fusion gene downstream of the SFFV promoter in a lentivirus encoding plasmid (a). To generate virus, we co-transfected 293T cells with pcl7CREeGFP, a plasmid encoding a foamyviral envelope, and a plasmid encoding viral polymerases. Transduced mast cells carrying the $Erk2^{flox/flox}$ allele demonstrated reduction in Erk2 protein, which was more notable in *E2-KO* samples as compared to *DKO* samples (b) (immunoblot was performed on unsorted mast cells following transduction, and some Erk2 signal is expected). Four week old mast cells were transduced with pcl7CREeGFP, and after four weeks of culture in IL-3, the putative *DKO* population ($Erk1^{-/-}Erk2^{flox/flox}$ cells that were Cre:eGFP^{+}) disappeared (c).

PD0325901 reduces mast cell infiltration in NF1-associated tumors.

Based on our findings of a critical requirement for Erk in mast cell cytopoiesis and SCF-stimulated proliferation, we hypothesized that PD0325901 would dampen mast cell invasion associated with tumorigenesis and maintenance in the *Nf1*$^{flox/-}$; *PeriostinCre*$^{+}$ tumor model. These mice harbor biallelic inactivation of *Nf1* in Schwann cell precursors and *Nf1*$^{+/-}$ supporting tissues, including the hematopoietic system (24, 82, 83, 86). As Yang et al have previously shown, *Nf1*$^{+/-}$ bone marrow accelerates tumor formation and progression in these mice, as compared to tumor mice transplanted with WT bone marrow (24). Although we had initially intended to transplant these mice with *Nf1*$^{+/-}$*Erk1*$^{-/-}$*Erk2*$^{flox/flox}$ hematopoietic stem cells, our prior studies suggested that *DKO* HSCs would fail to sustain hematopoiesis or generate mast cells and therefore preclude our ability to genetically study the consequence of dual *Erk* disruption on plexiform neurofibroma formation and maintenance.

We initiated the PD0325901 study in mice containing validated plexiform neurofibromas, as assessed by PET-CT using [^{18}F] fluorodeoxyglucose (FDG). Five tumor model mice were fed by oral gavage every day for six weeks with 12.5 mg/kg PD0325901. After the six-week treatment, the mice were killed and assessed. We found that this dose of PD0325901 moderately reduced the numbers of mast cells infiltrating the dorsal root ganglia of *Nf1*$^{flox/-}$; *PeriostinCre*$^{+}$ mice (Figure 37). However, we did not find a reduction in tumor size during the course of this treatment.

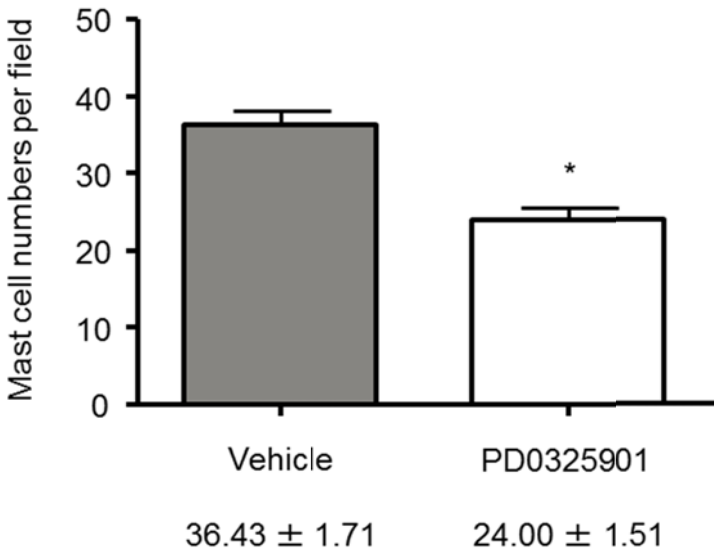
Mast cell numbers per field
50
40
30
20
10
0
*
Vehicle
PD0325901
36.43 ± 1.71
24.00 ± 1.51

Figure 37

Figure 37: PD0325901 reduces mast cell infiltration in a neurofibroma tumor model. *Nf1*$^{flox/-}$; *PeriostinCre*$^{+}$ tumor model mice with validated tumors were fed by oral gavage every day for six weeks with 12.5 mg/kg PD0325901 dissolved in 0.5% hydroxypropyl methylcellulose/0.2% Tween-80. After the six-week treatment, the mice were killed and their tissues assessed by histology. PD0325901 reduced mast cell infiltration to the hyperplastic dorsal root ganglia, as shown by quantification of mast cells per high powered field (n=5, *$p<0.01$, student's unpaired t-test).

DISCUSSION

The plexiform neurofibromas and myeloid leukemia that develop in individuals with Neurofibromatosis type 1 have no medical treatment. Both conditions create substantial morbidity and increase mortality. Specifically, nerve-impinging plexiform neurofibromas can compromise bowel and bladder dysfunction, cause sleeplessness and anorexia, and compress vital structures such as the airway, leading to suffering and death. JMML, by comparison, causes bone marrow failure and is universally fatal. Given these grim outlooks for the NF1 patient, we stress an emergent need for molecularly-targeted compounds in the management of NF1-associated tumors and leukemia.

Previous studies have shown that hyperactive Mek-Erk signaling in the hematopoietic compartment contributes to leukemic cell outgrowth as well as to the aberrant mast cell activity promoting the inflammatory microenvironment that underpins plexiform neurofibroma genesis and maintenance. Importantly, several studies have shown that *Nf1* deficient mast cells and myeloid progenitor cells demonstrate increased levels of phosphorylated Erk1/2 in response to multiple ligands, including SCF, a principal factor discussed throughout these studies.

Despite these correlative studies, little is known about the differential and combined roles of Erk1 and Erk2 in controlling SCF-mediated function in normal and diseased hematopoietic stem cells, myeloid progenitors, and mature mast cells. All prior studies in these cell types have relied on chemical Mek-Erk inhibition, principally in tissue culture and with the use of older generation agents (e.g. U0126, PD98059). Likewise, no report has heretofore explored Erk1 and

Erk2's contribution to stable, long-term hematopoiesis. While we performed these studies with an end goal of unraveling new treatments for NF1-associated disease, we focused our experiments on foundational experiments exploring Erk1 and Erk2 in hematopoiesis, myelopoiesis, and mast cell cytopoiesis and function. While these processes are prone to dysfunction in patients with genetic alterations of the *NF1* gene, they are also critical to host defense, blood generation, and homeostasis in many organisms. A better understanding of Erk1 and Erk2 in hematopoiesis not only informs the management of NF1-associated diseases, but is also informs fundamental physiological processes.

Our data overwhelmingly indicate that hematopoiesis and myelopoiesis require at least one isoform of Erk. Moreover, our genetic studies of mast cell cytopoiesis, our chemical-based experiments in mature mast cells, and our initial *DKO* genetic studies in primary cultured mast cells indicate a similar requirement for one isoform of Erk in SCF- and IL-3 mediated mast cell function. Intriguingly, our experiments indicate a broad dispensability for single Erk isoforms in hematopoiesis and SCF-mediated mast cell proliferation, although we resist a conclusion that these individual isoforms universally have no function in the presence of the other. Indeed, our own studies in osteoclasts have revealed that Erk1 critically contributes to multiple M-CSF-mediated osteoclast functions, including aberrant bone mineralization in animals transplanted long-term with *E1-KO* hematopoietic stem cells. Thus, our study reveals broad requirements for one isoform of Erk in hematopoiesis, but it does not preclude roles for Erk1 or Erk2 in specific cell lineages controlled by distinct ligand-receptor systems.

Erk and hematopoiesis

As shown here, Erk signaling critically contributes to long-term hematopoietic maintenance. As Erk1/2 activity appears to regulate cell differentiation, survival, and the G1/S transition in multiple primary cells and cell lines (114, 119, 121, 133, 192-197), we had generated at least three initial hypotheses as to the consequence of dual *Erk1/2* disruption in the hematopoietic system.

First, we hypothesized that *DKO* HSC frequency would expand relative to total marrow cellularity, representing a differentiation block, whereby HSCs could proliferate but not give rise to committed progeny. Because HSCs have a much lower proliferative index than their committed progeny (149, 150, 198), total bone marrow cellularity would still decrease and HSC number and frequency would increase. However, we found no evidence of increased HSC frequency in *DKO* bone marrow. Even so, we did find a mildly increased percentage of “lineage negative” and $CD150^{+}CD48/41^{-}$ cells, implying that at least some aspects of cell surface protein expression and perhaps differentiation require Erk. Specifically, *Erk* disruption abrogated the expression of c-kit on bone marrow cells, although it is difficult to conclude that this represents a differentiation block versus a primary proliferative deficiency (as exponentially expanding myeloid progenitors are c-kit-expressing). We also point to our colony forming assays, where *DKO* cells showed no colony formation capacity – in the case of a differentiation block, one would expect the rapid outgrowth of primitive, undifferentiated cells on highly

enriched media. In short, while we cannot rule out a differentiation block in *Erk*-disrupted HSCs, our data suggest preponderant defects in proliferation.

Second, we hypothesized that *DKO* HSCs would rapidly undergo apoptosis, leading to a decreased frequency of HSCs, hematopoietic collapse, anemia, and death. While all primary *DKO* animals died during or shortly after the polyIC regimen, we did not observe the catastrophic lethality seen in other apoptosis-inducing deletions (e.g. *Mx1Cre*$^{+}$*Cul4a*$^{flox/flox}$ mice, (199-201)). Moreover, we did not find substantial evidence of increased apoptosis in *DKO* spleen cells or bone marrow cells, and the *DKO* HSC frequency was not reduced. However, apoptosis can be difficult to detect in vivo, and we would expect cycle-arrested cells to eventually undergo cell death. Thus, increased apoptosis may be a reasonable consequence of failed proliferation, although we did not detect this phenomenon.

We also hypothesized that *Erk* disrupted HSCs would demonstrate an inability to synthesize DNA, as suggested by other studies arguing for Erk as the "master regulator" of the G1/S transition (reviewed in (114)). Surprisingly, though, we found that *DKO* HSCs incorporated BrdU and had increased nuclear material, even when assessed at different time points following the polyIC regimen. We considered that these BrdU^{+} and Pyronin Y/Hst positive HSCs may represent non-recombined cells rapidly proliferating to compensate for the loss of true *DKO* HSCs, but individually sorted HSCs failed to expand in culture. Likewise, few if any colonies formed when plating tens of thousands of bone marrow cells which would hypothetically contain equivalent numbers of HSCs to WT samples. These

data suggest to us a proliferative defect in *DKO* HSCs at a cell cycle stage beyond the G1/S transition.

Despite the mass of tissue culture data suggesting a primary role for Erk in the G1/S transition, our observations in the *DKO* HSC are not without precedence. Indeed, Erk can localize to kinetochores, spindle poles, and the midbody, leading others to hypothesize that Erk plays important roles in G2 and mitosis (202, 203). Moreover, *Erk1*/2 knockdown in engrafted epidermal keratinocytes induces G2/M arrest while knockdown in fibroblasts induces G1/S arrest, arguing that in certain cell types the G1/S transition does not depend upon Erk (115). Accordingly, Erk functions may vary by cell type, and established cell culture findings may not directly predict in vivo physiology.

Of note, our studies rely on genetic inhibition in vivo while most prior studies have relied on chemical inhibition or overexpression in vitro, secondary to stimulation by a defined growth factor. As such, Erk's modulation of the cell cycle could depend on a combination of structural interactions, kinase activities, and pathways initiated by multiple cytokines and growth factors. Future studies in the hematopoietic system could attempt to elucidate these mechanisms via restoration of transplanted HSCs with kinase-dead and other *Erk* variants prior to Cre induction. Although we are uncertain if these intricacies would directly elucidate our work with experimental therapies for NF1-associated disease, we postulate that increased mechanistic understanding will facilitate the development of targeted combinatorial therapies in the future. For example,

diseased HSCs could be induced to undergo cell cycle arrest and subsequently brought to apoptosis with a different, cycle stage-specific agent.

In addition to unraveling a novel proliferative consequence for *Erk* disruption in hematopoietic stem cells, our study critically complements a handful of other in vivo hematopoietic studies which, taken in isolation, may obfuscate the critical role for Erk pan-hematopoiesis. In the single previous assessment of dual *Erk1*/2 disruption using *Mx1Cre*, Yasuda et al reported defects in only pre-B cell expansion due to loss of Erk-dependent CREB and Elk1 activities (105). They did not assess myelopoiesis, long-term hematopoiesis, or HSC proliferation. Likewise, two other reports have shown that mice disrupted for *Erk1/2* in T cells (*pLck-cre* and *Cd4-Cre*) have greatly diminished T cell production and function (104, 204). Aggregating these findings with our findings, we have concluded that HSC proliferation and physiological hematopoiesis requires at least one Erk isoform.

Similarly, our study refines recent, conflicting conclusions derived from the use of Mek-Erk chemical inhibitors in tissue culture (reviewed in (109)). Mek inhibitors PD98059 and U0126 are used at micromolar concentrations, are prone to crystallization, and have potential off-target effects. Relying on these inhibitors, two reports have argued that Mek-Erk promotes monocyte generation while suppressing granulocytopoiesis via C/EBPα (107, 108). Contrastingly, Geest et al showed that that Mek-Erk activity controls granulocyte production from $CD34^{+}$ cells (106). And, Hsu et al suggested that Erk regulates GM colony formation from HSCs/MPPs but not from CMPs, thus implying Erk dispensability in later

precursors (110) while also arguing that Erk negatively regulates B cell production. However, our study and Yasuda et al have genetically shown that Erk positively regulates B cell production, and our colony forming assays demonstrate that *DKO* bone marrow cells (which contain phenotypically-confirmed MPPs, CMPs, GMPs, and MEPs) have little to no colony potential. Thus, our genetic data elucidate Erk1/2's importance in HSC proliferation, pan-myeloid colony formation, and stable hematopoiesis while obviating aspects of previous studies relying on chemical inhibitors in tissue culture.

Single Erk isoforms appear dispensable for hematopoietic stability, an important observation vis-à-vis recent debate over putative isoform-specific functions. For example, Erk1 negatively regulates splenic erythropoiesis (179) and fibroblast proliferation (128) while Erk2 positively regulates proliferation, survival, and differentiation in various cell types (116, 121). However, genetic studies in fibroblasts have shown both isoforms to positively contribute to proliferation, in a gene dose-dependent and isoform-independent manner (132, 133). Enhanced proliferation in some *Erk1*-disrupted cells, then, may result solely from Erk2 over-compensation (i.e. not from intrinsic negative-regulator properties). Although we detected no critical disparities between WT, *E1-KO*, and *E2-KO* hematopoietic stability, we observed reduced peripheral T cells in *E2-KO* HSC transplanted mice, recapitulating data from the previous studies using lymphocyte-specific Cre promoters (104, 204). We also examined $E1^{+/-}$*E2-KO* specimens, again finding no difference in marrow cellularity or colony formation.

Thus, we assert that each *Erk* isoform permits HSC proliferation and myelopoiesis in a binary fashion but that HSC BrdU incorporation and, potentially, S-phase entry, do not require Erk. While single isoforms appear dispensable for stable, long-term hematopoiesis, we have confirmed that Erk2 modulates T cell survival (following Fisher et al), and we have found that specific myeloid effector cells (e.g. osteoclasts) may demonstrate differential loss- or gain-of-function phenotypes secondary to *Erk1* and/or *Erk2* disruption. We reiterate that the conclusions regarding Erk function based on chemical inhibition in various cell culture systems may unnecessarily convolute our observation of a broad requirement for Erk in hematopoietic stem cell proliferation and myelopoiesis.

Taken together, our findings suggest that pharmacological Mek-Erk inhibition may be a powerful technique to modulate aspects of normal and diseased hematopoiesis. While we are principally interested in the treatment of NF1-associated leukemia and tumors, we also view the Ras-Raf-Mek-Erk axis as a critical ramifying junction in the control of normal hematopoiesis. Potentially, temporary pharmacological Mek-Erk inhibition will permit advanced, non-deleterious manipulation of the hematopoietic system.

As a potential example, recent studies have shown that treatment of mice with ACK2, an antibody directed against the c-kit antibody, induces hematopoietic stem cells to leave the bone marrow and enter the peripheral blood, allowing for a non-myeloablative HSC transplantation during this “window” period (205, 206). Such insights could allow medical practitioners to seamlessly

replace a diseased hematopoietic system while avoiding the morbidities associated with lethal irradiation and myeloablative chemotherapy. Because PD0325901 targets a critical node in the c-kit pathway, the use of this drug alone or in combination with niche clearing antibodies may accelerate egress, thus refining techniques of non-myeloablative transplantation (which are, as yet, in preclinical stages). We do not currently have data suggesting that *Erk* disruption induces niche clearance, and our genetic studies do not temporally fall within the "window" of mobilization, which typically occurs just a few days after HSC suppression. However, we anticipate discoveries to be made during hematopoietic studies of mice receiving systemic PD0325901 or other Mek-Erk inhibitors.

Finally, we view Mek-Erk pharmacological inhibition as a potentially crucial tool for modulating the course of NF1-associated JMML and other leukemia. As preliminary evidence, mice developing a virally-transformed, $Nf1^{-/-}$ leukemia lived three times as long when treated with PD0325901, although the mice still succumbed to their disease, putatively through cooperating mutations in genes encoding proteins within other pathways (157). Similarly, PD0325901 successfully treated mice harboring a myeloproliferative disease induced by an oncogenic Ras construct (158). Despite these promising studies, it remains unknown whether leukemic cell outgrowth can occur in the genetic absence of Erk1 and Erk2. To test this, we have initiated a long-term hematopoietic stem cell transplantation study assessing simultaneous *Nf1, Erk1,* and *Erk2* deletion, as shown in Figure 24. While we do not expect the results of this study to

immediately inform the treatment of NF1-associated leukemia – especially given our finding that normal hematopoiesis requires Erk – we expect to resolve the question as to whether more efficient and targeted Mek-Erk inhibitors can theoretically abolish hematopoiesis in both normal and diseased cells, regardless of cooperating mutations outside of the *Erk1* or *Erk2* locus.

Mast cells and future directions

In mouse models of plexiform neurofibroma formation, aberrant mast cell activity secondary to SCF-stimulation underpins tumor formation and maintenance. Multiple studies have shown that SCF-stimulated $Nf1^{+/-}$ mast cells have increased potency and latency in phospho-Erk1/2 signaling (reviewed in (82, 83)). However, the specific roles for Erk1 and Erk2 in the SCF-stimulated mast cell have not previously been examined genetically. In fact, functional studies of Erk activity have, as yet, relied on the older generation Mek-Erk inhibitor PD98059.

Here, we show that while Erk1 and Erk2 are largely dispensable for SCF-stimulated mast cell proliferation and cytokine synthesis, the Mek-Erk inhibitor PD0325901 efficiently prevents SCF-mediated mast cell proliferation at sub-micromolar concentrations. Throughout the course of our study, PD0325901 proved to be a potent, efficacious, stable, and highly-selective inhibitor of Mek-Erk activation. Accordingly, this molecule should serve as a valuable tool in the continued elaboration of Erk1/2 kinase functions in mast cells, especially as a complement to our ongoing development of genetic models. PD0325901 also has high oral bioavailability, making it an attractive candidate for clinical use. In

our mouse-based study of plexiform neurofibroma formation, PD0325901 treatment reduced mast cell infiltration to tumor tissue.

However, at the tested dosing schedule, PD0325901 did not reduce tumor burden. We first considered that our tested dose was not sufficient, as we were well below the toxic threshold (50-100 mg/kg) recorded in rodents (113). Additionally, we based our dosing schedule on a prior publication assessing PD0325901efficacy in inhibiting the growth of NF1-associated AML, but these transformed cells demonstrated an exquisite sensitivity to Mek-Erk inhibition, with a 10 to 100 fold lower IC_{50} for colony formation, as compared to normal bone marrow cells (157). Because neurofibroma-associated mast cells, including *Nf1*$^{+/-}$ mast cells, are not oncogenically transformed, the suppression of mast cell cytopoiesis in the hematopoietic system may require much higher circulating plasma levels of PD0325901.

However, based on our findings of a broad and critical requirement for Mek-Erk signaling in normal myelopoiesis, we have considered other consequences of high dose PD0325901 on hematopoietic stem cell and myeloid progenitor cell maintenance. As discussed above, our findings justify additional, foundational studies of myelopoiesis and in vivo mast cell function in the of PD0325901 treatment. To establish an effective PD0325901 dose for abrogating SCF-mediated mast cell cytopoiesis and recruitment to local tissue, we are implanting micro-osmotic pumps loaded with SCF into the subcutaneous tissue of WT mice, cohorts of which will receive increasing concentrations of PD0325901 by oral gavage. These findings should directly inform PD0325901's

efficacy in modulating mast cell pathophysiology in NF1-associated tumors, as deregulated Schwann cells similarly recruit mast cells to local tissues through secreted SCF.

Alternatively, PD0325901's potentiation of SCF-mediated cytokine production may lead to increased local inflammation. This increased biological activity could override the possible benefit of decreased mast cell numbers in tumor tissue. PD0325901 largely increased the level of cytokines found in the conditioned media of SCF-stimulated mast cells, including several factors known to recruit and activate macrophages (e.g. MIP, MCP). Hypothetically, activated macrophages can drive tumor vascularization, increase extracellular matrix remodeling and deposition, and further promote inflammatory microenvironments. These initial observations are challenging, and further studies will be required to weigh the benefits of mast cell number reduction against the possible short-term induction of cytokine synthesis and secretion.

The observation of increased cytokine production in PD0325901-treated mast cells also poses several mechanistic questions. We have postulated that PD0325901 potentiates cytokine synthesis through upregulation of PI-3K-dependent pathways, as a recent study has indicated a specific role for PI-3K-Akt signaling in the production of MCP-1 (207). Likewise, multiple studies have broadly implicated PI-3K in the modulation of IgE- and SCF-mediated cytokine production and release (208). In our biochemical studies, PD0325901-inhibited mast cells consistently demonstrated increased levels of phospho-Akt after four

to six hours of SCF stimulation, providing a temporal and mechanistic correlation to our observation of increased cytokine production in PD0325901-treated cells.

Hypothetically, translational level compensation for suppressed Mek-Erk signaling could increase activity in PI-3K-depedendent pathways. Several studies have shown that a decreased level of the mTOR-dependent protein IRS-1 leads to increased activation of PI-3K-Akt, a biochemical phenomenon which has plagued the clinical efficacy of mTOR inhibitors (e.g. Rapamycin) due to unintended Akt-mediated cellular mitogenesis (209). In our current line of inquiry, we are asking whether the loss of Mek-Erk activity reduces mTOR-mediated production of IRS-1, as Mek1/2-Erk1/2 have been shown to crosstalk with and potentiate the mTOR pathway (210). This reduction of IRS-1 could then disinhibit PI-3K-Akt signals and subsequent cytokine production if, indeed, cytokines primarily depend upon Akt-mediated signals.

To accomplish these goals, we are employing a variety of chemical and genetic approaches to further study SCF-stimulated primary cultured mast cells. As an example, we are assessing the effect of various inhibitors and genetic conditions on the level of the mRNAs encoding our identified cytokines. These experiments should not only elucidate the transcriptional level mechanism of control for cytokine production, but they will also ensure that PD0325901 does not simply potentiate cytokine levels through direct or indirect inhibition of secreted proteases.

We also observed mildly increased levels of phospho-Akt^{S473} and phospho-GSK3β^{S9} as well as deregulated total β-catenin levels in *E1-KO* and *E2-*

KO mast cells. These compensations within canonical and non-canonical PI-3K pathways may help normalize SCF-mediated mast cell function in the context of single *Erk* isoform disruption. Of note, *E1-KO* and *E2-KO* mast cells, while no different from WT in their SCF-mediated proliferative capacity, tended to produce more cytokine, although a larger sample size needs to be evaluated. These observations preliminarily reinforce the hypothesis that deregulated Akt signaling influences cytokine production.

Notwithstanding the deregulation of β-catenin signaling in *E1-KO* and *E2-KO* mast cells, the simple observation of SCF-induced β-catenin activity and translocation is a novel finding. As of May 2011, a PubMed search for “mast” and “catenin” reveals one relevant publication: an observation of SCF-stimulated β-catenin translocation in a mast cell leukemia line with the implication made that β-catenin activity here is correlated with oncogenesis (182). To our knowledge, no study has characterized β-catenin signaling in primary or untransformed mast cell physiology.

Intriguingly, recent investigations have unraveled intimate relationships between MAPK pathways and β-catenin. For example, Rac1-JNK signaling shuttles β-catenin to the nucleus during canonical Wnt signaling (180), and Erk1/2 can influence β-catenin levels through its phosphorylation of GSK3β (181). In the latter case, Erk physically interacts with GSK3β at a docking motif, phosphorylates it at threonine 43, and activates $p90^{rsk}$, which then phosphorylates GSK3β at serine 9 in a manner dependent on threonine 43 phosphorylation. Phosphorylated GSK3β disassociates from β-catenin, which

ceases its sequestration and degradation, allowing for its upregulation, phosphorylation, and translocation to the nucleus.

Following these observations, PD0325901 treatment of SCF-stimulated mast cells diminished the upregulation of β-catenin levels and prevented its nuclear translocation. Hypothetically, then, single *Erk* isoform disruption results in Akt hyperactivation and increased activity in Akt-GSK3β-β-catenin signaling, but the short-term silencing of Mek-Erk kinase activity abrogates this axis by preventing needed co-activating signals, such as phosphorylation of GSK3β at threonine 43. Our laboratory intends to elucidate this pathway genetically in *CRE:eGFP* lentivirus-treated *DKO* mast cells and in mast cells cultured from the bone marrow of *Mx1Cre*$^{+}$*Ctnnb1*$^{flox/flox}$ (β-catenin conditional knockout) mice. In all, we aim to assess the functional and biochemical aspects of β-catenin signaling in the mast cell, especially as it relates to signaling events in established c-kit-dependent pathways.

Finally, as with our hematopoietic studies, we found few differences in the proliferative kinetics between SCF-stimulated WT, *E1-KO*, and *E2-KO* mast cells. Our proliferation studies included thymidine incorporation assays, hemcytometer-based assays, and assays of total metabolic ability (e.g. MTT). In all of these experiments, shown and not shown, we rarely detected differences in the single *Erk KOs*, and when we did, the differences were unremarkable. By contrast, 100 nM PD0325901 efficiently inhibited total proliferative output and reduced thymidine and BrdU incorporation by about one-half. We did not detect an additional effect of PD0325901 in preventing completion of the cell cycle after S-

phase entry. We wonder how 100 nM PD0325901completely inhibited total proliferative output but reduced BrdU and thymidine incorporation by only about 50%. These data suggest that Erk's modulation of mast cell proliferation is not limited to DNA synthesis, as we had observed in *DKO* HSCs. Multiple putative explanations exist, including potential anti-proliferative or pro-apoptotic consequences of PD0325901-induced cytokine release. In short, more genetic studies of the elusive *DKO* mast cell are needed.

Conclusions

Prior to initiating our study of *Erk*-disrupted hematopoietic stem cells, we were surprised to be unable to generate *DKO* mast cells in tissue culture. In fact, this dramatic phenotype instigated our hematopoietic stem cell experiments. Multiple studies of SCF-stimulated mast cells have suggested that PI-3K-mediated pathways play the preponderant role in modulating mast cell cytopoiesis, proliferation, and migration (87, 96, 98, 101, 211-213). In the reports implicating Erk1/2 as a proliferative factor, SCF-stimulated mast cells required up to 50 μM of PD98059 to prevent proliferation, suggesting that signals in addition to the Ras-Raf-Mek-Erk cascade could contribute to cell cycle proliferation. Additionally, prior hematopoietic studies in tissue culture had implied that that Erk1/2 was dispensable in certain stages of myelopoiesis. Taken together, we labored under the assumption that *DKO* myeloid progenitors could give rise to *DKO* mast cells. Accordingly, we expected to test $Nf1^{+/-}$*DKO* mast cell function, biochemistry, and modulation of plexiform neurofibroma formation.

However, our colony assays and liquid culture experiments all indicated that mast cells could not be generated without one isoform of Erk. Based on these findings, we extended our investigation into the hematopoietic stem cell, performing long-term competitive transplantation studies to assess Erk-dependent hematopoiesis. Here, we found that the generation of nearly all myeloid cells requires one isoform of Erk, secondary to proliferative failure in the hematopoietic stem cell. Combined with other observations made in *Erk*-deficient B cells and T cells, we concluded that physiological hematopoiesis requires Erk.

These insights may inform finessed modulation of normal hematopoiesis and diseased bone marrow. Specifically, we are interested in silencing Mek-Erk activity in the treatment of NF1-associated plexiform neurofibromas, a strategy which we would hypothesize to succeed primarily through the dampening of an abnormally functioning hematopoietic system. However, our initial findings regarding potentiated cytokine synthesis have breathed an air of caution on this optimism. Notwithstanding, we also anticipate Mek-Erk inhibition as a suitable strategy for controlling NF1-associated leukemia, but the proliferative requirement for Mek-Erk activity in *Nf1*-deficient myeloid cells remains unknown.

Our data demonstrate that Erk1 and Erk2 constitute a crucial ramifying nexus for the transduction of cellular proliferative signals through multiple hematopoietic ligand-receptor systems. This nexus is so crucial, in fact, that the function of an individually-disrupted *Erk* isoform can typically be subsumed by its remaining complement, albeit with possible alterations in other biochemical pathways. These insights elucidate the importance of Erk signaling in myeloid

and hematopoietic stem cell biology and provide foundational evidence for potential uses of pharmacological Mek-Erk inhibitory agents. Our study ends with a note of caution, too, hinting that Mek-Erk inhibition may be a double-edged sword, thus imploring the need for further experimentation in mouse models of normal and diseased hematopoiesis.

REFERENCES

1. Friedman J, Gutmann, DH, Maccollin, M, Riccardi, VM. 1999. *Neurofibromatosis: phenotype, natural history, and pathogenesis.* Baltimore: The Johns Hopkins University Press. 381 pp.
2. Lubs ML, Bauer MS, Formas ME, Djokic B. 1991. Lisch nodules in neurofibromatosis type 1. *N Engl J Med* 324: 1264-6
3. Riccardi VM. 1991. Neurofibromatosis: past, present, and future. *N Engl J Med* 324: 1283-5
4. Riccardi VM. 2010. Neurofibromatosis type 1 is a disorder of dysplasia: the importance of distinguishing features, consequences, and complications. *Birth Defects Res A Clin Mol Teratol* 88: 9-14
5. Akenside M. 1768. Observations on cancers. *Med Trans Coll Phys Lond* 1: 64-92
6. Tilesius von Tilenau W. 1793. Historia pathologica singularis Cutis Turpitudinis: Jo Godofredi Rheinhardi viri L annorum. Leipzig, Germany: SL Crusius
7. Morse RP. 1999. Neurofibromatosis type 1. *Arch Neurol* 56: 364-5
8. von Recklinghausen F. 1882. *Uber die Multiplen Fibrome der Haut und ihre Beziehung zu Multiplen Neuromen*. Berlin: August Hirschwald
9. Gamble HJ, Goldby S. 1961. Mast cells in peripheral nerve trunks. *Nature* 189: 766-7
10. Baroni C. 1964. On the Relationship of Mast Cells to Various Soft Tissue Tumours. *Br J Cancer* 18: 686-91
11. Pineda A. 1965. Mast cells--their presence and ultrastructural characteristics in peripheral nerve tumors. *Arch Neurol* 13: 372-82
12. Olsson Y. 1971. Mast cells in human peripheral nerve. *Acta Neurol Scand* 47: 357-68
13. Isaacson P. 1976. Mast cells in benign nerve sheath tumours. *J Pathol* 119: 193-6
14. Greggio H. 1911. Les cellules granuleuses (Mastzellen) dans les tissus normaux et dans certaines maladies chirurgicales. *Arch. Med. Exp* 23: 323-75
15. Le LQ, Shipman T, Burns DK, Parada LF. 2009. Cell of origin and microenvironment contribution for NF1-associated dermal neurofibromas. *Cell Stem Cell* 4: 453-63
16. Zheng H, Chang L, Patel N, Yang J, Lowe L, Burns DK, Zhu Y. 2008. Induction of abnormal proliferation by nonmyelinating schwann cells triggers neurofibroma formation. *Cancer Cell* 13: 117-28
17. Wu J, Williams JP, Rizvi TA, Kordich JJ, Witte D, Meijer D, Stemmer-Rachamimov AO, Cancelas JA, Ratner N. 2008. Plexiform and dermal neurofibromas and pigmentation are caused by Nf1 loss in desert hedgehog-expressing cells. *Cancer Cell* 13: 105-16
18. Raffensperger J, Cohen R. 1972. Plexiform neurofibromas in childhood. *J Pediatr Surg* 7: 144-51

19. Serletis D, Parkin P, Bouffet E, Shroff M, Drake JM, Rutka JT. 2007. Massive plexiform neurofibromas in childhood: natural history and management issues. *J Neurosurg* 106: 363-7
20. McCaughan JA, Holloway SM, Davidson R, Lam WW. 2007. Further evidence of the increased risk for malignant peripheral nerve sheath tumour from a Scottish cohort of patients with neurofibromatosis type 1. *J Med Genet* 44: 463-6
21. Evans DG, Baser ME, McGaughran J, Sharif S, Howard E, Moran A. 2002. Malignant peripheral nerve sheath tumours in neurofibromatosis 1. *J Med Genet* 39: 311-4
22. Cavallaro G, Basile U, Polistena A, Giustini S, Arena R, Scorsi A, Zinnamosca L, Letizia C, Calvieri S, De Toma G. 2010. Surgical management of abdominal manifestations of type 1 neurofibromatosis: experience of a single center. *Am Surg* 76: 389-96
23. Wu J, Dombi E, Jousma E, Scott Dunn R, Lindquist D, Schnell BM, Kim MO, Kim A, Widemann BC, Cripe TP, Ratner N. 2011. Preclincial testing of Sorafenib and RAD001 in the Nf(flox/flox) ;DhhCre mouse model of plexiform neurofibroma using magnetic resonance imaging. *Pediatr Blood Cancer*
24. Yang FC, Ingram DA, Chen S, Zhu Y, Yuan J, Li X, Yang X, Knowles S, Horn W, Li Y, Zhang S, Yang Y, Vakili ST, Yu M, Burns D, Robertson K, Hutchins G, Parada LF, Clapp DW. 2008. Nf1-dependent tumors require a microenvironment containing Nf1+/-- and c-kit-dependent bone marrow. *Cell* 135: 437-48
25. Jakacki RI, Dombi E, Potter DM, Goldman S, Allen JC, Pollack IF, Widemann BC. 2011. Phase I trial of pegylated interferon-alpha-2b in young patients with plexiform neurofibromas. *Neurology* 76: 265-72
26. Widemann BC, Salzer WL, Arceci RJ, Blaney SM, Fox E, End D, Gillespie A, Whitcomb P, Palumbo JS, Pitney A, Jayaprakash N, Zannikos P, Balis FM. 2006. Phase I trial and pharmacokinetic study of the farnesyltransferase inhibitor tipifarnib in children with refractory solid tumors or neurofibromatosis type I and plexiform neurofibromas. *J Clin Oncol* 24: 507-16
27. Demestre M, Herzberg J, Holtkamp N, Hagel C, Reuss D, Friedrich RE, Kluwe L, Von Deimling A, Mautner VF, Kurtz A. 2010. Imatinib mesylate (Glivec) inhibits Schwann cell viability and reduces the size of human plexiform neurofibroma in a xenograft model. *J Neurooncol* 98: 11-9
28. Packer RJ, Rosser T. 2002. Therapy for plexiform neurofibromas in children with neurofibromatosis 1: an overview. *J Child Neurol* 17: 638-41; discussion 46-51
29. Franco CB, Chen CC, Drukker M, Weissman IL, Galli SJ. Distinguishing mast cell and granulocyte differentiation at the single-cell level. *Cell Stem Cell* 6: 361-8
30. Metz M, Piliponsky AM, Chen CC, Lammel V, Abrink M, Pejler G, Tsai M, Galli SJ. 2006. Mast cells can enhance resistance to snake and honeybee venoms. *Science* 313: 526-30

31. Kalesnikoff J, Galli SJ. 2008. New developments in mast cell biology. *Nat Immunol* 9: 1215-23
32. Galli SJ, Grimbaldeston M, Tsai M. 2008. Immunomodulatory mast cells: negative, as well as positive, regulators of immunity. *Nat Rev Immunol* 8: 478-86
33. Galli SJ, Tsai M. 2008. Mast cells: versatile regulators of inflammation, tissue remodeling, host defense and homeostasis. *J Dermatol Sci* 49: 7-19
34. Chabot B, Stephenson DA, Chapman VM, Besmer P, Bernstein A. 1988. The proto-oncogene c-kit encoding a transmembrane tyrosine kinase receptor maps to the mouse W locus. *Nature* 335: 88-9
35. Galli SJ, Tsai M, Wershil BK. 1993. The c-kit receptor, stem cell factor, and mast cells. What each is teaching us about the others. *Am J Pathol* 142: 965-74
36. Tsai M, Takeishi T, Thompson H, Langley KE, Zsebo KM, Metcalfe DD, Geissler EN, Galli SJ. 1991. Induction of mast cell proliferation, maturation, and heparin synthesis by the rat c-kit ligand, stem cell factor. *Proc Natl Acad Sci U S A* 88: 6382-6
37. Taylor AM, Galli SJ, Coleman JW. 1995. Stem-cell factor, the kit ligand, induces direct degranulation of rat peritoneal mast cells in vitro and in vivo: dependence of the in vitro effect on period of culture and comparisons of stem-cell factor with other mast cell-activating agents. *Immunology* 86: 427-33
38. Coussens LM, Werb Z. 2002. Inflammation and cancer. *Nature* 420: 860-7
39. Coussens LM, Werb Z. 2001. Inflammatory cells and cancer: think different! *J Exp Med* 193: F23-6
40. Hanahan D, Weinberg RA. 2000. The hallmarks of cancer. *Cell* 100: 57-70
41. Riccardi VM. 1981. Cutaneous manifestation of neurofibromatosis: cellular interaction, pigmentation, and mast cells. *Birth Defects Orig Artic Ser* 17: 129-45
42. Riccardi VM. 1987. Mast-cell stabilization to decrease neurofibroma growth. Preliminary experience with ketotifen. *Arch Dermatol* 123: 1011-6
43. Riccardi VM. 1993. A controlled multiphase trial of ketotifen to minimize neurofibroma-associated pain and itching. *Arch Dermatol* 129: 577-81
44. Bollag G, Clapp DW, Shih S, Adler F, Zhang YY, Thompson P, Lange BJ, Freedman MH, McCormick F, Jacks T, Shannon K. 1996. Loss of NF1 results in activation of the Ras signaling pathway and leads to aberrant growth in haematopoietic cells. *Nat Genet* 12: 144-8
45. Zhang YY, Vik TA, Ryder JW, Srour EF, Jacks T, Shannon K, Clapp DW. 1998. Nf1 regulates hematopoietic progenitor cell growth and ras signaling in response to multiple cytokines. *J Exp Med* 187: 1893-902
46. Ikuta K, Weissman IL. 1992. Evidence that hematopoietic stem cells express mouse c-kit but do not depend on steel factor for their generation. *Proc Natl Acad Sci U S A* 89: 1502-6

47. Barker D, Wright E, Nguyen K, Cannon L, Fain P, Goldgar D, Bishop DT, Carey J, Baty B, Kivlin J, et al. 1987. Gene for von Recklinghausen neurofibromatosis is in the pericentromeric region of chromosome 17. *Science* 236: 1100-2
48. Seizinger BR, Rouleau GA, Ozelius LJ, Lane AH, Faryniarz AG, Chao MV, Huson S, Korf BR, Parry DM, Pericak-Vance MA, et al. 1987. Genetic linkage of von Recklinghausen neurofibromatosis to the nerve growth factor receptor gene. *Cell* 49: 589-94
49. Fountain JW, Wallace MR, Bruce MA, Seizinger BR, Menon AG, Gusella JF, Michels VV, Schmidt MA, Dewald GW, Collins FS. 1989. Physical mapping of a translocation breakpoint in neurofibromatosis. *Science* 244: 1085-7
50. Wallace MR, Marchuk DA, Andersen LB, Letcher R, Odeh HM, Saulino AM, Fountain JW, Brereton A, Nicholson J, Mitchell AL, et al. 1990. Type 1 neurofibromatosis gene: identification of a large transcript disrupted in three NF1 patients. *Science* 249: 181-6
51. Viskochil D, Buchberg AM, Xu G, Cawthon RM, Stevens J, Wolff RK, Culver M, Carey JC, Copeland NG, Jenkins NA, et al. 1990. Deletions and a translocation interrupt a cloned gene at the neurofibromatosis type 1 locus. *Cell* 62: 187-92
52. Cawthon RM, Weiss R, Xu GF, Viskochil D, Culver M, Stevens J, Robertson M, Dunn D, Gesteland R, O'Connell P, et al. 1990. A major segment of the neurofibromatosis type 1 gene: cDNA sequence, genomic structure, and point mutations. *Cell* 62: 193-201
53. Marchuk DA, Saulino AM, Tavakkol R, Swaroop M, Wallace MR, Andersen LB, Mitchell AL, Gutmann DH, Boguski M, Collins FS. 1991. cDNA cloning of the type 1 neurofibromatosis gene: complete sequence of the NF1 gene product. *Genomics* 11: 931-40
54. Ledbetter DH, Rich DC, O'Connell P, Leppert M, Carey JC. 1989. Precise localization of NF1 to 17q11.2 by balanced translocation. *Am J Hum Genet* 44: 20-4
55. Fountain JW, Wallace MR, Brereton AM, O'Connell P, White RL, Rich DC, Ledbetter DH, Leach RJ, Fournier RE, Menon AG, et al. 1989. Physical mapping of the von Recklinghausen neurofibromatosis region on chromosome 17. *Am J Hum Genet* 44: 58-67
56. Li Y, O'Connell P, Breidenbach HH, Cawthon R, Stevens J, Xu G, Neil S, Robertson M, White R, Viskochil D. 1995. Genomic organization of the neurofibromatosis 1 gene (NF1). *Genomics* 25: 9-18
57. Shilyansky C, Lee YS, Silva AJ. 2010. Molecular and cellular mechanisms of learning disabilities: a focus on NF1. *Annu Rev Neurosci* 33: 221-43
58. Sergeyev AS. 1975. On the mutation rate of neurofibromatosis. *Humangenetik* 28: 129-38
59. Park VM, Pivnick EK. 1998. Neurofibromatosis type 1 (NF1): a protein truncation assay yielding identification of mutations in 73% of patients. *J Med Genet* 35: 813-20

60. Messiaen LM, Callens T, Mortier G, Beysen D, Vandenbroucke I, Van Roy N, Speleman F, Paepe AD. 2000. Exhaustive mutation analysis of the NF1 gene allows identification of 95% of mutations and reveals a high frequency of unusual splicing defects. *Hum Mutat* 15: 541-55
61. Maertens O, De Schepper S, Vandesompele J, Brems H, Heyns I, Janssens S, Speleman F, Legius E, Messiaen L. 2007. Molecular dissection of isolated disease features in mosaic neurofibromatosis type 1. *Am J Hum Genet* 81: 243-51
62. Praxedes LA, Pereira FM, Mazzeu JF, Costa SS, Bertola DR, Kim CA, Vianna-Morgante AM, Otto PA. 2010. An Illustrative Case of Neurofibromatosis Type 1 and NF1 Microdeletion. *Mol Syndromol* 1: 133-5
63. Dorschner MO, Sybert VP, Weaver M, Pletcher BA, Stephens K. 2000. NF1 microdeletion breakpoints are clustered at flanking repetitive sequences. *Hum Mol Genet* 9: 35-46
64. Wiest V, Eisenbarth I, Schmegner C, Krone W, Assum G. 2003. Somatic NF1 mutation spectra in a family with neurofibromatosis type 1: toward a theory of genetic modifiers. *Hum Mutat* 22: 423-7
65. Sabbagh A, Pasmant E, Laurendeau I, Parfait B, Barbarot S, Guillot B, Combemale P, Ferkal S, Vidaud M, Aubourg P, Vidaud D, Wolkenstein P. 2009. Unravelling the genetic basis of variable clinical expression in neurofibromatosis 1. *Hum Mol Genet* 18: 2768-78
66. Hawes JJ, Tuskan RG, Reilly KM. 2007. Nf1 expression is dependent on strain background: implications for tumor suppressor haploinsufficiency studies. *Neurogenetics* 8: 121-30
67. Upadhyaya M, Huson SM, Davies M, Thomas N, Chuzhanova N, Giovannini S, Evans DG, Howard E, Kerr B, Griffiths S, Consoli C, Side L, Adams D, Pierpont M, Hachen R, Barnicoat A, Li H, Wallace P, Van Biervliet JP, Stevenson D, Viskochil D, Baralle D, Haan E, Riccardi V, Turnpenny P, Lazaro C, Messiaen L. 2007. An absence of cutaneous neurofibromas associated with a 3-bp inframe deletion in exon 17 of the NF1 gene (c.2970-2972 delAAT): evidence of a clinically significant NF1 genotype-phenotype correlation. *Am J Hum Genet* 80: 140-51
68. Xu GF, O'Connell P, Viskochil D, Cawthon R, Robertson M, Culver M, Dunn D, Stevens J, Gesteland R, White R, et al. 1990. The neurofibromatosis type 1 gene encodes a protein related to GAP. *Cell* 62: 599-608
69. Gutmann DH, Collins FS. 1993. The neurofibromatosis type 1 gene and its protein product, neurofibromin. *Neuron* 10: 335-43
70. Gutmann DH, Boguski M, Marchuk D, Wigler M, Collins FS, Ballester R. 1993. Analysis of the neurofibromatosis type 1 (NF1) GAP-related domain by site-directed mutagenesis. *Oncogene* 8: 761-9
71. Martin GA, Viskochil D, Bollag G, McCabe PC, Crosier WJ, Haubruck H, Conroy L, Clark R, O'Connell P, Cawthon RM, et al. 1990. The GAP-related domain of the neurofibromatosis type 1 gene product interacts with ras p21. *Cell* 63: 843-9

72. DeClue JE, Papageorge AG, Fletcher JA, Diehl SR, Ratner N, Vass WC, Lowy DR. 1992. Abnormal regulation of mammalian p21ras contributes to malignant tumor growth in von Recklinghausen (type 1) neurofibromatosis. *Cell* 69: 265-73
73. McCormick F. 1989. ras GTPase activating protein: signal transmitter and signal terminator. *Cell* 56: 5-8
74. Vigil D, Cherfils J, Rossman KL, Der CJ. 2010. Ras superfamily GEFs and GAPs: validated and tractable targets for cancer therapy? *Nat Rev Cancer* 10: 842-57
75. Bourne HR, Sanders DA, McCormick F. 1990. The GTPase superfamily: a conserved switch for diverse cell functions. *Nature* 348: 125-32
76. Bourne HR, Sanders DA, McCormick F. 1991. The GTPase superfamily: conserved structure and molecular mechanism. *Nature* 349: 117-27
77. Hall A. 1990. The cellular functions of small GTP-binding proteins. *Science* 249: 635-40
78. Hall A. 1992. Signal transduction through small GTPases--a tale of two GAPs. *Cell* 69: 389-91
79. Le LQ, Parada LF. 2007. Tumor microenvironment and neurofibromatosis type I: connecting the GAPs. *Oncogene* 26: 4609-16
80. Dasgupta B, Gutmann DH. 2003. Neurofibromatosis 1: closing the GAP between mice and men. *Curr Opin Genet Dev* 13: 20-7
81. Costa RM, Silva AJ. 2003. Mouse models of neurofibromatosis type I: bridging the GAP. *Trends Mol Med* 9: 19-23
82. Staser K, Yang FC, Clapp DW. 2010. Plexiform neurofibroma genesis: questions of Nf1 gene dose and hyperactive mast cells. *Curr Opin Hematol* 17: 287-93
83. Staser K, Yang FC, Clapp DW. 2010. Mast cells and the neurofibroma microenvironment. *Blood* 116: 157-64
84. Cichowski K, Shih TS, Schmitt E, Santiago S, Reilly K, McLaughlin ME, Bronson RT, Jacks T. 1999. Mouse models of tumor development in neurofibromatosis type 1. *Science* 286: 2172-6
85. Zhu Y, Ghosh P, Charnay P, Burns DK, Parada LF. 2002. Neurofibromas in NF1: Schwann cell origin and role of tumor environment. *Science* 296: 920-2
86. Joseph NM, Mosher JT, Buchstaller J, Snider P, McKeever PE, Lim M, Conway SJ, Parada LF, Zhu Y, Morrison SJ. 2008. The loss of Nf1 transiently promotes self-renewal but not tumorigenesis by neural crest stem cells. *Cancer Cell* 13: 129-40
87. Ingram DA, Yang FC, Travers JB, Wenning MJ, Hiatt K, New S, Hood A, Shannon K, Williams DA, Clapp DW. 2000. Genetic and biochemical evidence that haploinsufficiency of the Nf1 tumor suppressor gene modulates melanocyte and mast cell fates in vivo. *J Exp Med* 191: 181-8
88. Yang FC, Chen S, Clegg T, Li X, Morgan T, Estwick SA, Yuan J, Khalaf W, Burgin S, Travers J, Parada LF, Ingram DA, Clapp DW. 2006. Nf1+/- mast cells induce neurofibroma like phenotypes through secreted TGF-beta signaling. *Hum Mol Genet* 15: 2421-37

89. Bajenaru ML, Donahoe J, Corral T, Reilly KM, Brophy S, Pellicer A, Gutmann DH. 2001. Neurofibromatosis 1 (NF1) heterozygosity results in a cell-autonomous growth advantage for astrocytes. *Glia* 33: 314-23
90. Simmons GW, Pong WW, Emnett RJ, White CR, Gianino SM, Rodriguez FJ, Gutmann DH. 2010. Neurofibromatosis-1 Heterozygosity Increases Microglia in a Spatially and Temporally Restricted Pattern Relevant to Mouse Optic Glioma Formation and Growth. *J Neuropathol Exp Neurol*
91. Daginakatte GC, Gianino SM, Zhao NW, Parsadanian AS, Gutmann DH. 2008. Increased c-Jun-NH2-kinase signaling in neurofibromatosis-1 heterozygous microglia drives microglia activation and promotes optic glioma proliferation. *Cancer Res* 68: 10358-66
92. Daginakatte GC, Gutmann DH. 2007. Neurofibromatosis-1 (Nf1) heterozygous brain microglia elaborate paracrine factors that promote Nf1-deficient astrocyte and glioma growth. *Hum Mol Genet* 16: 1098-112
93. Zhang Y, Taylor BR, Shannon K, Clapp DW. 2001. Quantitative effects of Nf1 inactivation on in vivo hematopoiesis. *J Clin Invest* 108: 709-15
94. Ballester R, Marchuk D, Boguski M, Saulino A, Letcher R, Wigler M, Collins F. 1990. The NF1 locus encodes a protein functionally related to mammalian GAP and yeast IRA proteins. *Cell* 63: 851-9
95. Ingram DA, Zhang L, McCarthy J, Wenning MJ, Fisher L, Yang FC, Clapp DW, Kapur R. 2002. Lymphoproliferative defects in mice lacking the expression of neurofibromin: functional and biochemical consequences of Nf1 deficiency in T-cell development and function. *Blood* 100: 3656-62
96. Yang FC, Ingram DA, Chen S, Hingtgen CM, Ratner N, Monk KR, Clegg T, White H, Mead L, Wenning MJ, Williams DA, Kapur R, Atkinson SJ, Clapp DW. 2003. Neurofibromin-deficient Schwann cells secrete a potent migratory stimulus for Nf1+/- mast cells. *J Clin Invest* 112: 1851-61
97. Khalaf WF, Yang FC, Chen S, White H, Bessler W, Ingram DA, Clapp DW. 2007. K-ras is critical for modulating multiple c-kit-mediated cellular functions in wild-type and Nf1+/- mast cells. *J Immunol* 178: 2527-34
98. McDaniel AS, Allen JD, Park SJ, Jaffer ZM, Michels EG, Burgin SJ, Chen S, Bessler WK, Hofmann C, Ingram DA, Chernoff J, Clapp DW. 2008. Pak1 regulates multiple c-Kit mediated Ras-MAPK gain-in-function phenotypes in Nf1+/- mast cells. *Blood* 112: 4646-54
99. Hiatt K, Ingram DA, Huddleston H, Spandau DF, Kapur R, Clapp DW. 2004. Loss of the nf1 tumor suppressor gene decreases fas antigen expression in myeloid cells. *Am J Pathol* 164: 1471-9
100. Hiatt KK, Ingram DA, Zhang Y, Bollag G, Clapp DW. 2001. Neurofibromin GTPase-activating protein-related domains restore normal growth in Nf1-/- cells. *J Biol Chem* 276: 7240-5
101. Yang FC, Kapur R, King AJ, Tao W, Kim C, Borneo J, Breese R, Marshall M, Dinauer MC, Williams DA. 2000. Rac2 stimulates Akt activation affecting BAD/Bcl-XL expression while mediating survival and actin function in primary mast cells. *Immunity* 12: 557-68

102. Ingram DA, Hiatt K, King AJ, Fisher L, Shivakumar R, Derstine C, Wenning MJ, Diaz B, Travers JB, Hood A, Marshall M, Williams DA, Clapp DW. 2001. Hyperactivation of p21(ras) and the hematopoietic-specific Rho GTPase, Rac2, cooperate to alter the proliferation of neurofibromin-deficient mast cells in vivo and in vitro. *J Exp Med* 194: 57-69
103. Chen S, Burgin S, McDaniel A, Li X, Yuan J, Chen M, Khalaf W, Clapp DW, Yang FC. 2010. Nf1-/- Schwann cell-conditioned medium modulates mast cell degranulation by c-Kit-mediated hyperactivation of phosphatidylinositol 3-kinase. *Am J Pathol* 177: 3125-32
104. Fischer AM, Katayama CD, Pages G, Pouyssegur J, Hedrick SM. 2005. The role of erk1 and erk2 in multiple stages of T cell development. *Immunity* 23: 431-43
105. Yasuda T, Sanjo H, Pages G, Kawano Y, Karasuyama H, Pouyssegur J, Ogata M, Kurosaki T. 2008. Erk kinases link pre-B cell receptor signaling to transcriptional events required for early B cell expansion. *Immunity* 28: 499-508
106. Geest CR, Buitenhuis M, Groot Koerkamp MJ, Holstege FC, Vellenga E, Coffer PJ. 2009. Tight control of MEK-ERK activation is essential in regulating proliferation, survival, and cytokine production of CD34+-derived neutrophil progenitors. *Blood* 114: 3402-12
107. Ross SE, Radomska HS, Wu B, Zhang P, Winnay JN, Bajnok L, Wright WS, Schaufele F, Tenen DG, MacDougald OA. 2004. Phosphorylation of C/EBPalpha inhibits granulopoiesis. *Mol Cell Biol* 24: 675-86
108. Jack GD, Zhang L, Friedman AD. 2009. M-CSF elevates c-Fos and phospho-C/EBPalpha(S21) via ERK whereas G-CSF stimulates SHP2 phosphorylation in marrow progenitors to contribute to myeloid lineage specification. *Blood* 114: 2172-80
109. Geest CR, Coffer PJ. 2009. MAPK signaling pathways in the regulation of hematopoiesis. *J Leukoc Biol* 86: 237-50
110. Hsu CL, Kikuchi K, Kondo M. 2007. Activation of mitogen-activated protein kinase kinase (MEK)/extracellular signal regulated kinase (ERK) signaling pathway is involved in myeloid lineage commitment. *Blood* 110: 1420-8
111. Brunet A, Pouyssegur J. 1997. Mammalian MAP kinase modules: how to transduce specific signals. *Essays Biochem* 32: 1-16
112. Roberts PJ, Der CJ. 2007. Targeting the Raf-MEK-ERK mitogen-activated protein kinase cascade for the treatment of cancer. *Oncogene* 26: 3291-310
113. Brown AP, Carlson TC, Loi CM, Graziano MJ. 2007. Pharmacodynamic and toxicokinetic evaluation of the novel MEK inhibitor, PD0325901, in the rat following oral and intravenous administration. *Cancer Chemother Pharmacol* 59: 671-9
114. Meloche S, Pouyssegur J. 2007. The ERK1/2 mitogen-activated protein kinase pathway as a master regulator of the G1- to S-phase transition. *Oncogene* 26: 3227-39

115. Dumesic PA, Scholl FA, Barragan DI, Khavari PA. 2009. Erk1/2 MAP kinases are required for epidermal G2/M progression. *J Cell Biol* 185: 409-22
116. Yao Y, Li W, Wu J, Germann UA, Su MS, Kuida K, Boucher DM. 2003. Extracellular signal-regulated kinase 2 is necessary for mesoderm differentiation. *Proc Natl Acad Sci U S A* 100: 12759-64
117. Ying QL, Wray J, Nichols J, Batlle-Morera L, Doble B, Woodgett J, Cohen P, Smith A. 2008. The ground state of embryonic stem cell self-renewal. *Nature* 453: 519-23
118. Yu J, Chau KF, Vodyanik MA, Jiang J, Jiang Y. 2011. Efficient feeder-free episomal reprogramming with small molecules. *PLoS One* 6: e17557
119. Lee KH, Chuang CK, Guo SF, Tu CF. 2011. Simple and Efficient Derivation of Mouse Embryonic Stem Cell Lines Using Differentiation Inhibitors or Proliferation Stimulators. *Stem Cells Dev*
120. Pages G, Guerin S, Grall D, Bonino F, Smith A, Anjuere F, Auberger P, Pouyssegur J. 1999. Defective thymocyte maturation in p44 MAP kinase (Erk 1) knockout mice. *Science* 286: 1374-7
121. Hatano N, Mori Y, Oh-hora M, Kosugi A, Fujikawa T, Nakai N, Niwa H, Miyazaki J, Hamaoka T, Ogata M. 2003. Essential role for ERK2 mitogen-activated protein kinase in placental development. *Genes Cells* 8: 847-56
122. Samuels IS, Karlo JC, Faruzzi AN, Pickering K, Herrup K, Sweatt JD, Saitta SC, Landreth GE. 2008. Deletion of ERK2 mitogen-activated protein kinase identifies its key roles in cortical neurogenesis and cognitive function. *J Neurosci* 28: 6983-95
123. Sturgill TW. 2008. MAP kinase: it's been longer than fifteen minutes. *Biochem Biophys Res Commun* 371: 1-4
124. Mazzucchelli C, Vantaggiato C, Ciamei A, Fasano S, Pakhotin P, Krezel W, Welzl H, Wolfer DP, Pages G, Valverde O, Marowsky A, Porrazzo A, Orban PC, Maldonado R, Ehrengruber MU, Cestari V, Lipp HP, Chapman PF, Pouyssegur J, Brambilla R. 2002. Knockout of ERK1 MAP kinase enhances synaptic plasticity in the striatum and facilitates striatal-mediated learning and memory. *Neuron* 34: 807-20
125. Ferguson SM, Fasano S, Yang P, Brambilla R, Robinson TE. 2006. Knockout of ERK1 enhances cocaine-evoked immediate early gene expression and behavioral plasticity. *Neuropsychopharmacology* 31: 2660-8
126. Fremin C, Bessard A, Ezan F, Gailhouste L, Regeard M, Le Seyec J, Gilot D, Pages G, Pouyssegur J, Langouet S, Baffet G. 2009. Multiple division cycles and long-term survival of hepatocytes are distinctly regulated by extracellular signal-regulated kinases ERK1 and ERK2. *Hepatology* 49: 930-9
127. Fremin C, Ezan F, Boisselier P, Bessard A, Pages G, Pouyssegur J, Baffet G. 2007. ERK2 but not ERK1 plays a key role in hepatocyte replication: an RNAi-mediated ERK2 knockdown approach in wild-type and ERK1 null hepatocytes. *Hepatology* 45: 1035-45

128. Vantaggiato C, Formentini I, Bondanza A, Bonini C, Naldini L, Brambilla R. 2006. ERK1 and ERK2 mitogen-activated protein kinases affect Ras-dependent cell signaling differentially. *J Biol* 5: 14
129. Bost F, Aouadi M, Caron L, Even P, Belmonte N, Prot M, Dani C, Hofman P, Pages G, Pouyssegur J, Le Marchand-Brustel Y, Binetruy B. 2005. The extracellular signal-regulated kinase isoform ERK1 is specifically required for in vitro and in vivo adipogenesis. *Diabetes* 54: 402-11
130. Agrawal A, Dillon S, Denning TL, Pulendran B. 2006. ERK1-/- mice exhibit Th1 cell polarization and increased susceptibility to experimental autoimmune encephalomyelitis. *J Immunol* 176: 5788-96
131. Guihard S, Clay D, Cocault L, Saulnier N, Opolon P, Souyri M, Pages G, Pouyssegur J, Porteu F, Gaudry M. The MAPK ERK1 is a negative regulator of the adult steady-state splenic erythropoiesis. *Blood* 115: 3686-94
132. Lefloch R, Pouyssegur J, Lenormand P. 2008. Single and combined silencing of ERK1 and ERK2 reveals their positive contribution to growth signaling depending on their expression levels. *Mol Cell Biol* 28: 511-27
133. Lefloch R, Pouyssegur J, Lenormand P. 2009. Total ERK1/2 activity regulates cell proliferation. *Cell Cycle* 8: 705-11
134. Satoh Y, Endo S, Ikeda T, Yamada K, Ito M, Kuroki M, Hiramoto T, Imamura O, Kobayashi Y, Watanabe Y, Itohara S, Takishima K. 2007. Extracellular signal-regulated kinase 2 (ERK2) knockdown mice show deficits in long-term memory; ERK2 has a specific function in learning and memory. *J Neurosci* 27: 10765-76
135. Shaikh TH, O'Connor RJ, Pierpont ME, McGrath J, Hacker AM, Nimmakayalu M, Geiger E, Emanuel BS, Saitta SC. 2007. Low copy repeats mediate distal chromosome 22q11.2 deletions: sequence analysis predicts breakpoint mechanisms. *Genome Res* 17: 482-91
136. Newbern J, Zhong J, Wickramasinghe RS, Li X, Wu Y, Samuels I, Cherosky N, Karlo JC, O'Loughlin B, Wikenheiser J, Gargesha M, Doughman YQ, Charron J, Ginty DD, Watanabe M, Saitta SC, Snider WD, Landreth GE. 2008. Mouse and human phenotypes indicate a critical conserved role for ERK2 signaling in neural crest development. *Proc Natl Acad Sci U S A* 105: 17115-20
137. Kinoshita T, Yoshida I, Nakae S, Okita K, Gouda M, Matsubara M, Yokota K, Ishiguro H, Tada T. 2008. Crystal structure of human mono-phosphorylated ERK1 at Tyr204. *Biochem Biophys Res Commun* 377: 1123-7
138. Srinivasan R, Zabuawala T, Huang H, Zhang J, Gulati P, Fernandez S, Karlo JC, Landreth GE, Leone G, Ostrowski MC. 2009. Erk1 and Erk2 regulate endothelial cell proliferation and migration during mouse embryonic angiogenesis. *PLoS One* 4: e8283
139. Fan HY, Liu Z, Shimada M, Sterneck E, Johnson PF, Hedrick SM, Richards JS. 2009. MAPK3/1 (ERK1/2) in ovarian granulosa cells are essential for female fertility. *Science* 324: 938-41

140. Imamura O, Pages G, Pouyssegur J, Endo S, Takishima K. 2010. ERK1 and ERK2 are required for radial glial maintenance and cortical lamination. *Genes Cells* 15: 1072-88
141. Matsushita T, Chan YY, Kawanami A, Balmes G, Landreth GE, Murakami S. 2009. Extracellular signal-regulated kinase 1 (ERK1) and ERK2 play essential roles in osteoblast differentiation and in supporting osteoclastogenesis. *Mol Cell Biol* 29: 5843-57
142. Kuhn R, Schwenk F, Aguet M, Rajewsky K. 1995. Inducible gene targeting in mice. *Science* 269: 1427-9
143. Kiel MJ, Acar M, Radice GL, Morrison SJ. 2009. Hematopoietic stem cells do not depend on N-cadherin to regulate their maintenance. *Cell Stem Cell* 4: 170-9
144. Larsson J, Ohishi M, Garrison B, Aspling M, Janzen V, Adams GB, Curto M, McClatchey AI, Schipani E, Scadden DT. 2008. Nf2/merlin regulates hematopoietic stem cell behavior by altering microenvironmental architecture. *Cell Stem Cell* 3: 221-7
145. Williams DE, Hangoc G, Cooper S, Boswell HS, Shadduck RK, Gillis S, Waheed A, Urdal D, Broxmeyer HE. 1987. The effects of purified recombinant murine interleukin-3 and/or purified natural murine CSF-1 in vivo on the proliferation of murine high- and low-proliferative potential colony-forming cells: demonstration of in vivo synergism. *Blood* 70: 401-3
146. Lantz CS, Boesiger J, Song CH, Mach N, Kobayashi T, Mulligan RC, Nawa Y, Dranoff G, Galli SJ. 1998. Role for interleukin-3 in mast-cell and basophil development and in immunity to parasites. *Nature* 392: 90-3
147. Tsai M, Shih LS, Newlands GF, Takeishi T, Langley KE, Zsebo KM, Miller HR, Geissler EN, Galli SJ. 1991. The rat c-kit ligand, stem cell factor, induces the development of connective tissue-type and mucosal mast cells in vivo. Analysis by anatomical distribution, histochemistry, and protease phenotype. *J Exp Med* 174: 125-31
148. Mikkola HK, Klintman J, Yang H, Hock H, Schlaeger TM, Fujiwara Y, Orkin SH. 2003. Haematopoietic stem cells retain long-term repopulating activity and multipotency in the absence of stem-cell leukaemia SCL/tal-1 gene. *Nature* 421: 547-51
149. Passegue E, Wagers AJ, Giuriato S, Anderson WC, Weissman IL. 2005. Global analysis of proliferation and cell cycle gene expression in the regulation of hematopoietic stem and progenitor cell fates. *J Exp Med* 202: 1599-611
150. Weissman IL, Shizuru JA. 2008. The origins of the identification and isolation of hematopoietic stem cells, and their capability to induce donor-specific transplantation tolerance and treat autoimmune diseases. *Blood* 112: 3543-53
151. Kiel MJ, Yilmaz OH, Iwashita T, Terhorst C, Morrison SJ. 2005. SLAM family receptors distinguish hematopoietic stem and progenitor cells and reveal endothelial niches for stem cells. *Cell* 121: 1109-21

152. Gothot A, Pyatt R, McMahel J, Rice S, Srour EF. 1997. Functional heterogeneity of human CD34(+) cells isolated in subcompartments of the G0 /G1 phase of the cell cycle. *Blood* 90: 4384-93
153. Darzynkiewicz Z, Juan G, Srour EF. 2004. Differential staining of DNA and RNA. *Curr Protoc Cytom* Chapter 7: Unit 7 3
154. Gothot A, Pyatt R, McMahel J, Rice S, Srour EF. 1998. Assessment of proliferative and colony-forming capacity after successive in vitro divisions of single human CD34+ cells initially isolated in G0. *Exp Hematol* 26: 562-70
155. Vermes I, Haanen C, Steffens-Nakken H, Reutelingsperger C. 1995. A novel assay for apoptosis. Flow cytometric detection of phosphatidylserine expression on early apoptotic cells using fluorescein labelled Annexin V. *J Immunol Methods* 184: 39-51
156. Sanchez I, Dynlacht BD. 2005. New insights into cyclins, CDKs, and cell cycle control. *Semin Cell Dev Biol* 16: 311-21
157. Lauchle JO, Kim D, Le DT, Akagi K, Crone M, Krisman K, Warner K, Bonifas JM, Li Q, Coakley KM, Diaz-Flores E, Gorman M, Przybranowski S, Tran M, Kogan SC, Roose JP, Copeland NG, Jenkins NA, Parada L, Wolff L, Sebolt-Leopold J, Shannon K. 2009. Response and resistance to MEK inhibition in leukaemias initiated by hyperactive Ras. *Nature* 461: 411-4
158. Lyubynska N, Gorman MF, Lauchle JO, Hong WX, Akutagawa JK, Shannon K, Braun BS. 2011. A MEK Inhibitor Abrogates Myeloproliferative Disease in Kras Mutant Mice. *Sci Transl Med* 3: 76ra27
159. Ingram DA, Wenning MJ, Shannon K, Clapp DW. 2003. Leukemic potential of doubly mutant Nf1 and Wv hematopoietic cells. *Blood* 101: 1984-6
160. Birnbaum RA, O'Marcaigh A, Wardak Z, Zhang YY, Dranoff G, Jacks T, Clapp DW, Shannon KM. 2000. Nf1 and Gmcsf interact in myeloid leukemogenesis. *Mol Cell* 5: 189-95
161. Thompson N, Lyons J. 2005. Recent progress in targeting the Raf/MEK/ERK pathway with inhibitors in cancer drug discovery. *Curr Opin Pharmacol* 5: 350-6
162. Wang JY, Wilcoxen KM, Nomoto K, Wu S. 2007. Recent advances of MEK inhibitors and their clinical progress. *Curr Top Med Chem* 7: 1364-78
163. Ciuffreda L, Del Bufalo D, Desideri M, Di Sanza C, Stoppacciaro A, Ricciardi MR, Chiaretti S, Tavolaro S, Benassi B, Bellacosa A, Foa R, Tafuri A, Cognetti F, Anichini A, Zupi G, Milella M. 2009. Growth-inhibitory and antiangiogenic activity of the MEK inhibitor PD0325901 in malignant melanoma with or without BRAF mutations. *Neoplasia* 11: 720-31
164. Henderson YC, Chen Y, Frederick MJ, Lai SY, Clayman GL. 2010. MEK inhibitor PD0325901 significantly reduces the growth of papillary thyroid carcinoma cells in vitro and in vivo. *Mol Cancer Ther* 9: 1968-76

165. Leyton J, Smith G, Lees M, Perumal M, Nguyen QD, Aigbirhio FI, Golovko O, He Q, Workman P, Aboagye EO. 2008. Noninvasive imaging of cell proliferation following mitogenic extracellular kinase inhibition by PD0325901. *Mol Cancer Ther* 7: 3112-21
166. Kinkade CW, Castillo-Martin M, Puzio-Kuter A, Yan J, Foster TH, Gao H, Sun Y, Ouyang X, Gerald WL, Cordon-Cardo C, Abate-Shen C. 2008. Targeting AKT/mTOR and ERK MAPK signaling inhibits hormone-refractory prostate cancer in a preclinical mouse model. *J Clin Invest* 118: 3051-64
167. Hennig M, Yip-Schneider MT, Wentz S, Wu H, Hekmatyar SK, Klein P, Bansal N, Schmidt CM. 2010. Targeting mitogen-activated protein kinase kinase with the inhibitor PD0325901 decreases hepatocellular carcinoma growth in vitro and in mouse model systems. *Hepatology* 51: 1218-25
168. Wentz SC, Wu H, Yip-Schneider MT, Hennig M, Klein PJ, Sebolt-Leopold J, Schmidt CM. 2008. Targeting MEK is effective chemoprevention of hepatocellular carcinoma in TGF-alpha-transgenic mice. *J Gastrointest Surg* 12: 30-7
169. Haura EB, Ricart AD, Larson TG, Stella PJ, Bazhenova L, Miller VA, Cohen RB, Eisenberg PD, Selaru P, Wilner KD, Gadgeel SM. 2010. A phase II study of PD-0325901, an oral MEK inhibitor, in previously treated patients with advanced non-small cell lung cancer. *Clin Cancer Res* 16: 2450-7
170. Rinehart J, Adjei AA, Lorusso PM, Waterhouse D, Hecht JR, Natale RB, Hamid O, Varterasian M, Asbury P, Kaldjian EP, Gulyas S, Mitchell DY, Herrera R, Sebolt-Leopold JS, Meyer MB. 2004. Multicenter phase II study of the oral MEK inhibitor, CI-1040, in patients with advanced non-small-cell lung, breast, colon, and pancreatic cancer. *J Clin Oncol* 22: 4456-62
171. Smith CK, Carr D, Mayhood TW, Jin W, Gray K, Windsor WT. 2007. Expression and purification of phosphorylated and non-phosphorylated human MEK1. *Protein Expr Purif* 52: 446-56
172. Smith CK, Windsor WT. 2007. Thermodynamics of nucleotide and non-ATP-competitive inhibitor binding to MEK1 by circular dichroism and isothermal titration calorimetry. *Biochemistry* 46: 1358-67
173. Leboeuf R, Baumgartner JE, Benezra M, Malaguarnera R, Solit D, Pratilas CA, Rosen N, Knauf JA, Fagin JA. 2008. BRAFV600E mutation is associated with preferential sensitivity to mitogen-activated protein kinase kinase inhibition in thyroid cancer cell lines. *J Clin Endocrinol Metab* 93: 2194-201
174. Liu D, Xing M. 2008. Potent inhibition of thyroid cancer cells by the MEK inhibitor PD0325901 and its potentiation by suppression of the PI3K and NF-kappaB pathways. *Thyroid* 18: 853-64
175. Pozo-Guisado E, Campbell DG, Deak M, Alvarez-Barrientos A, Morrice NA, Alvarez IS, Alessi DR, Martin-Romero FJ. 2010. Phosphorylation of STIM1 at ERK1/2 target sites modulates store-operated calcium entry. *J Cell Sci* 123: 3084-93

176. Blenkinsopp WK. 1967. Effect of tritiated thymidine on cell proliferation. *J Cell Sci* 2: 305-8
177. Cruikshank W, Little F. 2008. Interleukin-16: the ins and outs of regulating T-cell activation. *Crit Rev Immunol* 28: 467-83
178. Cavaillon JM. 1994. Cytokines and macrophages. *Biomed Pharmacother* 48: 445-53
179. Guihard S, Clay D, Cocault L, Saulnier N, Opolon P, Souyri M, Pages G, Pouyssegur J, Porteu F, Gaudry M. 2010. The MAPK ERK1 is a negative regulator of the adult steady-state splenic erythropoiesis. *Blood* 115: 3686-94
180. Wu X, Tu X, Joeng KS, Hilton MJ, Williams DA, Long F. 2008. Rac1 activation controls nuclear localization of beta-catenin during canonical Wnt signaling. *Cell* 133: 340-53
181. Ding Q, Xia W, Liu JC, Yang JY, Lee DF, Xia J, Bartholomeusz G, Li Y, Pan Y, Li Z, Bargou RC, Qin J, Lai CC, Tsai FJ, Tsai CH, Hung MC. 2005. Erk associates with and primes GSK-3beta for its inactivation resulting in upregulation of beta-catenin. *Mol Cell* 19: 159-70
182. Kajiguchi T, Lee S, Lee MJ, Trepel JB, Neckers L. 2008. KIT regulates tyrosine phosphorylation and nuclear localization of beta-catenin in mast cell leukemia. *Leuk Res* 32: 761-70
183. Hu T, Li C. 2010. Convergence between Wnt-beta-catenin and EGFR signaling in cancer. *Mol Cancer* 9: 236
184. Matsuda T, Cepko CL. 2007. Controlled expression of transgenes introduced by in vivo electroporation. *Proc Natl Acad Sci U S A* 104: 1027-32
185. Bender FL, Fischer M, Funk N, Orel N, Rethwilm A, Sendtner M. 2007. High-efficiency gene transfer into cultured embryonic motoneurons using recombinant lentiviruses. *Histochem Cell Biol* 127: 439-48
186. Gonzalez-Murillo A, Lozano ML, Alvarez L, Jacome A, Almarza E, Navarro S, Segovia JC, Hanenberg H, Guenechea G, Bueren JA, Rio P. Development of lentiviral vectors with optimized transcriptional activity for the gene therapy of patients with fanconi anemia. *Hum Gene Ther* 21: 623-30
187. Si Y, Pulliam AC, Linka Y, Ciccone S, Leurs C, Yuan J, Eckermann O, Fruehauf S, Mooney S, Hanenberg H, Clapp DW. 2008. Overnight transduction with foamyviral vectors restores the long-term repopulating activity of Fancc-/- stem cells. *Blood* 112: 4458-65
188. Leurs C, Jansen M, Pollok KE, Heinkelein M, Schmidt M, Wissler M, Lindemann D, Von Kalle C, Rethwilm A, Williams DA, Hanenberg H. 2003. Comparison of three retroviral vector systems for transduction of nonobese diabetic/severe combined immunodeficiency mice repopulating human CD34+ cord blood cells. *Hum Gene Ther* 14: 509-19
189. Rio P, Meza NW, Gonzalez-Murillo A, Navarro S, Alvarez L, Surralles J, Castella M, Guenechea G, Segovia JC, Hanenberg H, Bueren JA. 2008. In vivo proliferation advantage of genetically corrected hematopoietic stem cells in a mouse model of Fanconi anemia FA-D1. *Blood* 112: 4853-61

190. Furumoto Y, Brooks S, Olivera A, Takagi Y, Miyagishi M, Taira K, Casellas R, Beaven MA, Gilfillan AM, Rivera J. 2006. Cutting Edge: Lentiviral short hairpin RNA silencing of PTEN in human mast cells reveals constitutive signals that promote cytokine secretion and cell survival. *J Immunol* 176: 5167-71
191. Nakashima K, Sakurai F, Kawabata K, Mizuguchi H. 2008. Efficient gene delivery in human and rodent mast cells using adenovirus vectors. *J Control Release* 129: 215-22
192. Purcell NH, Wilkins BJ, York A, Saba-El-Leil MK, Meloche S, Robbins J, Molkentin JD. 2007. Genetic inhibition of cardiac ERK1/2 promotes stress-induced apoptosis and heart failure but has no effect on hypertrophy in vivo. *Proc Natl Acad Sci U S A* 104: 14074-9
193. Meloche S, Seuwen K, Pages G, Pouyssegur J. 1992. Biphasic and synergistic activation of p44mapk (ERK1) by growth factors: correlation between late phase activation and mitogenicity. *Mol Endocrinol* 6: 845-54
194. Voisin L, Saba-El-Leil MK, Julien C, Fremin C, Meloche S. 2010. Genetic demonstration of a redundant role of extracellular signal-regulated kinase 1 (ERK1) and ERK2 mitogen-activated protein kinases in promoting fibroblast proliferation. *Mol Cell Biol* 30: 2918-32
195. Pages G, Pouyssegur J. 2004. Study of MAPK signaling using knockout mice. *Methods Mol Biol* 250: 155-66
196. Volmat V, Pouyssegur J. 2001. Spatiotemporal regulation of the p42/p44 MAPK pathway. *Biol Cell* 93: 71-9
197. Pouyssegur J. 2000. Signal transduction. An arresting start for MAPK. *Science* 290: 1515-8
198. Kiel MJ, He S, Ashkenazi R, Gentry SN, Teta M, Kushner JA, Jackson TL, Morrison SJ. 2007. Haematopoietic stem cells do not asymmetrically segregate chromosomes or retain BrdU. *Nature* 449: 238-42
199. Waning DL, Li B, Jia N, Naaldijk Y, Goebel WS, HogenEsch H, Chun KT. 2008. Cul4A is required for hematopoietic cell viability and its deficiency leads to apoptosis. *Blood* 112: 320-9
200. Li B, Jia N, Waning DL, Yang FC, Haneline LS, Chun KT. 2007. Cul4A is required for hematopoietic stem-cell engraftment and self-renewal. *Blood* 110: 2704-7
201. Li B, Jia N, Kapur R, Chun KT. 2006. Cul4A targets p27 for degradation and regulates proliferation, cell cycle exit, and differentiation during erythropoiesis. *Blood* 107: 4291-9
202. Shapiro PS, Vaisberg E, Hunt AJ, Tolwinski NS, Whalen AM, McIntosh JR, Ahn NG. 1998. Activation of the MKK/ERK pathway during somatic cell mitosis: direct interactions of active ERK with kinetochores and regulation of the mitotic 3F3/2 phosphoantigen. *J Cell Biol* 142: 1533-45
203. Zecevic M, Catling AD, Eblen ST, Renzi L, Hittle JC, Yen TJ, Gorbsky GJ, Weber MJ. 1998. Active MAP kinase in mitosis: localization at kinetochores and association with the motor protein CENP-E. *J Cell Biol* 142: 1547-58

204. D'Souza WN, Chang CF, Fischer AM, Li M, Hedrick SM. 2008. The Erk2 MAPK regulates CD8 T cell proliferation and survival. *J Immunol* 181: 7617-29
205. Czechowicz A, Kraft D, Weissman IL, Bhattacharya D. 2007. Efficient transplantation via antibody-based clearance of hematopoietic stem cell niches. *Science* 318: 1296-9
206. Xue X, Pech NK, Shelley WC, Srour EF, Yoder MC, Dinauer MC. 2010. Antibody targeting KIT as pretransplantation conditioning in immunocompetent mice. *Blood* 116: 5419-22
207. Kuehn HS, Jung MY, Beaven MA, Metcalfe DD, Gilfillan AM. 2011. Prostaglandin E2 activates and utilizes mTORC2 as a central signaling locus for the regulation of mast cell chemotaxis and mediator release. *J Biol Chem* 286: 391-402
208. Kim MS, Radinger M, Gilfillan AM. 2008. The multiple roles of phosphoinositide 3-kinase in mast cell biology. *Trends Immunol* 29: 493-501
209. Easton JB, Kurmasheva RT, Houghton PJ. 2006. IRS-1: auditing the effectiveness of mTOR inhibitors. *Cancer Cell* 9: 153-5
210. Naegele S, Morley SJ. 2004. Molecular cross-talk between MEK1/2 and mTOR signaling during recovery of 293 cells from hypertonic stress. *J Biol Chem* 279: 46023-34
211. Sundstrom M, Alfredsson J, Olsson N, Nilsson G. 2001. Stem cell factor-induced migration of mast cells requires p38 mitogen-activated protein kinase activity. *Exp Cell Res* 267: 144-51
212. Tan BL, Yazicioglu MN, Ingram D, McCarthy J, Borneo J, Williams DA, Kapur R. 2003. Genetic evidence for convergence of c-Kit- and alpha4 integrin-mediated signals on class IA PI-3kinase and the Rac pathway in regulating integrin-directed migration in mast cells. *Blood* 101: 4725-32
213. Munugalavadla V, Sims EC, Borneo J, Chan RJ, Kapur R. 2007. Genetic and pharmacologic evidence implicating the p85 alpha, but not p85 beta, regulatory subunit of PI3K and Rac2 GTPase in regulating oncogenic KIT-induced transformation in acute myeloid leukemia and systemic mastocytosis. *Blood* 110: 1612-20

CURRICULUM VITAE

Karl W. Staser

Education

Indiana University
MD, expected May 2013.
PhD, Biochemistry and Molecular Biology, expected March 2012.

Howard Hughes Medical Institute (HHMI), Research Fellow, 2008-2009.

Harvard University, AB History and Literature, magna cum laude, 2002.

Professional Experience

Research Associate Positions
- Harvard University: Andy McMahon Laboratory, 2004-2005.
- Indiana University: Sidney Shaw Laboratory, 2005-2006.

McMaster-Carr Supply Company, Supervisor, 2002-2004 (Los Angeles, CA).

Medical Device Manufacturers Association, Intern, 2001 (Washington, DC).

Honors, Awards, and Fellowships

Medical/Graduate School

- NIH Medical Scientist Training Program (MSTP).
- Bowen Research Scholarship, Indiana University, 2006-2013.
- NIH T32 Cancer Biology Training Fellowship, 2009-2011.
- HHMI Research Fellowship, 2008-2009.
- Sigma Xi Research Award, 2010.
- International Society of Experimental Hematology, Travel Award, 2010.
- International Society of Experimental Hematology, Travel Award, 2011.
- American Society of Hematology Abstract Award, twice in 2011.
- William J. Wright Cancer Research Scholarship, 2011-2012.
- NIH F30 National Research Service Award 2012-2013 (projected).

Undergraduate

- John Harvard Scholarship and Harvard College Scholarship.
- National Merit Scholar.
- Coca-Cola Scholar.
- Robert C. Byrd National Scholar.

Publications

Staser K, Park SJ, Zeng Y, Rhodes SD, He YZ, Shew MA, Gehlhauen J, Cerabonna D, Yang FC, Clapp DW. Hematopoietic stem cell proliferation requires Erk. (Submission to *Blood*).

Staser K, Michels E, Shew M, Mwanthi M, FC Yang, Clapp DW, Park SJ. A Pak1-PP2A-Ezrin signaling axis coordinates IgE-dependent mast cell cytoskeletal organization and degranulation. (Submission to *Molecular and Cellular Biology*).

Lotze MT, Torte F, Keith B, Manfredi J, Spitz DR, Tycko B, Domann F,Chan T, Gary B, Livesey K, Lavik, A, Rao M, Veenstra J, Dean I, Hayan M, Coleman M, Staser K, Kadoch, C. Medical Training in Cancer Biology, Diagnosis, and Therapy. (Submission to *Journal of Clinical Oncology*).

Robertson K, Yang FC, Bowers D, Ho C, Hutchins G, Nalepa G, Croop J, Vik T, Denne S, Parada L, Hingtgen, Walsh L, Yu M, Pradhan K, Edwards-Brown M, Cohen M, Fletcher J, Travers J, Staser K, Lee M, Sherman M, Davis C, Miller L, Ingram D, Clapp W. Pilot phase II trial of imatinib mesylate in neurofibromatosis type 1 patients with plexiform neurofibromas. (In revision with *New England Journal of Medicine*).

Yu J, Valerius MT, Duah M, Staser K, Hansard J, Guo J, McMahon J, Vaughan J, Faria D, Georgas K, Rumballe B, Ren Q, Mayer AM, Junker J, Thiagarajan R, Machanick P, Gray P, van Oudenaarden A, Rowitch D, Stiles C, Ma Q, Grimmond S, Bailey T, Little M, McMahon AP. Identification of molecular compartments and genetic circuitry in the developing mammalian kidney. (In revision with *Development*).

Staser K and Yang FC. Single cell hematopoietic stem cell assay. *Encyclopedia of Systems Biology* (Springer International), 2012 (in press).

Staser K, Yang FC, and Clapp DW. Tumor/stromal interactions in plexiform neurofibromas: role of the hematopoietic system. *Annu Rev Pathol,* 2012 Feb 28;7:469-95, Epub 2011 Nov 7. PMID 22077553.

He Y, Staser K, Rhodes S, Liu Y, Wu X, Park SJ, Yuan J, Yang X, Li X, Chen S, Yang FC. *Erk1* positively regulates osteoclast differentiation and bone resorptive activity. *PLoS One*, 2011;6(9):e24780, Epub 2011 Sep 22. PMID 21961044.

Chen M, Burgin S, Staser K, He Y, Li X, Robinson M, Chan R, Ingram D, Clapp DW. Kinase Suppressor of Ras (KSR1) modulates multiple Kit-ligand-dependent mast cell functions. *Exp Hematol,* 2011 Oct;29(10):969-76, Epub 2011 Jul 1. PMID 21726514.

Staser K, Zollinger TW, Saywell RM, Kunapareddy S, Gibson PJ, Caine VA. Dietary Behaviors Associated with Fruit and Vegetable Consumption. *Prev Chronic Dis*, 2011 May 8(3):A66. PMID 21477506.

Stevenson DA, Yan J, He Y, Li H, Liu Y, Zhang Q, Guo Z, Zhang W, Yang D, Wu X, Hanson H, Li X, Staser K, Viskochil D, Carey J, Chen S, Miller L, Robertson K, Moyer-Mileur L, Yu, Menggang, Schwarz E, Pasquali M, Yang FC. Increased multiple osteoclast functions in individuals with neurofibromatosis type 1. *Am J Med Genet,* 2011 May;155(5)1050-9. PMID 21465658.

Staser K, Yang FC, Clapp DW. Plexiform neurofibroma genesis: questions of Nf1 gene dose and hyperactive mast cells. *Curr Opin Hematol*. 2010 Jul;17(4):287-93. PMID: 20571392.

Staser K, Yang FC, Clapp DW. Mast cells and the neurofibroma microenvironment. *Blood*. 2010 Jul 15;116(2):157-64.PMID: 2023397.

Abstracts/Presentations

He YZ, Staser K, Rhodes SD, Wu X, Zhang P, Chen S, Yang FC. Erk1 Plays Critical Role in Macrophage Development**.** American Society of Hematology Annual Meeting, December 10-13, 2011, San Diego, CA. Abstract Achievement Award.

Zheng Y, Staser K, Menon KM, Park SJ, Mwanthi M, Li J, Clapp, DW. Ezrin Regulates Hematopoietic Stem/Progenitor Cell Motility. American Society of Hematology Annual Meeting, December 10-13, 2011, San Diego, CA. Abstract Achievement Award.

Staser K, Park SJ, Shew MA, Michels EG, Mwanthi MM, Yang FC, Clapp DW. A Pak1-PP2A-ERM axis modulates IgE-mediated mast cell degranulation. International Society for Experimental Hematology (ISEH) Annual Meeting, Vancouver, Canada, August 25-28, 2011. (Oral) Travel award.

Staser K, Park SJ, He YZ, Shew MA, Rhodes SD, Li Y, Nalepa G, Yang FC, Clapp DW. Hematopoiesis requires Erk. Cancer Biology Training Consortium Annual Meeting, Tucson, AZ, November 5-7, 2010.

Staser K, Park SJ, He YZ, Shew MA, Rhodes SD, Li Y, Nalepa G, Yang FC, Clapp DW. Marrow repopulation and stem cell expansion requires ERK. International Society for Experimental Hematology (ISEH) Annual Meeting, Melbourne, Australia, September 15-18, 2010. (Oral) Travel award.

Staser K, Zollinger TW, Saywell RM, Kunapareddy S, Gibson PJ, Caine VA. Dietary Behaviors Associated with Fruit and Vegetable Consumption. American

College of Epidemiology annual meeting, San Francisco, CA, September 11-14, 2010.

Staser K, Park, SJ, Shew, MA, Yang, FC, Clapp, DW. Reciprocal yet critical roles for ERK1 and ERK2 in mast cell cytopoiesis and proliferation. MD/PhD Annual Conference, Keystone, CO, July 23-25, 2010.

Staser K, Park SJ, He YZ, Shew MA, Gehlhausen JR, Robinson MB, Li Y, Rhodes SD, Nalepa G, Yang FC, Clapp DW. Genetic evidence that myeloid proliferation requires ERK. American Society of Clinical Investigators (ASCI) Annual Meeting, Chicago, IL, April 23-25, 2010.

Staser K, Park SJ, Gehlhausen JR, Clapp DW. Erk1 negatively regulates SCF-dependent mast cell function via Erk2 and β-catenin interactions. Howard Hughes Medical Institute Annual Scholars/Fellows Meeting, Bethesda, MD, May 17-20, 2009.

Staser K, Hansard J, Yu J, Valerius MT, McMahon AP. KMAP: The Kidney Molecular Atlas Project. Harvard University Graduate School of Arts and Sciences Meetings, Cambridge, MA, May 2005.

Staser K, Valerius MT, Yu J, McMahon AP, Riboprobe Synthesis for In Situ Hybridization for the Kidney Molecular Atlas Project (KMAP)[protocol], July 2005, online at NIH/GUDMAP website, http://www.gudmap.org/Research/Protocols/McMahon/PlasmidProbeCloning.pdf.